frontiers
RESEARCH TOPICS

CELLULAR IMAGING AND EMERGING TECHNOLOGIES FOR ADULT NEUROGENESIS RESEARCH

Hosted by
Silvia De Marchis and Adam C. Puche

frontiers in
NEUROSCIENCE

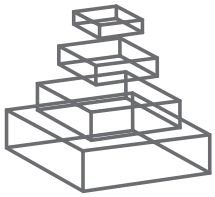

frontiers

Cover image provided by Ibbl sarl, Lausanne CH

ISSN 1664-8714
ISBN 978-2-88919-029-4
DOI 10.3389/978-2-88919-029-4

ABOUT FRONTIERS

Frontiers is more than just an open-access publisher of scholarly articles: it is a pioneering approach to the world of academia, radically improving the way scholarly research is managed. The grand vision of Frontiers is a world where all people have an equal opportunity to seek, share and generate knowledge. Frontiers provides immediate and permanent online open access to all its publications, but this alone is not enough to realize our grand goals.

FRONTIERS JOURNAL SERIES

The Frontiers Journal Series is a multi-tier and interdisciplinary set of open-access, online journals, promising a paradigm shift from the current review, selection and dissemination processes in academic publishing.
All Frontiers journals are driven by researchers for researchers; therefore, they constitute a service to the scholarly community. At the same time, the Frontiers Journal Series operates on a revolutionary invention, the tiered publishing system, initially addressing specific communities of scholars, and gradually climbing up to broader public understanding, thus serving the interests of the lay society, too.

DEDICATION TO QUALITY

Each Frontiers article is a landmark of the highest quality, thanks to genuinely collaborative interactions between authors and review editors, who include some of the world's best academicians. Research must be certified by peers before entering a stream of knowledge that may eventually reach the public - and shape society; therefore, Frontiers only applies the most rigorous and unbiased reviews.
Frontiers revolutionizes research publishing by freely delivering the most outstanding research, evaluated with no bias from both the academic and social point of view.
By applying the most advanced information technologies, Frontiers is catapulting scholarly publishing into a new generation.

WHAT ARE FRONTIERS RESEARCH TOPICS?

Frontiers Research Topics are very popular trademarks of the Frontiers Journals Series: they are collections of at least ten articles, all centered on a particular subject. With their unique mix of varied contributions from Original Research to Review Articles, Frontiers Research Topics unify the most influential researchers, the latest key findings and historical advances in a hot research area!
Find out more on how to host your own Frontiers Research Topic or contribute to one as an author by contacting the Frontiers Editorial Office: researchtopics@frontiersin.org

CELLULAR IMAGING AND EMERGING TECHNOLOGIES FOR ADULT NEUROGENESIS RESEARCH

Hosted By
Silvia De Marchis, University of Turin, Italy
Adam C. Puche, University of Maryland, USA

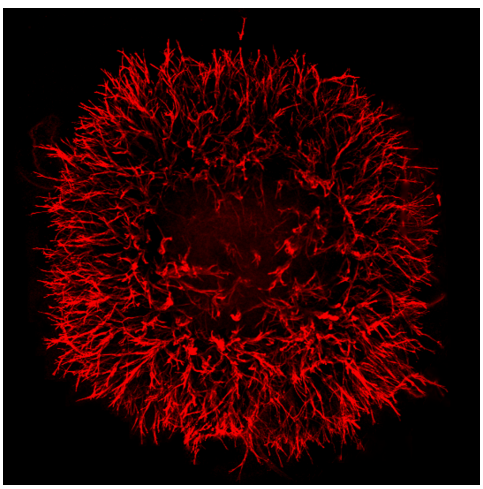

Over the past ten years a variety of cell imaging techniques have been applied to document different aspects of adult neurogenesis in the mammalian brain. Ranging from identification of stem/progenitor cells in the mature brain to imaging activation of adult generated neurons, cell imaging significantly contributed in the understanding of mechanisms and functions of adult neurogenesis. The idea for this special issue is to collect reviews covering the most recent developments in imaging strategies for adult neurogenesis research and to outline new challenges including their applicability to clinical neuroscience. New data papers could also be considered.

Table of Contents

frontiers in
NEUROSCIENCE

EDITORIAL
published: 03 April 2012
doi: 10.3389/fnins.2012.00041

Cellular imaging and emerging technologies for adult neurogenesis research

Silvia De Marchis[1,2]* and Adam C. Puche[3]

[1] *Department of Life Sciences and Systems Biology, University of Turin, Torino, Italy*
[2] *Neuroscience Institute Cavalieri Ottolenghi, NICO, Italy*
[3] *Department Anatomy and Neurobiology, University of Maryland School of Medicine, Baltimore, MD, USA*
**Correspondence: silvia.demarchis@unito.it*

The first report on the generation of new neurons in the adult mammalian brain occurred in the early 1960s, however, nearly 40 years passed before the scientific community generally recognized the existence of adult mammalian neurogenesis. Development of new technologies that facilitate the identification of newborn neurons in the early 1990s has been central to expanding our understanding of adult neurogenesis as a process influencing mammalian brain plasticity. Subsequently, the field of adult neurogenesis progressed tremendously thanks to continuous technical advances allowing *in vivo* and *in vitro* manipulations of adult neural progenitors. Today, a core understanding of various aspects of adult neurogenesis has emerged, including neural progenitor proliferation and fate-specification, and the migration, maturation, and synaptic integration of newborn neurons into functional circuits. However, numerous questions remain open. This research topic issue gathers a series of articles dedicated to major methodological advancements that have significantly contributed to progress in the understanding of adult neurogenesis in the mammalian brain. It includes six review articles that give a critical update of current approaches, outlining their strengths as well as their limitations, and the need of further improvement in technological tools to address specific key issues. Four methods articles dealing with new *in vitro*, *in vivo*, or *ex vivo* approaches to study adult neurogenesis together with one original research article are included.

In vitro assays are key tools for deciphering the cellular and molecular mechanisms of adult neurogenesis. Generally, adult neural precursor cells can be expanded *in vitro* using two different culture methodologies: neurospheres, or adherent monolayer cultures. Babu et al. (2011) present a detailed protocol for isolation and enrichment of neural precursor cells from mouse adult hippocampal neurons. They highlight potential modifications to the protocol useful for isolating and expanding precursor cells from other brain regions.

Newly generated neurons *in vivo* can be identified and/or manipulated by various approaches, such as the incorporation of nucleotide analogs, retrovirus-mediated gene transfer, and genetic methods using transgenic mice. Among nucleotide analog methods, bromodeoxyuridine (BrdU) has been the marker of choice in recent years. BrdU labeling of dividing cells allows various types of analysis including birth-dating, cell cycle analysis, and evaluation of survival of newly generated cells following different experimental paradigms. Sultan et al. (2011) present original data obtained by coupling BrdU and activated caspase-3 labeling to cellular mapping. They analyzed the number, spatial distribution, and apoptosis of newborn cells in the granule cell layer of the olfactory bulb following olfactory conditioning paradigms. This revealed a region-specific reduction in newborn cell death that correlates with the time point at which animals acquired the task. However, a key limitation of the BrdU method is its ability to recognize only a single pool of BrdU-positive cells at one time in the same animal. Llorens-Martín and Trejo (2011) describe the recent development of multiple birth-dating analyses involving the injection of different thymidine analogs (i.e., IdU and CldU) that can be unequivocally distinguished using specific antibodies. This method allows two to three cell subpopulations of different ages to be labeled in the same animal. Focusing on the hippocampus, the authors describe the main results obtained by this technique, outlining some of the key applications as well as the main concerns associated with multi-dating approaches.

Recent developments in genetic methods to identify and manipulate newborn neurons are invaluable tools to progress in the study of adult neurogenesis. Imayoshi et al. (2011) specifically discuss this topic describing the application of site-specific recombinases and the Tet inducible system in combination with transgenic or gene targeting strategy. They present several genetic models to suppress adult neurogenesis. An alternative method to deplete adult generated neurons is described in the article by Tan et al. (2011) that give technical details and results obtained by image-guided irradiation at different doses and survival time. Among the additional manipulation possibilities Imayoshi et al. (2011) also discuss the need to develop new genetic techniques to effectively increase neurogenesis in brain regions that are normally non-neurogenic. In a further refinement of genetic approaches, the review by Arenkiel (2011) describes approaches to reveal connectivity of newborn neurons in the adult brain, and to manipulate cell and circuit activity. He summarizes the current viral tracing methods, heterologous receptor expression systems, and optogenetic technologies that hold promise toward elucidating the wiring and circuit properties of adult-born neurons.

Two method papers detail new approaches to analyze integration of adult-born neurons relaying on immunohistochemical detection of endogenous markers. Rosenzweig and Wojtowicz (2011) describe the development of a method for *ex vivo* analysis of dendritic growth in immature adult-born hippocampal granule neurons. The method is based on laminar quantification of cell bodies, primary, secondary, and tertiary dendrites separately and independently from each other. The data demonstrate the suitability of this technique for analysis of dendritic growth and complexity comparing different experimental conditions. Luzzati et al. (2011) developed a new procedure suitable to analyze neurogenesis in parenchymal neurogenic niches, which represents a reliable alternative to the whole mount approaches to analyze cyto-architectural features of

adult germinative niche. The method, which is based on existing freeware software, combines confocal laser scanning microscopy and serial section reconstruction in order to span large volumes of brain tissue at cellular resolution. An example is described by investigating the morphology and spatial organization of a group of doublecortin-positive neuroblasts located in the lateral striatum of the late post-natal guinea pig.

The latest progress toward *in vivo* imaging of neurogenesis in animal models are discussed in the reviews by James et al. (2011) and Couillard-Despres et al. (2011). The first review centers on quantitative multi-photon microscopy applied to the dynamic study of SVZ-derived neuroblast migration in acute slices. In this paper James et al. (2011) present a brief overview of SVZ–neuroblast time-lapse imaging studies and the current knowledge of cellular patterns of SVZ–neuroblast migration, highlighting putative underlying regulatory mechanisms. They give technical useful suggestions for setting up a two-photon microscope imaging system and identifying several unsolved questions about SVZ–neuroblast migration. These questions might be addressed with current or emerging strategies to further harness the deep potential of two-photon microscopy.

Couillard-Despres et al. (2011) present a comprehensive review on *in vivo* monitoring of adult neurogenesis describing the use of magnetic resonance imaging (MRI), positron emission tomography (PET), and optical imaging with fluorescent or bioluminescent reporters. They compare the different approaches and outline one major challenge in the achievement of specificity and detection sensitivity for direct (e.g., iron oxide particles, [18F]-FLT) and indirect (i.e., the use of reporter-genes) labeling. The authors observe that, although preclinical settings in animal models offer the possibility to use transgenic reporter systems, the development of these imaging techniques to the study of adult neurogenesis in humans remains the ultimate goal. Studying human is further highlighted in the paper by Sierra et al. (2011). They detail the first data on adult human neurogenesis starting from methodologies directly imported from the rodent research. The authors describe new technologies specifically developed for the detection and quantification of neural stem cells in the living human brain. These technologies rely on the use of MRI, which is available in hospitals worldwide, and hold the potential to test the contribution of adult human neurogenesis to brain function in both health and disease.

REFERENCES

Arenkiel, B. R. (2011). Genetic approaches to reveal the connectivity of adult-born neurons. *Front. Neurosci.* 5:48. doi: 10.3389/fnins.2011.00048

Babu, H., Claasen, J.-H., Kannan, S., Rünker, A. E., Palmer, T., and Kempermann, G. (2011). A protocol for isolation and enriched monolayer cultivation of neural precursor cells from mouse dentate gyrus. *Front. Neurosci.* 5:89. doi: 10.3389/fnins.2011.00089

Couillard-Despres, S., Vreys, R., Aigner, L., and Van der Linden, A. (2011). In vivo monitoring of adult neurogenesis in health and disease. *Front. Neurosci.* 5:67. doi: 10.3389/fnins.2011.00067

Imayoshi, I., Sakamoto, M., and Kageyama, R. (2011). Genetic methods to identify and manipulate newly born neurons in the adult brain. *Front. Neurosci.* 5:64. doi: 10.3389/fnins.2011.00064

James, R., Kim, Y., Hockberger, P. E., and Szele, F. G. (2011). Subventricular zone cell migration: lessons from quantitative two-photon microscopy. *Front. Neurosci.* 5:30. doi: 10.3389/fnins.2011.00030

Llorens-Martín, M., and Trejo, J. L. (2011). Multiple birthdating analyses in adult neurogenesis: a line-up of the usual suspects. *Front. Neurosci.* 5:76. doi: 10.3389/fnins.2011.00076

Luzzati, F., Fasolo, A., and Peretto, P. (2011). Combining confocal laser scanning microscopy with serial section reconstruction in the study of adult neurogenesis. *Front. Neurosci.* 5:70. doi: 10.3389/fnins.2011.00070

Rosenzweig, S., and Wojtowicz, J. M. (2011). Analyzing dendritic growth in a population of immature neurons in the adult dentate gyrus using laminar quantification of disjointed dendrites. *Front. Neurosci.* 5:34. doi: 10.3389/fnins.2011.00034

Sierra, A., Encinas, J. M., and Maletic-Savatic, M. (2011). Adult human neurogenesis: from microscopy to magnetic resonance imaging. *Front. Neurosci.* 5:47. doi: 10.3389/fnins.2011.00047

Sultan, S., Lefort, J. M., Sacquet, J., Mandairon, N., and Didier, A. (2011). Acquisition of an olfactory associative task triggers a regionalized down-regulation of adult born neuron cell death. *Front. Neurosci.* 5:52. doi: 10.3389/fnins.2011.00052

Tan, Y.-F., Rosenzweig, S., Jaffray, D., and Wojtowicz, J. M. (2011). Depletion of new neurons by image guided irradiation. *Front. Neurosci.* 5:59. doi: 10.3389/fnins.2011.00059

Received: 24 February 2012; accepted: 14 March 2012; published online: 03 April 2012.

*Citation: De Marchis S and Puche AC (2012) Cellular imaging and emerging technologies for adult neurogenesis research. Front. Neurosci. **6**:41. doi: 10.3389/fnins.2012.00041*

This article was submitted to Frontiers in Neurogenesis, a specialty of Frontiers in Neuroscience.

frontiers in
NEUROSCIENCE

METHODS ARTICLE
published: 14 July 2011
doi: 10.3389/fnins.2011.00089

A protocol for isolation and enriched monolayer cultivation of neural precursor cells from mouse dentate gyrus

Harish Babu[1†], Jan-Hendrik Claasen[2,3,4†], Suresh Kannan[2], Annette E. Rünker[2], Theo Palmer[1] and Gerd Kempermann[2,3]*

[1] *Institute for Stem Cell Biology and Regenerative Medicine, Stanford University, Stanford, CA, USA*
[2] *CRTD, Center for Regenerative Therapies Dresden, DFG-Research Center for Regenerative Therapies Dresden, Dresden, Germany*
[3] *DZNE, German Center for Neurodegenerative Diseases, Dresden, Germany*
[4] *Department of Neurology, Medizinische Fakultät Carl Gustav Carus, Technische Universität Dresden, Dresden, Germany*

Edited by:
Silvia De Marchis, University of Turin, Italy

Reviewed by:
Silvia De Marchis, University of Turin, Italy
D. Chichung Lie, Helmholtz Zentrum Munchen German Research Center for Environmental Health, Germany

***Correspondence:**
Gerd Kempermann, DFG Research Center for Regenerative Therapies Dresden, Center for Regenerative Therapies Dresden, Tatzberg 47–49, 01307 Dresden, Germany.
e-mail: gerd.kempermann@crt-dresden.de

†Harish Babu and Jan-Hendrik Claasen have contributed equally to this work.

In vitro assays are valuable tools to study the characteristics of adult neural precursor cells under controlled conditions with a defined set of parameters. We here present a detailed protocol based on our previous original publication (Babu et al., 2007) to isolate neural precursor cells from the hippocampus of adult mice and maintain and propagate them as adherent monolayer cultures. The strategy is based on the use of Percoll density gradient centrifugation to enrich precursor cells from the micro-dissected dentate gyrus. Based on the expression of Nestin and Sox2, a culture-purity of more than 98% can be achieved. The cultures are expanded under serum-free conditions in Neurobasal A medium with addition of the mitogens Epidermal growth factor and Fibroblast growth factor 2 as well as the supplements Glutamax-1 and B27. Under differentiation conditions, the precursor cells reliably generate approximately 30% neurons with appropriate morphological, molecular, and electrophysiological characteristics that might reflect granule cell properties as their *in vivo* counterpart. We also highlight potential modifications to the protocol.

Keywords: hippocampus, progenitor cell, precursor cell, adult neurogenesis, *in vitro*

INTRODUCTION

In vitro cultures of adult hippocampal neural precursor cells and their differentiation into granule cell-like neurons is a key tool for deciphering the cellular and molecular mechanisms of adult neurogenesis. The sequence of adult neural precursor cell proliferation, neuronal differentiation, and subsequent integration into pre-existing neuronal circuitries occurs in the mature mammalian central nervous system throughout life (Kuhn et al., 1996; Ben Abdallah et al., 2010; Knoth et al., 2010).

Adult neural precursor cells reside in two distinct permissive microenvironments (neurogenic niches), the subventricular zone lining the lateral ventricle's wall and the subgranular zone of the hippocampal dentate gyrus (Reynolds and Weiss, 1992; Palmer et al., 1995). Adult neurogenesis represents a highly complex interaction among the many cellular and molecular components of the unique niche with the genetic setting of the precursor cells. On one hand, *in vitro* studies of neural precursor cells allow analyzing precursor cells independently of niche signals from their former neighboring cells. On the other hand, the culture conditions have to replace the niche at least to the degree required to maintain the cells. It does not pose considerable problems to extract neural precursor cells and bring them into culture, but it is difficult to maintain and expand them in a way preserving their intrinsic properties and allow differentiation into defined cellular phenotypes.

Generally, adult neural precursor cells can be expanded *in vitro* using two different culture forms: as neurospheres, non-adherent spherical clusters of cells, or as adherent monolayer cultures.

Neurospheres have several undisputed advantages, most notably their stunning ease of use. The cytoarchitecture within the spheres is suggested to provide a microenvironment that might be advantageous for the precursor cells to survive in non-physiological conditions *in vitro* (Bez et al., 2003). However this cellular organization is disadvantageous with respect to *in vitro* expansion of the "stem cells." Precursor cells inside the neurosphere have the tendency to differentiate resulting in increasing levels of cellular heterogeneity. With growing size neurospheres contain a more heterogeneous population of precursors with an external rim of rapidly dividing precursor cells and a core of differentiated postmitotic cells (Reynolds and Rietze, 2005) making frequent sphere dissociation inevitable. A reduced diffusion of growth factors into the sphere and a direct influence of already differentiated cells on the undifferentiated progeny may contribute to this layering effect. Other issues are the low efficiency of secondary sphere formation from dissociated single cells, and a tendency of floating cells to aggregate, making single-cell clonal analyses difficult to interpret. These and other caveats have been discussed in several critical comments and original publications (Jensen and Parmar, 2006; Singec et al., 2006; Jessberger et al., 2007; Marshall et al., 2007). Consequently, important modifications to the protocol have been suggested (Reynolds and Rietze, 2005; Rietze and Reynolds, 2006). Regardless, this culture form does have utility and has been the method of choice for multiple research projects including a side-by-side analysis of hippocampal cultures from rats and mice (Ray and Gage, 2006). For example, neurospheres might be rather faithful *in vitro* representations of the situation in the neurogenic niche and allowing to

study the interaction of different cell types during differentiation (Imbeault et al., 2009). The point is not that neurospheres are *per se* inferior to monolayers as precursor cell model but that both have their individual pros and cons and that for certain questions monolayers are clearly preferable.

Adherent monolayer cultures circumvent some of the problems associated with neurospheres because they represent a more homogeneous undifferentiated population of precursor cells. Cells are uniformly exposed to growth factors in culture medium that supports expansion by symmetrical cell division and inhibits spontaneous differentiation, a finding that was described for neural stem cells derived from pluripotent mouse embryonic stem (ES) cells and cortical neural stem cell lines from mouse fetuses (E16.5) by Conti and colleagues in 2005 (Conti and Cattaneo, 2005).

A second advantage of the monolayer culture is that cells can be directly monitored and investigated. The arrangement in one single layer facilitates appreciation of the morphology and size of the individual cell and the change over time, e.g., with videomicroscopy. This aspect becomes central in functional assays, e.g., based on conditional luciferase expression. The opportunity to monitor the appearance of undifferentiated and unimpaired cells is also important in order to choose comparable vital cultures for experiments. In contrast, the densely packed cellular clusters of neurospheres limit the experimental manipulation and analysis of individual cells. It needs to be noted, however, that *in vivo* precursor cells are never isolated and without contact to other cells. The situation in the culture dish is thus highly artificial and represents a highly reductionist setting. The advantages are paid for with limitations that require critical judgment of all results obtained with such model.

Despite the fact that the process of adult hippocampal neurogenesis has been found in almost all mammals studied including rats (Cameron et al., 1993), monkeys (Kornack and Rakic, 1999), humans (Eriksson et al., 1998), the vast majority of studies are done in mice. The first protocol to instruct the generation of a serum-free monolayer culture of neural precursor cells from the micro-dissected mouse dentate gyrus was developed in our laboratory by Babu et al. (2007), a method that was based on monolayer cultures originally described for rat hippocampal precursor cells (Palmer et al., 1995, 1997, 1999). Using micro-dissection and enrichment protocols, we could show that precursor cells from the mouse dentate gyrus were self-renewing and that upon differentiation their progeny developed into neurons with properties of hippocampal granule cells (Babu et al., 2007).

Although highly artificial, monolayer culture systems preserve the criteria of "stemness" in these cells. This is a virtually unlimited capacity to replicate (self-renewal) and the ability to generate the three principal cell types of the nervous system (multipotency), including neurons as indicated by immunocytochemistry and electrophysiology. The monolayer method has proven useful to study intrinsic regulatory mechanisms of neural precursor cells and details are provided here on the conditions that are required to establish a monolayer cell culture for long-term expansion. However, prolonged expansion of neural precursor cells might carry the risk of genomic instability and subsequent chromosomal aberration. We did not detect overt changes in our cultures during long-term passage with regard to morphology, self-renewal, or molecular profiling. This observation is in accordance with Foroni et al. (2007) who did not detect any cellular transformation or genetic instability, when propagating subventricular zone adult neural precursor for up to 1 year. Nevertheless, if late passages are to be used, karyotyping might be advisable.

Although the methods described here depict the direct isolation of neural stem and progenitor cells from the dentate gyrus and their subsequent cultivation, we found these methods also useful to transfer neurospheres to monolayer culture and for isolating and expanding precursor cells from other brain regions. The here-described protocol is essentially based on our original publication from 2007, but in addition to the original method considers a dissection method for dentate gyrus tissue that does not require micro-dissections from vibratome slices (compare Hagihara et al., 2009). The only major change from the original publication consists of the improved cell separation with one single Percoll gradient centrifugation step. A small change is the use of medium instead of artificial CSF to store cells during the preparation, because artificial CSF has no advantages.

For more than 3 years our protocol has been successfully used in a wide range of our research projects and has been taught to cooperating research groups and visiting scientists. The here-described protocol was used in recent publications by us (Babu et al., 2009) and our collaborators (Ramirez-Rodriguez et al., 2009), as well as independent researchers in original (Wong Po Foo et al., 2009) or slightly modified form (Boku et al., 2009; Liu et al., 2010; Luo et al., 2010a,b).

OVERVIEW OF THE PROCEDURE

Our neural precursor cell extraction protocol is based on Percoll gradient centrifugation that enables an enrichment of precursor cells for optimal culture conditions (Palmer et al., 1999).

The workflow is depicted in **Figure 1**. After separation of the hippocampus from the rest of the brain, the dentate gyrus is further isolated by micro-dissection from the adjacent walls of the lateral ventricles and *cornu ammonis* of the hippocampus to avoid a commixture of hippocampal neural precursor cells with other precursor cell populations. The excised tissue containing the neurogenic subgranular zone is then further dissociated into a single-cell suspension using an enzymatic solution supported by mechanical trituration steps with fire-polished Pasteur pipettes. In the ensuing step, neural precursor cells are separated from differentiated cells, myelin, and extracellular matrix using density gradient separation by a centrifugation step with 22% Percoll. Pelleted cells are separated from supernatant, washed, resuspended in chemically defined culture medium (Neurobasal A with supplements B27 and Glutamax-1 and growth factors EGF and FGF2) and plated on coated culture dishes. Two days after isolation neural precursor cells that have not yet attached to the surface are collected, centrifuged, and replated into the same culture dish with fresh medium. This enrichment step is necessary to ensure an optimal density for further cell expansion. From day 4 after cell extraction onwards, 75% of the culture medium is substituted every second day. In about 9–12 days 70–80% of the culture dish surface is populated and the culture is ready for the first passage.

The isolated and expanded cells display the typical morphology of adult neural precursor cells **Figures 2A–C** and express the typical neural precursor cell markers Nestin **Figure 3C**, or vimentin **Figure 3D.** Many cells also express the radial glia marker BLBP **Figure 3B** or transcription factor Id1 involved in self-renewal **Figure 3F.** In contrast, only few cells appear further committed to the neuronal lineage (expressing βIII-tubulin **Figure 3E**), and there are no identifiable

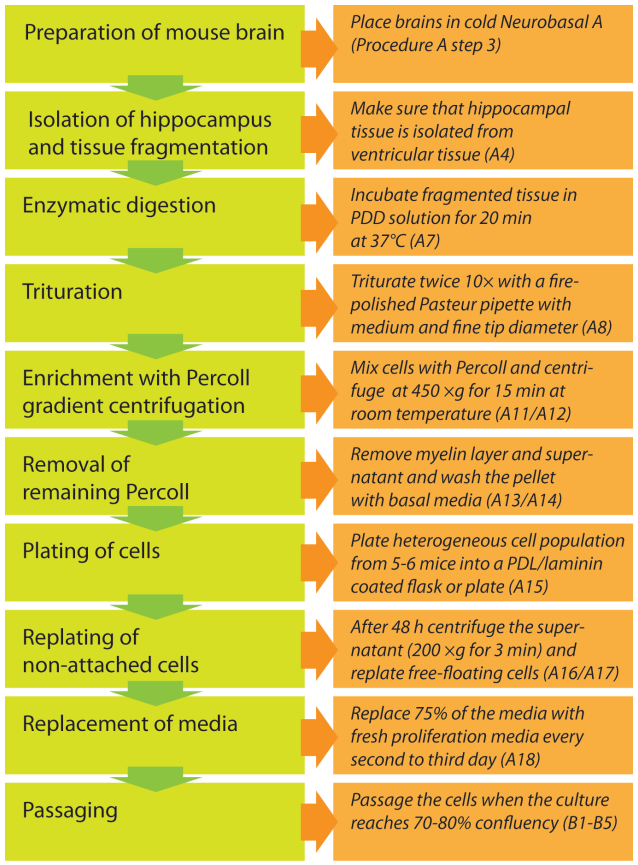

FIGURE 1 | Workflow diagram for the experimental procedure.

mature astrocytes (expressing S100β **Figure 3F**). Virtually all cells express Ki67, a cellular marker for proliferation **Figure 3A**. Similarly, incubation with BrdU, a thymidine analog that is incorporated during DNA synthesis, labels almost all cells, indicating robust proliferation of the cultured neural precursor cells (not shown here, but see figures in Babu et al., 2007). Under differentiation conditions, neural precursor cells gradually acquire the morphology of postmitotic neurons and astrocytes (**Figures2 D–F**).

MATERIAL

ANIMALS

- C57BL6/J (The Jackson Laboratory) female and/or male mice with an age of 7–9 weeks are used. Five to six mice of this strain are sufficient to establish a primary adult neural precursor cell culture. All animals are kept under standard housing conditions with a 12-h light/dark cycle and free access to food and water.

IMPORTANT! Experiments involving live animals must conform to experimenter's national and institutional rules and regulation.

3.2 REAGENTS

Culture medium

- Neurobasal A (Gibco, cat. no. 10888) or DMEM/F12 (Gibco, cat. no. 31330) for culture dish coating and cell separation procedure
- B27 Supplement (Gibco, cat. no. 17504)
- Glutamax-1 Supplement (Gibco, cat. no. 35050)
- Recombinant human Fibroblast growth factor 2 (FGF2; Peprotech, cat. no. 100-18B-B)

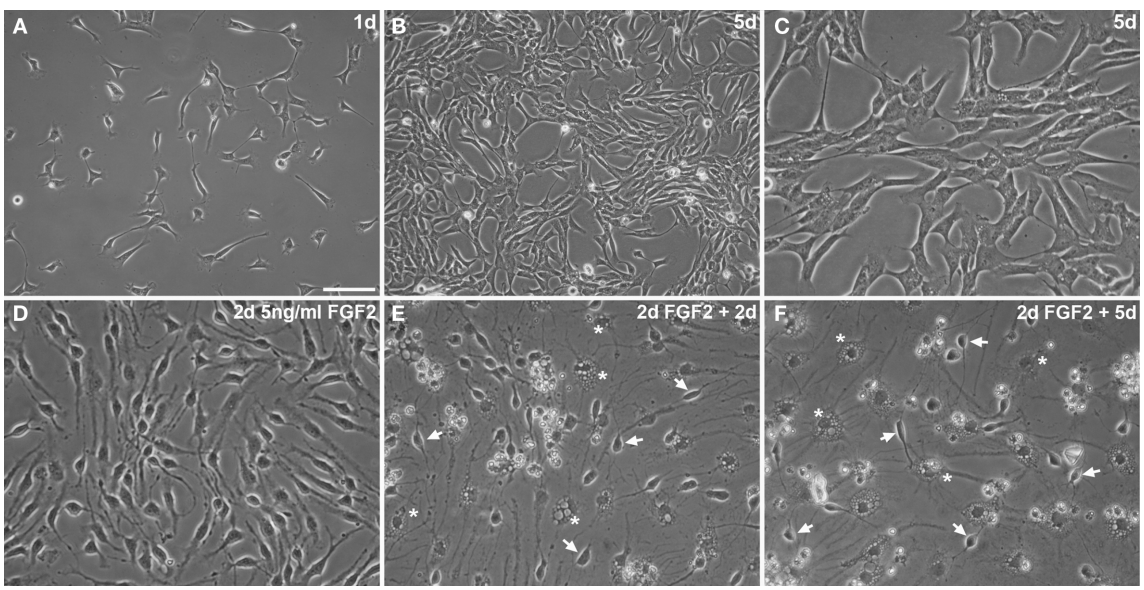

FIGURE 2 | Highly enriched neural precursor cells propagated as adherent monolayer cultures (A–C). Adherent precursor cells cultures under routine proliferation conditions 1 day **(A)** and 5 days after seeding [**(B)** about 80% confluent; higher magnification in **(C)**]. **(D–F)** Upon differentiation with 2 days of 5 ng/ml FGF2 **(D)** and subsequent complete growth factor depletion **(E,F)**, neural precursor cells change their morphology showing a progressively postmitotic and mature appearance of neuronal (arrows) and glial (asterisks) cells. Scale bar in **(A)**: 100 μm for **(A,B)**; 50 μm for **(C–F)**.

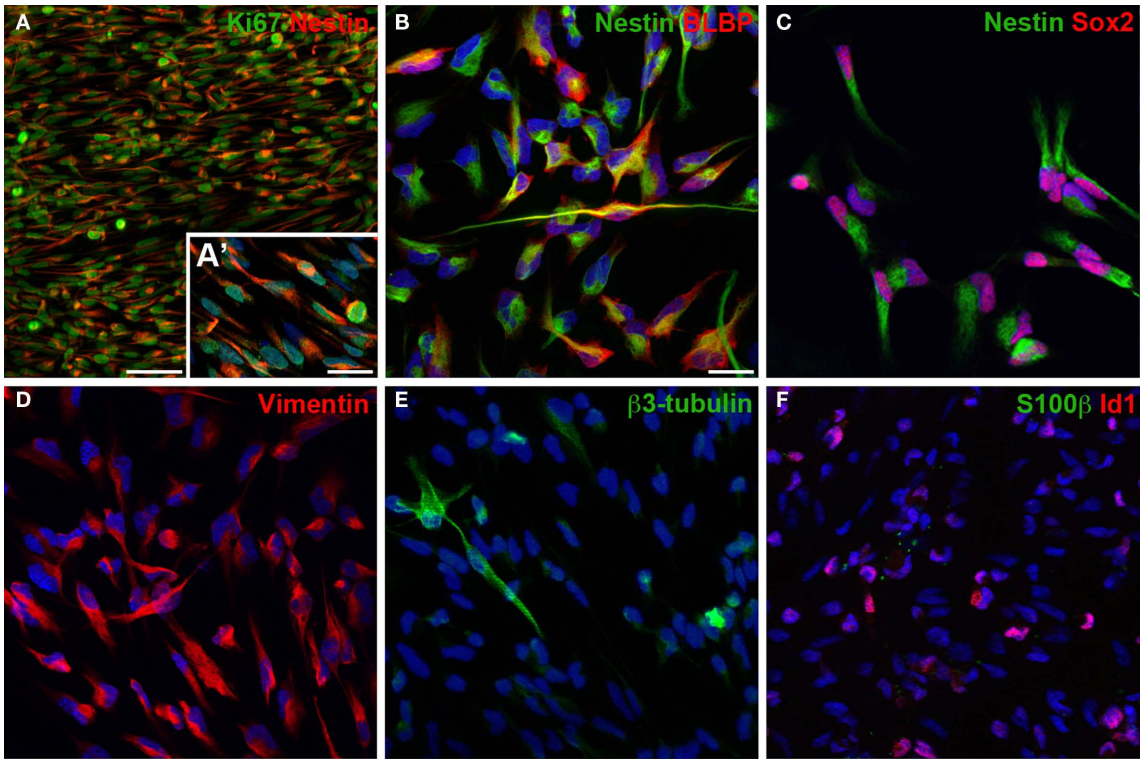

FIGURE 3 | In cultures of dentate gyrus neural precursor cells virtually all cells express cellular marker for proliferation, Ki67 (A), and for progenitor cells of the nervous system, such as Nestin (A–C), Sox2 (C) or vimentin (D). Many cells express also the radial glia marker BLBP **(B)** and Id1 **(F)**, a dominant-negative bHLH transcriptional regulator expressed in a fraction of adult neural stem cells important for their self-renewal capacity. Only few cells express β3-tubulin **(E)** indicating neuronally committed cells. No cells were positive for S100β **(F)**, a marker that labels mature astrocytes. Cells were grown until about 80% confluent (3–5 days) before fixing and staining. Blue stain in **(A–F)** is the nucleic dye DAPI. Scale bar in **(A)**: 50 μm, in **(A')** and **(B)** for **(A'–F)**: 20 μm.

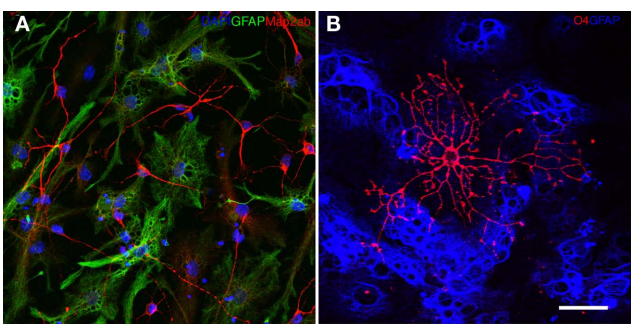

FIGURE 4 | (A) Neural precursor cells upon 6 days of differentiation generate Map2ab (red) positive neurons and GFAP positive (green) glial cells. The nuclei are stained with DAPI (blue). **(B)** Ten days of differentiation generates O4 (red) positive oligodendrocytes. GFAP positive glial cells are depicted in blue.

- Recombinant human Epidermal growth factor (EGF; Peprotech, cat. no. 100-15)
- Recombinant human Brain Derived Neurotrophic Factor (BDNF; Peprotech, cat. no. 450-02)
- Bovine serum albumin (BSA; Sigma, cat. no. A2153)
- D-Glucose (Sigma, cat. no. G7021)
- Retinoic acid (Sigma, cat. no. R2625)

Cell detachment
- Accutase (PAA, cat. no. L11-007)
- Ovomucoid trypsin inhibitor (Worthington, cat. no. 3085)
- Trypsin EDTA 10× (Gibco, cat. no. 15400054)

Cell extraction
- Papain (Worthington, cat. no. 3126)
- Dispase (Roche, cat. no. 10-165-859-001)
- DNase (Worthington, cat. no. 2139)
- Percoll (GE Healthcare, cat. no. 17-0891-01)
- PBS 10× (Gibco, cat. no. 70011)

Coating
- Laminin (Roche, cat. no. 11-243-217-001)
- Poly-D-Lysine (PDL; Sigma, cat. no. P1024)
- Ethanol 70% vol/vol
- PBS (Gibco, cat. no. 10010-023)
- H_2SO_4 (EMD, cat. no. SX1244-6)
- ddH_2O

Cell banking
- Dimethyl sulfoxide (DMSO; Sigma Aldrich, cat. no. D8418)

Immunocytochemistry

- Paraformaldehyde (PFA; Electron Microscopy Sciences, cat. no. 19210)
- Triton-X100 (Sigma, cat. no. T8787)
- Normal donkey serum (Jackson Immunoresearch, cat. no. 017-000-121)
- Hoechst 33258 (Gibco, cat. no. H3569)
- Mouse anti-Map2ab antibody (Sigma, cat. no. M1406; 1:500)
- Rabbit anti-GFAP antibody (Dako, cat. no. Z0334; 1:500)
- Mouse anti-O4 antibody (R&D Systems, cat. no. MAB1326; 1:100)
- Mouse anti-Nestin antibody (BD Pharmingen, cat. no. 611658; 1:200)
- Rabbit anti-Sox2 antibody (Chemicon, cat. no. AB5603; 1:500)
- Rabbit anti-Ki67 antibody (Novocastra, cat. no. NCL-Ki67p; 1:400)
- Rabbit anti-BLBP antibody (Abcam, cat. no. ab32423; 1:400)
- Goat anti-Vimentin antibody (Sigma, cat. no. V4630; 1:500)
- Rabbit anti-Id1 antibody (Biocheck, cat. no. BCH-1/37-2; 1:100)
- Mouse anti-β3-tubulin antibody (Promega, cat. no. G712A; 1:1000)
- Rabbit anti-S100b antibody (Swant, cat. no. 37A; 1:1000)

EQUIPMENT

- Inverted microscope
- Dissecting microscope
- Water bath (37°C)
- Horizontal laminar flow hood for sterile cell culture work
- Dissection instruments: micro-dissection scissors (FST, cat. no. 15010-11 or cat. no. 15000-10), fine forceps (FST, cat. no. 11251-20), spatula (FST, cat. no. 10093-13), fine scissors (FST, cat. no. 14090-09), surgical scissors (FST, cat. no. 14010-15), disposable scalpel
- Standard cell culture incubator (37°C, 5% CO_2, ≥95% humidity)
- Table top centrifuge with rotor capacity for 15 ml tubes
- Hemocytometer for cell counting
- Filter 0.22 μm (Millipore, cat. no. SE1M179M6)
- Polystyrene cell culture dishes: flasks with 0.2 μm vented plug seal, petri dishes, multiwell plates (BD Falcon)
- Pipettes, tubes, tips (BD Falcon)
- Cryogenic vial 1.2 ml (Corning, cat. no. 430487)
- Cryo 1°C freezing container (Nalgene, cat. no. 5100-0001)
- Coverglass slips 12 mm (Fisher, cat. no. 12-545-82)
- Pasteur pipettes (Fisher, cat. no. FB50623)
- Strainer 40 μm (BD Falcon, cat. no. 352340)

SET-UP

MATERIAL

Maintain strict sterile tissue culture practice!

BSA 0.1% wt/vol Dissolve BSA to a final concentration of 0.1% wt/vol in PBS and sterilize using a 0.22-μm filter.

Epidermal growth factor (EGF stock; 100 μg/ml) Dissolve EGF to a final concentration of 100 μg/ml in sterile PBS with 0.1% wt/vol BSA.

Fibroblast growth factor 2 (FGF2 stock; 100 μg/ml) Dissolve FGF2 to a final concentration of 100 μg/ml in sterile PBS with 0.1% wt/vol BSA. Store it in aliquots and avoid repeated freeze thaw cycles.

IMPORTANT! Stocks for BDNF, EGF, and FGF2 are stored in aliquots at −20°C for up to 6 months. After thawing, aliquots are kept at 4°C and used for maximal 2 weeks.

Basal growth medium Combine Neurobasal A (97 ml), B27 Supplement (2 ml), and Glutamax-1 (1 ml). This mixture is stable for 2 weeks at 4°C. We found that B27 supplemented with Vitamin A leads to higher cell viability than B27 without Vitamin A. Hence we recommend the use of B27 supplement including Vitamin A in standard media formulations. We have empirically determined that antibiotic-free medium is better at giving consistent results in our assays. To prevent the effect of penicillin and streptomycin on neural precursor cells beyond their traditional role as bactericidal agents we avoid using antibiotics in our culture medium. However using antibiotic-free media increases the risk of contaminations. It is up to the experimenter to calculate this risk.

Proliferation medium Add FGF2 (final concentration of 20 ng/ml) and EGF (final concentration of 20 ng/ml) to the basal growth medium just before use. Repeated freezing and thawing of the medium or growth factors can lead to a reduced effectiveness of the components. This severely effects the efficient derivation of differentiated cells from neural precursor cells. Cell lines can also be maintained with 10 ng/ml FGF2 and 10 ng/ml EGF in order to reduce consumption of the expensive growth factors. The activity of recombinant FGF2 can vary from lot to lot and a titration of FGF2 for peak mitogenesis on previously established cultures can be useful for determining the minimum dose required to maintain cells in an undifferentiated and rapidly dividing state.

IMPORTANT! Prolonged storage of medium with EGF and FGF2 leads to loss of mitogenic activity of growth factors within the medium. We recommend adding growth factors to the medium immediately before use.

Papain, Dispase and DNase mix (PDD) Prepare an enzymatic mixture of Papain (2.5 U/ml), Dispase (1 U/ml), and DNase (250 U/ml) in 100 ml Neurobasal A. Incubate the dilution for 30 min on a shaker at room temperature to get a clear solution. Filter sterilize by passing through a 0.22-μm filter. Freeze as single use aliquots.

Percoll buffer solution (Percoll-PBS) Dilute 9 ml of Percoll stock solution with 1 ml of 10× PBS. This constitutes the 100% Percoll buffer solution.

Glucose 2M Dissolve 36 g of D-Glucose in 100 ml ddH_2O. Filter sterilize the solution with a 0.22-μm filter. This solution can be stored at 4°C for 2 months.

Phosphate buffered saline with Glucose (PBS-G) Add 1.5 ml of 2M Glucose to 100 ml of PBS to get a final concentration of 30 mM Glucose. Warm this solution to 37°C before use. This solution can be preserved at 4°C for 2 months.

Dimethyl sulfoxide (DMSO) 10% vol/vol Add 1 ml of DMSO to 9 ml of cold proliferation medium. Prepare fresh each time before use. Mix DMSO well with the medium. DMSO is heavier and thus settles down if not mixed appropriately.

IMPORTANT! DMSO is harmful to health and can easily penetrate the skin. Therefore avoid any contact with this substance and wear the appropriate glove type.

Poly-D-Lysine (PDL) stock Prepare a 1000× stock by reconstituting Poly-D-Lysine at 10 mg/ml in ddH_2O. Prepare 500 µl aliquots in Eppendorf tubes and store at −20°C for max. 6–8 months. Tubes once thawed are maintained in 4°C and should not be refrozen.

H_2SO_4 2M Add 5.6 ml of concentrated H_2SO_4 to 44.4 ml of ddH_2O.

EQUIPMENT

Disinfect and clean the coverglass slips by incubating in a rotatory shaker for 2 days in 2M H_2SO_4 followed by multiple rinses in ddH_2O. Thoroughly dry by leaving the coverglass under the laminar flow hood for 1 day.

Fire-polish Pasteur pipettes by exposing the tip of the pipette to flame while rotating the pipette between hands. Round the sharp edges of the tip and prepare medium and fine tip diameters.

Poly-D-Lysine (PDL) coating of tissue culture surfaces Prepare a 10-µg/ml of PDL working solution in ddH_2O. Cover the required surface with this solution. Leave under the laminar flow hood overnight at room temperature. The following day, remove PDL and wash the surface three times with ddH_2O. Leave the surface to dry in the laminar flow hood. The dry coated surface can be stored at room temperature for future use and is stable for up to 6 months.

IMPORTANT! Avoid disinfection procedure of the laminar flow hood with UV-light during the coating process.

Laminin coating of tissue culture surfaces Prepare a working solution of 10 µg/ml of Laminin in Neurobasal A. Add the required amount to cover the PDL-coated surface and leave it in cell culture incubator at 37°C overnight. Use the plate next day for seeding cells. Laminin coated dishes can be stored at −20°C for up to 6 months.

IMPORTANT! Both Laminin and Neurobasal A have to be kept at 4°C when mixing and before adding to the PDL-coated surface. Laminin polymerizes at temperatures higher than 4°C, which would lead to uneven coating.

DETAILED PROTOCOL OF THE PROCEDURE

A. ISOLATION OF NEURAL PRECURSOR CELLS FROM MOUSE DENTATE GYRUS (3–3.5 H)

(1) Euthanize the mice with an appropriate method (e.g., overdose with anesthetics) approved by your institutional and national regulations.

(2) Disinfect head and neck of the mouse with 70% vol/vol ethanol. Decapitate the mouse with surgical scissors. Cut the skin sagittally along the midline till an arbitrary point between the eyes. Expose the skull free of overlying skin and subcutaneous tissue.

(3) Cut the skull mid-sagittally into two halves by cutting along the midline using fine scissors. This is done by incising the skull starting occipitally at the vertebral canal and then going forward toward the olfactory bulbs. The tip of the scissors should be kept close to the skull and away from the brain tissue to avoid damage. Further cross sections are made on either side from the vertebral canal laterally to the external auditory meatus. Reflect the overlying skull and expose the intact brain underneath. Carefully scoop out the brain and separate it from the rest of the calvarium. Place the brain in a 6-cm petri dish with cold Neurobasal A and remove the brains from remaining mice. Change to a clean 6 cm petri dish with fresh cold medium if the dish becomes bloody.

(4) Maintaining sterile working conditions, separate the cerebrum from the cerebellum, remove the meninges from the brain tissue and continue with dentate gyrus dissection:

(i) First option: dentate gyrus dissection from vibratome slices (this method has been used in the original publication Babu et al., 2007):

Section the brains coronally with a vibratome into 300 µm thick slices and collect those containing hippocampal tissue in cold Neurobasal A. Continue with dentate gyrus dissection using fine forceps under a dissecting microscope. Place an incision between the dentate gyrus and the ventricular wall of the lateral ventricle to avoid intermixture with subventricular zone neural precursor cells. As a next step transect along the hippocampal fissure and between the dentate gyrus and the CA3 region to free the dentate gyrus from the hippocampus (illustrated in Babu et al., 2007). Repeat with the remaining slices.

(ii) Second option: dentate gyrus dissection from entire hippocampus (this method is advantageous in our eyes but represents a change from the original publication Babu et al., 2007):

Cut the brain along the longitudinal fissure to divide both hemispheres. Continue the next steps under a dissection microscope. Remove the diencephalon, place the medial side of the hemisphere up, and resect the exposed hippocampus away from the neocortex. With the hippocampus isolated from the rest of the brain, separate the dentate gyrus from the hippocampus. Blood vessels running along the hippocampal fissure can be identified in the majority of animals. Place a longitudinal incision along the hippocampal fissure using these blood vessels as an anatomical landmark and mobilize the dentate gyrus. Free the knee-side of the dentate gyrus with an incision at the septal side of the hippocampal axis and liberate the dentate gyrus from CA1 and the lateral ventricle. Position the last cut almost at the temporal end of the hippocampal fissure and separate the hilar opening from CA3.

Watch the micro-dissection process from entire hippocampus in the movie provided as Supplementary File!

IMPORTANT! The dissection step carries the greatest risk of contamination and is thus ideally done with the microscope placed under a laminar flow hood. With adequate sterile work environment, however, these steps can also be performed outside the laminar flow hood. Dentate gyrus dissection from entire hippocampus demands greater technical skills compared to the technique using vibratome slices. However when performed accurately this technique is less time consuming and thus warrants a higher cell yield.

(5) Place the tissue in a 15-ml tube with cold Neurobasal A while dissecting the other animals. Avoid contact of the dissected tissue with blood-containing medium to prevent contamination with hematopoetic cells.

(6) With the pooled tissue in Neurobasal A accomplish the next steps in a sterile laminar flow hood. Chop the obtained tissue with a scalpel into small fragments.

(7) Incubate the dissected tissue in pre-warmed PDD enzyme mix for 20 min at 37°C. Add 1 ml of PDD per animal. The proteolytic enzymes digest the extracellular matrix and the intercellular adhesion proteins during the incubation step. The tissue still appears in one piece.

IMPORTANT! Do not use serum-containing medium to inhibit PDD as the proliferative ability of the recovered neural precursor cells significantly decreases in the presence of serum.

(8) Triturate carefully to obtain a single-cell suspension. Triturate first for 10 times with medium sized tip and then 10 times with fine sized tip fire-polished Pasteur pipettes.

IMPORTANT! Avoid frothing and bubbling. Entrapment of cells in air bubbles impairs their viability. Triturating with fire-polished Pasteur pipettes gently breaks the tissue and avoids sticking of cells to the tip.

(9) Plate the heterogeneous cell population from five to six mice in 1 ml proliferation medium into a PDL/Laminin coated 24-well plate.

(10) Add 3.9 ml of Neurobasal A equilibrated at room temperature to the recovered cell pellet.

(11) Add 1.1 ml of the Percoll buffer solution (Percoll-PBS) to the cell suspension for a final concentration of 22% vol/vol Percoll.

IMPORTANT! Make sure that the Percoll is well mixed with the cells and evenly distributed in the tube.

(12) Centrifuge for 15 min in a swinging bucket rotor at 450 × *g* at room temperature.

(13) After centrifugation a cell pellet at the bottom and a milky white layer on top should be visible. The supernatant contains buoyant non-dividing cells (astrocytes, neurons etc.) as well as myelin debris. Carefully discard the supernatant without disturbing the pellet containing the enriched neural precursor cell fraction.

IMPORTANT! Gently remove the supernatant, as the pellet may not be firmly attached to the bottom of the tube. If using vacuum suction, use at low intensity.

(14) Wash the cells three times with Neurobasal A. The medium allows for a better removal of the Percoll.

IMPORTANT! Thorough washing is important to completely remove Percoll. Residual Percoll results in poor attachment and survival of neural precursor cells after plating.

(15) Plate the heterogeneous cell population from five to six mice in 1 ml proliferation medium into a PDL/Laminin coated 24-well plate.

IMPORTANT! Do not let the Laminin coated surface dry between removing the Laminin containing solution and plating the cells. Drying alters the Laminin coating and hinders adhesion of the freshly plated precursor cells to vital extracellular matrix attachment proteins.

(16) Forty-eight hours after the initial isolation of the precursor cells, collect the medium with all floating cells that have not firmly attached to the surface yet.

IMPORTANT! Cover the PDL/Laminin coated surface with proliferation medium to avoid drying.

(17) Centrifuge the cell suspension at 200 × *g* for 3 min at room temperature in a swinging bucket rotor. Discard the supernatant and add fresh proliferation medium. Plate the cells back into the same culture dish. The final volume is about 200–250 μl/cm^2. Add FGF2 and EGF to a final concentration of 20 ng/ml each.

(18) On day 4 after isolation and plating, remove 75% of the medium and replace it with fresh proliferation medium. By now the precursor cells are firmly attached to the surface. To the total volume of the medium (100%) add fresh FGF2 and EGF to attain a final concentration of 20 ng/ml. Change 75% of medium every 2–3 days with fresh medium.

IMPORTANT! Monitor the color of the medium daily. Feed cells as frequently as required to avoid low pH.

(19) About 4–5 days after isolation and plating, the precursor cells will start to populate the tissue culture surface. At about 9–12 days the culture will produce colonies of adherent cells separated by areas devoid of cells. Secondary cultures that are derived from the first passage of the initially isolated cells will show uniform growth without time lag.

IMPORTANT! Do not allow the culture to grow to more than 80% confluence. A fully confluent culture will loose the precursor cell characteristics and undergo crisis with ensuing cell death.

B. PASSAGING (30 MIN)

(1) Discard the medium from the culture dish or flask and rinse once with warm PBS-G.

IMPORTANT! Do not let the cells incubate in PBS-G. Prolonged incubation can lead to cell detachment and thus loss of cells.

(2) For cell detachment we recommend two options:

(i) First option (Accutase):

Flood the surface of adherent neural precursor cells with Accutase. Return the culture back to the 37°C incubator and allow the cells to detach for 3 min. Accutase is a sterile ready-to-use solution especially developed for gentle cell dissociation. Three minutes of incubation is sufficient to detach the cells from the surface.

Immediately stop the digestive activity by diluting Accutase with 10 ml basal medium. Because Accutase digests itself, no additional enzyme inhibitors are required.

(ii) Second option (Trypsin):

Dilute 1 ml of 10× Trypsin EDTA (0.5% vol/vol) with 9 ml Neurobasal A to the final concentration of 0.05% vol/vol Trypsin and evenly cover cells with the solution. Return culture back to 37°C incubator and allow the cells to detach for 1 min.

Add the double amount of Ovomucoid Trypsin inhibitor stock solution directly to the cells to neutralize Trypsin. Gently swirl the culture dish to evenly mix the Trypsin inhibitor with the cell suspension. Avoid triturating the cells at this point or detaching them from the surface with mechanical force.

IMPORTANT! Do not prolong this incubation step beyond 1 min. Trypsin will digest membrane proteins leading to a poor recovery of the cells.

Results at this step are highly dependent on personal experience, skills, and preference. It is recommended that the reader experiments with different protocols to find the optimal conditions.

(3) Collect cells into a 15-ml conical tube and fill up to 10 ml with Neurobasal A. Centrifuge at 200 × *g* for 2 min at room temperature to pellet the dissociated cells.

IMPORTANT! It is essential to free the cells from Accutase and Trypsin. Residual amounts of these substances can interfere with attachment and maintenance of the precursor cells and their subsequent efficient differentiation into neurons and glia cells.

(4) After the final centrifugation step discard the supernatant and add fresh proliferation medium with 20 ng/ml of EGF and FGF2 to the pellet. Count the number of viable cells using a hemocytometer and Trypan blue.
(5) Plate 10^4 cells/cm^2 into culture dishes coated with PDL and Laminin for routine growth and maintenance of neural precursor cells. Disperse the cells evenly to prevent cell clumping and uneven intercellular interactions that may influence growth, proliferation, and preservation of their multipotential characteristics.

C. CRYOPRESERVATION OF NEURAL PRECURSOR CELLS (30 MIN)

(1) Collect the cells by using Accutase or Trypsin as described in **B** steps 1–3.
(2) Resuspend the pellet carefully in cold 10% vol/vol DMSO freezing solution with gentle agitation. Add enough DMSO freezing solution to obtain a final cell suspension of 10^6 cells ml.
(3) Immediately aliquot 500 µl of this cell suspension into 1.2 ml cryogenic vials. Place the vials in the Cryo 1°C freezing container and place it in −80°C for 2 days.
(4) Remove the vials from the −80°C freezer and place them into a liquid nitrogen tank for long-term storage.

D. THAWING FROZEN NEURAL PRECURSOR CELLS (20 MIN)

(1) For thawing frozen neural precursor cells transfer the vial from liquid nitrogen tank immediately into a 37°C water bath. After 1 min remove the vial from the water bath and dilute the content with 9 ml warm basal growth medium in a 15-ml centrifugation tube. Mix well to evenly resuspend the cells.

IMPORTANT! It is important to immediately add the thawn cells to warm medium (37°C) for efficient recovery. In general, mammalian cells are cryo-preserved by slow freezing while recovery of the cells is done by flash thawing at 37°C.

(2) Centrifuge the cell suspension at 200 × *g* for 2 min at room temperature. A pellet of the recovered cells should be visible on the bottom of the tube.
(3) Discard the supernatant and add fresh proliferation medium. Plate the cells on a PDL/Laminin coated culture dish at the appropriate density.
(4) Change medium the next day. Approximately 95% of the cells recover, when the protocol is rigorously followed. The cells can be used for any subsequent experimental assay as desired.

E. DIFFERENTIATION OF ADHERENT MONOLAYER NEURAL PRECURSOR CELLS (6–10 DAYS)

(1) Select flasks or dishes with neural precursor cells that are about 80% confluent. Detach cells with Accutase or Trypsin as indicated in **B** steps 1–4 and count the cells using a hemocytometer and Trypan blue.
(2) Plate 2 × 10^4 cells/cm^2 in proliferation medium onto PDL/Laminin coated 12 mm glass coverslips placed in a 24 multiwell plate. Place the cells in the humidified 37°C cell culture incubator.

IMPORTANT! Make sure that cell density is constant when comparing differentiation experiments. The fraction of neurons decreases with higher cell density suggesting that cell–cell interaction might influence fate programming of the precursor cells.

(3) After 48 h (differentiation day 0) discard the medium leaving the adhered neural precursor cells on the glass coverslips. Do not let dry. Add basal growth medium without growth factors (first option) or 5 ng/ml FGF2 (second option) to the culture and place the cells back into the incubator. At this stage, the cells can be fixed for immunocytochemistry and detection of neural precursor cell markers (e.g., Nestin, Sox2).
(4) Two days later (differentiation day 2) discard half of the medium (first option) or complete medium (second option) from the well and add basal growth medium without growth factors to the cells. Place cells back into the incubator.
(5) After 96 h (differentiation day 4) discard half of the medium and replace with equal amount of basal growth medium without growth factors.
(6) After 6 days from the start of the differentiation (8 days after plating) the cells can be fixed to assess differentiated progenies from the neural precursor cells. Neurons are visualized by immunocytochemistry for microtubule associated protein (Map2ab), astrocytes for glial fibrillary acidic protein (GFAP) and oligodendrocytes for O4.

IMPORTANT! Do not use β3-tubulin as a sole indicator of mature neuronal phenotypes since it can be expressed at the precursor cell stage. Complex neurite arborization and cell morphology are also useful indicators of neuronal differentiation.

(7) Further differentiation can be maintained by replacing 50% of the medium with basal growth medium every second day.

IMPORTANT! The here demonstrated "naïve" differentiation protocol was developed to manipulate as little as possible the intrinsic fate properties of neural precursor cells. Induction of the differentiation process of neural precursor cells *in vitro* by growth factor withdrawal is generally a stressful situation and accompanied by cell loss. We have empirically determined that the extent of cell death can be reduced by gradual reduction of FGF2. However this strategy needs further validation. The fraction of neuronal cells from the differentiating precursor cell pool can be further increased using BDNF (100 ng/ml) and retinoic acid (0.5 µM). Note that no side-by-side comparisons of the different protocols have been published, thus the exact impact of the different procedures on differentiation remains largely undetermined.

F. IMMUNOCYTOCHEMISTRY (2 DAYS)

(1) Remove the medium and fix the cells with 4% paraformaldehyde. Incubate for 20 min at room temperature.
(2) Wash 3× with PBS for 5 min each.
(3) Block non-specific sites by incubating the cells in PBS with 3% vol/vol donkey serum and 0.1% vol/vol Triton-X100 for 30 min at room temperature.

(4) Incubate cells in PBS with 3% vol/vol donkey serum and the appropriate concentration of primary antibody overnight with gentle shaking at 4°C.
(5) The following day remove the antibody mix and wash three times with PBS for 5 min each to remove excess antibody.
(6) After the final wash add donkey secondary antibodies conjugated to fluorophores diluted in PBS with 3% vol/vol donkey serum in appropriate dilution.
(7) Incubate for 1 h at room temperature with gentle shaking.
(8) Remove the secondary antibody and wash twice with PBS for 5 min.
(9) Incubate cells with Hoechst 33258 diluted in PBS (1:3000) for 10 min.
(10) Remove the dye and wash twice with PBS for 10 min.
(11) Mount the cover glass and visualize under the microscope.

TIMING

(A) Dissection and plating of adult dentate gyrus neural precursor cells: 3–3.5 h/12 days
Steps 1–5 Dentate gyrus dissection: 1 h
Steps 6–15 Isolation and plating of neural precursor cells: 2–2.5 h
Steps 16–19 Expansion of neural precursor cell culture: ≈12 days
(B) Passaging and replating of neural precursor cells:
Step 1–5: 30 min
(C) Cryopreservation of cells:
Steps 1–4: 30 min
(D) Thawing of frozen cells:
Steps 1–4: 20 min
(E) Differentiation:
Steps 1–7: 6–10 days
(F) Immunocytochemistry:
Steps 1–11: 2 days

EXPECTED RESULTS

When appropriately cultured, a 75-cm^2 flask that is ~ 80% confluent will contain about 7–8 × 10^6 cells. The typical appearance of adherent neural precursor cells under ideal culture conditions is shown in **Figures 2A–C**. Note that the neural precursor cells are phase bright with two to three processes. Cells in active mitosis are rounded and brighter than cells that are not in mitosis. Precursor cells of the murine dentate gyrus have a cell cycle length of about 20–21 h in culture. If maintained as suggested, the neural precursor cells can be passaged for extended periods (≈25 passages) without loss of multipotency and other precursor cell characteristics. However, extended passaging can be accompanied by increased chromosome aberration and reduced differentiation capacity.

Table 1 | Cultured adult hippocampal neural precursor cells differentiate (10 days of growth factor withdrawal) into the three principal cell types of the nervous system demonstrating their multipotent properties.

Phenotype	Percentage
Neurons	≈30%
Astrocytes	≈30%
Oligodendrocytes	≈1%
Undifferentiated	≈40%

Neurons generated from cultured adult hippocampal neural precursor cells using the present protocols typically display a resting membrane potential of −59 ± 4 mV and generate tetrodotoxin sensitive action potentials consistent with the expression of neuronal sodium channels (Babu et al., 2007).

An example of a neural precursor cell culture differentiated for 7 days is shown in **Figure 2F**. Immunocytochemically, neurons are detected by Map2ab, astrocytes by GFAP, and oligodendrocytes by O4 expression (**Figure 4**). O4-positive oligodendrocytes generated from adult neural precursor cells appear after 10 days of differentiation. **Table 1** depicts the estimated fraction of cells that are derived upon routine differentiation method described in this protocol.

SUPPLEMENTARY MATERIAL

The Supplementary Material for this article can be found online at http://www.frontiersin.org/neurogenesis/10.3389/fnins.2011.00089/abstract

MOVIE S1 | Micro-dissection and isolation of mouse dentate gyrus: the mouse brain is separated from the calvarium. The hippocampus that lies beneath the neocortex is dissected free from the rest of the brain. In the next step the dentate gyrus is isolated from the *cornu ammonis* by drawing a wedge through the hippocampal fissure.

REFERENCES

Babu, H., Cheung, G., Kettenmann, H., Palmer, T. D., and Kempermann, G. (2007). Enriched monolayer precursor cell cultures from micro-dissected adult mouse dentate gyrus yield functional granule cell-like neurons. *PLoS ONE* 2, e388. doi:10.1371/journal.pone.0000388

Babu, H., Ramirez-Rodriguez, G., Fabel, K., Bischofberger, J., and Kempermann, G. (2009). Synaptic network activity induces neuronal differentiation of adult hippocampal precursor cells through BDNF signaling. *Front. Neurosci.* 3:49. doi: 10.3389/neuro.22.001.2009

Ben Abdallah, N., Slomianka, L., Vyssotski, A. L., and Lipp, H. P. (2010). Early age-related changes in adult hippocampal neurogenesis in C57 mice. *Neurobiol. Aging* 31, 151–161.

Bez, A., Corsini, E., Curti, D., Biggiogera, M., Colombo, A., Nicosia, R. F., Pagano, S. F., and Parati, E. A. (2003). Neurosphere and neurosphere-forming cells: morphological and ultrastructural characterization. *Brain Res.* 993, 18–29.

Boku, S., Nakagawa, S., Masuda, T., Nishikawa, H., Kato, A., Kitaichi, Y., Inoue, T., and Koyama, T. (2009). Glucocorticoids and lithium reciprocally regulate the proliferation of adult dentate gyrus-derived neural precursor cells through GSK-3beta and beta-catenin/TCF pathway. *Neuropsychopharmacology* 34, 805–815.

Cameron, H. A., Woolley, C. S., McEwen, B. S., and Gould, E. (1993). Differentiation of newly born neurons and glia in the dentate gyrus of the adult rat. *Neuroscience* 56, 337–344.

Conti, L., and Cattaneo, E. (2005). Controlling neural stem cell division within the adult subventricular zone: an APPealing job. *Trends Neurosci.* 28, 57–59.

Eriksson, P. S., Perfilieva, E., Bjork-Eriksson, T., Alborn, A. M., Nordborg, C., Peterson, D. A., and Gage, F. H. (1998). Neurogenesis in the adult human hippocampus. *Nat. Med.* 4, 1313–1317.

Foroni, C., Galli, R., Cipelletti, B., Caumo, A., Alberti, S., Fiocco, R., and Vescovi, A. (2007). Resilience to transformation and inherent genetic and functional stability of adult neural stem cells ex vivo. *Cancer Res.* 67, 3725–3733.

Hagihara, H., Toyama, K., Yamasaki, N., and Miyakawa, T. (2009). Dissection of hippocampal dentate gyrus from adult mouse. *J. Vis. Exp.* 3000, 1–6.

Imbeault, S., Gauvin, L. G., Toeg, H. D., Pettit, A., Sorbara, C. D., Migahed, L., DesRoches, R., Menzies, A. S., Nishii, K., Paul, D. L., Simon, A. M., and Bennett, S. A. (2009). The extracellular matrix controls gap junction protein expression and function in postnatal hippocampal neural progenitor

cells. *BMC Neurosci.* 10, 13. doi: 10.1186/1471-2202-10-13

Jensen, J. B., and Parmar, M. (2006). Strengths and limitations of the neurosphere culture system. *Mol. Neurobiol.* 34, 153–161.

Jessberger, S., Clemenson, G. D. Jr., and Gage, F. H. (2007). Spontaneous fusion and nonclonal non-clonal growth of adult neural stem cells. *Stem Cells* 25, 871–874.

Knoth, R., Singec, I., Ditter, M., Pantazis, G., Capetian, P., Meyer, R. P., Horvat, V., Volk, B., and Kempermann, G. (2010). Murine features of neurogenesis in the human hippocampus across the lifespan from 0 to 100 Years. *PLoS ONE* 5, e8809. doi: 10.1371/journal.pone.0008809

Kornack, D. R., and Rakic, P. (1999). Continuation of neurogenesis in the hippocampus of the macaque monkey. *Proc. Natl. Acad. Sci. U.S.A.* 96, 5768–5773.

Kuhn, H. G., Dickinson-Anson, H., and Gage, F. H. (1996). Neurogenesis in the dentate gyrus of the adult rat: age-related decrease of neuronal progenitor proliferation. *J. Neurosci.* 16, 2027–2033.

Liu, C., Teng, Z. Q., Santistevan, N. J., Szulwach, K. E., Guo, W., Jin, P., and Zhao, X. (2010). Epigenetic regulation of miR-184 by MBD1 governs neural stem cell proliferation and differentiation. *Cell Stem Cell* 6, 433–444.

Luo, C. X., Jin, X., Cao, C. C., Zhu, M. M., Wang, B., Chang, L., Zhou, Q. G., Wu, H. Y., and Zhu, D. Y. (2010a). Bidirectional regulation of neurogenesis by neuronal nitric oxide synthase derived from neurons and neural stem cells. *Stem Cells* 28, 2041–2052.

Luo, Y., Shan, G., Guo, W., Smrt, R. D., Johnson, E. B., Li, X., Pfeiffer, R. L., Szulwach, K. E., Duan, R., Barkho, B. Z., Li, W., Liu, C., Jin, P., and Zhao, X. (2010b). Fragile x mental retardation protein regulates proliferation and differentiation of adult neural stem/progenitor cells. *PLoS Genet.* 6, e1000898. doi: 10.1371/journal.pgen.1000898

Marshall, G. P. II, Reynolds, B. A., and Laywell, E. D. (2007). Using the neurosphere assay to quantify neural stem cells in vivo. *Curr. Pharm. Biotechnol.* 8, 141–145.

Palmer, T. D., Markakis, E. A., Willhoite, A. R., Safar, F., and Gage, F. H. (1999). Fibroblast growth factor-2 activates a latent neurogenic program in neural stem cells from diverse regions of the adult CNS. *J. Neurosci.* 19, 8487–8497.

Palmer, T. D., Ray, J., and Gage, F. H. (1995). FGF-2-responsive neuronal progenitors reside in proliferative and quiescent regions of the adult rodent brain. *Mol. Cell. Neurosci.* 6, 474–486.

Palmer, T. D., Takahashi, J., and Gage, F. H. (1997). The adult rat hippocampus contains premordial neural stem cells. *Mol. Cell. Neurosci.* 8, 389–404.

Ramirez-Rodriguez, G., Klempin, F., Babu, H., Benitez-King, G., and Kempermann, G. (2009). Melatonin modulates cell survival of new neurons in the hippocampus of adult mice. *Neuropsychopharmacology* 34, 2180–2191.

Ray, J., and Gage, F. H. (2006). Differential properties of adult rat and mouse brain-derived neural stem/progenitor cells. *Mol. Cell. Neurosci.* 31, 560–573.

Reynolds, B. A., and Rietze, R. L. (2005). Neural stem cells and neurospheres – re-evaluating the relationship. *Nat. Methods* 2, 333–336.

Reynolds, B. A., and Weiss, S. (1992). Generation of neurons and astrocytes from isolated cells of the adult mammalian central nervous system. *Science* 255, 1707–1710.

Rietze, R. L., and Reynolds, B. A. (2006). Neural stem cell isolation and characterization. *Meth. Enzymol.* 419, 3–23.

Singec, I., Knoth, R., Meyer, R. P., Maciaczyk, J., Volk, B., Nikkhah, G., Frotscher, M., and Snyder, E. Y. (2006). Defining the actual sensitivity and specificity of the neurosphere assay in stem cell biology. *Nat. Methods* 3, 801–806.

Wong Po Foo, C. T., Lee, J. S., Mulyasasmita, W., Parisi-Amon, A., and Heilshorn, S. C. (2009). Two-component protein-engineered physical hydrogels for cell encapsulation. *Proc. Natl. Acad. Sci. U.S.A.* 106, 22067–22072.

Conflict of Interest Statement: The authors declare that the research was conducted in the absence of any commercial or financial relationships that could be construed as a potential conflict of interest.

Received: 11 March 2011; accepted: 28 June 2011; published online: 14 July 2011.

Citation: Babu H, Claasen J-H, Kannan S, Rünker AE, Palmer T and Kempermann G (2011) A protocol for isolation and enriched monolayer cultivation of neural precursor cells from mouse dentate gyrus. Front. Neurosci. ***5****:89. doi: 10.3389/fnins.2011.00089*

This article was submitted to Frontiers in Neurogenesis, a specialty of Frontiers in Neuroscience.

frontiers in
NEUROSCIENCE

ORIGINAL RESEARCH ARTICLE
published: 03 May 2011
doi: 10.3389/fnins.2011.00052

Acquisition of an olfactory associative task triggers a regionalized down-regulation of adult born neuron cell death

Sébastien Sultan, Julie M. Lefort, Joëlle Sacquet, Nathalie Mandairon and Anne Didier*

CNRS, UMR5020; INSERM, U1028; Lyon Neuroscience Research Center, Neuroplasticity and Neuropathology of olfactory perception Team, University of Lyon, Lyon; University Lyon1, Villeurbanne, France

Edited by:
Silvia De Marchis, University of Turin, Italy

Reviewed by:
Armen Saghatelyan, Université Laval, Canada
Isabelle Caillé, CNRS, France

****Correspondence:***
Anne Didier, Lyon Neuroscience Research Center, Université Lyon1, 50 Avenue Tony Garnier, 69007 Lyon, France.
e-mail: didier@olfac.univ-lyon1.fr

Associative olfactory learning increased survival of adult born granule interneurons in the olfactory bulb (OB) at regions which are specific to the learned odorant. However, the mechanism shaping this odor-specific distribution of newborn neurons and its temporal relationship with the learning process are unknown. In the present study, using Bromodeoxyuridine or activated-caspase3 labeling, newborn and apoptotic cells respectively were mapped in the granule cell layer (GCL) of the OB, just before, during, and at the end of odor conditioning or pseudo-conditioning in adult mice. Results indicate that before and during training, when the task is not yet acquired, conditioned and pseudo-conditioned animals displayed the same density of newborn neurons. However, at the end of the conditioning, when the animals mastered the task, the density of newborn cells remained elevated in conditioned animals while it decreased in pseudo-conditioned animals suggesting newborn cell death in that group. Indeed, using Activated-Caspase3/BrdU co-labeling, we found that the proportion of newborn cells among dying cells was reduced in conditioned animals mastering the task compared to non-expert conditioned or pseudo-conditioned animals. The overall level of cell death did not change across training and was similar in conditioned and pseudo-conditioned groups, indicating that BrdU-positive cells were spared to the detriment of non-labeled cells. In addition, a fine analysis of cell distribution showed an uneven distribution of apoptotic cells, with lower densities in the medial part of the GCL where the density of newborn cells is high in conditioned animals. We conclude that acquisition of the task triggered the rescue of newborn neurons by a targeted regulation of cell death.

Keywords: adult neurogenesis, olfactory bulb, cell death, learning, mice, BrdU, behavior

INTRODUCTION

New neurons are provided throughout life to the olfactory bulb (OB), the first central relay of olfactory information processing. These adult born neurons originate from stem cells proliferating in the subventricular zone of the lateral ventricles, giving birth to neuroblasts which then migrate to the OB. Within the OB, neuroblasts differentiate into inhibitory granules cells (GCs) for the majority of them and to a lesser extent into periglomerular cells, and integrate the bulbar circuit (Lledo et al., 2006). Dendritic and synaptic development of newborn cells take about 1 month, a critical period during which they are very sensitive to olfactory experience for their morphological (Kelsch et al., 2009; Livneh et al., 2009), neurochemical development (Bovetti et al., 2009), and their long-term survival (Petreanu and Alvarez-Buylla, 2002; Winner et al., 2002; Yamaguchi and Mori, 2005; Mandairon et al., 2006b; Mouret et al., 2008).

The OB is heavily involved in odor learning and memorization. For instances, electrophysiological recordings have shown that the response of mitral cells, the relay cells of the OB, are modified when the odor is coupled to a positive or negative reinforcement (Kay and Laurent, 1999) and bulbar network oscillations evolve with expertise in the task (Martin et al., 2004). Immediate early gene mapping also revealed cellular plasticity in the OB following learning (Salcedo et al., 2005; Mandairon et al., 2008; Busto et al., 2009; Moreno et al., 2009). All together these data indicate that the bulbar network undergoes experience-dependent plasticity. Inhibitory interneurons which interact through dendro-dendritic synapses with the mitral cells to shape the output message of the OB to higher olfactory centers, are involved in experience-dependent plasticity of the OB network (Shepherd et al., 2007).

Numerous studies over the last years have linked olfactory learning and memory to modulation of adult born GCs of the OB (Rochefort et al., 2002; Alonso et al., 2006; Mandairon et al., 2006a; Mouret et al., 2008; Lazarini et al., 2009; Moreno et al., 2009; Valley et al., 2009; Veyrac et al., 2009; Kermen et al., 2010; Sultan et al., 2010). In these studies, the number of newborn GCs was increased after olfactory enrichment or learning, suggesting that learning rescued some newborn neurons from the death which normally occurs during the first weeks after cell birth (Petreanu and Alvarez-Buylla, 2002; Winner et al., 2002; Mandairon et al., 2006b). These findings, together with the ability of newborn GCs to display long-term potentiation (Nissant et al., 2009) set the basis for the hypothesis that adult born cells could be important for olfactory learning or memory.

Recently, we have characterized further the role of adult born GCs in a paradigm of associative olfactory learning (Kermen et al., 2010; Sultan et al., 2010). We have shown that more adult born GCs survived after learning in odor-specific areas of the granule cell layer (GCL) and are required for long-term memory of the

task. However, the exact temporal relationship between survival of newborn cells and the learning process as well as the mechanism by which they are grouped in odor-specific areas are unknown.

To address this issue, we used cellular mapping to analyze the number, the spatial distribution, and the death of newborn cells in the GCL of the OB before, during, and after olfactory conditioning. Results reveal that the patterned distribution of adult born cells in the GCL after learning is due to a region-specific reduction in newborn cell death which correlates tightly with the time point at which animals have acquired the task.

MATERIALS AND METHODS

ANIMALS

Thirty-four male C57Black6/J mice (Charles River, L'Arbresles, France) aged 8 weeks at the beginning of the experiments were used. All mice were housed under a 12-h light/dark cycle in an environmentally controlled room. Mice had free access to water and food except during the olfactory learning period (see below). All behavioral training was conducted in the afternoon (14:00–17:00). Every effort was made to minimize both the number of animals used and their suffering during the experimental procedure in accordance with the European Community Council Directive of November 24, 1986 (86/609/EEC) and the University Lyon1 Ethical Committee.

EXPERIMENTAL SCHEME

Animals were injected with the cell division marker 5-Bromo-2′-deoxyuridine (BrdU) 13 days before the beginning of training, to allow newborn cells to migrate to the OB and to be in their critical period of development during training (Mandairon et al., 2006b; Mouret et al., 2008; Kelsch et al., 2009). Three days before the onset of conditioning, all the animals were submitted to a 3-day pre-training followed on D0 by a 5-day olfactory conditioning ($n = 17$) or pseudo conditioning ($n = 15$; see below). A retention test was performed 5 days after the end of conditioning. Animals were sacrificed at different time points: before conditioning (pre-training; $n = 5$), after 3 days of training ($n = 5$ conditioned and $n = 5$ pseudo-conditioned animals), after the complete conditioning at day 5 ($n = 5$ conditioned and $n = 5$ pseudo-conditioned animals) and 5-day post training ($n = 7$ conditioned and $n = 5$ pseudo-conditioned animals). A total of seven experimental groups were thus studied (**Figure 1A**). After behavioral testing, animals were sacrificed and histological techniques were applied to measure neurogenesis, neuronal differentiation, and cell death in the GCL.

BEHAVIORAL EXPERIMENTS

Experimental set up

All mice were tested on a computer-assisted 2-hole board apparatus (40 cm × 40 cm) run by specific software (Mandairon et al., 2009). The trial started by placing the mouse on the board, and the sequence and duration of nose poking into the holes (3 cm diameter, 4.5 cm deep) were automatically recorded. A polypropylene swab was placed at the bottom of the hole, covered with bedding. For trials involving odors, the swab was impregnated with 20 μL of pure odorant. The bedding was replaced after every trial. Between each trial, mice were put back in their home cage.

Olfactory associative learning

Odorants

+Limonene (Purity > 97%, Sigma-Aldrich, Saint Louis, MO, USA) was used in this experiment.

Pre-training

Mice were first trained to retrieve a reward (small bit of sweetened cereal, Kellogg's, Battle Creek, MI, USA) by digging through the bedding while no odor was present. The mouse was put in the start area and was allowed to dig for 2 min. During the first few trials the reward was placed on the top of the bedding of one of the holes. After several successful retrievals, the reward was buried deeper into the bedding. Pre-training was considered to be complete when a mouse could successfully retrieve a reward that was deeply buried in the bedding (from 8 to 12 trials).

Conditioning

During the olfactory learning experiments, water was continuously available, but the mice were food-deprived for 5 days before pre-training, to obtain a 5–10% reduction in body weight. Conditioning consisted of five sessions (one per day) of four trials (2 min per trial, inter trial interval of 15 min). For each trial, the mice were placed on the board and a reward (Kellogs's cereal) systematically associated with the odorant, was randomly placed in one of the two holes to avoid spatial learning. The other hole was not odorized and did not contain any reward. In the pseudo-conditioned groups, the reinforcement was randomly associated with either the odorized hole or the non-odorized hole. For each trial, the percentage of correct choice (first nose poke in the odorized hole) was recorded as indicative of learning.

Retention test

Five days after the last day of conditioning, mice were submitted to a retention test consisting in four trials of 2 min in the same conditions as during conditioning (inter trial interval of 15 min and presence of the reward in the odorized hole).

Data analysis

For each training session, correct choices were averaged within groups. Between groups comparisons were done using ANOVA for repeated measures and Student *t*-tests for pair's comparisons. Statistical significance was set at $p < 0.05$.

SACRIFICE

One hour after the last behavioral trial, the mice were deeply anesthetized (Pentobarbital, 0.2 mL/30 g) and killed by intracardiac perfusion of 50 ml of fixative (4% paraformaldehyde in phosphate buffer, pH 7.4). Brains were removed, post-fixed, cryoprotected in sucrose (20%), frozen rapidly and then stored at −20°C before sectioning with a cryostat (Jung).

5-BROMO-2′-DEOXYURIDINE (BrdU) ADMINISTRATION

BrdU (Sigma, 50 mg/kg in saline, three times at 2 h intervals) was injected 13 days before the behavioral training began in order to label a cohort of newborn cells arriving in the OB at the time of conditioning.

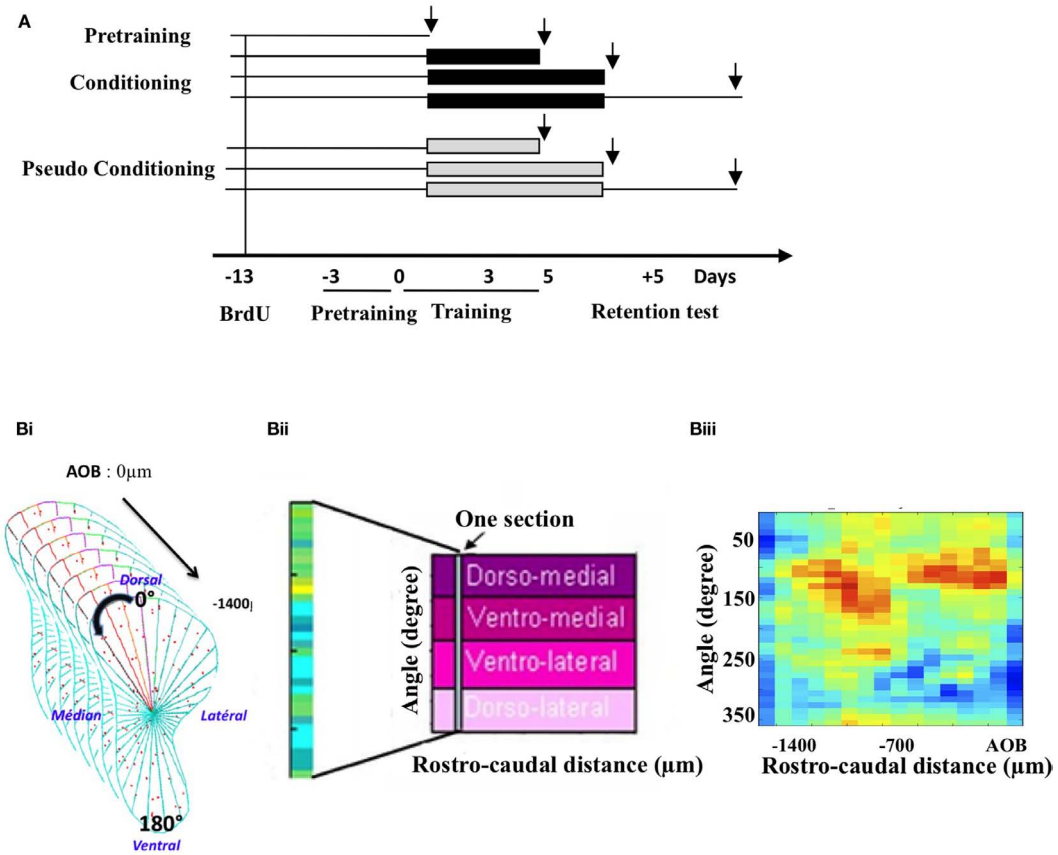

FIGURE 1 | Experimental design and cell mapping procedure. (A) Groups and timing of the experiment. Following a 3-day pre-training period, animals were submitted to an olfactory conditioning or pseudo-conditioning. They were sacrificed either before conditioning (pre-training) during (on day 3 and on day 5 of conditioning) or 5 days post conditioning, after a retention test. Black arrows indicate times of sacrifice, intervening 1 h after the last behavioral trial. To assess neurogenesis at these different time points, BrdU was administered 13 days before conditioning. **(B)** Principle of the labeled cell mapping method. Serial coronal sections of the OB were processed for BrdU or activated-caspase3 immunohistochemistry and every labeled cell was then counted on each section. The GCL was divided into 36 sectors of 10° and a density of labeled profiles was calculated for each sector **(Bi)**. The value of cell density obtained was then reported into a matrix in which one column represented all the sectors of one section. Sections were aligned along the rostro-caudal axis **(Bii)**. Finally, pseudo-color representation of the matrix was generated, giving a 2-dimension image of the density of labeled cells in the GCL. An example of such representation is given **(Biii)**.

BrdU IMMUNOCYTOCHEMISTRY

The protocol has been described previously (Mandairon et al., 2006a). Brains sections were first incubated in Target Retrieval Solution (Dako, Trappes, France) for 20 min at 98°C. After cooling for 20 min, they were treated with Triton 0.5% (SigmaX100) in phosphate buffered saline (PBS) for 30 min, then for 3 min with pepsin (0.43 U/ml in 0.1 N HCl, Sigma). Endogenous peroxidases were blocked with a solution of 3% H_2O_2 in 0.1 M PBS. Then, sections were incubated for 90 min in 5% normal horse serum, (Vector Laboratories, Burlingame, CA, USA) in 5% bovine serum albumin, (BSA, Sigma) and 0.125% Triton X-100 to block non-specific binding, and then incubated overnight at 4°C in a mouse anti-BrdU primary antibody (1/100, Chemicon, Temecula, CA, USA). Sections were then incubated in a horse biotinylated anti-mouse secondary antibody (1/200, Vector) for 2 h. Sections were then processed with avidin–biotin–peroxydase complex (ABC Elite Kit, Vector) for 30 min. Finally, sections were reacted in 0.05% 3,3-diaminobenzidine-tetra-hydrochloride (DAB, Sigma), 0.03% NiCL2, and 0.03% H_2O_2 in Tris–HCl buffer (0.05 M, pH 7.6), dehydrated in graded ethanols, and coverslipped in DPX.

ACTIVATED CASPASE 3 IMMUNOHISTOCHEMISTRY

We used the immunohistochemical detection of activated-caspase3 to detect apoptotic cell death. Brain sections were first rehydrated in PBS for 10 min, then incubated in H_2O_2 3% (prepared extemporaneously in PBS) for 20 min. Sections were then treated with Triton 0.5% (SigmaX100) BSA (2%), Goat serum (2%) in PBS for 1h. Then, sections were incubated for 1 h in 5% normal goat serum, (Vector Laboratories, Burlingame, CA, USA) in 5% bovine serum albumin, (BSA, Sigma) and 0.125% Triton X-100 to block non-specific binding, and then incubated for 48 h at 4°C in a rabbit anti-cleaved (activated) caspase 3 primary antibody (1/500, asp175 # 9661 Cell Signaling Technology). Sections were then incubated in a goat biotinylated anti-rabbit secondary antibody (1/200, Vector) for 1 h 30 min.

Sections were then processed with avidin–biotin–peroxydase complex (ABC Elite Kit, Vector) for 30 min. Finally, sections were reacted in 0.05% 3,3-diaminobenzidine-tetra-hydrochlor ide (DAB,Sigma), 0.03% NiCL2, and 0.03% H_2O_2 in Tris–HCl buffer (0.05 M, pH 7.6), dehydrated in graded ethanols, and coverslipped in DPX.

QUANTIFICATION OF BrdU-POSITIVE CELLS AND ACTIVATED CASPASE 3-POSITIVE CELLS

All cell counts were conducted blind with regards to the mouse status. Data were collected with the help of mapping software (Mercator Pro, Explora Nova, La Rochelle, France), coupled to a Zeiss microscope. In the GCL of the OB, every BrdU-positive cell was counted on 20 sections (14 μm thick, 70 μm intervals) of four to five mice per group. The number of positive cells was divided by the surface of the region of interest to yield the total density of labeled cells (number of labeled profiles/μm^2).

The same was done for activated-caspase3-positive cells. A recent study suggested that caspase3 is not only a key mediator of apoptosis but could also function as a regulatory molecule in synaptic plasticity (D'Amelio et al., 2009). In our study, activated-caspase3-positive cells were counted only if the nucleus was stained. This enabled us to consider them as apoptotic cells and not as neurons undergoing a process of synaptic plasticity. Data were analyzed by ANOVA followed by Student *t*-tests for pair's comparisons.

MAPPING OF BrdU-POSITIVE CELLS AND ACTIVATED CASPASE 3-POSITIVE CELLS IN THE GCL

This was done according to a previously described procedure (Mandairon et al., 2006a, 2008; Busto et al., 2009; Sultan et al., 2010). The GCL was divided into 36 sectors of 10° with a reference axis drawn parallel to the most ventral aspect of the subependymal layer of the OB (**Figure 1Bi**). The cell density (number of labeled profiles/μm^2) was calculated for each sector. Density values were then merged into arrays of 10° × 70 μm bins in which one column represents one section (**Figure 1Bii**). The most rostral aspect of the accessory OB served as an anatomical landmark to align the sections across animals. For each sector, means across animals were calculated to yield a map of mean cell density. A colored image plot of the data was constructed in Matlab v.6 (**Figure 1Biii**). SD maps were also constructed. Using Matlab, the 20% highest density bins were selected in BrdU-positive cell maps as well as the 20% lowest density bins in the activated-caspase3-positive cell maps. The overlapping bins were represented and counted. The percentage of overlapping bins (number of overlapping bins/number of bins selected × 100) was calculated and compared between groups using a *t*-test for comparisons of proportion (Mandairon et al., 2006a).

BrdU/NeuN DOUBLE LABELING AND ANALYSIS

To determine the phenotype of BrdU-positive cells in the GCL of the OB, we performed a BrdU/NeuN double-labeling using a rat anti-BrdU (1:100, Harlan Sera lab, Loughborough, UK) and a mouse anti-NeuN (1:500, Chemicon). Double-labelled cells were observed and analyzed by pseudo-confocal scanning microscopy using a Zeiss microscope equipped with the Apotome (n = 3–5 animals per group, 30–40 cells per animal). A percentage of double-labeled cells was calculated for each group and compared ANOVA and Student *t*-tests for pair's comparisons.

ACTIVATED-CASPASE3/BrdU DOUBLE LABELING AND ANALYSIS

To determine newborn cells death in the GCL, an activated caspase 3/BrdU double labeling was performed using a mouse anti-BrdU (1:100, Chemicon) and a rabbit anti anti-Activated caspase 3 (1:500, Cell signaling Technology) for 48 h at 4°C. Then, sections were incubated 2 h at room temperature in secondary antibodies (goat anti-mouse Alexa 546-coupled, 1:200, Molecular Probes, Invitrogen Oregon USA and goat biotinylated anti-rabbit, 1/200, Vector) followed by Streptavidin Alexa 488 (1:1000, Molecular Probe) for 90 min.

For data analysis, activated capspase3-positive cells were observed in each group (n = 3 animals per group, 8–10 cells per animal) and a percentage of BrdU-positive cells among activated-caspase3-positive cells was calculated for each group. Data were compared by ANOVA and Student *t*-tests for pair's comparisons.

RESULTS

TEMPORAL RELATIONSHIP BETWEEN LEARNING AND NEWBORN NEURON SURVIVAL

The global analysis of the behavioral data indicated that conditioned and pseudo-conditioned groups differed significantly [Group effect $F(1, 20) = 7.95$, $p < 0.05$; **Figure 2A**]. The success rate increased in conditioned animals [Day effect $F(4,44) = 4.99$, $p < 0.05$] but not in pseudo-conditioned animals [Day effect $F(4, 36) = 0.29$, $p > 0.05$], indicating that only the conditioned animals learnt the association between the odor and the reward. Success rates in conditioned animals significantly differed from those of pseudo-conditioned animals on day 5 of learning and 5 days post learning ($p < 0.05$ in both cases; **Figure 2A**).

In animals randomly selected before (pre-training), during (day 3 and 5) or after (day + 5) conditioning or pseudo-conditioning, we counted the density of BrdU-positive cells (**Figures 2B,D**) in the GCL. The density of adult born cells evolved with conditioning or pseudo-conditioning according to a different pattern [Group effect $F(6, 23) = 3.53$, $p < 0.05$]. In conditioned animals, the density of newborn cells was stable and similar to the pre-training level at all time points studied. Indeed, no difference was found between conditioned groups across time. In contrast, in pseudo-conditioned animals, newborn cell density decreased on day 5 and 5 days post training, compared to day 3 ($p < 0.05$; **Figure 2B**). Consequently, newborn cell density was significantly lower in pseudo-conditioned than in conditioned animals on day 5 of training and 5 days post training ($p < 0.05$). It is worth noting that the difference between conditioned and pseudo-conditioned animals with regard to newborn cell density appeared on day 5 of training, when the animals master the task. In contrast, on day 3 of training, at a time when the conditioned animals do not yet succeed in the task, the density of newborn cells was similar in conditioned and pseudo-conditioned groups. We also analyzed the level of neuronal differentiation of adult born cells across training using co-labeling of BrdU with the expression of the marker of mature neurons NeuN (**Figures 2C,E**). We found that the percentage of adult born neurons increased

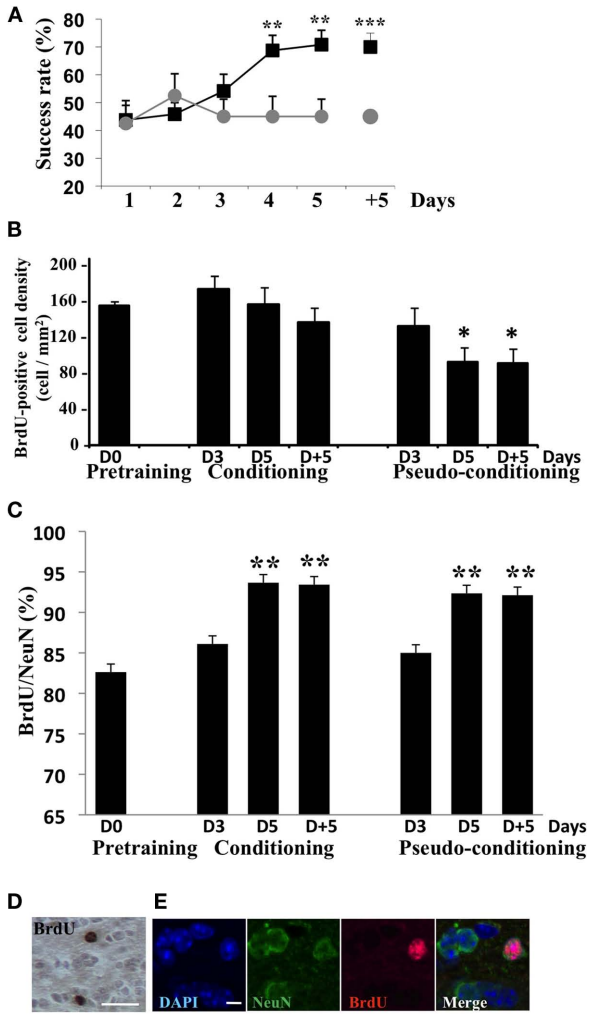

FIGURE 2 | Behavioral data and assessment of neurogenesis. (A) Success rate in conditioned and pseudo-conditioned animals during olfactory conditioning (day 1 to day 5) and in the retention test (day + 5). $^{**}p < 0.005$; $^{***}p < 0.0005$ for difference between conditioned and pseudo-conditioned groups. **(B)** Density in BrdU-positive cells in the GCL before (pre-training) during (D3 and D5) and after (D + 5) olfactory conditioning or pseudo-conditioning. $^{*}p < 0.05$ for difference from all other groups. **(C)** Percentage of BrdU-positive cells co-labeled with the neuronal marker NeuN in all experimental groups. $^{**}p < 0.005$ for difference from pre-training level and from D3 in conditioned and pseudo-conditioned groups. **(D)** BrdU-positive cells in the GCL, bar = 15 µm. **(E)** BrdU/NeuN double-labeled cell in the GCL. DAPI stains all nuclei. Bar = 5 µm.

significantly from about 80% to 90% between day 3 and day 5 of training [Group effect $F(6,23) = 4.32$, $p < 0.005$, $p < 0.05$ for difference between D3 and D5 in conditioned and pseudo-conditioned groups], and then remained stable between day 5 and 5 days post training. No difference was found between pre-training level and day 3 of training in any of the conditioned and pseudo-conditioned groups. These data indicated that the neuronal differentiation of newborn cells was completed 18-day post BrdU injections (13 days between BrdU injections and beginning of behavioral training + 5 days of training) and that this temporal pattern of differentiation was independent of learning.

All together, these results indicated that the increased newborn cell density observed at the end of conditioning was due to the rescue from death of newborn cells occurring once behavioral performances raised meaning when the animals master the task (**Figures 2A,B**). This prompted us to examine whether cell death differentially affected newborn cells in the different experimental groups.

NEWBORN NEURONS WERE SPARED BY CELL DEATH UPON ACQUISITION OF THE TASK

In order to further document the death of newborn cells in pseudo-conditioned animals and their rescue in conditioned animals, we performed activated-caspase3/BrdU double-labeling experiment in which we looked at the percentage of BrdU-positive cells among those expressing activated-caspase3 in the different experimental groups (**Figures 3A,B**). Results clearly showed that the percentage of newborn cells among dying cells decreased in conditioned animals on day 5 and 5 days post training, compared to the other groups [Group effect $F(6,14) = 20.93$, $p < 0.05$]. Furthermore, we counted activated-caspase3-positive cells in the GCL and found that their global density in the GCL was stable across time and groups [Group effect $F(6, 25) = 0.79$, $p > 0.05$; **Figures 3C,D**]. Taken together, these results indicated that the process of learning a new olfactory task was accompanied by the selective rescue of BrdU-positive cells from apoptotic death to the detriment of non-labeled cells.

SPATIO-TEMPORAL CORRELATION BETWEEN LOW CELL DEATH AND NEWBORN CELL SURVIVAL DURING LEARNING

In a previous study, we showed that after learning, newborn cells were found at odor-specific locations in the GCL (Sultan et al., 2010). To assess the contribution of cell death to this regionalization of newborn cells, activated-caspase3-positive cells were mapped in the GCL and we compared this distribution to that of BrdU-positive cells. In all groups, a higher density of newborn cells was retrieved in the medial and anterior parts of the GCL (red areas), while the lowest density was observed in the latero-posterior area (yellow–green to blue areas) (**Figure 4A**, upper panel). This distribution can be explained by the presence of a medio-lateral and a antero-posterior gradients in global cell density which we described previously in the GCL (Busto et al., 2009). Thus, in all groups, the gross distribution of newborn cells was coherent with the cell density in the GCL (**Figure 4A**, upper panel). To assess the effect of conditioning or pseudo conditioning on the distribution of BrdU-positive cells, we calculated the ratio of density values in the pre-training group to those of all other groups and depicted the results as color-coded maps of the ratio values (**Figure 4A**, lower panel). In conditioned animals, limited changes occurred in the lateral part of the GCL, accounting for the non-significant decrease in BrdU-positive cell density reported on **Figure 2B**. In contrast, in pseudo-conditioned animals, the ratio maps showed a loss of BrdU-positive cells, in line with the significant decreased in BrdU-cell density described in **Figure 2B**, and that this loss occurred broadly in the GCL.

The mapping of activated-caspase3-positive cells also revealed a non-uniform distribution of cell death (**Figure 4B**, upper panel). More specifically, in conditioned animals, visual inspection of the activated-

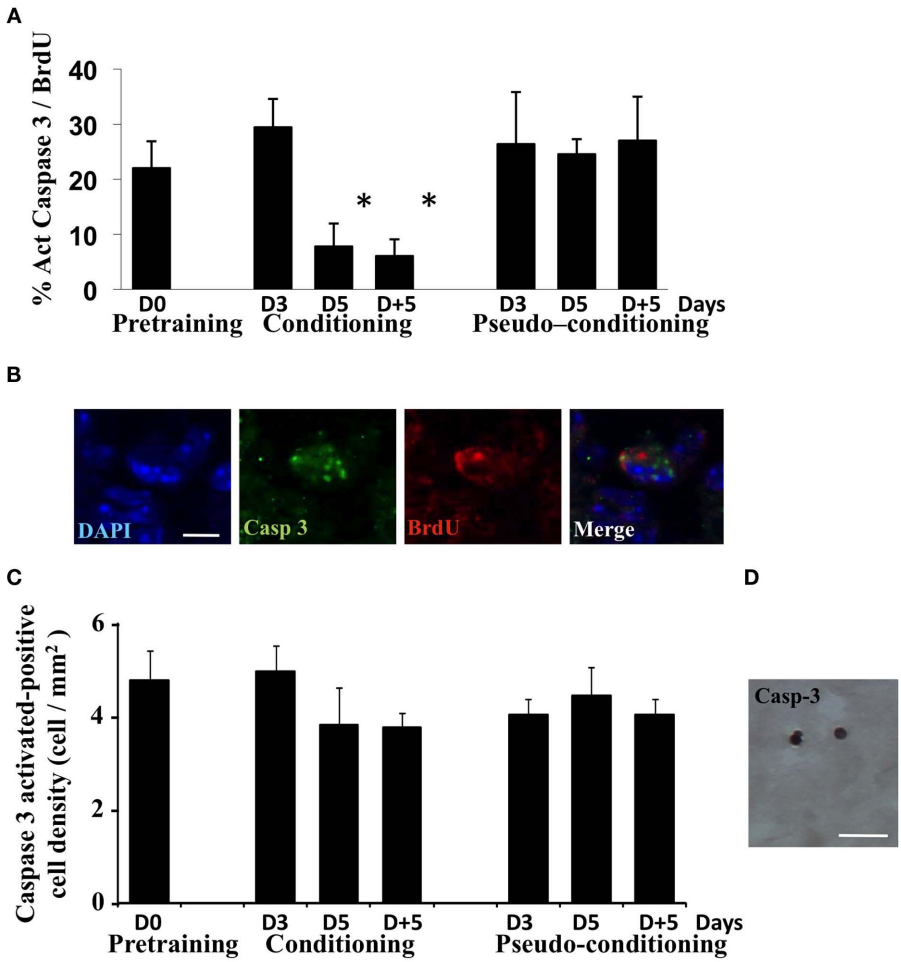

FIGURE 3 | Analysis of cell death during olfactory conditioning. **(A)** Percentage of activated-caspase3/BrdU double-labeled cells in the GCL. *$p < 0.05$ for difference from all other groups. **(B)** Activated-caspase3/BrdU double-labeled cell in the GCL. Bar = 5 μm. **(C)** Activated-caspase3-positive cell density in the GCL in all experimental groups. No significant difference was found. **(D)** Activated-caspase3-positive cells in the GCL. Bar = 15 μm.

caspase3-positive cell density indicated that it was lower in the medial part of the GCL (dark blue areas), where BrdU-positive cell density was the highest. Cell death was thus lower in the medial part of the GCL than what could be expected if it was simply proportional to global or newborn cell density. In order to directly relate newborn cell survival to lower level of cell death, we compared for each group the locations of high BrdU-positive cell density with those of low cell death density and quantify the overlap between these regions (see Materials and Methods; **Figure 4B**, lower panel). Interestingly, we found that the overlap between areas of high newborn and low cell death densities was located mostly to the medial part of the GCL, and was significantly higher in conditioned groups compared to pre-training or pseudo-conditioned groups (**Figure 4C**). Both BrdU and activated-caspase3 maps were highly reproducible within groups as illustrated by the SD maps, representing for each group, the SD value of the individual bins of the maps (**Figure 4D**). Taken together, these findings expanded the results of double-labeling experiment by suggesting that cell death was down-regulated in the areas of high density of BrdU-positive cells. However, on day 3 of conditioning, we found a high overlap of high BrdU- and low activated-caspase3-positive cell densities despite the fact that double labeling indicated that the proportion of newborn cells among dying cells was not yet decreased suggesting that, at this time point, newborn neurons were not spared more than preexisting cells.

In summary, our findings indicate that in close temporal correlation with the rise in success rate in the task, a down-regulation of cell death was targeted to newborn neurons on D5 and D + 5, allowing their rescue at specific locations of the GCL.

DISCUSSION

While the increase in newborn neurons following associative olfactory learning has been well documented (Alonso et al., 2006; Kermen et al., 2010; Sultan et al., 2010), the issue of when and how are newborn neurons selected to survive has not been investigated. In this study, using olfactory conditioning combined to double-labeling experiments and mapping of newborn or dying cells, we were able to show that cell death is regulated in the GCL of the OB during learning, allowing the learning-dependent rescue of newborn neurons. This conclusion is supported by the low pro-

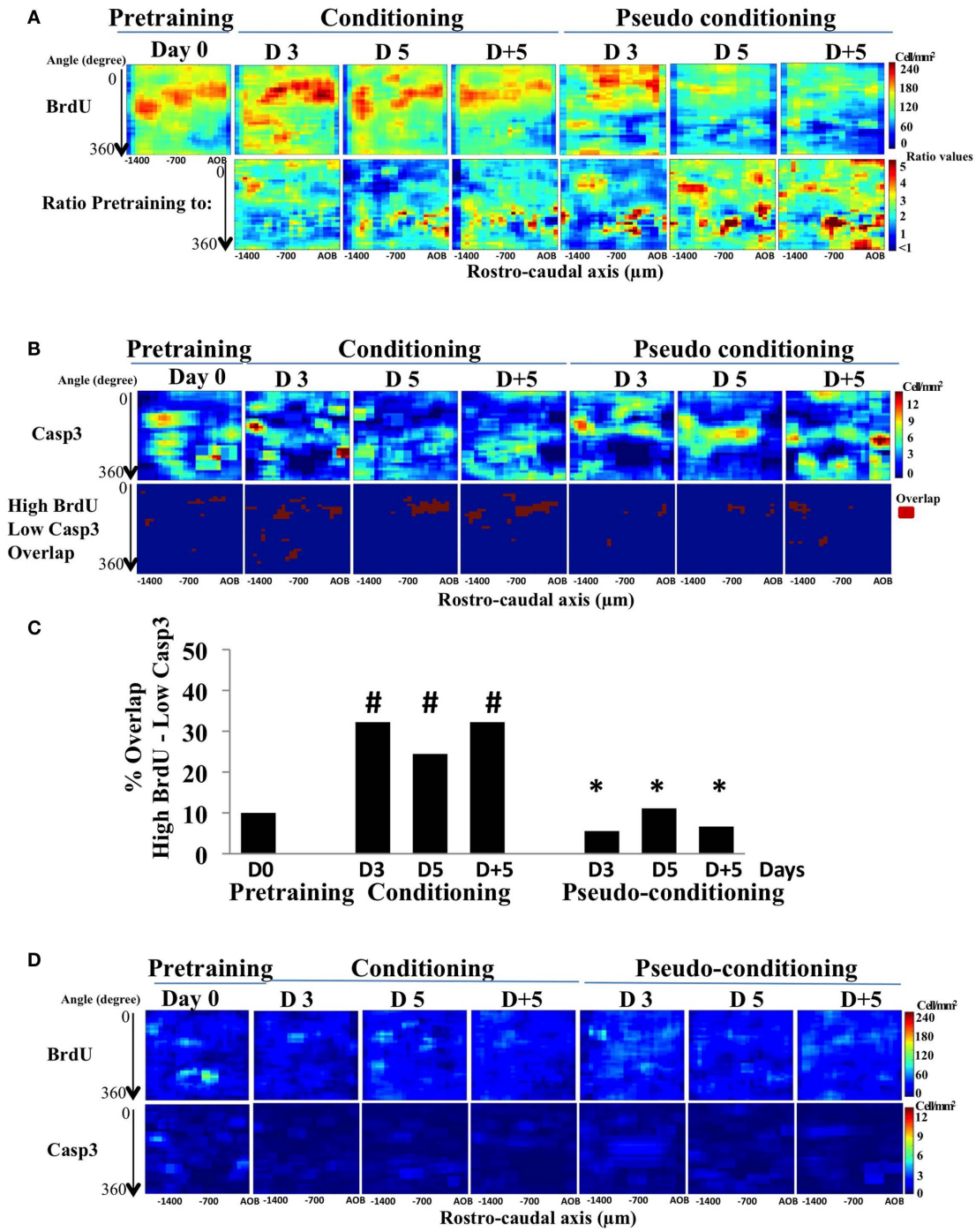

FIGURE 4 | BrdU- and activated-caspase3-positive cell mapping in the GCL. (A) Pseudo-color maps of Brdu-positive cells (BrdU; upper panel) and of the ratio BrdU-positive cell-density map of pre-training to all other groups (lower panel). **(B)** Activated-caspase3-positive (casp3) cell-density maps and maps of the overlap between high BrdU and low caspase3 cell densities. **(C)** Quantification of the overlap between high BrdU and low casp3. #$p < 0.05$ for difference from pre-training; *$p < 0.05$ for difference from corresponding time points in conditioned groups. **(D)** Maps of standard deviation (SD maps) associated with each bin of the BrdU- and activated-caspase3-postiive cell maps shown in **(A)**.

portion of newborn cells undergoing cell death during learning and by the temporal coincidence we found between the increase in newborn neuron survival and the decrease of the death of newborn cells. Several features of this regulatory process are of particular interest. First, we showed that it depended on learning since it occurred only in conditioned animals and not in pseudo-conditioned. Furthermore, it was closely correlated with the turning point of the learning curve. Indeed, it was only when animals

mastered the task (day 5 of learning) that newborn neurons death decreased suggesting that having learnt the task may protect newborn neurons from death. This is consistent with our previous study, in which we showed that day-to-day memory consolidation processes were necessary for newborn neuron survival (Kermen et al., 2010). Memory consolidation processes and associated signaling (Izquierdo et al., 2006) could contribute to protect newborn neurons from death. A good candidate for linking memory consolidation and survival is BDNF whose expression is involved in memory formation (Cunha et al., 2010) and which has been shown to stimulate newborn neurons formation (Zigova et al., 1998; Benraiss et al., 2001; Pencea et al., 2001; Bath et al., 2008; but see also, Galvao et al., 2008).

Second, in our experiment, we also showed that the overall level of cell death was unaffected across experimental groups. This observation together with the decreased in the death BrdU-labeled cells observed on D5 and D + 5, indicated that BrdU-negative GCs were subjected to higher level of cell death. Some uncertainty remains with regards to the age of these GCs in which cell death increased upon learning. They could be either older or younger than the labeled cells (more or less than 13 days old at the onset of training). Previous works showing that newborn neurons aged more than 30 days are suppressed by learning to the benefit of younger neurons (Mandairon et al., 2006a; Mouret et al., 2008) strongly suggest that the target of increased death are likely to be pre existing GCs. However, it can not be excluded that younger GCs may also undergo cell death.

Finally, thanks to our mapping approach, we found that cell death was lower in the areas where a high BrdU-positive cell density was retrieved during and after learning. These results support the idea of a regionalization of cell death. Interestingly, the target of cell death, newborn cells or pre-exisiting cells is likely to evolve with learning. Indeed, a mismatch was revealed by our study regarding cell death at 3 days of conditioning. At this time point, we found a high overlap between regions of high BrdU- and low activated-caspase3-positive cell densities but activated-caspase3/BrdU double labeling revealed no decrease in the proportion of newborn neurons among dying cells. It could thus be proposed that learning regulates cell death in two steps according to the learning process: a first early step with a down regulation of cell death occurring in high BrdU-positive cell density areas, without sparing newborn cells and a second step that could depend on the rise of performances and the strength of memory during which down regulation of cell death would target more specifically newborn neurons in these selected areas. Support to specific mechanisms occurring in newborn neurons and not older neurons upon memory formation is brought by the demonstration that newborn neurons selectively express long-term potentiation in the OB (Nissant et al., 2009).

The regulation of cell death we reported here thus shapes the temporal and spatial patterns of learning-dependent newborn neurons survival. These newborn neurons will be later on integrated in the network supporting long-term memory (Lazarini et al., 2009; Sultan et al., 2010). Based on these findings, one may predict that blocking cell death would alter the turn over of GCs and affect long-term memory. However, a recent study reported no effect of a pharmacological blockade by the pancaspase inhibitor Z-Vad (Mouret et al., 2009) on olfactory long-term memory. A possible explanation is that Z-Vad treatment decreased the overall level of cell death but did not prevent a learning-dependent protection of newborn neurons. Indeed, in this study conditioned animals displayed a lower level of cell death than pseudo-conditioned animals. This would imply that the absolute level of survival is less critical for memory than learning-dependent cell death regulation of newborn neurons.

In conclusion, this study demonstrates that newborn neurons are rescued from apoptotic death according to a specific time course closely following that of learning the associative task, through a process of regulation of cell death targeted to newborn cells as soon as the task is mastered.

ACKNOWLEDGMENTS

This work was supported by CNRS and University Claude Bernard Lyon 1 and the French ministry of research (Fellowship to Sébastien Sultan).

REFERENCES

Alonso, M., Viollet, C., Gabellec, M. M., Meas-Yedid, V., Olivo-Marin, J. C., and Lledo, P. M. (2006). Olfactory discrimination learning increases the survival of adult-born neurons in the olfactory bulb. *J. Neurosci.* 26, 10508–10513.

Bath, K. G., Mandairon, N., Jing, D., Rajagopal, R., Kapoor, R., Chen, Z. Y., Khan, T., Proenca, C. C., Kraemer, R., Cleland, T. A., Hempstead, B. L., Chao, M. V., and Lee, F. S. (2008). Variant brain-derived neurotrophic factor (Val66Met) alters adult olfactory bulb neurogenesis and spontaneous olfactory discrimination. *J. Neurosci.* 28, 2383–2393.

Benraiss, A., Chmielnicki, E., Lerner, K., Roh, D., and Goldman, S. A. (2001). Adenoviral brain-derived neurotrophic factor induces both neostriatal and olfactory neuronal recruitment from endogenous progenitor cells in the adult forebrain. *J. Neurosci.* 21, 6718–6731.

Bovetti, S., Veyrac, A., Peretto, P., Fasolo, A., and De Marchis, S. (2009). Olfactory enrichment influences adult neurogenesis modulating GAD67 and plasticity-related molecules expression in newborn cells of the olfactory bulb. *PLoS ONE* 4, e6359. doi: 10.1371/journal.pone.0006359

Busto, G. U., Elie, J. E., Kermen, F., Garcia, S., Sacquet, J., Jourdan, F., Marcel, D., Mandairon, N., and Didier, A. (2009). Expression of Zif268 in the granule cell layer of the adult mouse olfactory bulb is modulated by experience. *Eur. J. Neurosci.* 29, 1431–1439.

Cunha, C., Brambilla, R., and Thomas, K. L. (2010). A simple role for BDNF in learning and memory? *Front. Mol. Neurosci.* 3:1. doi: 10.3389/neuro.02.001.2010

D'Amelio, M., Cavallucci, V., and Cecconi, F. (2009). Neuronal caspase-3 signaling: not only cell death. *Cell Death Differ.* 17, 1104–1114.

Galvao, R. P., Garcia-Verdugo, J. M., and Alvarez-Buylla, A. (2008). Brain-derived neurotrophic factor signaling does not stimulate subventricular zone neurogenesis in adult mice and rats. *J. Neurosci.* 28, 13368–13383.

Izquierdo, I., Bevilaqua, L. R., Rossato, J. I., Bonini, J. S., Medina, J. H., and Cammarota, M. (2006). Different molecular cascades in different sites of the brain control memory consolidation. *Trends Neurosci.* 29, 496–505.

Kay, L. M., and Laurent, G. (1999). Odor- and context-dependent modulation of mitral cell activity in behaving rats. *Nat. Neurosci.* 2, 1003–1009.

Kelsch, W., Lin, C. W., Mosley, C. P., and Lois, C. (2009). A critical period for activity-dependent synaptic development during olfactory bulb adult neurogenesis. *J. Neurosci.* 29, 11852–11858.

Kermen, F., Sultan, S., Sacquet, J., Mandairon, N., and Didier, A. (2010). Consolidation of an olfactory memory trace in the olfactory bulb is required for learning-induced survival of adult-born neurons and long-term memory. *PLoS ONE* 5, e12118. doi: 10.1371/journal.pone.0012118

Lazarini, F., Mouthon, M. A., Gheusi, G., de Chaumont, F., Olivo-Marin, J. C., Lamarque, S., Abrous, D. N., Boussin, F. D., and Lledo, P. M. (2009). Cellular and behavioral effects of cranial irradiation of the subventricular zone in adult mice. *PLoS ONE* 4, e7017. doi: 10.1371/journal.pone.0007017

Livneh, Y., Feinstein, N., Klein, M., and Mizrahi, A. (2009). Sensory input enhances synaptogenesis of adult-born neurons. *J. Neurosci.* 29, 86–97.

Lledo, P. M., Alonso, M., and Grubb, M. S. (2006). Adult neurogenesis and functional plasticity in neuronal circuits. *Nat. Rev. Neurosci.* 7, 179–193.

Mandairon, N., Didier, A., and Linster, C. (2008). Odor enrichment increases interneurons responsiveness in spatially defined regions of the olfactory bulb correlated with perception. *Neurobiol. Learn. Mem.* 90, 178–184.

Mandairon, N., Sacquet, J., Garcia, S., Ravel, N., Jourdan, F., and Didier, A. (2006a). Neurogenic correlates of an olfactory discrimination task in the adult olfactory bulb. *Eur. J. Neurosci.* 24, 3578–3588.

Mandairon, N., Sacquet, J., Jourdan, F., and Didier, A. (2006b). Long-term fate and distribution of newborn cells in the adult mouse olfactory bulb: influences of olfactory deprivation. *Neuroscience* 141, 443–451.

Mandairon, N., Sultan, S., Rey, N., Kermen, F., Moreno, M., Busto, G., Farget, V., Messaoudi, B., Thevenet, M., and Didier, A. (2009). A computer-assisted odorized hole-board for testing olfactory perception in mice. *J. Neurosci. Methods* 180, 296–303.

Martin, C., Gervais, R., Hugues, E., Messaoudi, B., and Ravel, N. (2004). Learning modulation of odor-induced oscillatory responses in the rat olfactory bulb: a correlate of odor recognition? *J. Neurosci.* 24, 389–397.

Moreno, M. M., Linster, C., Escanilla, O., Sacquet, J., Didier, A., and Mandairon, N. (2009). Olfactory perceptual learning requires adult neurogenesis. *Proc. Natl. Acad. Sci. U.S.A.* 106, 17980–17985.

Mouret, A., Gheusi, G., Gabellec, M. M., de Chaumont, F., Olivo-Marin, J. C., and Lledo, P. M. (2008). Learning and survival of newly generated neurons: when time matters. *J. Neurosci.* 28, 11511–11516.

Mouret, A., Lepousez, G., Gras, J., Gabellec, M. M., and Lledo, P. M. (2009). Turnover of newborn olfactory bulb neurons optimizes olfaction. *J. Neurosci.* 29, 12302–12314.

Nissant, A., Bardy, C., Katagiri, H., Murray, K., and Lledo, P. M. (2009). Adult neurogenesis promotes synaptic plasticity in the olfactory bulb. *Nat. Neurosci.* 12, 728–730.

Pencea, V., Bingaman, K. D., Wiegand, S. J., and Luskin, M. B. (2001). Infusion of brain-derived neurotrophic factor into the lateral ventricle of the adult rat leads to new neurons in the parenchyma of the striatum, septum, thalamus, and hypothalamus. *J. Neurosci.* 21, 6706–6717.

Petreanu, L., and Alvarez-Buylla, A. (2002). Maturation and death of adult-born olfactory bulb granule neurons: role of olfaction. *J. Neurosci.* 22, 6106–6113.

Rochefort, C., Gheusi, G., Vincent, J. D., and Lledo, P. M. (2002). Enriched odor exposure increases the number of newborn neurons in the adult olfactory bulb and improves odor memory. *J. Neurosci.* 22, 2679–2689.

Salcedo, E., Zhang, C., Kronberg, E., and Restrepo, D. (2005). Analysis of training-induced changes in ethyl acetate odor maps using a new computational tool to map the glomerular layer of the olfactory bulb. *Chem. Senses* 30, 615–626.

Shepherd, G. M., Chen, W. R., Willhite, D., Migliore, M., and Greer, C. A. (2007). The olfactory granule cell: from classical enigma to central role in olfactory processing. *Brain Res. Rev.* 55, 373–382.

Sultan, S., Mandairon, N., Kermen, F., Garcia, S., Sacquet, J., and Didier, A. (2010). Learning-dependent neurogenesis in the olfactory bulb determines long-term olfactory memory. *FASEB J.* 24, 2355–2363.

Valley, M. T., Mullen, T. R., Schultz, L. C., Sagdullaev, B. T., and Firestein, S. (2009). Ablation of mouse adult neurogenesis alters olfactory bulb structure and olfactory fear conditioning. *Front. Neurosci.* 3:51. doi: 10.3389/neuro.22.003.2009

Veyrac, A., Sacquet, J., Nguyen, V., Marien, M., Jourdan, F., and Didier, A. (2009). Novelty determines the effects of olfactory enrichment on memory and neurogenesis through noradrenergic mechanisms. *Neuropsychopharmacology* 34, 786–795.

Winner, B., Cooper-Kuhn, C. M., Aigner, R., Winkler, J., and Kuhn, H. G. (2002). Long-term survival and cell death of newly generated neurons in the adult rat olfactory bulb. *Eur. J. Neurosci.* 16, 1681–1689.

Yamaguchi, M., and Mori, K. (2005). Critical period for sensory experience-dependent survival of newly generated granule cells in the adult mouse olfactory bulb. *Proc. Natl. Acad. Sci. U.S.A.* 102, 9697–9702.

Zigova, T., Pencea, V., Betarbet, R., Wiegand, S. J., Alexander, C., Bakay, R. A., and Luskin, M. B. (1998). Neuronal progenitor cells of the neonatal subventricular zone differentiate and disperse following transplantation into the adult rat striatum. *Cell Transplant.* 7, 137–156.

Conflict of Interest Statement: The authors declare that the research was conducted in the absence of any commercial or financial relationships that could be construed as a potential conflict of interest.

Received: 27 January 2011; accepted: 29 March 2011; published online: 03 May 2011.

Citation: Sultan S, Lefort JM, Sacquet J, Mandairon N and Didier A (2011) Acquisition of an olfactory associative task triggers a regionalized down-regulation of adult born neuron cell death. Front. Neurosci. ***5****:52. doi: 10.3389/fnins.2011.00052*

This article was submitted to Frontiers in Neurogenesis, a specialty of Frontiers in Neuroscience.

frontiers in
NEUROSCIENCE

REVIEW ARTICLE
published: 27 May 2011
doi: 10.3389/fnins.2011.00076

Multiple birthdating analyses in adult neurogenesis: a line-up of the usual suspects

María Llorens-Martín and José L. Trejo*

Department of Molecular, Cellular and Developmental Neurobiology, Cajal Institute, Madrid, Spain

Edited by:
Silvia De marchis, University of Turin, Italy

Reviewed by:
Muriel Koehl, Institut national de la santé et de la recherche médicale (Inserm), France
Helena Mira, Instituto de Salud Carlos III, Spain

***Correspondence:**
José L. Trejo, Department of Molecular, Cellular and Developmental Neurobiology, Cajal Institute, Av. Doctor Arce, 37, 28002 Madrid, Spain.
e-mail: jltrejo@cajal.csic.es

Analyzing the variation in different subpopulations of newborn neurons is central to the study of adult hippocampal neurogenesis. The acclaimed working hypothesis that different subpopulations of newborn, differentiating neurons could be playing different roles arouses great interest. Therefore, the physiological and quantitative analysis of neuronal subpopulations at different ages is critical to studies of neurogenesis. Such approaches allow cells of different ages to be identified by labeling them according to their probable date of birth. Until very recently, only neurons born at one specific time point could be identified in each experimental animal. However the introduction of different immunohistochemically compatible markers now enables multiple subpopulations of newborn neurons to be analyzed in the same animal as in a line-up, revealing the relationships between these subpopulations in response to specific influences or conditions. This review summarizes the current research carried out using these techniques and outlines some of the key applications.

Keywords: neurogenesis, dentate gyrus, dual birthdating, CldU, IdU, BrdU

INTRODUCTION

The accurate labeling of newborn cells in the adult brain poses a fundamental challenge in the study of adult neurogenesis. Adult brain neurogenesis is closely linked with learning and memory, and it has also been implicated in anxiety and depression (for recent reviews, see Aimone et al., 2010; Deng et al., 2010). Furthermore, many parameters associated with adult neurogenesis are altered in models of Alzheimer's and other neurodegenerative diseases, and in models of ischemia or schizophrenia. Adult neurogenesis has attracted considerable attention due to the cellular properties observed during this period, which may be adapted to rescue neuronal loss due to aging or neurodegenerative processes. In the adult hippocampus, newborn neurons are granule neurons of the dentate gyrus, whose precursors reside locally in the inner side of the granular layer, known as the subgranular zone (SGZ). The cells born in the adult dentate gyrus are derived from neural stem cells (NSC; type-1 cells); these cells are either quiescent (a small proportion) or divide slowly, to generate another group of rapidly dividing cells known as intermediate progenitor cells (type-2a cells). The progeny of these cells are neuroblasts that either continue to proliferate or exit the cell cycle to mature and differentiate into granule neurons, apparently indistinguishable from the rest of the dentate gyrus granule neurons. It will be important to note here that these cell populations can be traced using relatively specific markers (**Figure 1**). These markers can be easily used in conjunction with "birth-marking" labels to determine that the different subpopulations were actually born in the adult brain.

In recent years, the labeling of newly born cells in the adult brain has been almost overwhelmingly ruled by the use of 5-bromo-3′-deoxy-uridine (BrdU). "The underlying principle is straightforward: a permanent marker is brought into a cell of interest at the time point of division and the later fate of this cell is studied. Because the marker is persistent, it is possible to retrospectively conclude with confidence that a marked cell must have undergone cell division at the time when the marker was injected (*sic*)" (Kempermann, 2006). The protocol involves the administration of the thymidine analog (normally by intraperitoneal injection, and to a lesser extent via drinking water) which incorporates into the dual helix of any cell actively synthesizing DNA during the period the product remains systemically available and active in the body (usually around 2 h or less). After the animal is sacrificed, staining is detected by immunohistochemistry using antibodies specifically directed against the analog.

BrdU has been the marker of choice in recent years for several reasons, in part because this method requires no radioactivity unlike the use of tritiated thymidine, which for decades was used to label dividing cell populations during brain development. Furthermore, BrdU staining is readily detected by immunohistochemistry. The only significant drawback of this technique is the requirement to unmask the epitopes recognized by the primary antibody against BrdU using hydrochloric acid. Naturally there some other minor issues are involved in its use, though these have largely been solved over the years.

One of the most interesting parameters that can be assessed by the labeling of dividing cells is survival time, defined as the time between the incorporation of the BrdU and that of the animal's sacrifice. The age of labeled cells is equivalent to the survival time (i.e., cells are 1 month old if the animal injected with BrdU was sacrificed 1 month after BrdU injection).

A key limitation of this method is its ability to recognize only a single pool of BrdU incorporated into the body, regardless of when and how it was administered. This has significant implications: all incorporated BrdU is detected as a single signal, and hence, the cell populations that have incorporated BrdU are indistinguishable. Therefore, BrdU administration must be sufficiently discrete in time (depending on the experimental design)

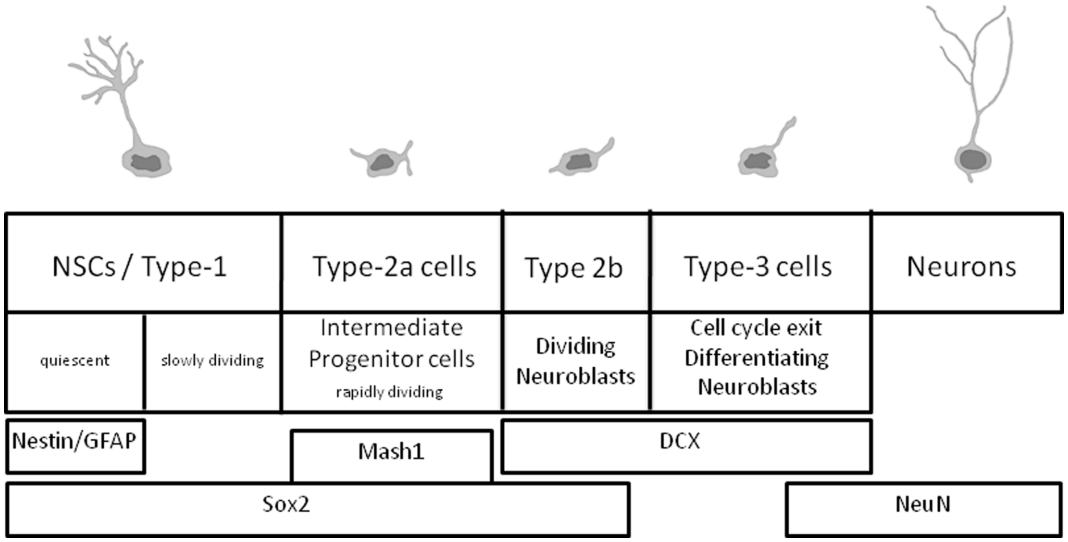

FIGURE 1 | Summary of the cell types in adult hippocampal neurogenesis and the expression of the main markers.

so that cell populations to be marked by BrdU are also consistent in terms of age. This issue is particularly important in short experiments (i.e., days). If the animal is injected with BrdU over *n* days, and sacrificed 1 week after the last injection, the cohort of labeled cells is considered to be between 7 and 7−*n* days old. Therefore, the injection rate in conjunction with the survival time can produce large differences, and in the worst cases, cell populations that are markedly heterogeneous in terms of age may be labeled equally. Within the framework of the experimental design, the investigator must judge what heterogeneity in terms of age can be accepted in the target cell population. In contrast, in a long-term survival experiment, several injections administered over consecutive days can label a cohort of cells that are subsequently identified as a single group, not taking into account the age difference between the cells marked by the first and the last injection.

This inherent limitation of BrdU labeling implies that each animal can only contain a population of cells marked, as homogeneous as possible in terms of age, precluding any distinction between cells of very different ages. BrdU injections at two times sufficiently separated would generate similarly labeled cells although they are very different. For this reason, the data from cell populations with qualitatively different ages has been achieved by using different experimental groups (different animals) that were subjected to different injection regimes of BrdU and/or different survival times (e.g., group A is sacrificed after 1 week to analyze 1 week old cells, while group B is sacrificed after 1 month to analyze 1 month old cells). This approach has generated a large amount of data. However, it is not a trivial matter that these comparisons between cell populations of different age, born in the adult brain, have been analyzed to date in different animals. It is clear that the study of possible direct relationships between subpopulations of qualitatively different age is strengthened considerably when performed in the same animal, avoiding potential confounding factors due to any intra-group variability between individuals. This problem can now be avoided by the use of a recent technique that permits two or three cell subpopulations of different ages to be labeled in the same animal.

This method involves the injection of the thymidine analogs 5-iodo-2′-deoxy-uridine (IdU) and 5-chloro-2′-deoxy-uridine (CldU), which can be unequivocally distinguished from one other using respective antibodies anti-CldU and anti-IdU, labeling two populations of different ages in the same animal.

It only takes a dual immunohistochemistry to detect the two cell populations of different age born in the adult brain, triple immunohistochemistry in the event that is also to characterize the phenotype of these two subpopulations.

The first attempts to cope with the problem were not so simple. Certainly, the first works reporting the separate detection of two different halogenated nucleotides that have been incorporated in DNA, used immunofluorescence dual-staining methods *in vitro* (Shibui et al., 1989; Bakker et al., 1991; Aten et al., 1992). However, these methods required complex histological procedures to distinguish between the two antibodies.

By using this technique, an early study by Manders et al. (1992) compared different replication patterns by using immunofluorescence dual staining of cell nuclei *in vitro*, after incorporating two independent markers of DNA replication in the same nucleus, and recording fluorescence signals with a dual-color confocal microscope. However, one of the first studies reporting the use of dual birthdate labeling in the brain used BrdU and IdU in human patients (Hoshino et al., 1992). The authors injected brain tumors patients with BrdU, followed 5 h later by IdU. The percentage of $BrdU^+$ cells was used to establish the S phase fraction, while the IdU/BrdU and BrdU/IdU ratios were used to establish the duration of the S phase and other parameters of cell cycle kinetics. Subsequently, Burns and Kuan (2005) were able to distinguish different cell populations depending on the embryonic day the cells were generated during cortical development, by using antibodies raised in different species (rat and mouse) to distinguish two deoxyuridines

(again BrdU and IdU), and further incubation with species-specific secondary antibodies conjugated to different fluorophores. This method permits the separate evaluation of dual-labeled cells (BrdU and IdU signal) and single-labeled cells (BrdU signal). This way, the authors also demonstrated the length of the S phase of neural progenitor cells in the adult mouse dentate gyrus.

CHARACTERIZATION AND SET-UP

A number of papers have described different approaches to implement these protocols. In most of them, both thymidine analogs were injected in the same animal to a number of individuals. The first consideration must be the analog dose injected. For this purpose, three important factors have to be taken into account in the use of two thymidine analogs at a time: (i) the absence of cross-reactivity in the immunohistochemistry, (ii) the possibility to detect them along with markers of lineage/differentiation, making possible the identification of the maturational state of the newborn cell/neuron and nevertheless, (iii) the ability to quantify the number of these cells by means of stereology. Each of these requirements can be fulfilled by the use of equimolar administration of CldU and IdU to the animals, as demonstrated by Vega and Peterson (2005).

For this goal, we have used in mice doses of CldU and IdU that are equimolar to the BrdU dose. Specifically, we use to prepare it according to the 50 mg/kg bw BrdU dose. This dose was selected because the cells with a nucleus completely filled by the labeling at this dose, or a nucleus containing easily identifiable patches of chromatin marked by the fluorophore at this dose, can clearly be identified as cells that were in S phase in time of administration of the thymidine analog, thus preventing to analyze cells with a weak incorporation possibly due to DNA repair or other unknown factors. The doses used were 42.75 mg/kg bw for CldU and 56.75 mg/kg bw for IdU. The use of saturating doses of BrdU, CldU, and IdU has been described previously by Leuner et al. (2009).

Nevertheless, the doses of thymidine analogs used in the literature vary considerably. One of the most common approaches is to administer a first analog over a 2–3 week period, and after a variable intermediate period without labeling (see Re-entering the cell cycle), then the second analog over a subsequent 2–3 week period. This protocol has usually been achieved by administering the nucleosides in drinking water (see for example Maslov et al., 2004; Gobeske et al., 2009) at 1 mg/ml both nucleosides, while Bonaguidi et al. (2008) used 1.15 mg/ml CldU and 0.85 mg/ml IdU with 2.5% sucrose. Other approaches consist of intraperitoneal injection of the analogs. This way the doses used has been heterogeneous either, see for example Bauer and Patterson (2005) using 16.67 mg/ml CldU in saline and 10 mg/ml IdU in PBS/NaOH, pH 8.0, while Gobeske et al. (2009), Mira et al. (2010), and Stone et al. (2010) used 10 mg/ml CldU in saline and IdU equimolar to CldU, what means to use doses adjusted volumetrically to the molar equivalent of 50 mg/kg BrdU for each animal. The authors used 42.5 mg/kg CldU and 57.5 mg/kg IdU.

Although a number of authors used doses of CldU and IdU equimolar to that of BrdU, this BrdU dose itself varies in the literature from 50 mg/kg bw BrdU (as used by ourselves), some others used equimolar doses to 100 mg/kg bw (for example Breunig et al., 2007). A number of other authors have published the use of equimolar doses but not mentioning to what BrdU dose.

Despite the variability in the protocols used, and despite the completely different injection regimes used, all these studies report reliable and consistent labeling. In our studies, CldU can easily be prepared in 0.9% saline. IdU by using 0.1 M PBS with 2 drops of 5N NaOH added per 10–15 ml PBS. This solution was then heated 2–3 times in a microwave oven without boiling and vigorously stirred manually.

The next parameter to be taken into account is the survival time. Several groups have used different survival times in different groups of animals to characterize and set-up the technique. Specifically, we injected CldU and IdU at different time points in the same animals and they were then sacrificed either 24 h or 2 weeks after the last injection.

Finally, mice were anesthetized with pentobarbital, transcardially perfused with saline followed by 4% paraformaldehyde in phosphate buffer (PB). The brains were removed, post-fixed overnight in the same fixative and sectioned with a vibratome (50 µm thick sections). The slices were pre-incubated with 0.5% Triton X-100 and 0.1% bovine serum albumin, and then dual immunohistochemistry was performed. Briefly, we used rat anti-CldU antibody (Accuratechemicals 1:500) and a mouse anti-IdU antibody (BD Biosciences 1:500) overnight. Primary antibodies were detected by using secondary Alexa-conjugated antibodies from Molecular Probes (1:1,000): Alexa 488 conjugated donkey anti-rat for the anti-CldU antibody, Alexa 594 conjugated donkey anti-mouse for the anti-IdU antibody overnight, and the reverse fluorophore-conjugated antibodies for the control experiments switching the colors of the secondary antibodies. Sections were counterstained finally with DAPI (Calbiochem 1:1,000) for 10 min.

We found and consistently replicate the result that cells were labeled in decreasing numbers with increasing survival time, as expected, and this was consistent for both analogs. In addition, the number of cells dual labeled for CldU and IdU ($CldU^+/IdU^+$ cells) in the same animal also decreases as the time between injections of each thymidine analog increased, as is expected (see **Figure 2** taken from Llorens-Martin et al., 2010).

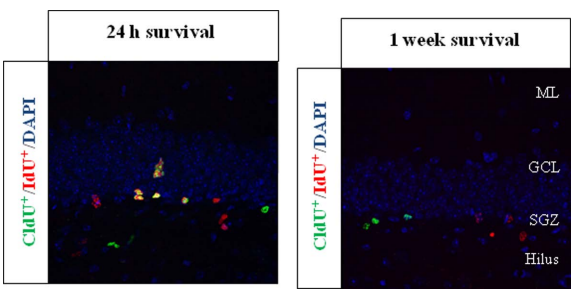

FIGURE 2 | Representative pictures of $CldU^+$ and IdU^+ cells in set-up experiments. The thymidine analogs were injected in the same individuals separated by either 24 h or 1 week; BrdU-equimolecular dosages of CldU and IdU were injected. Animals were then sacrificed 2 h after the last injection. We found that the injection of different thymidine analogs separated by more than 1 day (1 week survival) led to no overlapping of the labeling, while in the 24 h experiment a huge proportion of cells were co-labeled, as expected. The labeling was assessed in the hippocampal dentate gyrus of adult mice. The pictures were registered from 50 µm thick coronal sections, and both are taken from Llorens-Martin et al. (2010). ML, molecular layer; GCL, granule cell layer; SGZ, subgranular zone.

Other authors had previously demonstrated the feasibility and reliability of both analogs to produce a replicable and consistent labeling of dividing cells. In this way, Vega and Peterson (2005) showed that simultaneous equimolar delivery of both IdU and CldU co-labeled all cells with both markers. Next they demonstrated that the administration of equimolar concentrations of IdU and CldU 1 day apart is able to label three populations of proliferative cells (one of the markers or both together).

In a different experiment, we changed the order of the injections with respect to our design mentioned above; some animals were injected CldU first and later IdU, while other animals were injected in reverse order. The quality of aforementioned labeling unchanged whatever the order in which the analogs were injected. The number of cells obtained after 24 h survival either with CldU or IdU, and the number of cells obtained after 2 weeks survival by injecting CldU or IdU, were consistently similar.

Bonaguidi et al. (2008) performed a number of interesting control experiments. By labeling with IdU and CldU separated in time by several weeks, the authors could see in the granule cell layer (GCL) of the hippocampal dentate gyrus that older cells were located farther within the GCL than younger cells, consistent with labeling two temporally distinct precursor populations. Besides, dual-labeled cells were found in very low numbers.

Our experiments have all been performed in mice, like many other authors. However, a number of studies have reported similar protocols, and importantly, similar results about the reliability of the technique by using rats. Problems of specificity, cross-reactivity, and feasibility of the technique, don't therefore seem to rely on the species the experiments have been carried out up to date.

We have never encountered cross-reactivity problems of the antibodies in tissue from mice. Cross-reactivity has not been a major problem frequently reported in the literature, except for the early works by Shibui et al. (1989) by using BrdU and IdU, or the work by Aten et al. (1992) by using CldU and IdU detected by means of anti-BrdU antibodies specific for BrdU-CldU or only BrdU. The former work required complicated histological procedures to ensure the specificity of staining, while the second one required the use of a high-salt buffer to differentially remove binding from each substrate. None of these problems are common today with the commercially available antibodies.

TROUBLESHOOTING

The simplicity of the protocols reviewed here makes this technique affordable and easy to implement. There are no special considerations to take into account in dealing with the development of the technique (except for the commentaries on cross-reactivity above mentioned). However, we will mention a couple of minor issues: the first is the consideration on the order in which the analogs are injected into animals in experimental designs aimed at scoring two subpopulations of qualitatively different age. Although we have seen experimentally that CldU/IdU can be administered in any order obtaining identical results in the type and quality of cell labeling, we first administered in our experiments CldU, and IdU later, because the long-term experiments course with a significant non-negligible increase in body weight of animals, which forces to inject large amounts of the second analog. Due to the considerably greater cost of the current commercially available CldU versus IdU, we inject CldU first, when the animals are smaller, allowing to considerably save product.

The second is relative to the dissolution of the IdU. IdU has a low solubility in water. This should not be a problem if one has in mind a couple of considerations. First, the product should be prepared immediately prior to injection, taking great care to its dissolution (see above). Second, if the experiment includes a large number of animals, the product may begin to precipitate and crystallize after half an hour of its dissolution. In this case, the product must be re-diluted, or, if it is expected to spend more than half an hour to inject all animals, the product can be prepared in two batches.

CONCERNS

The use of thymidine analogs CldU and IdU might hit a last hurdle: the sensitivity and specificity of these analogs was not enough to carry out reliable studies (Leuner et al., 2009). Of course, if the sensitivity is somewhat lower than that of BrdU, it is not a relevant issue if we are not interested in calculating an estimate of the actual number of cells in the tissue under study. If this were the case, the analysis of the data would suffer with this concern. But for comparative studies of experimental animal groups treated equally, the differential sensitivity with respect to BrdU is not relevant, because it is not here to estimate the actual number of cells in S phase at the time of injection to survive until sacrificing the animal, but rather to compare the apparent number of these cells between experimental groups. This assertion deserves a deeper discussion: it is not that our estimate (the number of labeled cells, obtained by using similar CldU and IdU), is biased. By contrast, the differential relative sensitivities of CldU and IdU, among themselves and with BrdU, and the greater penetration and specificity of the respective antibodies will simply yield estimates of the number of labeled cells that are not intrinsically comparable, but each marker itself is not biased. In a word, different analogs produce different data accuracy in terms of sensitivity, but we have no *prime facie* evidence that the resulting estimator is biased. Therefore, it is quite useful for comparison between experimental groups. It is not, however, to compare studies from different authors if some use BrdU and other CldU, for example, or if the object of study is to estimate the actual number of surviving cells that were in S phase at the time of injection.

SOME RESULTS AND DISCUSSION

Labeling of cell nucleus with the thymidine analog BrdU has been used to identify proliferating cells for years (see for example Wojtowicz and Kee, 2006). The progression through S phase is considered a hallmark event to birthdate a cell. CldU and IdU can reliably be used in the same way (Vega and Peterson, 2005). "Because neurons are strictly postmitotic, a BrdU-positive neuron that is detected *some time* after BrdU injection must have originated from a cell that divided at exactly the time when BrdU was systemically available (*sic*)" (Kempermann, 2006). CldU and IdU are known from 45 years ago, and its potential for dual labeling has been used in cytometry over the last 30 years (for a recent review, see for example Yokochi and Gilbert, 2007). However, its application for the studies of adult neurogenesis

has not begun until the middle of the last decade, including the analysis of its ability to be used to identify transplanted cells to the central nervous system (see Burns et al., 2006 for a study of the potential for transfer of thymidine analogs from grafted cells to dividing host cells).

CORRELATIONS BETWEEN CELL POPULATIONS OF DIFFERENT AGE

One of the biggest advantages of studying two cell populations of qualitatively different age in the same animal is that any hypothetical relationship between such populations can be analyzed directly. For example, one obvious and direct relationship, the possible influence of higher or lower rate of survival of an older cell population on the survival rate of the younger cell population, for instance, can be ruled out by analyzing the correlation between the numbers of cells in each population. The higher or lower number of older newborn cells can be correlated significantly with greater or lesser number of younger newborn cells. So we can discard or not a working hypothesis based on the premise that the quantity of one population could affect the survival of the other subpopulation. So far, this analysis would be performed by evaluating the effect of a given treatment on two experimental groups made of different animals, each group with a unique different labeling, one group to study a population of age X, and another group to study the population of age 2X, for example. The results would take the following form: the effect of treatment is that the survival of the younger population X is increased (or vice versa), while the survival of the older population 2X decreases (or vice versa). In this format, no further conclusions could be drawn, but most important, it is always possible to argue that unknown factors may have influenced the difference in treatment effect, what we call a group effect.

By contrast, with two immunohistochemically compatible markers as CldU and IdU, the analysis could be done by evaluating the effect of treatment on only one group of animals, avoiding the group effect. The results would take the following form: the effect of treatment is that the survival of X increases (or decreases), while 2X survival decreases (or increases), and a statistically significant correlation (or not) exists between both populations, in the sense that the animals with a higher number of 2X old cells, have fewer X old cells, for example. This conclusion alone allows to assess a hypothesis formulated as "the number of adult-born neurons surviving a treatment or condition in a given brain region, affects or modulates the survival of neurons born at a later stage in the same region."

A quantitative approach as specified, on the number of new neurons, can also be adapted to assess a number of different morphological features, such as the degree of maturation of new neurons, the expression of other markers of differentiation, the number of dendritic branches, the number of synaptic buttons, etc. Such an approach has been recently used by Tronel et al. (2010), to demonstrate that spatial learning influences the development of the dendritic trees of the newborn neurons through different, interrelated ways depending on the age and differentiation stage of the different subpopulations of new cells.

All assumptions made about the possible influence of a population of old new neurons on young new neurons arise from the possibility of studying both subpopulations coexisting together in the same tissue, coexisting in a single section of one animal, in the same way as suspects must be identified in a line-up in which they are all placed together in front of the witness. This method, when possible, is significantly more reliable than attempting to identify suspects by just looking at them one at a time. Similarly, any comparison of different populations is most effective when performed in the same animal. This immediately rules out possible artifacts or unknown interfering factors that could contribute to the effects observed in different animals.

In a recent study, our group addressed the issue that environmental enrichment (EE) specifically modulates hippocampal neurogenic cell populations over time (Llorens-Martin et al., 2010). We used the dual-birthdating to study two subpopulations of newborn neuron in mice: those born at the beginning and at the end of enrichment. In this way, we demonstrate that while short-term cell survival is upregulated after an initial 1 week period of enrichment, after long-term enrichment (2 months) neither cell proliferation nor the survival of the younger newly born cell populations are distinguishable from that observed in non-enriched control mice. In addition, we show that the survival of older newborn neurons alone (i.e., those born at the beginning of the enrichment) is higher than in controls, due to the significantly lower levels of cell death. These findings suggested an early selective, long-lasting effect of EE on the neurons born in the initial stages of enrichment. Therefore, we could conclude that EE induces differential effects on distinct subpopulations of newborn neurons depending on the age of the immature cells.

A different and elegant approach of this analysis was used by Bauer and Patterson (2005) to distinguish between nucleoside incorporation due to either cell proliferation or DNA repair/apoptosis, by injection of IdU and CldU before and after brain irradiation, respectively. With this approach, the authors were able to compare the putative incorporation of nucleoside during DNA repair (after irradiation, through a possible increase in CldU labeling due to cell proliferation plus DNA repair) and the IdU incorporation (due to cell proliferation only). They reported evidences that nucleosides are not significantly incorporated during DNA repair in the adult brain, and that labeling is not detected in dying postmitotic neurons.

Similarly, CldU and IdU injection before or after EE or running were used to analyze the promoting effect of physical-cognitive activity on the different cell subpopulations involved in the neurogenic process, by means of a complete battery of neurogenic markers (Gobeske et al., 2009). Thus, CldU or IdU labeling, together with cell lineage identity assessment (by means of Sox2 or GFAP for NSC, nestin for early progenitors, doublecortin for young neurons, and NeuN for mature neurons) enabled the authors to conclude the role of the signaling pathway they were interested (BMP) in the neurogenic process and its role as a mediator of the procognitive and proneurogenic effects of enrichment and exercise. Importantly, they demonstrated that both exercise and *noggin* increased proliferation across the lineage: from progenitors to neuroblasts, but also that increased medium-term survival (7–10 days). This work is a very good example of how the dual-birthdating technique can be combined with a battery of molecular markers to better characterize the cellular subpopulations under study.

Obviously, the approaches listed here are only the first assays using CldU and IdU (together with other techniques) that have been published applied to the analysis of adult neurogenesis. Many others are possible and will be published shortly. Just to mention a few of them, one interesting possibility might be the use of retroviruses to infect dividing cells in the dentate GCL of adult animals. Recently, Tronel et al. (2010) published an interesting study demonstrating that learning-induced changes in new neurons are long-lasting and specific to adult-born neurons in the dentate gyrus. For this purpose, the authors labeled newborn neurons by infecting the dentate gyrus with a retrovirus with a ubiquitous, long-term GFP-expressing promoter. On the same day, animals were administered BrdU. This way the authors could show the influence of learning on the length of dendrites of 3-month old newborn neurons (BrdU labeled). This type of analysis will be extended further in the near future by the use of dual-birthdating, by incorporating both CldU and IdU, and retrovirus infection at different time points. A recent review about these last approaches and its combination with dual-birthdating markers has been published by Landgren and Curtis (2010).

A different approach has been used to distinguish between newborn granule neurons in the adult dentate gyrus (labeled with IdU) and the granule neurons born during development (CldU). With this technique, Stone et al. (2010) have demonstrated that the integration rates of dentate granule neurons into memory networks does not appear to depend on the developmental stage of generation of granule cells, and that a functional equivalence between the different developmental stages exist.

DUAL-BIRTHDATING AND BEHAVIOR

The comparison of two neuronal populations of different ages in the same animal can be particularly informative when combined with behavioral analyses. Until very recently, and even today, many studies have evaluated the effect of a treatment or an animal's condition on their behavior and on neurogenesis in separate groups of animals. Thus, these studies were required to consider the possible effects of behavioral testing on the survival or proliferation of newborn neurons. Many other studies accounted for this possible influence by quantifying neurogenesis both in groups of animals undergoing behavioral tests and in untested animals (see e.g., Llorens-Martin et al., 2007). It is obvious that after taking into account the possible effect of behavior on neurogenesis, the most interesting studies of neurogenesis and behavior should be carried out in the same animals. For example, it is of great interest to determine whether a treatment or condition has anxiolytic and/or procognitive effects, and increases adult hippocampal neurogenesis in the same animal. However, this whole approach should be made in duplicate to assess a second subpopulation of new neurons of different age. Up to date, the problem was that in this case, it could always be argued that they were different animals, and that the response in behavioral tests could differ between experimental groups in a way that influenced neurogenesis.

In contrast, using two immunohistochemically compatible markers in the same animal, which also undergoes a behavioral testing, it is now possible to test the hypothesis whether the implementation of a behavior, or the effect of a treatment or condition on such behavior is related to a variation in an old or young neurogenic population and not the other, because everything is quantified in the same animal (taken into account once again the possibility of the influence of behavioral tests on neurogenesis, as already mentioned).

One of the earliest and best examples about how to take advantage of this kind of approach is the elegant work by the laboratory of Nora Abrous (Dupret et al., 2007). The authors injected rats with IdU 7 days before a water maze training in order to label the newborn cells for which survival should be increased by learning. CldU was injected 3 days before the start of the training in order to label newly born cells that, as stated in the working hypothesis, might die as a consequence of learning. They found that learning promoted the survival of IdU-labeled cells generated 1 week before exposure to the task, while decreased the survival of CldU-labeled cells that were born 3 days before the start of the training. Both groups of data were associated with the corresponding decreases and increases in positive labeled pyknotic nuclei, respectively. This way the authors showed that learning-induced increases in survival and apoptosis of newborn cells are interrelated processes, and that learning promotes survival of relatively mature neurons, apoptosis of more immature cells, and finally, proliferation of neural precursors.

DIFFERENT STIMULI OR RE-EXPOSITION TO A STIMULUS AND DUAL LABELING OF NEWBORN NEURONS

A different and interesting target where the present approach can be quite useful deals with the re-exposition of animals to given stimuli. Our laboratory has addressed recently the issue whether the antidepressant and proneurogenic effects of EE are different in animals that are naïve or pre-exposed to the stress inducing helplessness, and whether these differential effects are exerted on distinct neurogenic subpopulations (Llorens-Martín, Tejeda and Trejo, submitted). The repeated exposure to a forced swimming stressor was analyzed together with the effects of EE on different neurogenic populations distinguished by age and differentiation state, by means of using CldU and IdU at separated times in the same animals. We have found that younger cells are more sensitive and responsive to the conditions, both the positive and negative effects. These data will be relevant to identify the cell populations that are the targets of stress, depression, and enrichment, and that form part of the mechanism responsible for mood dysfunctions.

TEMPORAL DISCRIMINATION OF CELL CYCLE

All the approaches described so far takes advantage of the use of the two markers in distinct neuronal populations generated at distinct times. But a second approach that is now possible to address through the use of two immunohistochemically compatible markers, benefits from the use of the two markers very close in time. A first benefit of such an approach is to analyze the effect of a given treatment on proliferation or immediate survival, compared with the effect on short-term survival. An interesting study that took advantage of this benefit of dual labeling is the work by Thomas et al. (2007). The authors tested the hypothesis whether an acute psychosocial stress affected proliferation, short-term survival or immediate survival. They used sequential thymidine analog administration (CldU and IdU) as follows: three consecutive days of twice-daily (every 12 h) injections of either IdU (the first 2 days)

or CldU (the third day). Next, the animals were sacrificed either on day forth or 7 days later. This way, the authors were able to temporally discriminate DNA replication, by administering equimolar doses of CldU and IdU that, in turn, were equimolar of BrdU usual doses. As stress session took place in the third day, when CldU was injected, the authors could demonstrate that short-term survival but not initial proliferation or immediate survival was altered in response to stress.

RE-ENTERING THE CELL CYCLE

The use of two deoxyuridines has been used to analyze cell populations able to eventually re-enter the cell cycle. Adult neurogenic niches are characterized for having a rapidly dividing population of proliferative progenitors, and a slowly dividing population of NSC that maintain themselves and generate the progenitors; the latter population therefore retain for longer times a nucleoside label. The approach consists of an initial period of administration of the first analog (2–3 weeks) during which NSC, proliferative progenitors, and a proportion of more differentiated cells will become labeled. However, only some cells will retain labeling, either slowly dividing NSC or differentiated cells (cells which did not dilute the labeling due to active division). The surviving population that retain label for long periods can next be distinguished by administration of a 2–3 weeks second round of a second analog, that will be incorporated only by NSC. Maslov et al. (2004) used this approach with IdU and CldU to establish whether cells that retain a first nucleoside over long periods eventually re-enter the cell cycle in the subependymal zone (SVZ) of the lateral ventricles. Bonaguidi et al. (2008) did the same in the SGZ of the hippocampal dentate gyrus, to demonstrate that the SGZ contains a small population of slowly dividing NSC.

With a similar approach, other works have analyzed the distinct subpopulations of newborn cells able to exit or re-enter the cell cycle after a manipulation of a putative regulative factor is made [like for example in the study of Notch by Breunig et al. (2007)]. And recently, the different properties, morphologies, and mechanisms controlling maintenance and differentiation of distinct subpopulations of NSC in the adult dentate gyrus GCL, has been explored by Lugert et al. (2010) by using CldU and IdU separated by 1–6 or 11 days in different sets of experiments, to demonstrate that two distinguishable populations of NSC exist in the SGZ (quiescent and actively dividing), and importantly, some of these cells can reversibly change its properties to reconstitute the quiescent or the dividing subpopulations, a process involving Notch.

By using the same reasoning above mentioned, this approach let Mira et al. (2010) demonstrate the delicate equilibrium between neural stem cell proliferation and quiescence in the SGZ, supposedly intended to prevent the premature depletion of NSC activity in the mature brain. The authors used the BMP signaling pathway and noggin in a way similar to that above mentioned, to study the consequences of depleting the pool of quiescent NSC. They used CldU at the time when noggin was administered, and IdU several weeks later, thereby $CldU^+$ cells retaining label are either NSCs that do not dilute the nucleoside or cells that have matured to granule neurons. That way, the authors could analyze the NSCs that re-entered the cell cycle by means of the dual labeling with IdU. Some other authors have used the same strategy, for example to analyze the effect of LIF on NSCs from ventricular zone (Bauer and Patterson, 2006). A recent review of these approaches and its technical details has been published (Tuttle et al., 2010).

A second benefit stems from the fact that whether the time difference in the administration of the two markers is short enough, it is likely that a proportion of cells that captured the first analog during S phase of cell cycle can be detected in a new round of S phase of the cycle with the second analog. This possibility opens the door to studies in which a particular treatment or condition may have an influence on cell cycle re-entry in neurogenic subpopulations during short time periods, and to study the intermediate progenitor cells subpopulation. One such study has been published recently (Brandt et al., 2010), designed to distinguish between cell cycle exit and continued division at the progenitor cell level. Specifically, the authors analyze the proportion of type-2b/3 cells re-entering S phase by labeling the cells by means of the two thymidine analogs. This way, Brandt and collaborators have demonstrated that running promotes both proliferation and cell cycle exit of DCX^+ type-3 precursors.

MULTIPLE LABELING

Recent work (Chehrehasa et al., 2009) has shown the possibility to label two different populations of dividing cells by means of BrdU (revealed by immunohistochemistry as mentioned), and EdU (the thymidine analog 5-ethyl-2′-deoxyuridine, detected by click chemistry; Bradford and Clarke, 2011). However, several laboratories including ours are experiencing some complications to implement triple labeling including EdU, because some of the commercially available antibodies against CldU or IdU cross-react with EdU.

We do not doubt that soon we will see the solution of these transient technical problems and we will witness the chance to label more than two subpopulations of cycling cells in the same animal by using three markers. The only limits will be the number of both secondary antibodies and colors separated enough to be clearly differentiated in the confocal microscope we can get.

CONCLUSION

We think that the possibility of reliably detecting dual labels of cell birthdating ("birth-marking" labels; Kempermann, 2006) represents a qualitative improvement in the tools available to analyze adult neurogenesis, as we demonstrate in the studies cited here. The ability to unequivocally identify separate subpopulations of newborn neurons, according to their age, each with putative different maturational states and in turn, different properties, will continue to improve (however, see the interesting insight by Eisch and Mandyam, 2007) advancing in the analysis of the role/s of the immature new neurons, because the properties of different populations of newborn neurons and their influence in the performance of different behaviors will be fully understood only when studied in the same animal.

ACKNOWLEDGMENT

The authors wish to thank Gonzalo S. Tejeda for his help with the setup and performance of some experiments mentioned in this manuscript, Dr. Mark Sefton for his assistance in revising the manuscript, and Simona Gradari for her contribution to the drawings in **Figure 1**. This work was supported by a grant from Spanish Ministerio de Educación y Ciencia, BFU2007-60195/BFI, to José L. Trejo.

REFERENCES

Aimone, J. B., Deng, W., and Gage, F. H. (2010). Adult neurogenesis: integrating theories and separating functions. *Trends Cogn. Sci.* (*Regul. Ed.*) 14, 325–337.

Aten, J. A., Bakker, P. J., Stap, J., Boschman, G. A., and Veenhof, C. H. (1992). DNA dual labelling with IdUrd and CldUrd for spatial and temporal analysis of cell proliferation and DNA replication. *Histochem. J.* 24, 251–259.

Bakker, P. J., Stap, J., Tukker, C. J., van Oven, C. H., Veenhof, C. H., and Aten, J. (1991). An indirect immunofluorescence dual staining procedure for the simultaneous flow cytometric measurement of iodo- and chlorodeoxyuridine incorporated into DNA. *Cytometry* 12, 366–372.

Bauer, S., and Patterson, P. H. (2005). The cell cycle-apoptosis connection revisited in the adult brain. *J. Cell Biol.* 171, 641–650.

Bauer, S., and Patterson, P. H. (2006). Leukemia inhibitory factor promotes neural stem cell self-renewal in the adult brain. *J. Neurosci.* 26, 12089–12099.

Bonaguidi, M. A., Peng, C. Y., McGuire, T., Falciglia, G., Gobeske, K. T., Czeisler, C., and Kessler, J. A. (2008). Noggin expands neural stem cells in the adult hippocampus. *J. Neurosci.* 28, 9194–9204.

Bradford, J. A., and Clarke, S. T. (2011). Dual-pulse labeling using 5-ethynyl-2′-deoxyuridine (EdU) and 5-bromo-2′-deoxyuridine (BrdU) in flow cytometry. *Curr. Protoc. Cytom.* Chapter 7, Unit7 38, PMID 21207361.

Brandt, M. D., Maass, A., Kempermann, G., and Storch, A. (2010). Physical exercise increases Notch activity, proliferation and cell cycle exit of type-3 progenitor cells in adult hippocampal neurogenesis. *Eur. J. Neurosci.* 32, 1256–1264.

Breunig, J. J., Silbereis, J., Vaccarino, F. M., Sestan, N., and Rakic, P. (2007). Notch regulates cell fate and dendrite morphology of newborn neurons in the postnatal dentate gyrus. *Proc. Natl. Acad. Sci. U.S.A.* 104, 20558–20563.

Burns, K. A., and Kuan, C. Y. (2005). Low doses of bromo- and iododeoxyuridine produce near-saturation labeling of adult proliferative populations in the dentate gyrus. *Eur. J. Neurosci.* 21, 803–807.

Burns, T. C., Ortiz-Gonzalez, X. R., Gutierrez-Perez, M., Keene, C. D., Sharda, R., Demorest, Z. L., Jiang, Y., Nelson-Holte, M., Soriano, M., Nakagawa, Y., Luquin, M. R., Garcia-Verdugo, J. M., Prosper, F., Low, W. C., and Verfaillie, C. M. (2006). Thymidine analogues are transferred from prelabeled donor to host cells in the central nervous system after transplantation: a word of caution. *Stem Cells* 24, 1121–1127.

Chehrehasa, F., Meedeniya, A. C., Dwyer, P., Abrahamsen, G., and Mackay-Sim, A. (2009). EdU, a new thymidine analogue for labelling proliferating cells in the nervous system. *J. Neurosci. Methods* 177, 122–130.

Deng, W., Aimone, J. B., and Gage, F. H. (2010). New neurons and new memories: how does adult hippocampal neurogenesis affect learning and memory? *Nat. Rev. Neurosci.* 11, 339–350.

Dupret, D., Fabre, A., Dobrossy, M. D., Panatier, A., Rodriguez, J. J., Lamarque, S., Lemaire, V., Oliet, S. H., Piazza, P. V., and Abrous, D. N. (2007). Spatial learning depends on both the addition and removal of new hippocampal neurons. *PLoS Biol.* 5, e214. doi: 10.1371/journal.pbio.0050214

Eisch, A. J., and Mandyam, C. D. (2007). Adult neurogenesis: can analysis of cell cycle proteins move us "Beyond BrdU"? *Curr. Pharm. Biotechnol.* 8, 147–165.

Gobeske, K. T., Das, S., Bonaguidi, M. A., Weiss, C., Radulovic, J., Disterhoft, J. F., and Kessler, J. A. (2009). BMP signaling mediates effects of exercise on hippocampal neurogenesis and cognition in mice. *PLoS One* 4, e7506. doi: 10.1371/journal.pone.0007506

Hoshino, T., Ito, S., Asai, A., Shibuya, M., Prados, M. D., Dodson, B. A., Davis, R. L., and Wilson, C. B. (1992). Cell kinetic analysis of human brain tumors by in situ dual labelling with bromodeoxyuridine and iododeoxyuridine. *Int. J. Cancer* 50, 1–5.

Kempermann, G. (2006). *Adult Neurogenesis*. New York: Oxford University Press.

Landgren, H., and Curtis, M. A. (2010). Locating and labeling neural stem cells in the brain. *J. Cell. Physiol.* 226, 1–7.

Leuner, B., Glasper, E. R., and Gould, E. (2009). Thymidine analogue methods for studies of adult neurogenesis are not equally sensitive. *J. Comp. Neurol.* 517, 123–133.

Llorens-Martin, M., Tejeda, G. S., and Trejo, J. L. (2010). Differential regulation of the variations induced by environmental richness in adult neurogenesis as a function of time: a dual birthdating analysis. *PLoS One* 5, e12188. doi: 10.1371/journal.pone.0012188

Llorens-Martin, M. V., Rueda, N., Martinez-Cue, C., Torres-Aleman, I., Florez, J., and Trejo, J. L. (2007). Both increases in immature dentate neuron number and decreases of immobility time in the forced swim test occurred in parallel after environmental enrichment of mice. *Neuroscience* 147, 631–638.

Lugert, S., Basak, O., Knuckles, P., Haussler, U., Fabel, K., Gotz, M., Haas, C. A., Kempermann, G., Taylor, V., and Giachino, C. (2010). Quiescent and active hippocampal neural stem cells with distinct morphologies respond selectively to physiological and pathological stimuli and aging. *Cell Stem Cell* 6, 445–456.

Manders, E. M., Stap, J., Brakenhoff, G. J., van Driel, R., and Aten, J. A. (1992). Dynamics of three-dimensional replication patterns during the S-phase, analysed by dual labelling of DNA and confocal microscopy. *J. Cell. Sci.* 103, 857–862.

Maslov, A. Y., Barone, T. A., Plunkett, R. J., and Pruitt, S. C. (2004). Neural stem cell detection, characterization, and age-related changes in the subventricular zone of mice. *J. Neurosci.* 24, 1726–1733.

Mira, H., Andreu, Z., Suh, H., Lie, D. C., Jessberger, S., Consiglio, A., San Emeterio, J., Hortiguela, R., Marques-Torrejon, M. A., Nakashima, K., Colak, D., Gotz, M., Farinas, I., and Gage, F. H. (2010). Signaling through BMPR-IA regulates quiescence and long-term activity of neural stem cells in the adult hippocampus. *Cell Stem Cell* 7, 78–89.

Shibui, S., Hoshino, T., Vanderlaan, M., and Gray, J. W. (1989). Dual labeling with iodo- and bromodeoxyuridine for cell kinetics studies. *J. Histochem. Cytochem.* 37, 1007–1011.

Stone, S. S., Teixeira, C. M., Zaslavsky, K., Wheeler, A. L., Martinez-Canabal, A., Wang, A. H., Sakaguchi, M., Lozano, A. M., and Frankland, P. W. (2010). Functional convergence of developmentally and adult-generated granule cells in dentate gyrus circuits supporting hippocampus-dependent memory. *Hippocampus*, doi: 10.1002/hipo.20845. [Epub ahead of print].

Thomas, R. M., Hotsenpiller, G., and Peterson, D. A. (2007). Acute psychosocial stress reduces cell survival in adult hippocampal neurogenesis without altering proliferation. *J. Neurosci.* 27, 2734–2743.

Tronel, S., Fabre, A., Charrier, V., Oliet, S. H., Gage, F. H., and Abrous, D. N. (2010). Spatial learning sculpts the dendritic arbor of adult-born hippocampal neurons. *Proc. Natl. Acad. Sci. U.S.A.* 107, 7963–7968.

Tuttle, A. H., Rankin, M. M., Teta, M., Sartori, D. J., Stein, G. M., Kim, G. J., Virgilio, C., Granger, A., Zhou, D., Long, S. H., Schiffman, A. B., and Kushner, J. A. (2010). Immunofluorescent detection of two thymidine analogueues (CldU and IdU) in primary tissue. *J. Vis. Exp.* 46, 2166.

Vega, C. J., and Peterson, D. A. (2005). Stem cell proliferative history in tissue revealed by temporal halogenated thymidine analogue discrimination. *Nat. Methods* 2, 167–169.

Wojtowicz, J. M., and Kee, N. (2006). BrdU assay for neurogenesis in rodents. *Nat. Protoc.* 1, 1399–1405.

Yokochi, T., and Gilbert, D. M. (2007). Replication labeling with halogenated thymidine analogues. *Curr. Protoc. Cell Biol.* Chapter 22, Unit 22 10, PMID 18228503.

Conflict of Interest Statement: The authors declare that the research was conducted in the absence of any commercial or financial relationships that could be construed as a potential conflict of interest.

*Received: 20 January 2011; accepted: 17 May 2011; published online: 27 May 2011. Citation: Llorens-Martín M and Trejo JL (2011) Multiple birthdating analyses in adult neurogenesis: a line-up of the usual suspects. Front. Neurosci. **5**:76. doi: 10.3389/fnins.2011.00076*

This article was submitted to Frontiers in Neurogenesis, a specialty of Frontiers in Neuroscience.

frontiers in
NEUROSCIENCE

REVIEW ARTICLE
published: 02 May 2011
doi: 10.3389/fnins.2011.00064

Genetic methods to identify and manipulate newly born neurons in the adult brain

Itaru Imayoshi[1,2,3]*, Masayuki Sakamoto[1,4,5] and Ryoichiro Kageyama[1,4]*

[1] *Institute for Virus Research, Kyoto University, Kyoto, Japan*
[2] *The Hakubi Center, Kyoto University, Kyoto, Japan*
[3] *Japan Science and Technology Agency, Precursory Research for Embryonic Science and Technology, Japan*
[4] *Japan Science and Technology Agency, Core Research for Evolutional Science and Technology, Japan*
[5] *Graduate School of Biostudies, Kyoto University, Kyoto, Japan*

Edited by:
Silvia De Marchis, University of Turin, Italy

Reviewed by:
Claudio Giachino, Max Planck Institute, Germany
Michele Studer, INSERM, France

***Correspondence:**
Itaru Imayoshi and Ryoichiro Kageyama, Institute for Virus Research, Kyoto University, Shogoin-Kawahara, Sakyo-ku, Kyoto 606-8507, Japan.
e-mail: iimayosh@virus.kyoto-u.ac.jp; rkageyam@virus.kyoto-u.ac.jp

Although mammalian neurogenesis is mostly completed by the perinatal period, new neurons are continuously generated in the subventricular zone of the lateral ventricle and the subgranular zone of the hippocampal dentate gyrus. Since the discovery of adult neurogenesis, many extensive studies have been performed on various aspects of adult neurogenesis, including proliferation and fate-specification of adult neural stem cells, and the migration, maturation and synaptic integration of newly born neurons. Furthermore, recent research has shed light on the intensive contribution of adult neurogenesis to olfactory-related and hippocampus-mediated brain functions. The field of adult neurogenesis progressed tremendously thanks to technical advances that facilitate the identification and selective manipulation of newly born neurons among billions of pre-existing neurons in the adult central nervous system. In this review, we introduce recent advances in the methodologies for visualizing newly generated neurons and manipulating neurogenesis in the adult brain. Particularly, the application of site-specific recombinases and Tet inducible system in combination with transgenic or gene targeting strategy is discussed in further detail.

Keywords: adult neurogenesis, neural stem cells, Cre/loxP, CreERT2, transgenic mice, nestin

INTRODUCTION

It is now widely accepted that in mammals, including humans, newly born neurons are continuously generated and incorporated into the functional neural network of the adult brain (McKay, 1997; Gage, 2000; Temple, 2001; Ming and Song, 2005; Imayoshi et al., 2008, 2009). Neurogenesis in the mature adult brain was first reported by Altman and colleagues using a [H^3]-thymidine-incorporation labeling method in the dentate gyrus (DG) of the rat hippocampus (Altman and Das, 1965). They published a series of research articles describing neurogenesis in various regions of the adult rat brain, including the neocortex and olfactory bulb (OB; Altman, 1966, 1969). The long-term survival of newly born neurons in the hippocampus has also been demonstrated (Kaplan and Hinds, 1977). The development of a bromodeoxyuridine (BrdU)-incorporation labeling method enabled us to analyze the characteristics of newly born neurons in combination with immunohistochemistry. Adult neurogenesis has been observed with BrdU incorporation in all mammals examined, including humans (Eriksson et al., 1998).

In the rodent brain, neurogenesis predominantly occurs in two brain regions, the subventricular zone (SVZ) of the lateral ventricles and the subgranular zone (SGZ) of the hippocampal DG (Alvarez-Buylla et al., 2001; Lledo et al., 2006; Zhao et al., 2006). A large number of neurons born in the SVZ migrate into the OB and become local interneurons (granule cells and periglomerular cells), while neurons born in the SGZ migrate into the granule cell layer and become granule cells of the DG. Newly born neurons are incorporated into the functional neural networks of the OB and the DG, suggesting a significant impact of adult neurogenesis on neural circuit plasticity, and various brain functions, including learning and memory (van Praag et al., 2002; Carleton et al., 2003; Kee et al. 2007; Adam and Mizrahi, 2010; Deng et al., 2010; Lazarini and Lledo, 2011). Neurogenesis outside these two regions appears to be extremely limited in the intact adult mammalian central nervous system (CNS). After pathological stimulation, such as brain insults or seizures, adult neurogenesis appears to occur in regions otherwise considered to be non-neurogenic, such as the striatum and neocortex (Ming and Song, 2005; Gould, 2007).

The field of adult neurogenesis progressed thanks to technical advances that facilitate the identification and selective manipulation of newly born neurons among billions of pre-existing neurons in the adult CNS (Deng et al., 2010; Kelsch et al., 2010; Lacar et al., 2010). Newly generated neurons can be identified and/or manipulated by various approaches, such as the incorporation of nucleotide analogs, retrovirus-mediated gene transfer, and genetic methods using transgenic mice. The ablation of neural stem/progenitor cells using irradiation, with antimitotic drugs, or the transgenic expression of toxin genes are common strategies to study the functional importance of adult neurogenesis. Accumulating evidence has suggested a correlation between the magnitude of adult neurogenesis and an animal's cognitive ability. In this review, we discuss the experimental approaches to visualize newly generated neurons and manipulate neurogenesis in the adult brain, especially focusing on genetic methods.

NEUROGENESIS FROM NEURAL STEM CELLS IN THE ADULT BRAIN

In the adult brain, neural stem cells (NSCs) exist principally in two regions: the SVZ of the lateral ventricle and the SGZ of the hippocampal DG (Kriegstein and Alvarez-Buylla, 2009), where neurogenesis occurs continuously. The SVZ is a layer extending along the lateral wall of the lateral ventricle and contains many dividing cells. A large number of neurons born in the SVZ migrate into the OB, forming a rostral migratory stream, and differentiate into local interneurons. A subset of glial fibrillary acidic protein (GFAP)-positive cells (Type-B cells) function as NSCs in the adult SVZ. Type-B cells divide slowly and give rise to rapidly proliferating "transit-amplifying cells" (Type-C cells), which then generate migrating neuroblasts (Type-A cells) after several cell divisions. Type-B cells have the ultrastructural features of astrocytes and express GFAP, a canonical astrocyte marker protein (Doetsch et al., 1997, 1999; Pastrana et al., 2009; **Figure 1A**). Thus, NSCs gradually undergo changes in proliferation and differentiation competencies in the developing and adult brain (Kriegstein and Alvarez-Buylla, 2009).

In the SGZ of the adult hippocampal DG, Type-1 NSCs have astrocytic features and are marked by GFAP (Seri et al., 2004; Zhao et al., 2006; Suh et al., 2007). Although these cells have a proliferative capacity, they cycle much slower than the Type-2 progenitor cells that follow. While Nestin, Sox2, and brain lipid-binding protein (BLBP) are also expressed in Type-1 cells, the expression persists into the Type-2 cell stages (Steiner et al., 2006). NeuroD and Doublecortin (Dcx) appear in Type-2b cells, the later stage of Type-2 cells, and persist into postmitotic but immature granule cell precursors. Finally, these cells mature into NeuN/calbindin/Prox1-positive granule cell neurons in the DG (**Figure 1B**). Notch signaling is highly activated in Type-B cells of the SVZ of the lateral ventricle and Type-1 cells of the SGZ of the DG (Ehm et al., 2010; Imayoshi et al., 2010; Lugert et al., 2010; **Figure 1**).

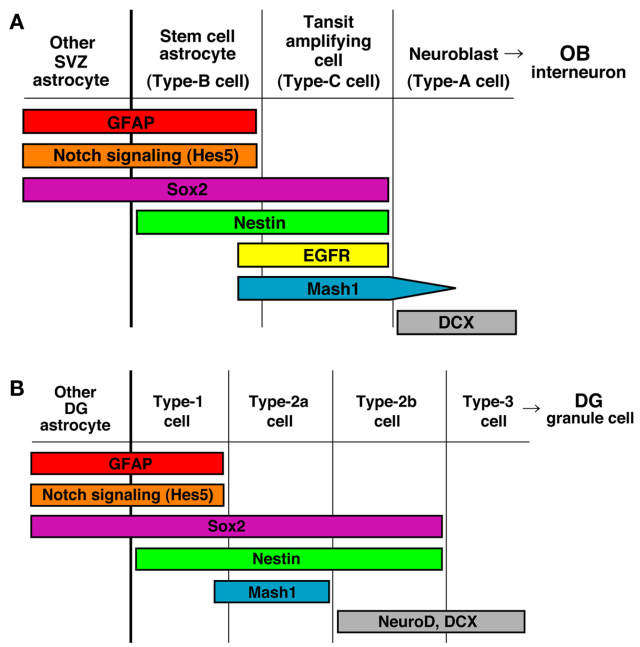

FIGURE 1 | Current view of the sequence of neurogenesis from NSCs in the adult brain. (A) Generation of new interneurons in the olfactory bulb (OB) from NSCs in the subventricular zone of the lateral ventricle (SVZ/LV). **(B)** Generation of new granular neurons in the dentate gyrus (DG) of the hippocampus from NSCs in the subgranular zone (SGZ).

CreER TRANSGENIC MICE TO MANIPULATE ADULT NEURAL STEM/PROGENITOR CELLS

Site-specific recombinases (SSRs) have proven to be useful tools in the analysis of gene function and the genetic manipulation of restricted cell populations (Branda and Dymecki, 2004). SSRs can induce the deletion, insertion or inversion of DNA sequences by breaking and joining DNA molecules at specific sites (Nagy, 2000; Wu et al., 2007). The most widely used SSR in cultured mammalian cells and animals is the P1 bacteriophage-derived Cre, a member of the λ integrase family that recognizes homotypic 34-bp loxP recognition sites. Cre recombinase efficiently excises DNA, which is flanked by two directly repeated loxP recognition sites, in mammalian cells. By crossing transgenic mice expressing Cre in a cell type-specific manner with reporter mice, we can trace the lineage of the progeny of Cre expressing cells with reporter gene expression such as GFP and LacZ. In reporter mice, a reporter gene is under the control of a ubiquitous promoter such as CAG (a combination of the chicken beta-actin promoter and the cytomegalovirus immediate-early enhancer) and the Rosa26 promoter; however the expression of the reporter gene is interrupted by a loxP-flanked transcriptional STOP cassette. In these mice, recombination by Cre results in the removal of the STOP cassette and permanent expression of the reporter protein.

Temporal control of Cre-mediated recombination can be achieved by using the ligand-dependent chimeric recombinase CreER. CreER is constructed by fusing Cre to the mutated ligand-binding domain (LBD) of the estrogen receptor (Metzger et al., 1995; Feil et al., 1997). In transgenic mice, CreER is activated by the administration of tamoxifen, a synthetic estrogen antagonist, but not by natural ligands of LBD such as 17β-estradiol (Indra et al., 2000; Li et al., 2000).

Several groups have generated transgenic mice using the *nestin* promoter and enhancer (**Table 1**). Nestin is an intermediate filament protein specifically expressed by neural stem/progenitor cells in the developing nervous system and the adult brain (Lendahl et al., 1990), and the second intron of the *nestin* gene contains a neural stem/progenitor cell-specific enhancer (Zimmerman et al., 1994; Mignone et al., 2004; Imayoshi et al., 2006, 2008; Lagace et al., 2007). In Nestin-CreER transgenic embryos, CreER is specifically expressed in the ventricular zone of the developing CNS and, in mice expressing CreER at an appropriate level, Cre recombinase activity is efficiently induced in NSCs by the administration of tamoxifen. Nestin is expressed in the SVZ and SGZ of the adult brain (Doetsch et al., 1997), and in Nestin-CreER transgenic mice, NSCs and transit-amplifying cells express CreER. In the presence of tamoxifen, Cre-mediated recombination occurs efficiently in NSCs, and the majority of newborn neurons generated from such recombined NSCs were labeled with reporter gene expression after tamoxifen treatment (Carlén et al., 2006; Imayoshi et al., 2006, 2008;

Table 1 | CreER-expressing mice for Cre/loxP gene targeting in adult neurogenesis research.

Promoter/transcription unit	CreER variant	Technique	Reference
Nestin promoter + 2nd intron enhancer	CreERT2	Tg	Imayoshi et al. (2006, 2008)
Nestin promoter + Nestin exons 1–3 including the 2nd intron	CreERT2	Tg	Lagace et al. (2007)
Nestin 2nd intron/HSV-TK promoter	CreERT2	Tg	Balordi and Fishell (2007)
Nestin 2nd intron/hsp68 mini promoter	CreERT2	Tg	Carlén et al. (2006)
Nestin promoter + Nestin exons 1–3 including the 2nd intron	CreERT2	Tg	Giachino and Taylor (2009)
Nestin promoter + 2nd intron enhancer	CreERTM	Tg	Kuo et al. (2006)
Nestin 2nd intron/hsp68 mini promoter	CreERTM	Tg	Burns et al. (2007)
Nestin promoter + 2nd intron enhancer	CreERT2	Tg	Chen et al. (2009)
Sox2 5′ telencephalic enhancer/promoter	CreERT2	Tg	Favaro et al. (2009)
TLX BAC	CreERT2	Tg	Liu et al. (2008)
Gli1 locus	CreERT2	KI	Ahn and Joyner (2005)
FGFR3 PAC	iCreERT2	Tg	Young et al. (2010)
human GFAP promoter	CreERT2	Tg	Favaro et al. (2009)
human GFAP promoter	CreERTM	Tg	Chow et al. (2008)
GLAST locus	CreERT2	KI	Mori et al. (2006), Ninkovic et al. (2007)
GLAST BAC	CreERT2	Tg	Slezak et al. (2007)
Cx30 BAC	CreERT2	Tg	Slezak et al. (2007)
Aqp4 BAC	CreERT2	Tg	Slezak et al. (2007)
Ascl1 BAC	CreERTM	Tg	Kim et al. (2007)
Dlx1/2 intergenic enhancer i12	CreERT2	Tg	Batista-Brito et al. (2008)
DCX BAC	CreERT2	Tg	Cheng et al. (2010)
DCX promoter	CreERT2	Tg	Zhang et al. (2010)

BAC, bacterial artificial chromosome; PAC, phage artificial chromosome; Tg, transgenic; KI, knock-in.

Kuo et al., 2006; Balordi and Fishell, 2007; Burns et al., 2007; Lagace et al., 2007; Chen et al., 2009; Giachino and Taylor, 2009). Although the *nestin* promoter/enhancer is highly active in NSCs in the adult brain, undesired transgene expression, such as in ependymal cells and specific neuronal subtypes, was observed. Using other promoter sequences or gene loci of NSC-specific genes, for example Sox2, Tlx, Gli1, and FGFR3, several CreER driver transgenic mouse strains have been reported and efficient tamoxifen-dependent recombination was observed (**Table 1**); however, undesired transgene expression, especially in specific neuronal subtypes was also observed (Ahn and Joyner, 2005; Liu et al., 2008; Favaro et al., 2009; Young et al., 2010).

In CreER transgenic mice in which the expression of the transgene is regulated by an astrocyte-specific gene, adult neurogenesis can be targeted, because adult NSCs express astrocyte-specific genes, such as GFAP, GLAST, Cx30, and aquaporin4 (**Table 1**; Ganat et al., 2006; Mori et al., 2006; Slezak et al., 2007; Chow et al., 2008). In these transgenic mice, efficient recombination was observed in adult NSCs in a tamoxifen-dependent manner, but one concern is that recombination is also induced in all astrocytes, including non-neurogenic cells, and it may affect the behavior of NSCs in a non-cell-autonomous manner.

To achieve efficiently inducible CreER transgenic mice, it is important to identify a founder line in which CreER expression is optimal. Most adult neural stem/progenitor specific promoter sequences also induce transgene expression in NSCs during development, and in many cases their promoter activities are rather stronger in embryonic NSCs. In the absence of tamoxifen, CreER is trapped in the cytoplasm, but when CreER is expressed too much, CreER is not retained in the cytoplasm and significant amounts translocate into the nucleus, resulting in tamoxifen-independent recombination. Therefore, too-high level of CreER expression results in tamoxifen-independent recombination in NSCs during development and disturb adult NSC-specificity (Imayoshi et al., 2006; Chen et al., 2009). Conversely, too-low level of CreER expression impairs efficient tamoxifen-dependent recombination and induce recombination only in a subset of adult NSCs. The expression level and spatial pattern of transgenes could be affected by the transgene-copy number and chromosomal integration site. In the case of CreER knock-in mice, the expression level of CreER is determined by the activity of the original promoter from the targeted locus; therefore, we have to carefully select the targeting gene locus.

Various inducible CreER variants have been reported, among them, from our experience, CreER^{T2} developed in the Chambon laboratory is the most superior with respect to its induction by tamoxifen (Feil et al., 1997). ER^{T2}CreER^{T2}, in which ER^{T2} is fused to the N- and C-terminus of Cre (Casanova et al., 2002), has more tightly controlled inducibility than CreER^{T2}, tamoxifen-independent leaky recombination is greatly reduced in the ER^{T2}CreER^{T2} variant, but higher expression levels than for CreER^{T2} are required for efficient recombination (Casanova et al., 2002; Matsuda and Cepko, 2007). ER^{T2}CreER^{T2} is more suitable than CreER^{T2} for transgenic constructs whose promoter activities are very strong, or for fate-mapping or lineage-trace experiments that require strictly specific recombination in adult NSCs.

For the activation of CreER by tamoxifen or its metabolite 4-hydroxy-tamoxifen (4-OHT), intraperitoneal (I.P.) injection or oral gavage are commonly used. When high dose (e.g., 10 mg per 30 g mouse weigh) tamoxifen treatment is required, I.P. injection is sometimes detrimental to the health of the recipient mouse, especially if tamoxifen is dissolved in corn oil. The effects of tamoxifen treatment itself on mouse health should be minimal, and, from our experience, oral gavage is less harmful to health than I.P. injection for high doses of tamoxifen.

VISUALIZATION OF NEUROGENESIS

Transgenic mice expressing CreER in adult NSCs are crossed with reporter mouse strains containing a floxed STOP sequence upstream of GFP or LacZ as a read out for recombinase activity (**Table 2**; Branda and Dymecki, 2004). In double transgenic mice, in the presence of tamoxifen, CreER is released from its cytoplasmic sequestration and translocated to the nucleus (activated). The Cre reporter allele undergoes recombination in cells expressing activated CreER, resulting in permanent marker (GFP or LacZ) expression in marked NSCs and their descendants (Metzger et al., 1995).

The Rosa26-stop-LacZ knock-in reporter mouse has most commonly been used (Soriano, 1999). As the Rosa26 locus is active in almost all cells, the Rosa26 promoter has been used to drive widespread expression of marker genes in transgenic mice (Zambrowicz et al., 1997). Although X-gal staining to detect LacZ expression has very strong sensitivity and a low background signal, immunostaining for LacZ protein is occasionally difficult. As LacZ localizes in the cell body, it is difficult to clearly visualize cellular shapes, such as the axons or dendrites of neurons. GFP or its variants spread more diffusely than LacZ throughout cells, and fine cellular structures are more easily visualized during immunostaining for GFP than for LacZ. Rosa26-stop-ECFP/EGFP/EYFP knock-in reporter strains were developed and widely used in double- or triple-color immunostaining with various antibodies (Mao et al., 2001; Srinivas et al., 2001).

Using the ubiquitous CAG promoter, several transgenic Cre reporter strains have been developed (**Table 2**; Lobe et al., 1999; Kawamoto et al., 2000; Novak et al., 2000; Vintersten et al., 2004). Although CAG promoter transgenic mice are able to induce higher levels of reporter expression than the Rosa26 promoter in most cells, the promoter activity is silenced in some cells and not completely ubiquitous probably due to unfavorable chromatin configurations. To overcome this problem, several reporter strains were recently developed in which reporter constructs under the control of the CAG promoter were knocked into the Rosa26 locus. The expression of exogenous promoters inserted into this locus is not restricted by unfavorable chromatin configurations (Strathdee et al., 2006). Rosa26-knock-in Cre reporter strains with the CAG promoter have stronger reporter expression than the normal Rosa26 reporter and, additionally a single copy is introduced thereby avoiding problems associated with a large multicopy array. One of these reporter mice, the Rosa26-mTmG reporter (Muzumdar et al., 2007), induces the membrane-bound expression of EGFP after recombination. In this reporter mouse, fine cellular structures, especially axons of neurons, could be clearly visualized by its strong EGFP expression in the plasma membrane. Recently, Rosa26 knock-in Cre reporter

Table 2 | Site-specific recombinases (SSRs)-responsive effector mice.

Promoter/transcription unit	Technique	STOP cassette	Reporter/effector	Reference
Rosa26 locus	KI	loxP-flanked	LacZ	Soriano (1999)
Rosa26 locus	KI	loxP-flanked	ECFP	Srinivas et al. (2001)
Rosa26 locus	KI	loxP-flanked	EYFP	Srinivas et al. (2001)
Rosa26 locus	KI	loxP-flanked	EGFP	Mao et al. (2001)
CAG	Tg	loxP-flanked	PLAP	Lobe et al. (1999)
CAG	Tg	loxP-flanked	EGFP	Novak et al. (2000)
CAG	Tg	loxP-flanked	DsRed	Vintersten et al. (2004)
CAG	Tg	loxP-flanked	EGFP	Kawamoto et al. (2000)
CAG (Rosa26 locus)	KI	loxP-flanked	mEGFP	Muzumdar et al. (2007)
Rosa26 locus + CAG	KI	loxP-flanked	tdTomato	Madisen et al. (2010)
Tau locus	KI	loxP-flanked	mEGFP	Hippenmeyer et al. (2005)
Rosa26 locus	KI	loxP-flanked	DTA	Brockschnieder et al. (2006)
Rosa26 locus	KI	loxP-flanked	diphtheria toxin receptor	Buch et al. (2005)
Rosa26 locus	KI	FRT-flanked	PLAP	Awatramani et al. (2001)
Rosa26 locus	KI	FRT-flanked	LacZ	Possemato et al. (2002)
Rosa26 locus	KI	attP/B-flanked	LacZ	Raymond and Soriano (2007)
Rosa26 locus	KI	rox-flanked	LacZ	Anastassiadis et al. (2009)
Rosa26 locus	KI	loxP-flanked and FRT-flanked	PLAP	Awatramani et al. (2003)
Rosa26 locus + CAG	KI	loxP-flanked and FRT-flanked	WGA-ires-EGFP	Farago et al. (2006)
Rosa26 locus + CAG	KI	loxP-flanked and FRT-flanked	EGFP	Sousa et al. (2009), Miyoshi and Fishell (2006)
Rosa26 locus + CAG	KI	loxP-flanked and FRT-flanked	tetanus toxin light chain	Kim et al. (2009)

Tg, transgenic; KI, knock-in.

strain series with the CAG promoter were reported by the Allen institute (Madisen et al., 2010). Among them, the Rosa26-CAG-stop-tdTomato reporter strain is very useful in live imaging experiments, because tdTomato is the brightest available red fluorescent protein and is excited with a 543 nm laser, which is less toxic for cells than a 488 nm laser.

Endogenous Rosa26 promoter activity is very low in astrocytes compared with other neural cell types (Garcia et al., 2010), and the expression of the reporter protein is often undetectable in astrocytes. Unfortunately, this may lead to severe misunderstandings in fate-mapping experiments. As the CAG promoter is active in astrocytes, Rosa26 knock-in reporter strains with the CAG promoter are more suitable for fate-mapping experiments.

In some cases, reporter expression in other cell types (e.g., astrocytes, oligodendrocytes, and NSCs) disturbs the observation of fine structures of marked newly born neurons. Several Cre reporter strains have been developed in which reporter protein expression is driven by neuron-specific promoters. One of these reporter mice, the Tau-stop-mGFP knock-in mouse, can induce the membrane-bound expression of EGFP driven by the endogenous neuron-specific Tau promoter, which is very useful for the visualization of axon targeting by newborn neurons (Hippenmeyer et al., 2005). However, it is important to check in advance that the Tau promoter is active in the newly born neurons of interest.

Several groups have been developed CreER driver strains in which CreER is expressed in transit-amplifying cells and neuroblasts, but not in NSCs (**Table 1**). In the Ascl1-CreER and Dlx1/2-CreER lines, after the administration of tamoxifen, Cre-mediated recombination is specifically induced in transit-amplifying cells (Kim et al., 2007; Batista-Brito et al., 2008). The DCX-CreER line is able to induce recombination in immature newborn neurons (Cheng et al., 2010; Zhang et al., 2010). Importantly, as CreER is not expressed in NSCs, these lines allow pulse labeling of newborn neurons within a short time-window, thereby facilitating the analysis of the differentiation and integration of adult-born new neurons at specific time points.

Recently the Lois group and Mizrahi group reported elegant experimental methods for the genetic labeling of the synapses of adult-born neurons (Kelsch et al., 2008, 2009; Livneh et al., 2009). The visualization of pre- and post-synaptic terminals can be achieved by the expression of fluorescent proteins fused to proteins specifically located in synapses. For instance, synaptophysin is a protein localized in neurotransmitter vesicles that is selectively located at presynaptic terminals and can be used to identify release sites on axon terminals. PSD95, a scaffolding protein that is restricted to clusters in the post-synaptic density of most glutamatergic synapses, has been used to identify post-synaptic terminals. To achieve the sparse and modest expression of these fusion proteins, they adapted retrovirus-mediated gene transfer to adult NSCs.

Relatively little is known about the connectivity of newborn neurons within mature circuits of the adult brain (Deng et al., 2010). How new neurons make synaptic connections with mature circuits is an open question. Several genetically encoded synaptic tracers are used to characterize the connections between neurons. Genetically encoded tracer molecules, such as wheat germ agglutinin (WGA) or tetanus toxin- fragment C (TTC), can be transported trans-synaptically (Luo et al., 2008). Fusion proteins of these tracer molecules and GFP, LacZ, alkaline phosphatase, or Cre can also be transported trans-synaptically (Luo et al., 2008). The application of these genetically encoded synaptic tracers, or recently developed monosynaptic rabies virus technology (Wickersham et al., 2007; Miyamichi et al., 2011), may elucidate the connectivity of newly born neurons in neuronal circuitry and contribute to a functional understanding of the lifelong addition of new neurons in the adult brain.

GENETIC MANIPULATION OF ADULT NEUROGENESIS

Several methods have been developed to manipulate neurogenesis in the adult brain. The majority of studies have examined the consequences of the suppression of neurogenesis on cognitive performance (Deng et al., 2010). The traditional approaches for ablating neurogenesis are anti-mitotic drug treatments or irradiation. These treatments are able to selectively disrupt cell cycle progression in neural stem/progenitor cells, because these cells are more sensitive to these treatments than differentiated neurons. After treatment, neurogenesis is strongly though not fully blocked (Wojtowicz, 2006; Gould, 2007). Although these methods are effective in reducing neurogenesis, they have considerable side effects in animals, such as general health deterioration and inflammation.

Recently, several transgenic mouse lines have been generated for more specific suppression of adult neurogenesis. In GFAP-TK and Nestin-TK mice, the targeted expression of herpes simplex virus thymidine kinase (HSV-TK) in NSCs is combined with the delivery of the nucleotide analog ganciclovir (GCV), resulting in specific and inducible ablation of dividing GFAP- or Nestin-expressing cells (**Figure 2A**; Garcia et al., 2004; Saxe et al., 2006; Deng et al., 2009; Singer et al., 2009). In both transgenic mice, adult neurogenesis was severely reduced after GCV treatment. Although other proliferating populations expressing GFAP or Nestin could be affected throughout the body, these transgenic strategies are highly specific. Theoretically, this model affects dividing NSCs, and quiescent NSCs should not be affected, which allows investigators to transiently reduce neurogenesis, and after the cessation of GCV infusion, active neurogenesis resumes. Although it was reported that the recovery of neurogenesis after drug withdrawal, was slow and incomplete, possibly because of quiescent NSC population was also affected by the prolonged infusion of GCV, these transgenic models are very useful as temporally regulated and reversible methods for the manipulation of adult NSCs.

In the Nestin-CreER/NSE-DTA mouse (Imayoshi et al., 2008), the expression of a suicide gene (diphtheria toxin fragment A, DTA) is selectively induced in newly generated neurons. NSE-DTA mice carry the loxP-STOP-loxP-IRES-DTA gene cassette, which was knocked into the 3′-non-coding region of the neuron-specific enolase (NSE) gene (**Figure 2B**). Crossing NSE-DTA mice with Nes-CreER mice and administering tamoxifen led to the deletion of the STOP cassette in NSCs. When these NSCs began neuronal differentiation, DTA was expressed from the NSE locus, thereby killing the cells.

The induction of apoptotic cell death in NSCs was achieved in Nestin-rtTA/TRE-Bax mice (**Figure 2C**; Dupret et al., 2008). This model is based on the reverse tetracycline-controlled transactivator (rtTA)-regulated system (Tet-On system). The activation of transgenes with doxycycline (Dox) treatment, a tetracycline analog,

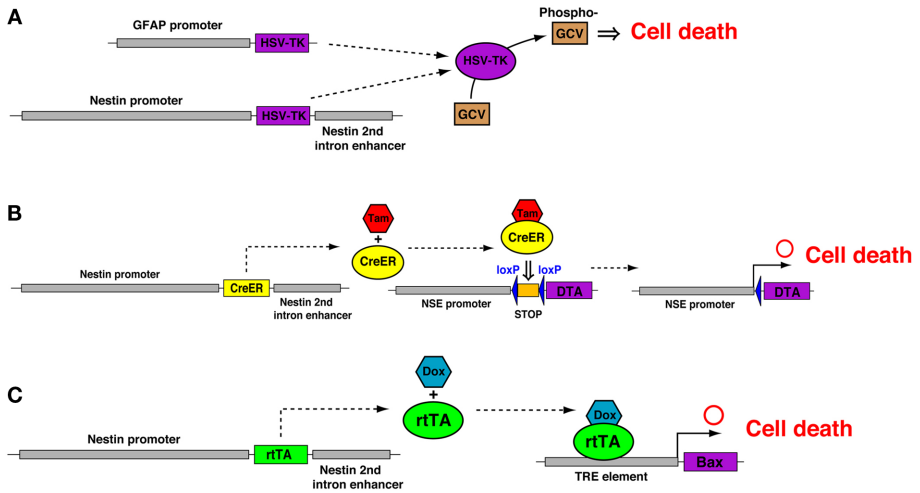

FIGURE 2 | Genetic methods to suppress adult neurogenesis. **(A)** Administration of Ganciclovir (GCV) to mice carrying the transgene (GFAP-TK or Nestin-TK) results in death of dividing cells expressing herpes simplex virus thymidine kinase (HSV-TK). HSV-TK produces toxic metabolites that disrupt DNA synthesis and result in the death of dividing cells. **(B)** In the Nestin-CreER/NSE-DTA mouse, Nestin-CreER drives the expression of a tamoxifen (Tam)-inducible form of Cre in NSCs and a Cre-inducible diphtheria toxin fragment A (DTA) is engineered into the locus of the neuron-specific enolase (NSE) gene. Activated CreER leads to the recombination of loxP sites and removal of the STOP cassette upstream of the DTA gene, thus allowing the expression of DTA from the NSE promoter. **(C)** In the Nestin-rtTA/TRE-Bax mice, doxycycline (Dox) activates the rtTA protein, which binds to seven TetO sequences (TRE) to drive the expression of the pro-apoptotic protein Bax, which activates the apoptosis pathway in NSCs.

resulted in the overexpression of the pro-apoptotic protein Bax in nestin-expressing cells. This resulted in the increased cell death of neural stem/progenitor cells, consequently cell proliferation and neurogenesis were reduced, albeit not totally blocked.

In addition to the application of these suicide genes, the increased understanding of the molecular mechanisms regulating adult neurogenesis allows investigators to develop new techniques to block neurogenesis (Mu et al., 2010). For example, blockade of several important signaling cascades responsible for the proliferation or maintenance of NSCs, such as Notch (Breunig et al., 2007; Ables et al., 2010; Ehm et al., 2010; Imayoshi et al., 2010), Shh (Lai et al., 2003; Balordi and Fishell, 2007), Wnt (Lie et al., 2005), and BMP (Lim et al., 2000; Mira et al., 2010) signaling can manipulate the behavior of NSCs. Incomplete maintenance and premature neuronal differentiation will deplete the neural stem pool and, consequently, reduce the supply of new neurons. Conversely, increased stem cell maintenance at the expense of proper neuronal differentiation will impair the ability of NSCs to generate a sufficient number of new neurons.

As most of the available genetic methods aim to reduce neurogenesis, it is important to develop genetic techniques that are able to increase the magnitude of neurogenesis. One important question in the adult neurogenesis research field is why new neurons are supplied only to the OB and hippocampal DG. To address this issue, genetic methods that can forcibly induce neurogenesis in ectopic brain regions, such as the cerebral cortex, are hoped for.

There is growing evidence that adult neurogenesis intensely contributes to neural circuit plasticity (Deng et al., 2010). Adult-born DG granule cells exhibit stronger synaptic plasticity than mature granule cells, as indicated by their lower threshold for the induction of long-term potentiation (LTP) and their higher LTP amplitude (Schmidt-Hieber et al., 2004; Ge et al., 2007). LTP formation between centrifugal projections from the piriform cortex and adult-born granule cells in the OB was reported. Interestingly, the synaptic plasticity of young newborn neurons in the OB occurs during a narrow time-window when new neurons are initially added to the circuit (Gao and Strowbridge, 2009; Nissant et al., 2009). The transgenic expression of genetically encoded tools that can modulate LTP formation, such as constitutively active CREB or dominant negative GluR1, may shed light on the functional significance of neuron addition on neural circuit plasticity.

Several technologies have been recently developed to control the activity of genetically specified neural populations. Chemically triggered activating or silencing genetic technologies include RASSLs (Alexander et al., 2009), MISTs (Karpova et al., 2005), AlstR (Tan et al., 2006), GluClab (Lerchner et al., 2007), TRPV1 (Arenkiel et al., 2008), and modified GABA-A receptors (Wulff et al., 2007). Optogenetic tools that allow for the fast stimulation and inhibition of genetically targeted neuronal populations on the millisecond timescale have recently been developed. The light-gated cation channel Channelrhodopsin-2 (ChR2) and the light-driven chloride ions pump halorhodopsin are powerful and versatile tools for controlling neuronal activity (Zhang et al., 2007). The feasibility of using optogenetics to precisely control the activity of adult-born OB interneurons has been recently reported (Bardy et al., 2010). These technical advances in the fine manipulation of adult-born neurons will contribute to unveil the functional significance of adult neurogenesis.

COMBINATIONAL USE OF OTHER SSRs AND THE TET SYSTEM WITH THE Cre/LoxP SYSTEM

In addition to the Cre/loxP system, other SSR systems, such as the Flp/FRT, PhiC31/att, and Dre/rox systems, have been used as powerful tools for genome manipulation in mice (Branda and Dymecki, 2004). The Cre/loxP system is most widely used to manipulate the

mouse genome *in vivo*, because it is more efficient than the other SSR systems, although recent studies reported that codon-optimized versions of SSRs (e.g., Flpo, PhiC31o, and codon-improved Dre) had similar recombination efficiencies as Cre (Raymond and Soriano, 2007; Anastassiadis et al., 2009). Similar to the Cre/loxP system, these SSRs are able to induce intra-molecular recombination between their recognition sites when oriented in the same direction *in cis*, including the deletion of the flanked sequence (Raymond and Soriano, 2007). As Cre, Flp, PhiC31, and Dre recognize different target sequences, the combined use of these recombinases would facilitate more sophisticated genetic manipulation of restricted cell populations.

For example, intersectional genetic strategies using Cre and Flp have been reported (**Figure 3**; Awatramani et al., 2003; Farago et al., 2006; Miyoshi and Fishell, 2006; Sousa et al., 2009). In the Rosa26 knock-in intersectional reporter mice (e.g., R26::FLAP, RC::PFwe, and RCE:dual), dual recombinase responsive indicator alleles were designed, that express marker proteins only when Cre and Flp have been expressed in the same cell. As the majority of genes in the developing nervous system are expressed in multiple cell populations, these intersectional approaches provide important means to reduce complexity, such that smaller subpopulations of genetically defined cells can be targeted.

As the majority of adult NSC-specific genes are expressed in the SVZ of the lateral ventricle and the SGZ of the DG, most CreER driver strains (e.g., Nestin-CreER and GLAST-CreER) induce recombination in both NSCs. In order to selectively manipulate NSCs either in the SVZ or the SGZ, Cre- and Flp-mediated intersectional strategies will be useful. The increased understanding of the molecular mechanisms regulating adult neurogenesis will identify candidate genes for Flp-expressing transgenic mice. Several members of the basic helix–loop–helix (bHLH) or homeobox gene families are selectively expressed in precursors or stem cells in the germinal zone of the adult brain. Alternatively, regulatory elements of the genes responsible for neurotransmitter identity (e.g., glutamatergic for the DG and GABAergic for the OB) could be attractive candidates for Flp-expressing transgenic mice.

Recently the Dymecki group reported an elegant strategy applying a Cre- and Flp-mediated intersectional approach to the functional investigation of genetically defined neuronal populations (**Figure 3**; Kim et al., 2009). RC::PFtox mice express the tetanus toxin light chain (tox), an inhibitor of vesicular neurotransmission, only when Cre and Flp have been expressed in the same cell. The development of intersectional transgenic mice with various effectors, for example, neurotoxins, optogenetic tools, neuronal activity modulators, etc., will contribute to the more sophisticated manipulation of newly born neurons in the adult brain.

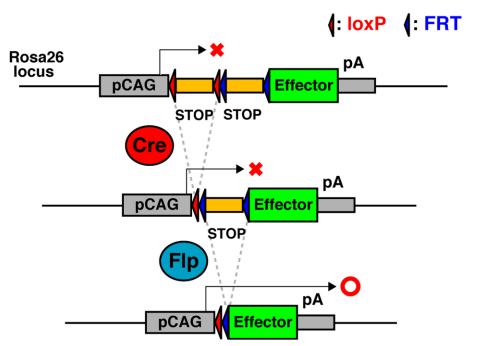

FIGURE 3 | Schematic of Cre- and Flp-dual recombinase responsive allele. The effector-encoding sequence is interrupted by a loxP-flanked STOP cassette followed by a FRT-flanked STOP cassette. The effector protein expresses only when Cre and Flp have been expressed in the same cell.

The tetracycline-controlled transactivator (tTA)-dependent systems (Gossen and Bujard, 1992) have been used for inducible gene expression in adult NSCs. tTA is a fusion protein between the tetracycline repressor from the Tn10 tetracycline resistance operon of *Escherichia coli* and the C-terminal domain of the VP16 transcription factor from HSV. The resulting hybrid transcriptional activator can trigger expression from a cognate promoter made of minimal promoter sequences placed downstream from multiple repeats of the tetracycline operator (tetO). tTA is constitutively active but its activity can be blocked by tetracycline or analogs such as Dox. The reverse tTA (rtTA), obtained by random mutagenesis of tTA, has the opposite features of tTA. It is constitutively silent but needs Dox to bind to the tetO sequences and induce gene transcription. Combined with tissue-specific promoters, the tetracycline-inducible system is able to provide transgenic mice with inducible, reversible, and spatially controlled transgene expression. As conditional expression systems with SSRs depend on the permanent intra-molecular recombination between their recognition sites, including the deletion of the flanked sequence, transgene expression is basically irreversible. The combinational use of the Tet system with the SSRs-mediated conditional expression systems will achieve the reversible manipulation of newly born neurons.

ELECTROPORATION IN THE POSTNATAL BRAIN

Although the use of transgenic or gene targeted mice has proved to be a powerful strategy for the manipulation of adult neurogenesis, we often suffer from the fact that transgenesis via oocyte injection or gene knock-in by homologous recombination in embryonic stem cells are time consuming and expensive. Gene transfer through the injection of plasmid DNA into embryos followed by electric pulses (electroporation) has developed into an important tool for functional analyses *in vivo* (Matsuda and Cepko, 2004; Shimogori and Ogawa, 2008). *In utero* electroporation in rodents is widely used, and more recently, gene transfer into postnatal neural tissues, including the postnatal and adult SVZ have been demonstrated (Barnabé-Heider et al., 2008; Boutin et al., 2008; Chesler et al., 2008). The lateral ventricle is readily accessible through minimally invasive techniques during the neonatal period. After electroporation, injected plasmid DNAs are incorporated into radial glial cells that populate the neonatal SVZ and send processes along the lateral ventricle. Electroporated radial glial cells differentiate into ependymal cells and SVZ astrocytes during the neonatal period. A subset of SVZ astrocytes generate transit-amplifying cells and neuroblasts, which migrate to the OB. Therefore, neonatal electroporation enables the visualization or manipulation of early postnatal neurogenesis. However, there is an important limitation of neonatal electroporation, plasmid dilution over the course of successive cell divisions results in lower and undetectable expression levels of transfected genes after several weeks of electroporation (Lacar et al., 2010). The use of vectors encoding transposons

will permit genetic integration and the permanent expression of transfected genes in adult NSCs (Sato et al., 2007). Alternatively, electroporation of SSR-containing plasmids into the neonatal brain of transgenic mice with SSR-specific STOP cassettes, will achieve the prolonged expression of the gene of interest in adult NSCs and newborn neurons. An alternative approach is the electroporation of adult mice (Barnabé-Heider et al., 2008); however, this approach is technically more challenging and more damaging to the animals since it requires the use of a stereotactic frame.

Although we focused mainly on the transgenic or gene targeting approaches for the visualization and manipulation of adult neurogenesis in this review, virus vectors can also mediate efficient gene transfer in adult NSCs and newly born neurons (Consiglio et al., 2004).

CONCLUSION

Since the discovery of adult neurogenesis, many extensive studies have been performed on various aspects of adult neurogenesis. Postdevelopmental neurogenesis is found to be an evolutionarily conserved phenomenon, and functional importance on brain activities has just begun to be unveiled. Further understanding of adult neurogenesis will lead to the development of novel therapies for functional recovery after disease, trauma, or pathological aging.

ACKNOWLEDGMENTS

This work was supported by the Grants-in-aid from the Ministry of Education, Culture, Sports, Science and Technology of Japan. Itaru Imayoshi was supported by JST PRESTO program.

REFERENCES

Ables, J. L., Decarolis, N. A., Johnson, M. A., Rivera, P. D., Gao, Z., Cooper, D. C., Radtke, F., Hsieh, J., and Eisch, A. J. (2010). Notch1 is required for maintenance of the reservoir of adult hippocampal stem cells. *J. Neurosci.* 30, 10484–10492.

Adam, Y., and Mizrahi, A. (2010). Circuit formation and maintenance – perspectives from the mammalian olfactory bulb. *Curr. Opin. Neurobiol.* 20, 134–140.

Ahn, S., and Joyner, A. L. (2005). In vivo analysis of quiescent adult neural stem cells responding to sonic hedgehog. *Nature* 437, 894–897.

Alexander, G. M., Rogan, S. C., Abbas, A. I., Armbruster, B. N., Pei, Y., Allen, J. A., Nonneman, R. J., Hartmann, J., Moy, S. S., Nicolelis, M. A., McNamara, J. O., and Roth, B. L. (2009). Remote control of neuronal activity in transgenic mice expressing evolved G protein-coupled receptors. *Neuron* 63, 27–39.

Altman, J. (1966). Autoradiographic and histological studies of postnatal neurogenesis. II. A longitudinal investigation of the kinetics, migration and transformation of cells incorporating tritiated thymidine in infant rats, with special reference to postnatal neurogenesis in some brain regions. *J. Comp. Neurol.* 1966, 431–474.

Altman, J. (1969). Autoradiographic and histological studies of postnatal neurogenesis. IV. Cell proliferation and migration in the anterior forebrain, with special reference to persisting neurogenesis in the olfactory bulb. *J. Comp. Neurol.* 137, 433–457.

Altman, J., and Das, G. D. (1965). Autoradiographic and histological evidence of postnatal hippocampal neurogenesis in rats. *J. Comp. Neurol.* 124, 319–335.

Alvarez-Buylla, A., Garcia-Verdugo, J. M., and Tramontin, A. D. (2001). A unified hypothesis on the lineage of neural stem cells. *Nat. Rev. Neurosci.* 2, 287–293.

Anastassiadis, K., Fu, J., Patsch, C., Hu, S., Weidlich, S., Duerschke, K., Buchholz, F., Edenhofer, F., and Stewart, A. F. (2009). Dre recombinase, like Cre, is a highly efficient site-specific recombinase in *E. coli*, mammalian cells and mice. *Dis. Model. Mech.* 2, 508–515.

Arenkiel, B. R., Klein, M. E., Davison, I. G., Katz, L. C., and Ehlers, M. D. (2008). Genetic control of neuronal activity in mice conditionally expressing TRPV1. *Nat. Methods* 5, 299–302.

Awatramani, R., Soriano, P., Mai, J. J., and Dymecki, S. (2001). An Flp indicator mouse expressing alkaline phosphatase from the ROSA26 locus. *Nat. Genet.* 29, 257–259.

Awatramani, R., Soriano, P., Rodriguez, C., Mai, J. J., and Dymecki, S. M. (2003). Cryptic boundaries in roof plate and choroid plexus identified by intersectional gene activation. *Nat. Genet.* 35, 70–75.

Balordi, F., and Fishell, G. (2007). Mosaic removal of hedgehog signaling in the adult SVZ reveals that the residual wild-type stem cells have a limited capacity for self-renewal. *J. Neurosci.* 27, 4248–4259.

Bardy, C., Alonso, M., Bouthour, W., and Lledo, P. M. (2010). How, when, and where new inhibitory neurons release neurotransmitters in the adult olfactory bulb. *J. Neurosci.* 30, 17023–17034.

Barnabé-Heider, F., Meletis, K., Eriksson, M., Bergmann, O., Sabelström, H., Harvey, M. A., Mikkers, H., and Frisén, J. (2008). Genetic manipulation of adult mouse neurogenic niches by *in vivo* electroporation. *Nat. Methods* 5, 89–96.

Batista-Brito, R., Close, J., Machold, R., and Fishell, G. (2008). The distinct temporal origins of olfactory bulb interneuron subtypes. *J. Neurosci.* 28, 3966–3975.

Boutin, C., Diestel, S., Desoeuvre, A., Tiveron, M. C., and Cremer, H. (2008). Efficient *in vivo* electroporation of the postnatal rodent forebrain. *PLoS ONE* 3, e1883. doi: 10.1371/journal.pone.0001883

Branda, C. S., and Dymecki, S. M. (2004). Talking about a revolution: the impact of site-specific recombinases on genetic analysis in mice. *Dev. Cell* 6, 7–28.

Breunig, J. J., Silbereis, J., Vaccarino, F. M., Sestan, N., and Rakic, P. (2007). Notch regulates cell fate and dendrite morphology of newborn neurons in the postnatal dentate gyrus. *Proc. Natl. Acad. Sci. U.S.A.* 104, 20558–20563.

Brockschnieder, D., Pechmann, Y., Sonnenberg-Riethmacher, E., and Riethmacher, D. (2006). An improved mouse line for Cre-induced cell ablation due to diphtheria toxin A, expressed from the Rosa26 locus. *Genesis* 44, 322–327.

Buch, T., Heppner, F. L., Tertilt, C., Heinen, T. J., Kremer, M., Wunderlich, F. T., Jung, S., and Waisman, A. (2005). A Cre-inducible diphtheria toxin receptor mediates cell lineage ablation after toxin administration. *Nat. Methods* 2, 419–426.

Burns, K. A., Ayoub, A. E., Breunig, J. J., Adhami, F., Weng, W. L., Colbert, M. C., Rakic, P., and Kuan, C. Y. (2007). Nestin-CreER mice reveal DNA synthesis by nonapoptotic neurons following cerebral ischemia hypoxia. *Cereb. Cortex* 17, 2585–2592.

Carlén, M., Meletis, K., Barnabé-Heider, F., and Frisén, J. (2006). Genetic visualization of neurogenesis. *Exp. Cell Res.* 312, 2851–2859.

Carleton, A., Petreanu, L. T., Lansford, R., Alvarez-Buylla, A., and Lledo, P. M. (2003). Becoming a new neuron in the adult olfactory bulb. *Nat. Neurosci.* 6, 507–518.

Casanova, E., Fehsenfeld, S., Lemberger, T., Shimshek, D. R., Sprengel, R., and Mantamadiotis, T. (2002). ER-based double iCre fusion protein allows partial recombination in forebrain. *Genesis* 34, 208–214.

Chen, J., Kwon, C. H., Lin, L., Li, Y., and Parada, L. F. (2009). Inducible site-specific recombination in neural stem/progenitor cells. *Genesis* 47, 122–131.

Cheng, X., Li, Y., Huang, Y., Feng, X., Feng, G., and Xiong, Z. Q. (2010). Pulse labeling and long-term tracing of newborn neurons in the adult subgranular zone. *Cell Res.* 12, 338–349.

Chesler, A. T., Le Pichon, C. E., Brann, J. H., Araneda, R. C., Zou, D. J., and Firestein, S. (2008). Selective gene expression by postnatal electroporation during olfactory interneuron neurogenesis. *PLoS ONE* 3, e1517. doi: 10.1371/journal.pone.0001517

Chow, L. M., Zhang, J., and Baker, S. J. (2008). Inducible Cre recombinase activity in mouse mature astrocytes and adult neural precursor cells. *Transgenic Res.* 17, 919–928.

Consiglio, A., Gritti, A., Dolcetta, D., Follenzi, A., Bordignon, C., Gage, F. H., Vescovi, A. L., and Naldini, L. (2004). Robust in vivo gene transfer into adult mammalian neural stem cells by lentiviral vectors. *Proc. Natl. Acad. Sci. U.S.A.* 101, 14835–14840.

Deng, W., Aimone, J. B., and Gage, F. H. (2010). New neurons and new memories: how does adult hippocampal neurogenesis affect learning and memory? *Nat. Rev. Neurosci.* 11, 339–350.

Deng, W., Saxe, M. D., Gallina, I. S., and Gage, F. H. (2009). Adult-born hippocampal dentate granule cells undergoing maturation modulate learning and memory in the brain. *J. Neurosci.* 29, 13532–13542.

Doetsch, F., Caille, I., Lim, D. A., Garcia-Verdugo, J. M., and Alvarez-Buylla, A. (1999). Subventricular zone astrocytes are neural stem cells in the adult mammalian brain. *Cell* 97, 703–716.

Doetsch, F., Garcia-Verdugo, J. M., and Alvarez-Buylla, A. (1997). Cellular composition and three-dimensional

organization of the subventricular germinal zone in the adult mammalian brain. *J. Neurosci.* 17, 5046–5061.

Dupret, D., Revest, J. M., Koehl, M., Ichas, F., De Giorgi, F., Costet, P., Abrous, D. N., and Piazza, P. V. (2008). Spatial relational memory requires hippocampal adult neurogenesis. *PLoS ONE* 3, e1959. doi:10.1371/journal.pone.0001959

Ehm, O., Göritz, C., Covic, M., Schaffner, I., Schwarz, T. J., Karaca, E., Kempkes, B., Kremmer, E., Pfrieger, F. W., Espinosa, L., Bigas, A., Giachino, C., Taylor, V., Frisén, J., and Lie, D. C. (2010). RBPJkappa-dependent signaling is essential for long-term maintenance of neural stem cells in the adult hippocampus. *J. Neurosci.* 30, 13794–13807.

Eriksson, P. S., Perfililieva, E., Bjork-Eriksson, T., Alborn, A. M., Nordborg, C., Peterson, D. A., and Gage, F. H. (1998). Neurogenesis in the adult human hippocampus. *Nat. Med.* 4, 1313–1317.

Farago, A. F., Awatramani, R. B., and Dymecki, S. M. (2006). Assembly of the brainstem cochlear nuclear complex is revealed by intersectional and subtractive genetic fate maps. *Neuron* 20, 205–218.

Favaro, R., Valotta, M., Ferri, A. L., Latorre, E., Mariani, J., Giachino, C., Lancini, C., Tosetti, V., Ottolenghi, S., Taylor, V., and Nicolis, S. K. (2009). Hippocampal development and neural stem cell maintenance require Sox2-dependent regulation of Shh. *Nat. Neurosci.* 12, 1248–1256.

Feil, R., Wagner, J., Metzger. D., and Chambon, P. (1997). Regulation of Cre recombinase activity by mutated estrogen receptor ligand-binding domains. *Biochem. Biophys. Res. Commun.* 237, 752–757.

Gage, F. H. (2000). Mammalian neural stem cells. *Science* 287, 1433–1438.

Ganat, Y. M., Silbereis, J., Cave, C., Ngu, H., Anderson, G. M., Ohkubo, Y., Ment, L. R., and Vaccarino, F. M. (2006). Early postnatal astroglial cells produce multilineage precursors and neural stem cells *in vivo*. *J. Neurosci.* 26, 8609–8621.

Gao, Y., and Strowbridge, B. W. (2009). Long-term plasticity of excitatory inputs to granule cells in the rat olfactory bulb. *Nat. Neurosci.* 12, 731–733.

Garcia, A. D., Doan, N. B., Imura, T., Bush, T. G., and Sofroniew, M. V. (2004). GFAP-expressing progenitors are the principal source of constitutive neurogenesis in adult mouse forebrain. *Nat. Neurosci.* 7, 1233–1241.

Garcia, A. D., Petrova, R., Eng, L., and Joyner, A. L. (2010). Sonic hedgehog regulates discrete populations of astrocytes in the adult mouse forebrain. *J. Neurosci.* 30, 13597–13608.

Ge, S., Yang, C. H., Hsu, K. S., Ming, G. L., and Song, H. (2007). A critical period for enhanced synaptic plasticity in newly generated neurons of the adult brain. *Neuron* 54, 559–566.

Giachino, C., and Taylor, V. (2009). Lineage analysis of quiescent regenerative stem cells in the adult brain by genetic labelling reveals spatially restricted neurogenic niches in the olfactory bulb. *Eur. J. Neurosci.* 30, 9–24.

Gossen, M., and Bujard, H. (1992). Tight control of gene expression in mammalian cells by tetracycline-responsive promoters. *Proc. Natl. Acad. Sci. U.S.A.* 89, 5547–5551.

Gould, E. (2007). How widespread is adult neurogenesis in mammals? *Nat. Rev. Neurosci.* 8, 481–488.

Hippenmeyer, S., Vrieseling, E., Sigrist, M., Portmann, T., Laengle, C., Ladle, D. R., and Arber, S. (2005). A developmental switch in the response of DRG neurons to ETS transcription factor signaling. *PLoS Biol.* 3, e159. doi:10.1371/journal.pbio.0030159

Imayoshi, I., Ohtsuka, T., Metzger, D., Chambon, P., and Kageyama, R. (2006). Temporal regulation of Cre recombinase activity in neural stem cells. *Genesis* 44, 233–238.

Imayoshi, I., Sakamoto, M., Ohtsuka, T., and Kageyama, R. (2009). Continuous neurogenesis in the adult brain. *Dev. Growth Differ.* 51, 379–386.

Imayoshi, I., Sakamoto, M., Ohtsuka, T., Takao, K., Miyakawa, T., Yamaguchi, M., Mori, K., Ikeda, T., Itohara, S., and Kageyama, R. (2008). Roles of continuous neurogenesis in the structural and functional integrity of the adult forebrain. *Nat. Neurosci.* 11, 1153–1161.

Imayoshi, I., Sakamoto, M., Yamaguchi, M., Mori, K., and Kageyama, R. (2010). Essential roles of Notch signaling in maintenance of neural stem cells in developing and adult brains. *J. Neurosci.* 30, 3489–3498.

Indra, A. K., Li, M., Brocard, J., Warot, X., Bornert, J. M., Gérard, C., Messaddeq, N., Chambon, P., and Metzger, D. (2000). Targeted somatic mutagenesis in mouse epidermis. *Horm. Res.* 54, 296–300.

Kaplan, M. S., and Hinds, J. W. (1977). Neurogenesis in the adult rat: electron microscopic analysis of light radioautographs. *Science* 197, 1092–1094.

Karpova, A. Y., Tervo, D. G., Gray, N. W., and Svoboda, K. (2005). Rapid and reversible chemical inactivation of synaptic transmission in genetically targeted neurons. *Neuron* 48, 727–735.

Kawamoto, S., Niwa, H., Tashiro, F., Sano, S., Kondoh, G., Takeda, J., Tabayashi, K., and Miyazaki, J. (2000). A novel reporter mouse strain that expresses enhanced green fluorescent protein upon Cre-mediated recombination. *FEBS Lett.* 470, 263–268.

Kee, N., Teixeira, C. M., Wang, A. H., and Frankland, P. W. (2007). Preferential incorporation of adult-generated granule cells into spatial memory networks in the dentate gyrus. *Nat. Neurosci.* 10, 355–362.

Kelsch, W., Lin, C. W., and Lois, C. (2008). Sequential development of synapses in dendritic domains during adult neurogenesis. *Proc. Natl. Acad. Sci. U.S.A.* 105, 16803–16808.

Kelsch, W., Lin, C. W., Mosley, C. P., and Lois, C. (2009). A critical period for activity-dependent synaptic development during olfactory bulb adult neurogenesis. *J. Neurosci.* 29, 11852–11858.

Kelsch, W., Sim, S., and Lois, C. (2010). Watching synaptogenesis in the adult brain. *Annu. Rev. Neurosci.* 33, 131–149.

Kim, E. J., Leung, C. T., Reed, R. R., and Johnson, J. E. (2007). *In vivo* analysis of Ascl1 defined progenitors reveals distinct developmental dynamics during adult neurogenesis and gliogenesis. *J. Neurosci.* 27, 12764–12774.

Kim, J. C., Cook, M. N., Carey, M. R., Shen, C., Regehr, W. G., and Dymecki, S. M. (2009). Linking genetically defined neurons to behavior through a broadly applicable silencing allele. *Neuron* 63, 305–315.

Kriegstein, A., and Alvarez-Buylla, A. (2009). The glial nature of embryonic and adult neural stem cells. *Annu. Rev. Neurosci.* 32, 149–184.

Kuo, C. T., Mirzadeh, Z., Soriano-Navarro, M., Rasin, M., Wang, D., Shen, J., Sestan, N., Garcia-Verdugo, J., Alvarez-Buylla, A., Jan, L. Y., and Jan, Y. N. (2006). Postnatal deletion of Numb/Numblike reveals repair and remodeling capacity in the subventricular neurogenic niche. *Cell* 127, 1253–1264.

Lacar, B., Young, S. Z., Platel, J. C., and Bordey, A. (2010). Imaging and recording subventricular zone progenitor cells in live tissue of postnatal mice. *Front. Neurosci.* 4:43. doi:10.3389/fnins.2010.00043

Lagace, D. C., Whitman, M. C., Noonan, M. A., Ables, J. L., DeCarolis, N. A., Arguello, A. A., Donovan, M. H., Fischer, S. J., Farnbauch, L. A., Beech, R. D., DiLeone, R. J., Greer, C. A., Mandyam, C. D., and Eisch, A. J. (2007). Dynamic contribution of nestin-expressing stem cells to adult neurogenesis. *J. Neurosci.* 27, 2623–2629.

Lai, K., Kaspar, B. K., Gage, F. H., and Schaffer, D. V. (2003). Sonic hedgehog regulates adult neural progenitor proliferation *in vitro* and *in vivo*. *Nat. Neurosci.* 6, 21–27.

Lazarini, F., and Lledo, P. M. (2011). Is adult neurogenesis essential for olfaction? *Trends Neurosci.* 34, 20–30.

Lendahl, U., Zimmerman, L. B., and McKay, R. D. G. (1990). CNS stem cells express a new class of intermediate filament protein. *Cell* 60, 585–595.

Lerchner, W., Xiao, C., Nashmi, R., Slimko, E. M., van Trigt, L., Lester, H. A., and Anderson, D. J. (2007). Reversible silencing of neuronal excitability in behaving mice by a genetically targeted, ivermectin-gated Cl- channel. *Neuron* 54, 35–49.

Li, M., Indra, A. K., Warot, X., Brocard, J., Messaddeq, N., Kato, S., Metzger, D., and Chambon, P. (2000). Skin abnormalities generated by temporally controlled RXRalpha mutations in mouse epidermis. *Nature* 407, 633–636.

Lie, D. C., Colamarino, S. A., Song, H. J., Désiré, L., Mira, H., Consiglio, A., Lein, E. S., Jessberger, S., Lansford, H., Dearie, A. R., and Gage, F. H. (2005). Wnt signalling regulates adult hippocampal neurogenesis. *Nature* 437, 1370–1375.

Lim, D. A., Tramontin, A. D., Trevejo, J. M., Herrera, D. G., García-Verdugo, J. M., and Alvarez-Buylla, A. (2000). Noggin antagonizes BMP signaling to create a niche for adult neurogenesis. *Neuron* 28, 713–726.

Liu, H. K., Belz, T., Bock, D., Takacs, A., Wu, H., Lichter, P., Chai, M., and Schutz, G. (2008). The nuclear receptor tailless is required for neurogenesis in the adult subventricular zone. *Genes Dev.* 22, 2473–2478.

Livneh, Y., Feinstein, N., Klein, M., and Mizrahi, A. (2009). Sensory input enhances synaptogenesis of adult-born neurons. *J. Neurosci.* 29, 86–97.

Lledo, P. M., Alonso, M., and Grubb, M. S. (2006). Adult neurogenesis and functional plasticity in neuronal circuits. *Nat. Rev. Neurosci.* 7, 179–193.

Lobe, C. G., Koop, K. E., Kreppner, W., Lomeli, H., Gertsenstein, M., and Nagy, A. (1999). Z/AP, a double reporter for cre-mediated recombination. *Dev. Biol.* 208, 281–292.

Lugert, S., Basak, O., Knuckles, P., Haussler, U., Fabel, K., Goetz, M., Haas, C. A., Kempermann, G., Taylor, V., and Giachino, C. (2010). Quiescent and active hippocampal neural stem cells with distinct morphologies respond selectively to physiological and pathological stimuli and aging. *Cell Stem Cell* 6,445–456.

Luo, L., Callaway, E. M., and Svoboda, K. (2008). Genetic dissection of neural circuits. *Neuron* 57, 634–660.

Madisen, L., Zwingman, T. A., Sunkin, S. M., Oh, S. W., Zariwala, H. A., Gu, H., Ng, L. L., Palmiter, R. D., Hawrylycz, M. J., Jones, A. R., Lein, E. S., and Zeng, H. (2010). A robust and high-throughput Cre reporting and characterization system for the whole mouse brain. *Nat. Neurosci.* 13, 133–140.

Mao, X., Fujiwara, Y., Chapdelaine, A., Yang, H., and Orkin, S. H. (2001). Activation of EGFP expression by Cre-mediated excision in a new ROSA26 reporter mouse strain. *Blood* 97, 324–326.

Matsuda, T., and Cepko, C. L. (2004). Electroporation and RNA interference in the rodent retina in vivo and in vitro. *Proc. Natl. Acad. Sci. U.S.A.* 101, 16–22.

Matsuda, T., and Cepko, C. L. (2007). Controlled expression of transgenes introduced by *in vivo* electroporation. *Proc. Natl. Acad. Sci. U.S.A.* 104, 1027–1032.

McKay, R. (1997). Stem cell in the central nervous system. *Science* 276, 66–71.

Metzger, D., Clifford, J., Chiba, H., and Chambon, P. (1995). Conditional site-specific recombination in mammalian cells using a ligand-dependent chimeric Cre recombinase. *Proc. Natl. Acad. Sci. U.S.A.* 92, 6991–6995.

Mignone, J. L., Kukekov, V., Chiang, A., Steindler, D., and Enikolopov, G. (2004). Neural stem and progenitor cells in nestin-GFP transgenic mice. *J. Comp. Neurol.* 469, 311–324.

Ming, G., and Song, H. J. (2005). Adult neurogenesis in the mammalian central nervous system. *Annu. Rev. Neurosci.* 28, 223–250.

Mira, H., Andreu, Z., Suh, H., Lie, D. C., Jessberger, S., Consiglio, A., San Emeterio, J., Hortigüela, R., Marqués-Torrejón, M. A., Nakashima, K., Colak, D., Götz, M., Fariñas, I., and Gage, F. H. (2010). Signaling through BMPR-IA regulates quiescence and long-term activity of neural stem cells in the adult hippocampus. *Cell Stem Cell* 7, 78–89.

Miyamichi, K., Amat, F., Moussavi, F., Wang, C., Wickersham, I., Wall, N. R., Taniguchi, H., Tasic, B., Huang, Z. J., He, Z., Callaway, E. M., Horowitz, M. A., and Luo, L. (2011). Cortical representations of olfactory input by trans-synaptic tracing. *Nature* 472, 191–196.

Miyoshi, G., and Fishell, G. (2006). Directing neuron-specific transgene expression in the mouse CNS. *Curr. Opin. Neurobiol.* 16, 577–584.

Mori, T., Tanaka, K., Buffo, A., Wurst, W., Kühn, R., and Götz, M. (2006). Inducible gene deletion in astroglia and radial glia – a valuable tool for functional and lineage analysis. *Glia* 54, 21–34.

Mu, Y., Lee, S. W., and Gage, F. H. (2010). Signaling in adult neurogenesis. *Curr. Opin. Neurobiol.* 20, 416–423.

Muzumdar, M. D., Tasic, B., Miyamichi, K., Li, L., and Luo, L. (2007). A global double-fluorescent Cre reporter mouse. *Genesis* 45, 593–605.

Nagy, A. (2000). Cre recombinase: the universal reagent for genome tailoring. *Genesis* 26, 99–109.

Ninkovic, J., Mori, T., and Götz, M. (2007). Distinct modes of neuron addition in adult mouse neurogenesis. *J. Neurosci.* 27, 10906–10911.

Nissant, A., Bardy, C., Katagiri, H., Murray, K., and Lledo, P. M. (2009). Adult neurogenesis promotes synaptic plasticity in the olfactory bulb. *Nat. Neurosci.* 12, 728–730.

Novak, A., Guo, C., Yang, W., Nagy, A., and Lobe, C. G. (2000). Z/EG, a double reporter mouse line that expresses enhanced green fluorescent protein upon Cre-mediated excision. *Genesis* 28, 147–155.

Pastrana, E., Cheng, L. C., and Doetsch, F. (2009). Simultaneous prospective purification of adult subventricular zone neural stem cells and their progeny. *Proc. Natl. Acad. Sci. U.S.A.* 106, 6387–6392.

Possemato, R., Eggan, K., Moeller, B. J., Jaenisch, R., and Jackson-Grusby, L. (2002). Flp recombinase regulated lacZ expression at the ROSA26 locus. *Genesis* 32, 184–186.

Raymond, C. S., and Soriano, P. (2007). High-efficiency FLP and PhiC31 site-specific recombination in mammalian cells. *PLoS ONE* 2, e162. doi:10.1371/journal.pone.0000162

Sato, Y., Kasai, T., Nakagawa, S., Tanabe, K., Watanabe, T., Kawakami, K., and Takahashi, Y. (2007). Stable integration and conditional expression of electroporated transgenes in chicken embryos. *Dev. Biol.* 305, 616–624.

Saxe, M. D., Battaglia, F., Wang, J. W., Malleret, G., David, D. J., Monckton, J. E., Garcia, A., D., Sofroniew, M. V., Kandel, E. R., Santarelli, L., Hen, R., and Drew, M. R. (2006). Ablation of hippocampal neurogenesis impairs contextual fear conditioning and synaptic plasticity in the dentate gyrus. *Proc. Natl. Acad. Sci. U.S.A.* 103, 17501–17506.

Schmidt-Hieber, C., Jonas, P., and Bischofberger, J. (2004). Enhanced synaptic plasticity in newly generated granule cells of the adult hippocampus. *Nature* 429, 184–187.

Seri, B., Garcia-Verdugo, J. M., Collado-Morente, L., McEwen, B. S., and Alvarez-Buylla, A. (2004). Cell types, lineage, and architecture of the germinal zone in the adult dentate gyrus. *J. Comp. Neurol.* 478, 359–378.

Shimogori, T., and Ogawa, M. (2008). Gene application with in utero electroporation in mouse embryonic brain. *Dev. Growth Differ.* 50, 499–506.

Singer, B. H., Jutkiewicz, E. M., Fuller, C. L., Lichtenwalner, R. J., Zhang, H., Velander, A. J., Li, X., Gnegy, M. E., Burant, C. F., and Parent, J. M. (2009). Conditional ablation and recovery of forebrain neurogenesis in the mouse. *J. Comp. Neurol.* 514, 567–582.

Slezak, M., Göritz, C., Niemiec, A., Frisén, J., Chambon, P., Metzger, D., and Pfrieger, F. W. (2007). Transgenic mice for conditional gene manipulation in astroglial cells. *Glia* 55, 1565–1576.

Soriano, P. (1999). Generalized lacZ expression with the ROSA26 Cre reporter strain. *Nat. Genet.* 21, 70–71.

Sousa, V. H., Miyoshi, G., Hjerling-Leffler, J., Karayannis, T., and Fishell, G. (2009). Characterization of Nkx6-2-derived neocortical interneuron lineages. *Cereb. Cortex* 19 (Suppl. 1), i1–i10.

Srinivas, S., Watanabe, T., Lin, C. S., William, C. M., Tanabe, Y., Jessell, T. M., and Costantini, F. (2001). Cre reporter strains produced by targeted insertion of EYFP and ECFP into the ROSA26 locus. *BMC Dev. Biol.* 1, 4. doi:10.1186/1471-213X-1-4

Steiner, B., Klempin, F., Wang, L., Kott, M., Kettenmann, H., and Kempermann, G. (2006). Type-2 cells as link between glial and neuronal lineage in adult hippocampal neurogenesis. *Glia* 54, 805–814.

Strathdee, D., Ibbotson, H., and Grant, S. G. (2006). Expression of transgenes targeted to the Gt(ROSA)26Sor locus is orientation dependent. *PLoS ONE* 1, e4. doi:10.1371/journal.pone.0000004

Suh, H., Consiglio, A., Ray, J., Sawai, T., D-Amour, K. A., and Gage, F. H. (2007). *In vivo* fate analysis reveals the multipotent and self-renewal capacities of Sox2+ neural stem cells in the adult hippocampus. *Cell Stem Cell* 1, 515–528.

Tan, E. M., Yamaguchi, Y., Horwitz, G. D., Gosgnach, S., Lein, E. S., Goulding, M., Albright, T. D., and Callaway, E. M. (2006). Selective and quickly reversible inactivation of mammalian neurons *in vivo* using the Drosophila allatostatin receptor. *Neuron* 51, 157–170.

Temple, S. (2001). The development of neural stem cells. *Nature* 414, 112–117.

van Praag, H., Schinder, A. F., Christie, B. R., Toni, N., Palmer, T. D., and Gage, F. H. (2002). Functional neurogenesis in the adult hippocampus. *Nature* 415, 1030–1034.

Vintersten, K., Monetti, C., Gertsenstein, M., Zhang, P., Laszlo, L., Biechele, S., and Nagy, A. (2004). Mouse in red: red fluorescent protein expression in mouse ES cells, embryos, and adult animals. *Genesis* 40, 241–246.

Wickersham, I. R., Lyon, D. C., Barnard, R. J., Mori, T., Finke, S., Conzelmann, K. K., Young, J. A., and Callaway, E. M. (2007). Monosynaptic restriction of transsynaptic tracing from single, genetically targeted neurons. *Neuron* 53, 639–647.

Wojtowicz, J. M. (2006). Irradiation as an experimental tool in studies of adult neurogenesis. *Hippocampus* 16, 261–266.

Wu, S., Ying, G., Wu, Q., and Capecchi, M. R. (2007). Toward simpler and faster genome-wide mutagenesis in mice. *Nat. Genet.* 39, 922–930.

Wulff, P., Goetz, T., Leppä, E., Linden, A. M., Renzi, M., Swinny, J. D., Vekovischeva, O. Y., Sieghart, W., Somogyi, P., Korpi, E. R., Farrant, M., and Wisden, W. (2007). From synapse to behavior: rapid modulation of defined neuronal types with engineered GABAA receptors. *Nat. Neurosci.* 10, 923–929.

Young, K. M., Mitsumori, T., Pringle, N., Grist, M., Kessaris, N., and Richardson, W. D. (2010). An Fgfr3-iCreER(T2) transgenic mouse line for studies of neural stem cells and astrocytes. *Glia* 58, 943–953.

Zambrowicz, B. P., Imamoto, A., Fiering, S., Herzenberg, L. A., Kerr, W. G., and Soriano, P. (1997). Disruption of overlapping transcripts in the ROSA beta geo 26 gene trap strain leads to widespread expression of beta-galactosidase in mouse embryos and hematopoietic cells. *Proc. Natl. Acad. Sci. U.S.A.* 94, 3789–3794.

Zhang, J., Giesert, F., Kloos, K., Vogt Weisenhorn, D. M., Aigner, L., Wurst, W., and Couillard-Despres, S. (2010). A powerful transgenic tool for fate mapping and functional analysis of newly generated neurons. *BMC Neurosci.* 11,158. doi:10.1186/1471-2202-11-158

Zhang, F., Wang, L. P., Brauner, M., Liewald, J. F., Kay, K., Watzke, N., Wood, P. G., Bamberg, E., Nagel, G., Gottschalk, A., and Deisseroth, K. (2007). Multimodal fast optical interrogation of neural circuitry. *Nature* 446, 633–639.

Zhao, C., Teng, E. M., Summers, R. G. Jr., Ming, G. L., and Gage, F. H. (2006). Distinct morphological stages of dentate granule neuron maturation in the adult mouse hippocampus. *J. Neurosci.* 26, 3–11.

Zimmerman, L., Lendahl, U., Cunningham, M., McKay, R., Parr, B., Gavin, B., Mann, J., Vassileva, G., and

McMahon, A. (1994). Independent regulatory elements in the nestin gene direct transgene expression to neural stem cells or muscle precursors. *Neuron* 12, 11–24.

Conflict of Interest Statement: The authors declare that the research was conducted in the absence of any commercial or financial relationships that could be construed as a potential conflict of interest.

Received: 31 January 2011; accepted: 19 April 2011; published online: 02 May 2011.

Citation: Imayoshi I, Sakamoto M and Kageyama R (2011) Genetic methods to identify and manipulate newly born neurons in the adult brain. Front. Neurosci. ***5****:64. doi: 10.3389/fnins.2011.00064*
This article was submitted to Frontiers in Neurogenesis, a specialty of Frontiers in Neuroscience.

frontiers in
NEUROSCIENCE

REVIEW ARTICLE
published: 05 April 2011
doi: 10.3389/fnins.2011.00048

Genetic approaches to reveal the connectivity of adult-born neurons

Benjamin R. Arenkiel [1,2,3]*

[1] Department of Molecular and Human Genetics, Baylor College of Medicine, Houston, TX, USA
[2] Department of Neuroscience, Baylor College of Medicine, Houston, TX, USA
[3] Jan and Dan Duncan Neurological Research Institute at Texas Children's Hospital, Baylor College of Medicine, Houston, TX, USA

Edited by:
Silvia De Marchis, University of Turin, Italy

Reviewed by:
Alan Carleton, University of Geneva, Switzerland
Serena Bovetti, University of Turin, Italy

***Correspondence:**
Benjamin R. Arenkiel, Department of Molecular and Human Genetics, Jan and Dan Duncan Neurological Research Institute, Baylor College of Medicine, 1250 Moursund Street, Suite 1165.0, Houston, TX 77030, USA.
e-mail: arenkiel@bcm.edu

Much has been learned about the environmental and molecular factors that influence the division, migration, and programmed cell death of adult-born neurons in the mammalian brain. However, detailed knowledge of the mechanisms that govern the formation and maintenance of functional circuit connectivity via adult neurogenesis remains elusive. Recent advances in genetic technologies now afford the ability to precisely target discrete brain tissues, neuronal subtypes, and even single neurons for vital reporter expression and controlled activity manipulations. Here, I review current viral tracing methods, heterologous receptor expression systems, and optogenetic technologies that hold promise toward elucidating the wiring diagrams and circuit properties of adult-born neurons.

Keywords: neurogenesis, synapse, circuit, viruses, optogenetics, heterologous, trans-synaptic, monosynaptic

INTRODUCTION

The ongoing addition of new neurons to adult brain circuits represents a remarkable mode of both cellular and structural plasticity. In mammals, two main areas support continued neurogenesis: the subgranular zone (SGZ) of the dentate gyrus in the hippocampus, and the subventricular zone (SVZ) of the lateral ventricle (Alvarez-Buylla and Temple, 1998; Ming and Song, 2005; Zhao et al., 2008). Neurons born in the SGZ migrate short distances to the dentate granule cell layer and differentiate into dentate granule cells (Song et al., 2002), whereas those born in the SVZ migrate anteriorly and differentiate into inhibitory interneurons of the olfactory bulb, including both granule and periglomerular cells (Lledo and Saghatelyan, 2005; Bovetti et al., 2007). It is generally thought that turnover, replacement, or *de novo* integration of newborn neurons into these brain regions may be important for different forms of learning, memory, mood control, and/or perception (Gheusi et al., 2000; Santarelli et al., 2003; Kempermann et al., 2004; Imayoshi et al., 2008; Zhang et al., 2008; Breton-Provencher et al., 2009).

Since the discovery of adult neurogenesis nearly four decades ago (Altman and Das, 1965a,b), a great deal of emphasis has been placed on better understanding the mechanisms underlying this phenomenon for potential therapeutic avenues in cell-based tissue repair. Similar in many ways to normal neurodevelopment, adult neurogenesis shares several conserved molecular and genetic programs that influence progenitor cell division, migration, neuronal differentiation, and circuit integration (Esposito et al., 2005; Duan et al., 2008). However, whereas in embryogenesis where most of the nervous system develops in concert, adult-born neurons must navigate through the established cellular and extracellular environments of the mature brain. Because the mechanisms of adult-born neuron circuit integration come under the dynamic influence of preexisting tissues and brain structures, this represents a strikingly different scenario than early brain development. Newborn neurons in the adult must make their way into established brain circuits via a host of different guidance and survival cues, including a milieu of membrane-bound and secreted factors, functioning neuronal networks, and a range of different synaptic and extrasynaptic inputs. In addition, it is now appreciated that numerous extrinsic physiological and pathological processes that affect overall brain function also directly influence adult-born neuron circuit integration (Zhao et al., 2008; Ma et al., 2009; Suh et al., 2009).

Several elegant electrophysiological, electron microscopy, and *in vivo* imaging studies in rodents have begun to identify the types of synaptic interactions that accompany the development and integration of newborn neurons into adult brain circuits (Belluzzi et al., 2003; Carleton et al., 2003; Ming and Song, 2005; Mizrahi et al., 2006; Toni et al., 2008; Livneh et al., 2009; Panzanelli et al., 2009; Whitman and Greer, 2009). Although several principles of adult-born neuron birth, migration, and integration into adult brain circuits are similar between the hippocampus and olfactory system, they also contrast in many ways. Notable differences include the terminal cell types generated, migration distances, and final patterns of connectivity. Our knowledge continues to expand with regards to the exact forms of synaptic and/or neuromodulatory input that adult-born neurons receive during sequential stages of neuronal maturation and circuit integration in both systems.

In the hippocampal formation, newborn neurons are known to receive local GABAergic inputs during early stages of integration. Similar to what occurs in development, this GABAergic drive is considered to be excitatory and capable of depolarizing newborn neurons (Overstreet Wadiche et al., 2005; Ge et al., 2006, 2007). Also during this time, newborn dentate granule cells begin to establish contacts with their CA3 targets. With maturation, GABAergic input from local interneurons becomes inhibitory, and new excitatory

synaptic inputs are made onto the newborn neurons from the entorhinal cortex. Alongside the known connectivity onto the neurons themselves, the neurogenic niche of the hippocampus also receives extensive input from several brain regions, including the septum, ventral tegmental area, locus coeruleus, median raphe nucleus, and supramammillary region (Freund and Buzsaki, 1996; Zhao et al., 2008; **Figure 1**). It remains unknown how these different types of inputs modulate the incorporation, survival, and maturation of granule cells in the dentate gyrus and their importance for learning and memory.

Similar to the hippocampus, the survival, integration, and maturation of newborn neurons in the olfactory bulb is thought to require excitatory drive from multiple brain regions onto the developing granule cells (Pathania et al., 2010). As the newborn olfactory bulb neurons migrate anteriorly, mature, and take residence within local bulbar networks, they first receive GABAergic input (Belluzzi et al., 2003; Carleton et al., 2003), followed shortly after by local inputs from olfactory sensory neurons, mitral cells, and various short axon cell types (Shepherd, 2004). However, some of the first contacts onto newborn granule and periglomerular cells are thought to come from centrifugal fibers (Panzanelli et al., 2009). The number and type of centrifugal inputs to the bulb is vast, including connections from the anterior olfactory nucleus, piriform, periamygdaloid, and lateral entorhinal cortices, as well as neuromodulatory input from the nucleus of the diagonal band, raphe nuclei, and locus coeruleus (Shipley and Ennis, 1996; Whitman and Greer, 2009). Interestingly, both of the neurogenic regions in the brain have inputs from common structures (**Figure 1**).

In both scenarios it takes roughly 1 month for adult-born neurons to become synaptically integrated into functional brain circuits. Ultimately, only about one half of all neurons born at any given time point survive this process and escape cell death, a phenomenon that is thought to be activity-dependent (van Praag et al., 1999; Petreanu and Alvarez-Buylla, 2002; Rochefort et al., 2002; Leuner et al., 2004; Alonso et al., 2006; Ma et al., 2009). Considering the timing, diversity, and nature of the inputs to adult neurogenic regions and the neurons born from them, it is reasonable to speculate that signals from both centrifugal and local pathways likely play discrete roles at different stages of newborn neuron survival and circuit integration. However, it remains to be determined which of these different inputs make direct synaptic contacts onto newborn neurons, and when during circuit integration they might act.

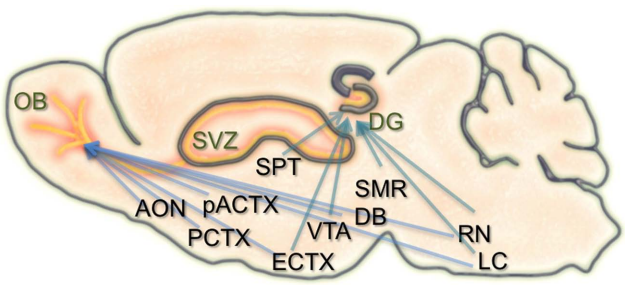

FIGURE 1 | Schematic of the inputs to regions of adult neurogenesis and circuit formation. Illustration of a sagittal section through the rodent brain. Orange areas depict regions of adult neurogenesis and circuit development. Blue arrows extending to the olfactory bulb (OB), and dentate gyrus (DG) originate from brain structures that have inputs to these areas. Many of these structures have inputs to both the OB and DG. SVZ, subventricular zone; AON, anterior olfactory nucleus; PCTX, piriform cortex; pACTX, periamygdaloid cortex; SPT, septum; ECTX, entorhinal cortex; VTA, ventral tegmental area; DB, nucleus of the diagonal band; SMR, supramammillary region; RN, raphe nucleus; LC, locus coeruleus.

Given the complexity of the synaptic networks, the shear number and types of cells that make up the brain, and the dynamic interplay between the various intrinsic and extrinsic factors known to influence adult neurogenesis, many of the detailed molecular programs that underlie the circuit integration process remain elusive. In order to better understand the mechanisms that link the environment and sensory experience to the genetic pathways and molecules that facilitate ongoing synapse and circuit formation in the adult brain, it is essential to first crack the neuroanatomical code of cellular connectivity made onto newborn neurons as they form synapses and circuits. Identifying the precise neuronal subtypes that provide inputs onto adult-born neurons promises to reveal key molecular pathways that facilitate and govern this fascinating phenomenon. With such knowledge, genetic manipulations aimed at promoting the synthetic enrichment of adult-born neurons to target brain regions become imaginable. To date, this goal has remained a challenge.

We have now entered an astounding new era of molecular and genetic neuroscience. Through experimental creativity and novel genetic engineering methods, recent technological advances now allow investigators to mark, manipulate, and image neurons and their associated synaptic networks (Arenkiel and Ehlers, 2009; O'Connor et al., 2009). With the ability to precisely target discrete brain tissues, neuronal subtypes, and even single neurons for vital reporter expression and controlled activity manipulations, we are now afforded the opportunity to query previously intractable aspects of brain wiring (Luo et al., 2008). On the forefront of this endeavor lies a widespread interest to better understand the molecular mechanisms that govern adult-born neuron circuit integration. Here I review current viral tracing methods, heterologous receptor expression systems, and optogenetic technologies that hold promise toward elucidating the wiring diagrams and circuit properties of adult-born neurons. In addition, these technologies allow for direct manipulation of circuit activity, which will undoubtedly reveal unknown roles of adult neurogenesis in normal brain function, animal behavior, and perhaps provide clues toward harnessing adult-born neurons for cell-based circuit repair.

LABELING THE LIVING BRAIN

Owing to the complexity of the mammalian brain, it has remained a major challenge to decipher the patterns of connectivity made onto and by newborn neurons as they integrate into circuits of the adult brain. With major advances in both molecular genetics and light microscopy, our ability to query not only neuronal morphologies, but also the molecular and cellular composition of individual neurons and their associated synaptic networks has become possible. Marking and manipulating neurons through transgenic and gene targeting technologies in the rodent (Brinster et al., 1981; Capecchi, 1989) now allows investigators to "program" neuronal subsets with unprecedented precision (Arenkiel and Ehlers, 2009).

Arguably, one of the most influential contributions to contemporary neuroscience has been the use of fluorescent proteins (FPs; Shimomura et al., 1962; Chalfie et al., 1994) and their targeted expression in living neurons of the mammalian brain tissue. The wide array of FPs available provides an ever-expanding toolbox of vital reporters and gene expression tags (Feng et al., 2000; Giepmans et al., 2006). Applications for these proteins range from vital reporters expressed throughout the cytoplasm to subcellular protein fusion tags, which together can be used to monitor the process of circuit integration *in vivo* using both electrophysiological methods and fluorescent imaging.

Beyond merely marking cells for identification, a number of other methods have been developed to exploit the vital properties of FPs to investigate neuronal properties. For example, superecliptic pHluorin, which fluoresces at neutral pH but is quenched at acidic pH, can be used to monitor the trafficking and exchange of intracellular compartments within neurons (Miesenbock et al., 1998). This variant allows direct imaging of membrane dynamics, exocytosis and endocytosis of synaptic receptors, and neurotransmitter release *in vitro* and *in vivo* (Bozza et al., 2004; Fernandez-Alfonso et al., 2006; Park et al., 2006; Kennedy et al., 2010). More recently, a new method termed GFP reconstitution across synaptic partners (GRASP) shows promise for revealing synaptic interactions between contacting neurons. By tethering split GFP fragments to separate pre- and post-synaptic proteins, reconstitution of GFP fluorescence can be observed when genetically targeted cells form synaptic pairs (Feinberg et al., 2008). Although this technology has been successfully applied to reveal invertebrate synapses, it has yet to be demonstrated in rodents (Gordon and Scott, 2009).

The range of FP reporters for visualizing neuronal morphologies, cellular dynamics, and synapse function continues to expand. However, perhaps the single-most limiting factor for using FPs in neuroscience is our incomplete knowledge of neuronal gene regulation. Often transgenic reporters fail to recapitulate endogenous patterns of gene expression, or such patterns are too broad to identify neuronal subtypes with cellular precision. The introduction of gene targeting and BAC transgenics has helped circumvent many of these issues (Gong et al., 2003), but at times low levels of "single-copy" reporter expression can be experimentally limiting. Further characterization of cell type-specific promoter activities to drive targeted FP expression in discrete neuronal populations will certainly expand the ability for precise spatiotemporal neuroanatomical investigation. Ultimately however, the exploitation of FPs and their cast of variants has allowed investigators to genetically probe adult-born neuron circuit integration with limits only bounded by experimental creativity.

TRANS-SYNAPTIC CIRCUIT TRACING

A major goal toward understanding mechanisms of neuronal development, synapse formation, and circuit wiring has been to elucidate nodes and patterns of synaptic connectivity. A creative angle to address this challenge has been the incorporation of genes encoding FPs and FP-fusion proteins into neurotropic viral vectors, which show the innate ability to infect neurons and trans-synaptically spread throughout the nervous system (Kuypers and Ugolini, 1990; Callaway, 2008).

Two types of viruses that have been broadly employed for this purpose include rabies and herpes. Herpes viruses belong to a family of double-stranded DNA viruses, while rabies belongs to a family of negative-strand RNA viruses (Voyles, 1993). Although evolutionarily different, they are both endowed with the unique ability to bind to and infect neuronal cells. This cell type-specific infectivity is conferred to the viruses via their mature enveloped coat particles, which are made of both host membrane and virally encoded glycoproteins. The composite envelope proteins are the determinants that mediate neuronal membrane recognition and subsequent neuron-to-neuron infection by binding to membrane surface receptors.

Herpes viruses have been used to label neural circuits for years. Two common tracing strains are herpes simplex virus-1 (HSV-1; Lilley et al., 2001) and pseudorabies virus (PRV; Enquist, 2002). Both of these variants predominantly spread in a retrograde direction, and each has been effectively applied to dissect synapse and circuit connections in the rodent brain (Callaway, 2008). However, one limitation to using the herpes viruses for circuit analysis is polysynaptic spreading. Due to the vast cohort of cell types within brain tissue, the number of synapses formed on each of those cells, and the high degree of interconnectivity in intact neural circuits, this approach still poses a challenge to dissect precise patterns of neural connectivity. To simplify trans-synaptic circuit analysis, Wickersham et al. (2007b) devised a clever coat protein complementation strategy that allows for monosynaptic tracing of neuronal connections using a pseudotyped rabies virus (RV). Not to be confused with PRV (which as stated above is actually a herpes virus), pseudotyping a viral particle refers to synthetically modifying the viral envelope to recognize a foreign receptor not normally present on the membranes of mammalian neurons. The strategy will be briefly discussed below, and for further reference also see Wickersham et al. (2007a), Arenkiel and Ehlers (2009), Hasenstaub and Callaway (2010).

The RV gene encoding its glycoprotein (termed G) has been the primary target for genetic modification and RV vector engineering. Removal of G from the RV genome renders the virus both incapable of generating infective particles and replication incompetent. However, even in the absence of the native glycoprotein gene, RV is still capable of expressing its genome. Thus, G can be replaced with sequences encoding FPs or FP-tagged biomolecules to generate RV vectors for vital reporter expression (Wickersham et al., 2007a). To make these replication incompetent viruses useful for circuit tracing studies, they must be "armed" by providing an envelope *in trans* by propagating and packaging the particles *in vitro* using cell lines engineered to synthesize the required glycoprotein.

To perform monosynaptic circuit tracing and target FP-expressing RV to desired neuronal subsets, the particles can first be pseudotyped with the foreign coat protein EnvA from avian sarcoma leukosis virus, which specifically binds to a class of avian membrane proteins called TVA receptors (Barnard et al., 2006). Genetic targeting of neuronal subsets for TVA expression directs RV infection to only those neurons. To facilitate monosynaptic tracing, Wickersham et al. (2007a) added a clever twist on this approach. By introducing a plasmid that encodes the wildtype RV G-protein, the disarmed EGFP-expressing virus is now able to undergo one round of subsequent infection to presynaptic partners of TVA-targeted

neurons. Since only the initially infected neuron contains G, viral spread ceases after one round of monosynaptic jumping. Including a plasmid encoding a red FP allows the cell originally targeted for infection to be identified amongst the monosynaptic network of GFP labeled cells (**Figure 2**). Of course it must be considered that true monosynaptic tracing is dependent on targeting individual neurons for the expression of G. If for example synaptically coupled cells both harbor G, but only one of them serves as the primary source cell of TVA-mediated infection, then viral spread can become multisynaptic through subsequent rounds of viral packaging in presynaptic partners. Monosynaptic tracing control thus depends directly upon the precision of neuronal targeting for the RV tracing components.

This new technology now makes it feasible to dissect complicated patterns of neuronal connectivity with synaptic precision (Stepien et al., 2010; Weible et al., 2010). Targeting adult-born neurons for monosynaptic circuit tracing holds certain promise toward elucidating the numbers, types, and synaptic inputs that might usher and/or promote the formation and maintenance of functional circuit integration. Unfortunately however, much needs to be learned about the viral mechanisms of infectivity, trans-synaptic propagation, and replication to make viral tracing methods broadly applicable for detailed circuit analysis throughout the nervous system. For example, one major limitation to viral-mediated circuit tracing using either HSV or RV type vectors is the inevitable deterioration of neuronal cell health with time (Callaway, 2008). Whereas the HSV particles show rapid and high levels of expression within 1–2 days, they also show a lytic-type phase of replication that induces neuronal loss within 1–2 weeks. Although most neurons appear to tolerate RV infection for longer periods of time, they too eventually show signs of dysfunction and poor health beyond 2 weeks. In addition, not much is known regarding the exact tropism for the various viruses to infect particular subtypes of neurons. Although it is clear that viral particles can cross axo-dendritic, dendro-dendritic, glutamatergic, and GABAergic synapses (Willhite et al., 2006; Wickersham et al., 2007b; Stepien et al., 2010; Miyamichi et al., 2011; Rancz et al., 2011), the different efficacies of transfer have not been determined. Preferential binding of viral particles to different types of presynaptic proteins must exist, which would ultimately result in more efficient transfer of viruses between certain synaptic pairs. This information is currently unknown, thus it remains a challenge to reliably perform unbiased quantitative circuit analysis using viruses over extended periods of time.

Although current trans-synaptic circuit tracing methods are in their infancy, with further understanding of the viral mechanisms, and a subsequent "re-tooling" of existing vectors, one can easily imagine that this experimental avenue for intact circuit mapping will become indispensable. Moreover, this methodology holds definite promise to address outstanding questions in adult neurogenesis, ranging from identification of the types of connections that

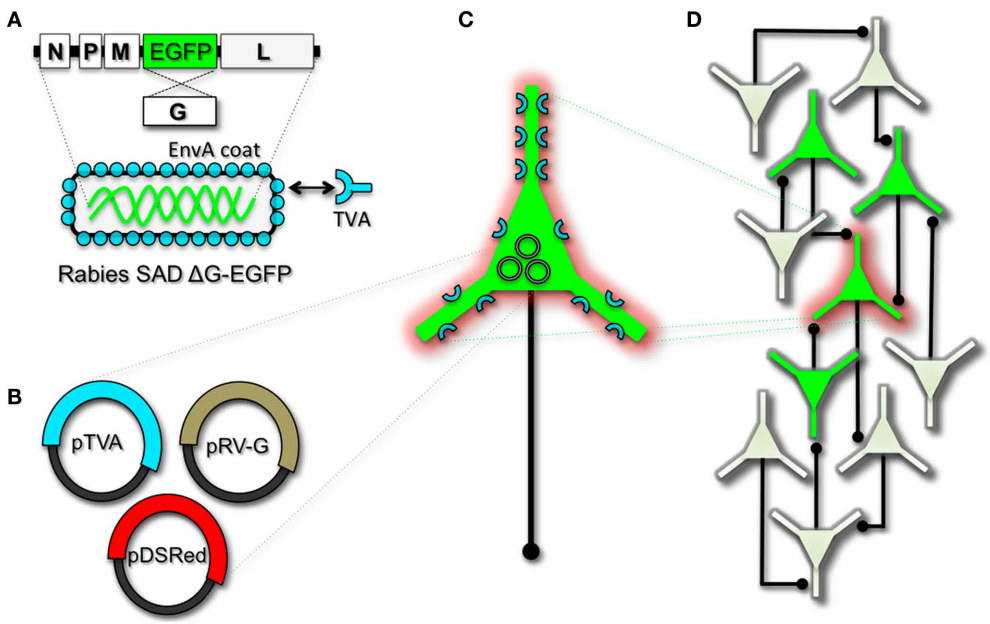

FIGURE 2 | Engineering and pseudotyping rabies virus (RV) for transneuronal tracing. (A) RV can be genetically engineered to express EGFP by replacing the genomic sequence encoding the G coat protein. The genetically modified G-deletion mutant RV must be propagated *in vitro* to supply a coat protein. The particle can thus be pseudotyped by providing a foreign coat protein such as EnvA, which originates from the avian leukosis virus and binds specifically to it its cognate receptor TVA. EnvA pseudotyped RV can be used to selectively infect neurons that have been genetically targeted for TVA expression. By including additional constructs that encode the wildtype G-capsid protein and a red-colored "cell fill" **(B)**, the modified RV can be genetically targeted to individual neurons for restricted circuit mapping and monosynaptic tracing **(C).** Since no endogenous receptors exist in the mammalian brain for EnvA, only neurons that are programmed to express TVA are capable of being infected by the EnvA pseudotyped virions. Because the wildtype G-protein sequence has been deleted from the RV genome, G must be supplied by complementation to allow trans-synaptic spread from the neurons targeted for infection. **(D)** Viral spread ceases monosynaptically due to the absence of G in unmodified neuronal populations.

are dynamically made and broken during circuit development, to exposing the complete cohort of input types that are observed in mature circuits within the intact brain.

MANIPULATING CELL AND CIRCUIT ACTIVITY

Earmarking neuronal subsets and their associated networks for has been invaluable toward our current understanding of neuronal morphologies and circuit architecture. However, to fully understand the cellular and molecular mechanisms that guide adult-born neuron synapse formation and circuit integration, we must be able to probe neuronal connectivity. Recent advances in genetically encoded actuators now provide this possibility. Technologies such as heterologous receptor or channel expression, optogenetics, and genetically encoded synaptic toxins are beginning to allow functional circuit mapping with synaptic precision (Luo et al., 2008; Arenkiel and Ehlers, 2009; **Figure 3**). By targeting pre- or post-synaptic cell

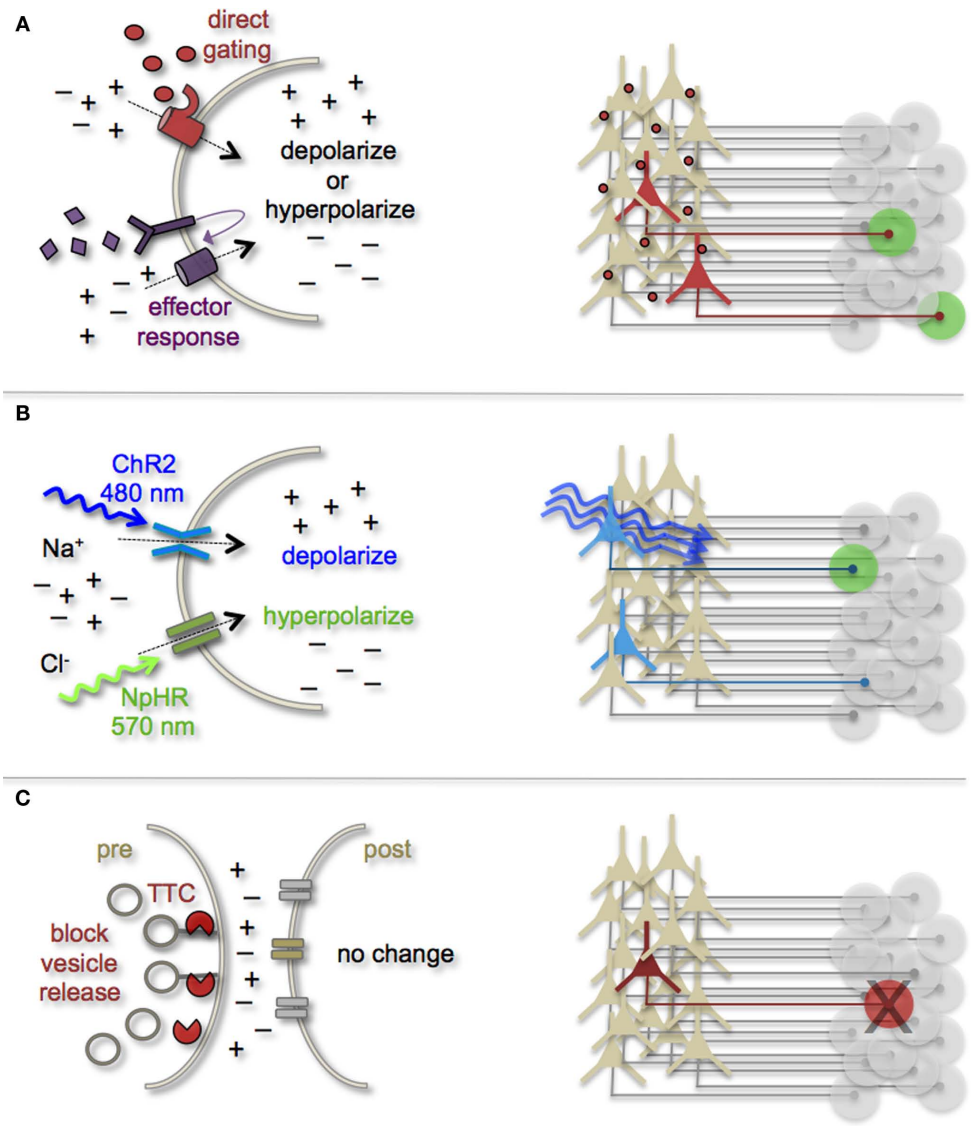

FIGURE 3 | Genetic strategies to mark and manipulate neurons and circuits. (A) Neurons can be targeted for heterologous receptor expression. These foreign receptors can be either directly or indirectly gated by application of exogenous ligands (depicted as red ovals and purple diamonds). Left: heterologous receptor activation via application of synthetic ligands can be used to change a neuron's ionic equilibrium and thus firing properties. Right: depending on molecular properties, exogenous ligands spread variably throughout brain tissue. All neurons expressing the heterologous receptors are capable of being activated and driving target cell responses (represented as green circles). **(B)** Expression of light-gated channels can be used to modulate neuronal firing with photons. Left: ChR-2 is a non-selective cation channel that responds optimally to blue light. Photostimulating this channel results in positive inward currents, depolarization, and neuronal firing. NpHR is a photoactive chloride pump that responds optimally to greenish-yellow light. Photostimulating this pump protein results in negative inward currents, hyperpolarization, and neuronal silencing. Right: FP-fusion reporters can be used to identify cells that express photoresponsive proteins (represented by blue coloring). Only neurons expressing the photoresponsive channels and receive photons show light activated modulation, whereas downstream circuit targets can be monitored for post-synaptic photo responses (green coloring). **(C)** Targeted expression of synaptic toxins in neurons can be used to block synaptic vesicle release and inhibit neurotransmission to post-synaptic targets. TTC, tetanus toxin.

types for activity manipulations, coupled with functional imaging and/or electrophysiological recordings, it is now possible to genetically dissect circuit nodes by monitoring evoked synthetic output responses. Some of the earliest efforts to genetically control neuronal output relied on engineered expression of heterologous receptors in neurons that normally do not show their presence. For example, expression of modified opiate receptors in the brains of transgenic mice showed that introducing synthetic exogenous ligands could activate neuronal subsets (Zhao et al., 2003). To date, numerous variations on this theme have proven effective for both driving neuronal excitability and inhibition. Models for promoting depolarization and increased neuronal firing have spanned custom G-protein-coupled receptors designed for sensitivity to synthetic ligands (Conklin et al., 2008), hyperdopaminergic drive through ectopic acetylcholine receptor activation (Drenan et al., 2008), and conditional expression and activation of the rat TRPV1 receptor in select population of neurons (Arenkiel et al., 2008). Methods to induce hyperpolarization or inhibit action potential generation have included targeted expression of the *Drosophila* allostatin receptor and the *C. elegans* ivermectin channel, which promote opening of inward-rectifying K^+ channels or chloride channels respectively (Tan et al., 2006; Lerchner et al., 2007; Wehr et al., 2009). Orthogonal strategies to these methods have been to genetically express small-molecules for inactivation of synaptic transmission (Karpova et al., 2005), or toxins that disrupt synaptic transmission (Harms et al., 2005; Ehlers et al., 2007).

In several models mentioned above, temporal control of neuronal activity (excitatory or inhibitory) is gained by providing the target molecule's "designer" ligand (**Figure 3A**). It must be cautioned, that although these avenues for manipulating neuronal output by the introduction of exogenous ligands are still bounded by biophysical properties of the ligands themselves. In many cases, it has been notoriously difficult to predict a ligands efficacy for crossing the mammalian blood–brain barrier, as well as determining the binding kinetics for the engineered receptor within the complex tissue environment that comprises the brain. Not all genetically encoded channel systems require the presence or absence of a ligand to influence neuronal firing however. It is also possible to directly modify the excitability of a cell by overexpressing or ectopically expressing ion-specific channels to alter a neuron's ionic equilibrium. In fact, this experimental design has been previously implemented to directly query how changes in membrane excitability influence the ability for newborn neurons in the olfactory system to survive and integrate into bulbar circuits (Lin et al., 2010). Within the last few years, genetic manipulation of neuronal activity has rapidly moved beyond expression of ectopic ligand-gated and rectifying channels. Light responsive proteins now facilitate control of neuronal firing with fast kinetics and millisecond precision. The burgeoning field of optogenetics provides the means to either increase neuronal firing by targeted expression of the Channelrhodopsins, or decrease firing with Halorhodopsins (Zhang et al., 2007a, 2010). The Channelrhodopsins comprise a family of light-gated cation channels that were originally identified and cloned from the green algae *Chlamydomonas reinhardtii* (Nagel et al., 2005), whereas the Halorhodopsins are light-driven chloride ion pumps from halobacteria (Chow et al., 2010). Each of these classes of light responsive proteins is gated by different photo spectra. Channelrhodopsin-2 (ChR-2) shows a peak response to blue light (480 nm; Nagel et al., 2003), whereas NpHR responds optimally to greenish-yellow light (570 nm; Zhang et al., 2007b; **Figure 3B**). Not only can these photoresponsive channels be used independently to turn neurons "on" or "off," but they can also be used in combination to provide control over both states by toggling the color of light used for photoillumination (Han and Boyden, 2007; Zhang et al., 2007b). The power of this of technology has transformed modern circuit mapping in living brain tissue. Thus far, applications have ranged from microcircuit analysis to long-range connectivity studies *in vivo* (Arenkiel et al., 2007; Petreanu et al., 2007; Wang et al., 2007). Additionally, optogenetic mapping of deep brain circuits has begun to reveal previously unknown patterns of connectivity that underlie complex behaviors and neuropsychiatric disorders (Deisseroth, 2010; Lin et al., 2011).

Aside from a handful of recent elegant studies (Toni et al., 2008; Bardy et al., 2010), optogenetic technology has not been broadly applied to investigate adult-born neuron circuit integration *in vivo*. It is intriguing to contemplate different experimental designs that might be used to genetically dissect the input/output relationships between pre- and post-synaptic connections that are made during the circuit integration process. This might be accomplished by selectively targeting neuronal subtypes with known inputs onto newborn neurons for photostimulation, or photoinactivation. Alternatively, optogenetic reporters could be expressed in newborn neuron populations at different stages of circuit development to assess cell autonomous effects of activity upon survival, synapse formation, and circuit maintenance. An appealing consideration for using optogenetics in this line of experimentation is the versatility of subtype-specific targeting, as well as the dynamic range of neuronal control that is possible. However, it must still be acknowledged that optogenetic technology still remains relatively nascent. In all of its elegance, experimental applications are still bounded by the biophysical parameters of delivering light into the brain. Aside from superficial target domains such as the cortex, or perhaps the surface of the olfactory bulb, photon delivery requires invasive brain surgery and/or the introduction of foreign material such as fiber optics into target deep brain tissues for photostimulation. Nonetheless, these new methods for genetically marking and manipulating cells of the olfactory system hold great promise to broaden our understanding of the activity-dependent mechanisms that underlie adult-born neuron circuit integration.

CONCLUDING REMARKS

To date, many of the experimental methods that have been used to investigate the propensity for adult-born neurons to find their way into functional circuits have relied on direct imaging or recording the electrophysiological properties of newborn neurons at different stages of development. Through this cumulative work we have gained a wealth of knowledge about the amazing capacity of the adult brain to continually remodel its own structure and function. We now have the power to dissect neuron and circuit activities with genetic precision, as well as label and identify synaptically coupled neural networks. Once we begin to reveal the various pre- and post-synaptic cell types that comprise adult-born neuronal circuits, we then might be able to probe the synaptic contributions of discrete inputs to promote and/or guide adult circuitogenesis. These new technologies not only provide new avenues for our continual learning

about neural development and circuit formation, but they also may reveal novel insights into the fundamental principles that underlie the phenomenon of adult neurogenesis. A comprehensive understanding of this elusive and intriguing process will require creative and multifaceted experimental inquiry. The brain's map is nothing less than extremely complex; understanding the dynamic and plastic properties of continued "wiring" will require our best efforts.

ACKNOWLEDGMENTS

I would like to thank Tom Newpher, Mirjana Maletic-Savatic, Jeff Neul, and Jennifer Selever for thoughtful comments on this manuscript. Also, I would like to apologize for those primary works not referenced here due to space limitations. Funding through the McNair Foundation, NINDS award R00NS064171, and NARSAD supported this work.

REFERENCES

Alonso, M., Viollet, C., Gabellec, M. M., Meas-Yedid, V., Olivo-Marin, J. C., and Lledo, P. M. (2006). Olfactory discrimination learning increases the survival of adult-born neurons in the olfactory bulb. *J. Neurosci.* 41, 10508–10513.

Altman, J., and Das, G. D. (1965a). Autoradiographic and histological evidence of postnatal hippocampal neurogenesis in rats. *J. Comp. Neurol.* 124, 319–335.

Altman, J., and Das, G. D. (1965b). Postnatal origin of microneurones in the rat brain. *Nature* 207, 953–956.

Alvarez-Buylla, A., and Temple, S. (1998). Stem cells in the developing and adult nervous system. *J. Neurobiol.* 36, 105–110.

Arenkiel, B. R., and Ehlers, M. D. (2009). Molecular genetics and imaging technologies for circuit-based neuroanatomy. *Nature* 461, 900–907.

Arenkiel, B. R., Klein, M. E., Davison, I. G., Katz, L. C., and Ehlers, M. D. (2008). Genetic control of neuronal activity in mice conditionally expressing TRPV1. *Nat. Methods* 5, 299–302.

Arenkiel, B. R., Peca, J., Davison, I. G., Feliciano, C., Deisseroth, K., Augustine, G. J., Ehlers, M. D., and Feng, G. (2007). In vivo light-induced activation of neural circuitry in transgenic mice expressing channelrhodopsin-2. *Neuron* 54, 205–218.

Bardy, C., Alonso, M., Bouthour, W., and Lledo, P. M. (2010). How, when, and where new inhibitory neurons release neurotransmitters in the adult olfactory bulb. *J. Neurosci.* 30, 17023–17034.

Barnard, R. J., Elleder, D., and Young, J. A. (2006). Avian sarcoma and leukosis virus-receptor interactions: from classical genetics to novel insights into virus-cell membrane fusion. *Virology* 344, 25–29.

Belluzzi, O., Benedusi, M., Ackman, J., and LoTurco, J. J. (2003). Electrophysiological differentiation of new neurons in the olfactory bulb. *J. Neurosci.* 23, 10411–10418.

Bovetti, S., Peretto, P., Fasolo, A., and De Marchis(2007). Spatio-temporal specification of olfactory bulb interneurons. *J. Mol. Histol.* 38, 563–569.

Bozza, T., McGann, J. P., Mombaerts, P., and Wachowiak, M. (2004). In vivo imaging of neuronal activity by targeted expression of a genetically encoded probe in the mouse. *Neuron* 42, 9–21.

Breton-Provencher, V., Lemasson, M., Peralta, M. R. III, and Saghatelyan, A. (2009). Interneurons produced in adulthood are required for the normal functioning of the olfactory bulb network and for the execution of selected olfactory behaviors. *J. Neurosci.* 29, 15245–15257.

Brinster, R. L., Chen, H. Y., Trumbauer, M., Senear, A. W., Warren, R., and Palmiter, R. D. (1981). Somatic expression of herpes thymidine kinase in mice following injection of a fusion gene into eggs. *Cell* 27, 223–231.

Callaway, E. M. (2008). Transneuronal circuit tracing with neurotropic viruses. *Curr. Opin. Neurobiol.* 18, 617–623.

Capecchi, M. R. (1989). Altering the genome by homologous recombination. *Science* 244, 1288–1292.

Carleton, A., Petreanu, L. T., Lansford, R., Alvarez-Buylla, A., and Lledo, P. M. (2003). Becoming a new neuron in the adult olfactory bulb. *Nat. Neurosci.* 6, 507–518.

Chalfie, M., Tu, Y., Euskirchen, G., Ward, W. W., and Prasher, D. C. (1994). Green fluorescent protein as a marker for gene expression. *Science* 263, 802–805.

Chow, B. Y., Han, X., Dobry, A. S., Qian, X., Chuong, A. S., Li, M., Henninger, M. A., Belfort, G. M., Lin, Y., Monahan, P. E., and Boyden, E. S. (2010). High-performance genetically targetable optical neural silencing by light-driven proton pumps. *Nature* 463, 98–102.

Conklin, B. R., Hsiao, E. C., Claeysen, S., Dumuis, A., Srinivasan, S., Forsayeth, J. R., Guettier, J. M., Chang, W. C., Pei, Y., McCarthy, K. D., Nissenson, R. A., Wess, J., Bockaert, J., and Roth, B. L. (2008). Engineering GPCR signaling pathways with RASSLs. *Nat. Methods* 5, 673–678.

Deisseroth, K. (2010). Controlling the brain with light. *Sci. Am.* 303, 48–55.

Drenan, R. M., Grady, S. R., Whiteaker, P., McClure-Begley, T., McKinney, S., Miwa, J. M., Bupp, S., Heintz, N., McIntosh, J. M., Bencherif, M., Marks, M. J., and Lester, H. A. (2008). In vivo activation of midbrain dopamine neurons via sensitized, high-affinity alpha 6 nicotinic acetylcholine receptors. *Neuron* 60, 123–136.

Duan, X., Kang, E., Liu, C. Y., Ming, G. L., and Song, H. (2008). Development of neural stem cell in the adult brain. *Curr. Opin. Neurobiol.* 18, 108–115.

Ehlers, M. D., Heine, M., Groc, L., Lee, M. C., and Choquet, D. (2007). Diffusional trapping of GluR1 AMPA receptors by input-specific synaptic activity. *Neuron* 54, 447–460.

Enquist, L. W. (2002). Exploiting circuit-specific spread of pseudorabies virus in the central nervous system: insights to pathogenesis and circuit tracers. *J. Infect. Dis.* 186(Suppl. 2), S209–S214.

Esposito, M. S., Piatti, V. C., Laplagne, D. A., Morgenstern, N. A., Ferrari, C. C., Pitossi, F. J., and Schinder, A. F. (2005). Neuronal differentiation in the adult hippocampus recapitulates embryonic development. *J. Neurosci.* 25, 10074–10086.

Feinberg, E. H., Vanhoven, M. K., Bendesky, A., Wang, G., Fetter, R. D., Shen, K., and Bargmann, C. I. (2008). GFP reconstitution across synaptic partners (GRASP) defines cell contacts and synapses in living nervous systems. *Neuron* 57, 353–363.

Feng, G., Mellor, R. H., Bernstein, M., Keller-Peck, C., Nguyen, Q. T., Wallace, M., Nerbonne, J. M., Lichtman, J. W., and Sanes, J. R. (2000). Imaging neuronal subsets in transgenic mice expressing multiple spectral variants of GFP. *Neuron* 28, 41–51.

Fernandez-Alfonso, T., Kwan, R., and Ryan, T. A. (2006). Synaptic vesicles interchange their membrane proteins with a large surface reservoir during recycling. *Neuron* 51, 179–186.

Freund, T. F., and Buzsaki, G. (1996). Interneurons of the hippocampus. *Hippocampus* 6, 347–470.

Ge, S., Goh, E. L., Sailor, K. A., Kitabatake, Y., Ming, G. L., and Song, H. (2006). GABA regulates synaptic integration of newly generated neurons in the adult brain. *Nature* 439, 589–593.

Ge, S., Pradhan, D. A., Ming, G. L., and Song, H. (2007). GABA sets the tempo for activity-dependent adult neurogenesis. *Trends Neurosci.* 30, 1–8.

Gheusi, G., Cremer, H., McLean, H., Chazal, G., Vincent, J. D., and Lledo, P. M. (2000). Importance of newly generated neurons in the adult olfactory bulb for odor discrimination. *Proc. Natl. Acad. Sci. U.S.A.* 97, 1823–1828.

Giepmans, B. N., Adams, S. R., Ellisman, M. H., and Tsien, R. Y. (2006). The fluorescent toolbox for assessing protein location and function. *Science* 312, 217–224.

Gong, S., Zheng, C., Doughty, M. L., Losos, K., Didkovsky, N., Schambra, U. B., Nowak, N. J., Joyner, A., Leblanc, G., Hatten, M. E., and Heintz, N. (2003). A gene expression atlas of the central nervous system based on bacterial artificial chromosomes. *Nature* 425, 917–925.

Gordon, M. D., and Scott, K. (2009). Motor control in a *Drosophila* taste circuit. *Neuron* 61, 373–384.

Han, X., and Boyden, E. S. (2007). Multiple-color optical activation, silencing, and desynchronization of neural activity, with single-spike temporal resolution. *PLoS ONE* 2, e299. doi: 10.1371/journal.pone.0000299

Harms, K. J., Tovar, K. R., and Craig, A. M. (2005). Synapse-specific regulation of AMPA receptor subunit composition by activity. *J. Neurosci.* 25, 6379–6388.

Hasenstaub, A. R., and Callaway, E. M. (2010). Paint it black (or red, or green): optical and genetic tools illuminate inhibitory contributions to cortical circuit function. *Neuron* 67, 681–684.

Imayoshi, I., Sakamoto, M., Ohtsuka, T., Takao, K., Miyakawa, T., Yamaguchi, M., Mori, K., Ikeda, T., Itohara, S., and Kageyama, R. (2008). Roles of continuous neurogenesis in the structural and functional integrity of the adult forebrain. *Nat. Neurosci.* 11, 1153–1161.

Karpova, A. Y., Tervo, D. G., Gray, N. W., and Svoboda, K. (2005). Rapid and reversible chemical inactivation of synaptic transmission in genetically targeted neurons. *Neuron* 48, 727–735.

Kempermann, G., Wiskott, L., and Gage, F. H. (2004). Functional significance of adult neurogenesis. *Curr. Opin. Neurobiol.* 14, 186–191.

Kennedy, M. J., Davison, I. G., Robinson, C. G., and Ehlers, M. D. (2010). Syntaxin-4 defines a domain for activity-dependent exocytosis in dendritic spines. *Cell* 141, 524–535.

Kuypers, H. G., and Ugolini, G. (1990). Viruses as transneuronal tracers. *Trends Neurosci.* 13, 71–75.

Lerchner, W., Xiao, C., Nashmi, R., Slimko, E. M., van Trigt, L., Lester, H. A., and

Anderson, D. J. (2007). Reversible silencing of neuronal excitability in behaving mice by a genetically targeted, ivermectin-gated Cl-channel. *Neuron* 54, 35–49.

Leuner, B., Mendolia-Loffredo, S., Kosorovitskiy, T., Samburg, D., Gould, E., and Shors, T. J. (2004). Learning enhances the survival of neurons beyond the time when the hippocampus is required for memory. *J. Neurosci.* 24, 7477–7481.

Lin, C. W., Sim, S., Ainsworth, A., Okada, M., Kelsch, W., and Lois, C. (2010). Genetically increased cell-intrinsic excitability enhances neuronal integration into adult brain circuits. *Neuron* 65, 32–39.

Lin, D., Boyle, M. P., Dollar, P., Lee, H., Lein, E. S., Perona, P., and Anderson, D. J. (2011). Functional identification of an aggression locus in the mouse hypothalamus. *Nature* 470, 221–226.

Livneh, Y., Feinstein, N., Klein, M., and Mizrahi, A. (2009). Sensory input enhances synaptogenesis of adult-born neurons. *J. Neurosci.* 29, 86–97.

Lilley, C. E., Branston, R. H., and Coffin, R. S. (2001). Herpes simplex virus vectors for the nervous system. *Curr. Gene Ther.* 1, 339–358.

Lledo, P. M., and Saghatelyan, A. (2005). Integrating new neurons into the adult olfactory bulb: joining the network, life-death decisions, and the effects of sensory experience. *Trends Neurosci.* 28, 248–254.

Luo, L., Callaway, E. M., and Svoboda, K. (2008). Genetic dissection of neural circuits. *Neuron* 57, 634–660.

Ma, D. K., Kim, W. R., Ming, G. L., and Song, H. (2009). Activity-dependent extrinsic regulation of adult olfactory bulb and hippocampal neurogenesis. *Ann. N. Y. Acad. Sci.* 1170, 664–673.

Miesenbock, G., De Angelis, D. A., and Rothman, J. E. (1998). Visualizing secretion and synaptic transmission with pH-sensitive green fluorescent proteins. *Nature* 394, 192–195.

Ming, G. L., and Song, H. (2005). Adult neurogenesis in the mammalian central nervous system. *Annu. Rev. Neurosci.* 28, 223–250.

Miyamichi, K., Amat, F., Moussavi, F., Wang, C., Wickersham, I., Wall, N. R., Taniguchi, H., Tasic, B., Huang, Z. J., He, Z., Callaway, E. M., Horowitz, M. A., and Luo, L. (2011). Cortical representations of olfactory input by trans-synaptic tracing. *Nature*, doi:10.1038/nature09714.

Mizrahi, A., Lu, J., Irving, R., Feng, G., and Katz, L. C. (2006). In vivo imaging of juxtaglomerular neuron turnover in the mouse olfactory bulb. *Proc. Natl. Acad. Sci. U.S.A.* 103, 1912–1917.

Nagel, G., Szellas, T., Huhn, W., Kateriya, S., Adeishvili, N., Berthold, P., Ollig, D., Hegemann, P., and Bamberg, E. (2003). Channelrhodopsin-2, a directly light-gated cation-selective membrane channel. *Proc. Natl. Acad. Sci. U.S.A.* 100, 13940–13945.

Nagel, G., Szellas, T., Kateriya, S., Adeishvili, N., Hegemann, P., and Bamberg, E. (2005). Channelrhodopsins: directly light-gated cation channels. *Biochem. Soc. Trans.* 33, 863–866.

O'Connor, D. H., Huber, D., and Svoboda, K. (2009). Reverse engineering the mouse brain. *Nature* 461, 923–929.

Overstreet Wadiche, L., Bromberg, D. A., Bensen, A. L., and Westbrook, G. L. (2005). GABAergic signaling to newborn neurons in dentate gyrus. *J. Neurophysiol.* 94, 4528–4532.

Panzanelli, P., Bardy, C., Nissant, A., Pallotto, M., Sassoe-Pognetto, M., Lledo, P. M., and Fritschy, J. M. (2009). Early synapse formation in developing interneurons of the adult olfactory bulb. *J. Neurosci.* 29, 15039–15052.

Park, M., Salgado, J. M., Ostroff, L., Helton, T. D., Robinson, C. G., Harris, K. M., and Ehlers, M. D. (2006). Plasticity-induced growth of dendritic spines by exocytic trafficking from recycling endosomes. *Neuron* 52, 817–830.

Pathania, M., Yan, L. D., and Bordey, A. (2010). A symphony of signals conducts early and late stages of adult neurogenesis. *Neuropharmacology* 58, 865–876.

Petreanu, L., and Alvarez-Buylla, A. (2002). Maturation and death of adult-born olfactory bulb granule neurons: role of olfaction. *J. Neurosci.* 22, 6106–6113.

Petreanu, L., Huber, D., Sobczyk, A., and Svoboda, K. (2007). Channelrhodopsin-2-assisted circuit mapping of long-range callosal projections. *Nat. Neurosci.* 10, 663–668.

Rancz, E. A., Franks, K. M., Schwarz, M. K., Pichler, B., Schaefer, A. T., and Margrie, T. W. (2011). Transfection via whole-cell recording in vivo: bridging single-cell physiology, genetics and connectomics. *Nat. Neurosci.* 14, 527–532.

Rochefort, C., Gheusi, G., Vincent, J. D., and Ledo, P. M. (2002). Enriched odor exposure increases the number of newborn neurons in the adult olfactory bulb and improves odor memory. *J. Neurosci.* 22, 2679–2689.

Santarelli, L., Saxe, M., Gross, C., Surget, A., Battaglia, F., Dulawa, S., Weisstaub, N., Lee, J., Duman, R., Arancio, O., Belzung, C., and Hen, R. (2003). Requirement of hippocampal neurogenesis for the behavioral effects of antidepressants. *Science* 301, 805–809.

Shepherd, G. M. (2004). *The Synaptic Organization of the Brain*, 5th Edn. New York: Oxford University Press.

Shimomura, O., Johnson, F. H., and Saiga, Y. (1962). Extraction, purification and properties of aequorin, a bioluminescent protein from the luminous hydromedusan, *Aequorea*. *J. Cell. Comp. Physiol.* 59, 223–239.

Shipley, M. T., and Ennis, M. (1996). Functional organization of olfactory system. *J. Neurobiol.* 30, 123–176.

Song, H. J., Stevens, C. F., and Gage, F. H. (2002). Neural stem cells from adult hippocampus develop essential properties of functional CNS neurons. *Nat. Neurosci.* 5, 438–445.

Stepien, A. E., Tripodi, M., and Arber, S. (2010). Monosynaptic rabies virus reveals premotor network organization and synaptic specificity of cholinergic partition cells. *Neuron* 68, 456–472.

Suh, H., Deng, W., and Gage, F. H. (2009). Signaling in adult neurogenesis. *Annu. Rev. Cell Dev. Biol.* 25, 253–275.

Tan, E. M., Yamaguchi, Y., Horwitz, G. D., Gosgnach, S., Lein, E. S., Goulding, M., Albright, T. D., and Callaway, E. M. (2006). Selective and quickly reversible inactivation of mammalian neurons in vivo using the *Drosophila* allatostatin receptor. *Neuron* 51, 157–170.

Toni, N., Laplagne, D. A., Zhao, C., Lombardi, G., Ribak, C. E., Gage, F. H., and Schinder, A. F. (2008). Neurons born in the adult dentate gyrus form functional synapses with target cells. *Nat. Neurosci.* 11, 901–907.

van Praag, H., Christie, B. R., Sejnowski, T. J., and Gage, F. H. (1999). Running enhances neurogenesis, learning, and long-term potentiation in mice. *Proc. Natl. Acad. Sci. U.S.A.* 96, 13427–13431.

Voyles, B. A. (1993). *The Biology of Viruses*, 1st Edn. St. Louis: Mosby-Year Book.

Wang, H., Peca, J., Matsuzaki, M., Matsuzaki, K., Noguchi, J., Qiu, L., Wang, D., Zhang, F., Boyden, E., Deisseroth, K., Kasai, H., Hall, W. C., Feng, G., and Augustine, G. J. (2007). High-speed mapping of synaptic connectivity using photostimulation in channelrhodopsin-2 transgenic mice. *Proc. Natl. Acad. Sci. U.S.A.* 104, 8143–8148.

Wehr, M., Hostick, U., Kyweriga, M., Tan, A., Weible, A. P., Wu, H., Wu, W., Callaway, E. M., and Kentros, C. (2009). Transgenic silencing of neurons in the mammalian brain by expression of the allatostatin receptor (AlstR). *J. Neurophysiol.* 102, 2554–2562.

Weible, A. P., Schwarcz, L., Wickersham, I. R., Deblander, L., Wu, H., Callaway, E. M., Seung, H. S., and Kentros, C. G. (2010). Transgenic targeting of recombinant rabies virus reveals monosynaptic connectivity of specific neurons. *J. Neurosci.* 30, 16509–16513.

Whitman, M. C., and Greer, C. A. (2009). Adult neurogenesis and the olfactory system. *Prog. Neurobiol.* 89, 162–175.

Wickersham, I. R., Finke, S., Conzelmann, K. K., and Callaway, E. M. (2007a). Retrograde neuronal tracing with a deletion-mutant rabies virus. *Nat. Methods* 4, 47–49.

Wickersham, I. R., Lyon, D. C., Barnard, R. J., Mori, T., Finke, S., Conzelmann, K. K., Young, J. A., and Callaway, E. M. (2007b). Monosynaptic restriction of transsynaptic tracing from single, genetically targeted neurons. *Neuron* 53, 639–647.

Willhite, D. C., Nguyen, K. T., Masurkar, A. V., Greer, C. A., Shepherd, G. M., and Chen, W. R. (2006). Viral tracing identifies distributed columnar organization in the olfactory bulb. *Proc. Natl. Acad. Sci. U.S.A.* 103, 12592–12597.

Zhang, C. L., Zou, Y., He, W., Gage, F. H., and Evans, R. M. (2008). A role for adult TLX-positive neural stem cells in learning and behaviour. *Nature* 451, 1004–1007.

Zhang, F., Aravanis, A. M., Adamantidis, A., de Lecea, L., and Deisseroth, K. (2007a). Circuit-breakers: optical technologies for probing neural signals and systems. *Nat. Rev. Neurosci.* 8, 577–581.

Zhang, F., Wang, L. P., Brauner, M., Liewald, J. F., Kay, K., Watzke, N., Wood, P. G., Bamberg, E., Nagel, G., Gottschalk, A., and Deisseroth, K. (2007b). Multimodal fast optical interrogation of neural circuitry. *Nature* 446, 633–639.

Zhang, F., Gradinaru, V., Adamantidis, A. R., Durand, R., Airan, R. D., de Lecea, L., and Deisseroth, K. (2010). Optogenetic interrogation of neural circuits: technology for probing mammalian brain structures. *Nat. Protoc.* 5, 439–456.

Zhao, C., Deng, W., and Gage, F. H. (2008). Mechanisms and functional implications of adult neurogenesis. *Cell* 132, 645–660.

Zhao, G. Q., Zhang, Y., Hoon, M. A., Chandrashekar, J., Erlenbach, I., Ryba, N. J., and Zuker, C. S. (2003). The receptors for mammalian sweet and umami taste. *Cell* 115, 255–266.

Conflict of Interest Statement: The author declares that the research was conducted in the absence of any commercial or financial relationships that could be construed as a potential conflict of interest.

Received: 11 January 2011; accepted: 24 March 2011; published online: 05 April 2011.
*Citation: Arenkiel BR (2011) Genetic approaches to reveal the connectivity of adult-born neurons. Front. Neurosci. **5**:48. doi: 10.3389/fnins.2011.00048*
This article was submitted to Frontiers in Neurogenesis, a specialty of Frontiers in Neuroscience.

frontiers in
NEUROSCIENCE

METHODS ARTICLE
published: 21 April 2011
doi: 10.3389/fnins.2011.00059

Depletion of new neurons by image guided irradiation

Y.-F. Tan[1], S. Rosenzweig[1], D. Jaffray[2] and J. M. Wojtowicz[1]*

[1] *Department of Physiology, Faculty of Medicine, University of Toronto, Toronto, ON, Canada*
[2] *Radiation Oncology, Princess Margaret Hospital, University of Toronto, Toronto, ON, Canada*

Edited by:
Silvia De Marchis, University of Turin, Italy

Reviewed by:
Tatsunori Seki, Tokyo Medical University, Japan
Gilles Gheusi, Institut Pasteur, France

***Correspondence:**
J. M. Wojtowicz, Department of Physiology, University of Toronto, Medical Sciences Building, Third Floor, 1 King's College Circle, Toronto, ON, Canada M5S 1A8.
e-mail: martin.wojtowicz@utoronto.ca

Ionizing radiation continues to be a relevant tool in both imaging and the treatment of cancer. Experimental uses of focal irradiation have recently been expanded to studies of new neurons in the adult brain. Such studies have shown cognitive deficits following radiation treatment and raised caution as to possible unintentional effects that may occur in humans. Conflicting outcomes of the effects of irradiation on adult neurogenesis suggest that the effects are either transient or permanent. In this study, we used an irradiation apparatus employed in the treatment of human tumors to assess radiation effects on rat neurogenesis. For subjects we used adult male rats (Sprague-Dawley) under anesthesia. The irradiation beam was directed at the hippocampus, a center for learning and memory, and the site of neurogenic activity in adult brain. The irradiation was applied at a dose-rate 0.6 Gy/min for total single-fraction, doses ranging from 0.5 to 10.0 Gy. The animals were returned to home cages and recovered with no sign of any side effects. The neurogenesis was measured either 1 week or 6 weeks after the irradiation. At 1 week, the number of neuronal progenitors was reduced in a dose-dependent manner with the 50% reduction at 0.78 Gy. The dose–response curve was well fitted by a double exponential suggesting two processes. Examination of the tissue with quantitative immunohistochemistry revealed a dominant low-dose effect on neuronal progenitors resulting in 80% suppression of neurogenesis. This effect was partially reversible, possibly due to compensatory proliferation of the remaining precursors. At higher doses (>5 Gy) there was additional, nearly complete block of neurogenesis without compensatory proliferation. We conclude that notwithstanding the usefulness of irradiation for experimental purposes, the exposure of human subjects to doses often used in radiotherapy treatment could be damaging and cause cognitive impairments.

Keywords: adult neurogenesis, dentate gyrus, radiation, radiotherapy, hippocampus, imaging

INTRODUCTION

Ionizing radiation has emerged as a standard method in animal studies on functional effects of adult neurogenesis (Wojtowicz, 2006). It is the only method that is currently available for relatively uninvasive deletion of new neurons in selected brain regions in a dose-dependent manner. It can be used on any species and its effects are readily translated to humans (Monje et al., 2002; Monje and Palmer, 2003). With the advent of improved focusing methods combined with brain imaging the irradiation beam can be applied to brain targets as small as a few millimeters in diameter. In this study, we employed such an approach to construct a dose–response curve showing effects of irradiation on the population of neuronal progenitors in the hippocampus, a brain structure involved in spatial and episodic memory (Cohen and Eichenbaum, 1993). Previous studies generally used one or two doses and focused on the mechanisms of cell depletion. Several studies have established that within hours of the treatment many of the proliferating cells die through apoptosis (Peissner et al., 1999; Mizumatsu et al., 2003). This is consistent with the established vulnerability of the mitotically active cells to radiation. However, there are indications of other damaging processes as well. Inflammation with the resulting release of toxic cytokines (Monje et al., 2003), destruction of blood capillaries (Monje et al., 2003) and killing of quiescent stem cells (Encinas et al., 2008) have been reported. There are conflicting reports on irreversible and reversible nature of these effects (Tada et al., 2000; Ben Abdallah et al., 2007). This is an important issue since behavioral tests require a stable baseline of neurogenesis at a given level, presumably lower than in the intact brain. If the effects of irradiation are in fact reversible the factors that can speed up or enhance its recovery are of importance in clinical practice where irradiation is used to treat malignant tumors often with unavoidable collateral damage on the surrounding tissue. If the effects are irreversible, the cause of the permanent damage should be understood since it could influence the mechanism of the remaining neurogenesis and the properties of the surviving neurons. This study shows that dose-dependence is bimodal and can be accounted for by low-dose reversible and high-dose irreversible effects of irradiation.

METHODS

SUBJECTS

Thirty 12-week-old male S-D rats (Charles River) were used in this study.

The animals were allowed to acclimate in the facility for 1 week after the delivery. All procedures were approved by the University of Toronto and University Hospital Network ethics committees.

IRRADIATION

Just prior to irradiation the animals were anesthetized with IP injection of ketamine/xylazine at 85/5 mg/kg. Animals were placed one by one on the treatment couch of the irradiation unit (Elekta Synergy)

and aligned at the intersection of isocenter marking lasers just in front of the ears (**Figure 1**). The shielded door to the treatment room was shut and the animal imaged using the integrated cone-beam CT system (imaging dose of <0.03 Gy) to obtain an outline of the skull together with the body landmarks such as oral cavity, ear canals, etc. The graphical representation of the isocenter of the treatment beam was aligned with the approximate location of the hippocampus as determined from a pre-existing MRI and CT scan from a generic rat. The position of the rat with respect to the actual isocenter was then automatically adjusted using the robotic table of the treatment unit. The dosimetry with the resulting fields as seen from the side and from the front was done using Pinnacle software (**Figure 2**). Thus the 98, 80, 60%, isodose level were seen superimposed on the image of the skull aligned with the approximate location of the hippocampus. The dose-rate of irradiation was 0.6 Gy/min and the total dose was obtained by irradiating equally from each side (left and right lateral beams). Doses were applied over the range from 0.5 to 10 Gy with three animals per dose. The treatment unit is referenced to the National Research Council of Canada (NRCC) radiation dosimetry standards through the

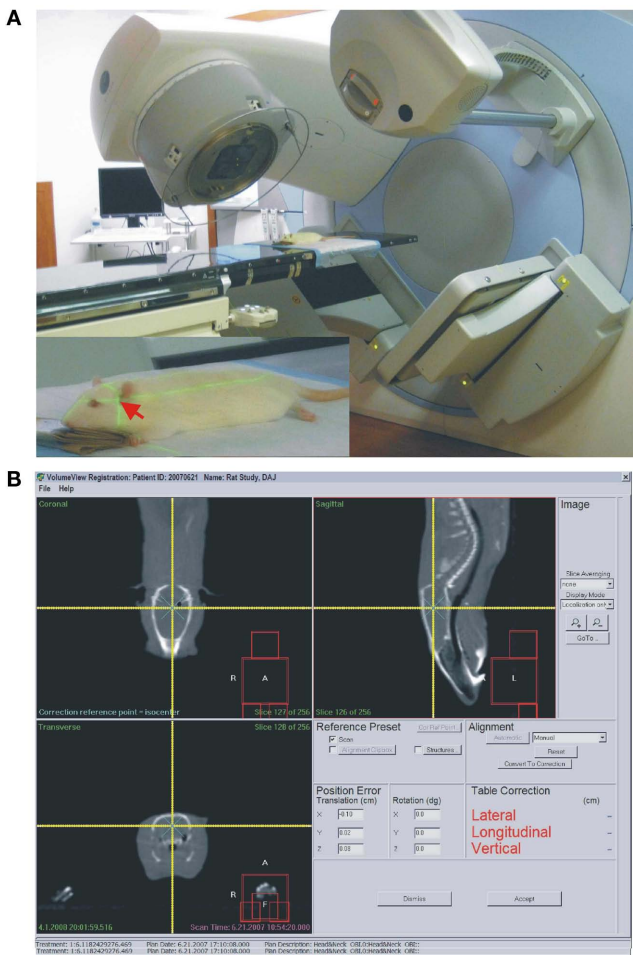

FIGURE 1 | (A) Elekta synergy CT system used for imaging and irradiation in this study. Same system is also used for human radiotherapy. Inset. Red arrow points at the approximate location of the hippocampus at the intersection of the two guiding laser beams. **(B)** Screen-print of the targeting and dosimetry software allowing visualization of the rat's skull (white outline). The intersection of two yellow beams indicates the center point of the irradiation (isocenter).

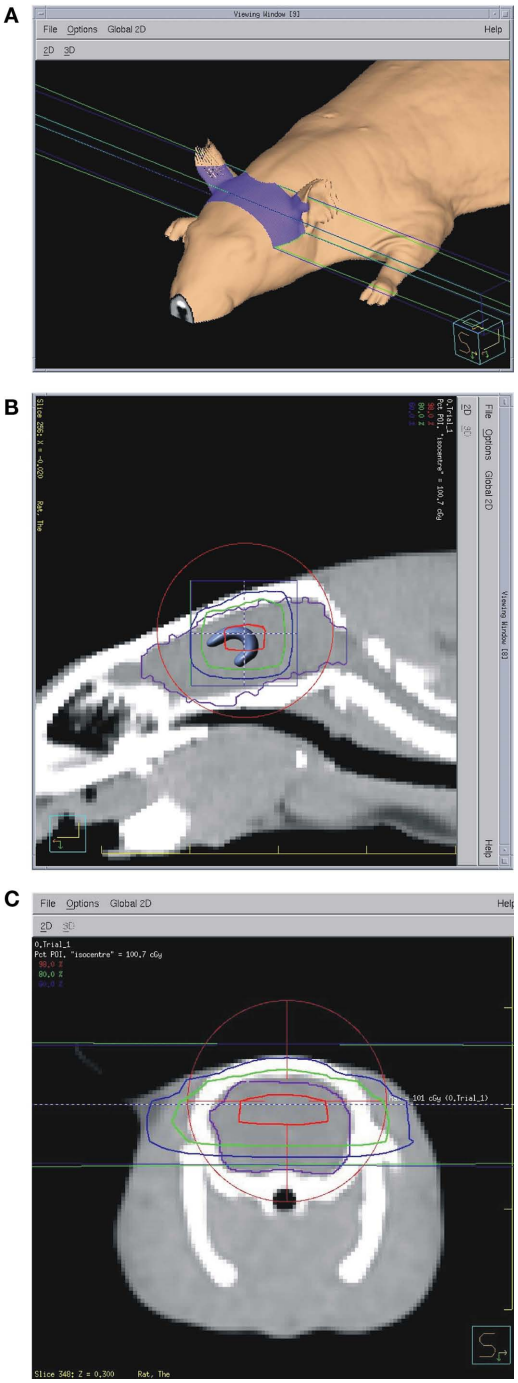

FIGURE 2 | (A) Dosimetry data show approximate irradiated area on the animal's skin. **(B)** Saggital CT scan with 98% dose (red), 80% dose (green), and 60% dose (blue) outlines. Brain outline is shown in purple and the hippocampus is sketched in the location determined from a brain atlas. Red circle and blue square are part of the targeting software with cross-hairs (visible only with zoom-in) at the isocenter. **(C)** Frontal view with the same isodose outlines.

American Association of Physicists in Medicine TG-51 dosimetry protocol. Monitor units used for the irradiation were derived from the clinical dosimetry database of the Princess Margaret Hospital's Radiation Medicine Program. Sham controls were anesthetized but not imaged or irradiated. Following treatment, the animals were transferred to home cages and kept for 1 week or 6 weeks in standard conditions. There was no effect of the treatment on animal's behavior and no side effects such as hair loss or weight loss. The weights of the control animals ($n = 3$) were 394.7 before, and 425.7 g 1 week after treatment. The weights of the 10 Gy (the highest dose) irradiated animals ($n = 3$) were 392.7 g before treatment and 425.7 g 1 week after treatment.

BrdU ADMINISTRATION

5-Bromo-2-deoxyuridine (BrdU; Sigma, St. Louis, MO, USA) was dissolved in phosphate-buffered saline (PBS) containing 10 mM NaOH for a final concentration of BrdU 20 mg/ml. The solution was injected i.p. at a dose of 200 mg/kg of body weight at 9 AM and again at 9 PM on the 14th day after irradiation. The dose of BrdU was chosen to allow for maximal labeling of cells born during a 24-h period according the previously described procedures (McDonald and Wojtowicz, 2005).

PERFUSION AND TISSUE PREPARATION

Most animals were perfused at 1 week after irradiation with three animals per irradiation dose. This time point was chosen on the basis of published data showing a peak of proliferation following cell birth (McDonald and Wojtowicz, 2005). Several additional animals were perfused at 6 weeks, allowing measurement of cell survival and examination of long-term effects of irradiation on cell differentiation and maturation. Following intracardiac perfusion with PBS and 4% paraformaldehyde, the right hippocampus was sectioned into three parts – dorsal, medial, and ventral – and post-fixed overnight in 4% paraformaldehyde at 4°C. Serial 30 μm sections of all segments were cut with a vibratome resulting in 200–250 sections per animal. One in 10 transverse sections were sampled using a systematic random sampling procedure along the dorso-ventral extent of the hippocampus.

IMMUNOHISTOCHEMISTRY

Procedures for detection of calbindin (CaBP), doublecortin (DCX), Ki67, and BrdU were the same as described in several research and methods articles recently published by us (Kee et al., 2002; McDonald and Wojtowicz, 2005; Wojtowicz and Kee, 2006). Primary antibodies, dilutions, and incubation times were as follows: CaBP (Chemicon AB1778), 1:200, 72 h at 4°C; DCX (Santa Cruz; C-18, sc-8066), 1:200, 24 h at 4°C; Ki67 (Vector labs. VP-K451), 1:200, 18 h at room temp.; BrdU (Cedarlane, OBT0030), 1:200, 24 h at 4°C). The secondary antibodies were tagged with Alexa 594 (red) or 488 (green) fluorophores (Molecular Probes). Selected sections were stained for a microglia marker ED1 as described previously (Tan et al., 2010).

DATA ANALYSIS

Cells were counted in each of the sampled sections (20–25 sections per animal for each marker at each time point). In all experiments with 1-week survival, the cell counts were expressed per dentate gyrus (unilateral) by counting all labeled cells in the subgranular zone of the dentate gyrus in sampled sections and multiplying the average by the total number of sections per animal. In experiments with 6-weeks survival, the cells were counted per section, since we wished to compare three regions (dorsal, middle, and ventral) of the dentate gyrus with regard to effects of radiation. In these experiments, BrdU/CaBP double-labeled cells were examined under a confocal microscope (Leica, TC, SSL).

Statistical analysis was done using SigmaPlot 8 and SigmaStat 3.0 software. Data sets were analyzed with one-way or two-way ANOVA, as appropriate, and passed the normality and equal variance tests. All values given in the text and in figures show mean and standard errors.

RESULTS

Post-irradiation status of neurogenesis was assessed 1 week after treatment. This time point was chosen because previous BrdU tracing experiments revealed maximal density of the immature and proliferating cells at that time (McDonald and Wojtowicz, 2005). In addition, brain trauma, such as ischemia, produces maximal rebound neurogenesis 1 week after treatment (Tada et al., 2000; Dash et al., 2001; Sharp et al., 2002). Thus, the 1-week time point is an important milestone in normal and pathological cell development.

To examine possible effects of this procedure on neurogenesis we examined a wide range of doses, beginning with very low levels and spanning the previously used higher doses. As expected we observed strong inhibitory effect of high doses, but surprisingly even a low dose of 1 Gy had clear, pronounced effect (**Figure 3**). The irradiation produced statistically significant reductions in the total number of DCX+ cells per dentate gyrus at all doses (ANOVA, with pairwise comparisons between the control and the irradiated groups, $P = 0.001$). We showed this decrease using another marker of neurogenesis, PSA-NCAM, that labels young neurons in the similar age range, but has very different chemical characteristics and entirely different cellular distribution (Seki and Arai, 1993). The controls and the 5 Gy-irradiated groups showed similar cell counts using DCX and PSA-NCAM labeling, 21.334 ± 1028, 2.150 ± 567 for DCX and 21.308 ± 654, 1.839 ± 652 for PSA-NCAM, respectively. This confirmed that irradiation had a robust effect on cell number and was not marker-specific.

Densities of the proliferating Ki67+ cells in the same animals were not reduced at any of the doses. In fact, the proliferation appeared to be enhanced at the intermediate doses of 2, 3, and 4 Gy (ANOVA, $F = 3.978$, $P = 0.016$) compared to controls. These results suggest that reduced proliferation is either not the cause of lowered neurogenesis or that a delayed compensatory increase in proliferation occurred as a result of the initial insult. The observed increase in proliferation cannot instantly compensate for the underlying decrease in neurogenesis but could account for its recovery within a few weeks.

We next analyzed the dose–response relationship by fitting the DCX data to a double exponential curve with four parameters corresponding to the maxima and the rate constants of the two exponential components (**Figure 4**). A good fit to the data suggests two processes, one with a maximum of 80% suppression and sharp rising rate constant with a half dose of 0.78 Gy, and the other with

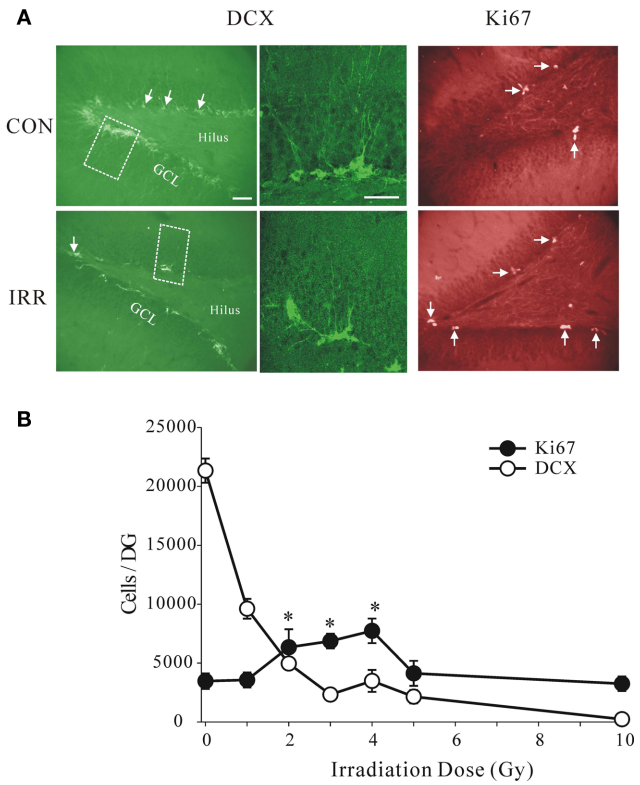

FIGURE 3 | (A) Images of transverse sections through the dentate gyrus stained for doublecortin (DCX), a marker of neuroblasts and young neurons, and for Ki67, a marker for proliferating cells. Note that the number of DCX-positive cells was reduced by irradiation (IRR), while the number of Ki67-positive cells was increased. The enlarged areas (broken line) are shown in the images in the middle showing typical morphology of normal young neurons in control animal and the immature morphology in irradiated animal. Dose of irradiation was 4 Gy and the survival time was 1 week after treatment. Calibration bars are 50 μm. **(B)** Absolute numbers of DCX+ and Ki67+ cells per dentate gyrus at different doses. Note sharp dose–response dependence at low doses and a near complete depletion of DCX+ cells at the highest dose (10 Gy). The number of proliferating cells was significantly increased at 2, 3, and 4 Gy (asterisks, ANOVA, $P = 0.016$), but there was no change at the lowest and the highest doses.

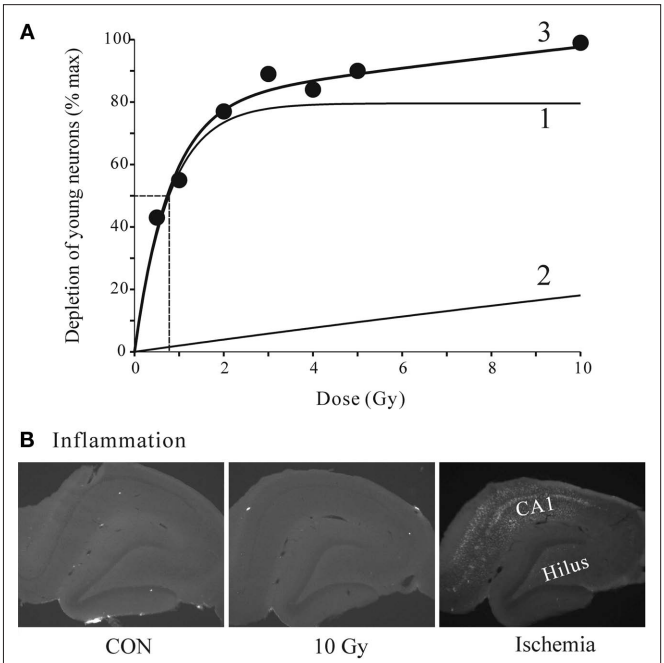

FIGURE 4 | (A) Quantitative dose–response relationship for effects of radiation on DCX-positive young neurons. The data points were fitted to a double exponential (3) with a fast (1) and a slow (2) component. Half-maximal dose of 0.78 Gy is shown by dashed lines. The parameters were: $\max_1 = 79.6$, $a_1 = 1.28$. $\max_2 = 99.7$, $a_2 = 0.022$. Regression analysis $F_{3,6} = 32.06$, $P = 0.0088$. **(B)** Representative images of tissue sections from control and 10 Gy irradiated animals at 1-week time point stained for microglia inflammation marker ED1. There was no detectable staining even at the highest dose (10 Gy) used in this study. For positive control the tissue from another study (Tan et al., 2010) shows clear microglia signal in CA1 and the Hilus 1 week after global ischemia.

the 100% suppression and half maximal dose of 45.5 Gy. Together, they completely account for the data and suggest a bimodal mechanism. Transient inflammation has been reported after irradiation (Monje et al., 2003; Noonan et al., 2010) at the doses similar to the ones used in this study. However, none of our animals tested at 1 week or 6 weeks post-irradiation showed any sign of inflammation even at the highest irradiation dose of 10 Gy (**Figure 4B**). The tissue from the study by Tan et al. (2010) where global ischemia induced prominent activation of microglia in CA1 and the Hilus was used as positive control. Thus, neither the reversible nor irreversible effects of irradiation were directly related to inflammation. Examination of the dorsal, medial and ventral thirds of the dentate gyrus showed no differences in the proportional effects of irradiation on Ki67+ or DCX+ cells. Thus all data are reported as average changes per whole dentate gyrus. This is specifically illustrated for the 6-week data set (**Figure 6**, below), but also applicable to all data sets in this study.

We investigated the possibility that increased proliferation at moderate doses of irradiation can compensate for the loss of DCX+ cells. In this experiment we exposed the animals to 3 Gy, which at 1 week causes suppression of neurogenesis by nearly 90% but increases proliferation by over two-fold. We hypothesized that with time the increased proliferation of the precursors should compensate for the initial cell loss. The results are consistent with this hypothesis. The number of Ki67+ cells was significantly higher in the irradiated animals at 1 week post-irradiation. Two-way ANOVA, taking time (1 or 6 weeks) and treatment (control or irradiation) as variables, shows a significant effect of time ($F_{1,11} = 39.26$, $P < 0.001$) and treatment ($F_{1,11} = 18.06$, $P = 0.003$) and significant interactions ($F_{1,11} = 8.86$, $P = 0.018$). In particular, with regard to the above hypothesis, the treatment had a significant effect at 1 week ($P < 0.0001$) but not at 6 weeks ($P = 0.39$). In contrast, the number of DCX+ cells was significantly reduced at 1-week time point. Two-way ANOVA shows a significant effect of time ($F_{1,11} = 32.63$, $P < 0.001$) and treatment ($F_{1,11} = 128.73$, $P < 0.001$) and significant interactions ($F_{1,11} = 76.63$, $P < 0.001$). In particular, the treatment had a significant effect at 1 week ($P < 0.0001$) but not at 6 weeks ($P = 0.10$). These data are presented graphically using the relative values (irradiated/control) to show the recovery of the effects at 6 weeks. The absolute values for cell numbers are given in the legend of **Figure 5**.

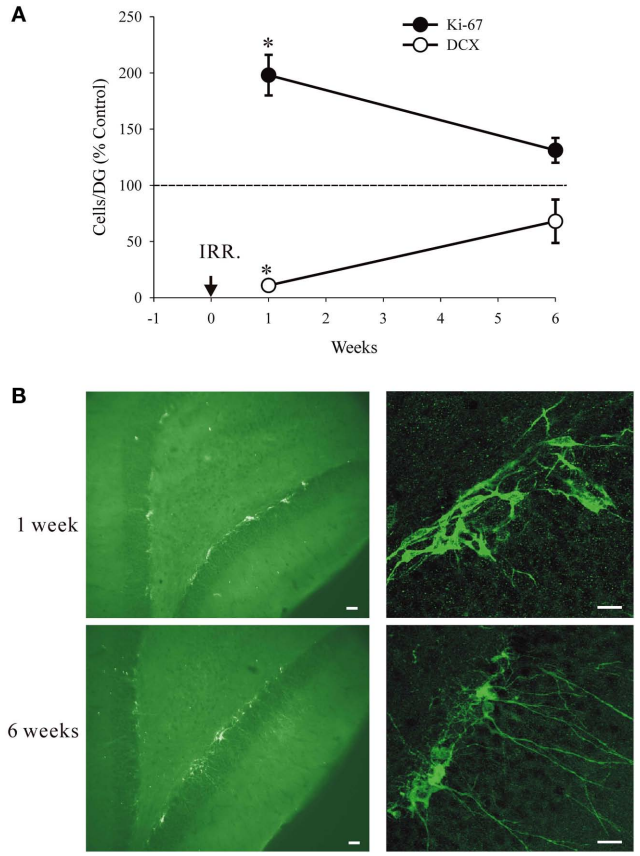

FIGURE 5 | Recovery from irradiation at 3Gy. (A) Relative numbers of DCX+ and Ki67+ cells at 1 week and at 6 weeks after treatment (IRR). The numbers of DCX+ cells and Ki67+ cells at 1 week, but not at 6 weeks were significantly different from controls (asterisks). The absolute values for cell numbers per DG were as follows: For Ki67 at 1 week 3.464 ± 657.6 (controls) and 6.860 ± 1.084.3 (irradiated). For Ki67 at 6 weeks 1.919 ± 204.3 (controls) and 2.516 ± (irradiated). For DCX at 1 week 21.334 ± 1.781.4 (controls) and 2.327 ± 180.7 (irradiated). For DCX at 6 weeks 7.654 ± 979.7 (controls) and 5.203 ± 2562.1 (irradiated). The reduced cell numbers at 6 vs. 1 week for controls are due to expected decline with animal's age. All values are means and standard errors (n = 3 in each group). **(B)** Typical immature appearance of the DCX+ cells at 1 week and a more normal appearance with longer dendrites at 6 weeks. Calibration bars are 20 μm in all cases.

In the next experiment we showed that the remaining proliferation after irradiation resulted in the production of mature neurons, albeit at lower rates. Two groups of animals, 3 Gy irradiated and sham controls, were injected with BrdU at 2 weeks and killed at 6 weeks after irradiation, thus allowing 4 weeks for neuronal maturation of the BrdU-tagged neurons. The surviving neurons were co-labeled for BrdU and calbindin (CaBP), a neuronal marker that is expressed during neuronal maturation (McDonald and Wojtowicz, 2005). In this case we show separately the total number of BrdU+ and BrdU/CaBP+ cells and we include the distribution among the three hippocampal regions (**Figure 6**).

DISCUSSION

High energy radiation surrounds us in the environment, it is also used in high doses in ionizing X-ray procedures, various imaging devices such as CT scans, and in radiotherapy for treatment of cancer or benign conditions (Koh et al., 2006). One specialized application of the ionizing radiation is to inhibit growth of endogenous stem cells in adult brain in order to assess their function in normal physiology and in potential regeneration of the brain tissue (Saxe et al., 2006; Wojtowicz, 2006). The present study examined the effects of irradiation on the hippocampus, a key brain structure involved in learning and memory. There is now convincing evidence that inhibition of adult neurogenesis in the dentate gyrus, the integral part of the hippocampus, affects some types of learning and memory in experimental animals. In particular, the memory that relates past events to context is very sensitive to reduced neurogenesis (Winocur et al., 2006; Wojtowicz et al., 2008; Hernandez-Rabaza et al., 2009). With continuing use of the irradiation in animal experiments on neurogenesis it is important to understand the mechanisms and dose dependence of the treatment. It is also useful to assess the extent of cell depletion along the dorso-ventral axis of the hippocampus. Dorsal and ventral regions are unevenly involved in various behaviors and recent evidence suggests that neurogenesis is also polarized (Snyder et al., 2008). Our results show that the targeting procedure ensures uniform effects of radiation in all regions of the hippocampus along its dorso-ventral axis (**Figure 6**).

There exists conflicting evidence with regard to the duration of radiation effects. In most studies the effects were irreversible (Wojtowicz, 2006), but in others, either spontaneous or experimentally induced recovery has been observed (Monje et al., 2003; Rola et al., 2004; Ben Abdallah et al., 2007). Our new data reconcile these discrepancies by showing that the effects of irradiation are bimodal. There appear to be a low-dose effect of irradiation that is associated with enhanced compensatory proliferation of precursors and, a high dose effect that lacks such compensation. Most of previous reports of the irreversible effects on neurogenesis used the doses in the higher range, above 5 Gy. The lower doses, below 5 Gy may be reversible by allowing sufficient time for recovery after treatment. However, it is also apparent that full recovery is unlikely since according to the exponential model shown in **Figure 4A** the high dose effect begins from 0 and grows steadily with dosage. This finding appears ominous for possible side effects of radiotherapy that uses large doses (>50 Gy) in fractions of 1-2 Gy (Laack and Brown, 2004; Barani et al., 2007). It can also be expected that even some forms of imaging such as CT scans, that require significant exposure to radiation, may affect neurogenesis. It should be noted that the irreversible effects are not necessarily due to persistent inflammation since our irradiation procedure did not produce any detectable inflammation (**Figure 4B**). Unlike in our previous studies where we used pentobarbital anesthesia (Wojtowicz, 2006), the present study utilized a more common ketamine/xylazine anesthesia. Thus, the proposed protective action of the pentobarbital does not seem to be necessary to prevent the inflammation at least in the dose range utilized here.

The apparent increase in proliferation at lower doses (**Figure 3**) may seem paradoxical but in fact is in agreement with the well established compensatory or rebound response of proliferation to various types of brain injury including ischemia or mechanical trauma (Dash et al., 2001; Kee et al., 2001; Sharp et al., 2002). There is no doubt that proliferation is reduced within 24 h of the irradiation but the rebound at 1 week suggests a homeostatic mechanism that compensates for

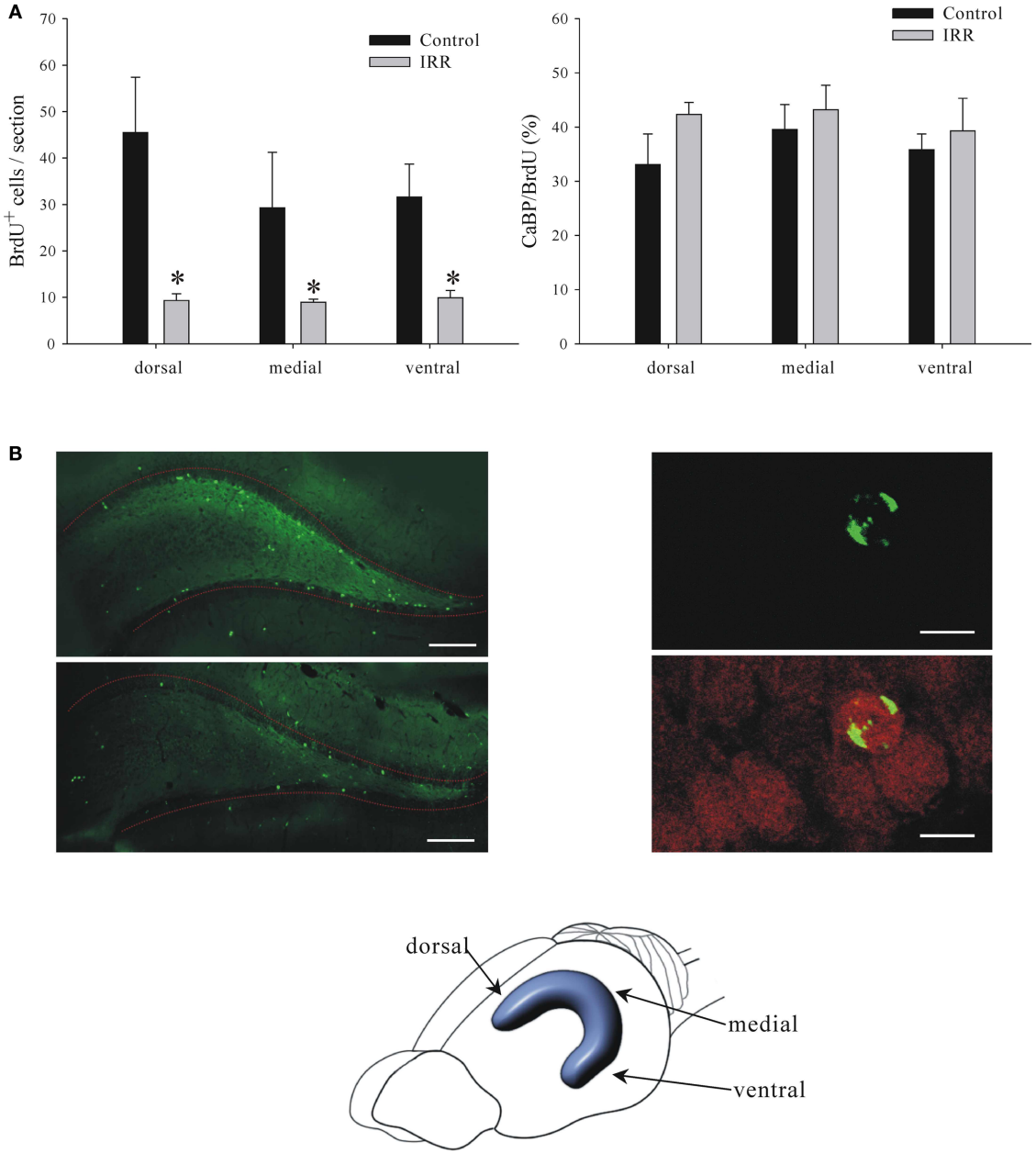

FIGURE 6 | Details of reduced neurogenesis at 6 weeks after irradiation (IRR). (A) Left. Graph shows numbers of BrdU+ cells in dorsal, medial, and ventral portions of the dentate gyrus. Reduction of neurogenesis in irradiated animals was equal and significant in all three regions (two-way ANOVA, $P = 0.001$). Right. Graph shows ratios of CaBP+ cells to the total number of BrdU+ cells in the three regions. There were no significant differences between regions or treatment (two-way ANOVA, $P = 0.645$) indicating that the irradiation is equally effective in all three regions and there is no effect on cell maturation. **(B)** Panels show examples of images stained for BrdU (left panel) or BrdU and CaBP (right panel). BrdU is shown in green and CaBP is shown in red. Calibration bars are 200 and 15 μm in left and right panels, respectively.

the initial damage. This partial recovery seems to take the course of *de novo* renewal of the young cell population. Accordingly, the DCX+ cells observed at 1 week of recovery are very similar to 1-week-old neurons in their normal development (McDonald and Wojtowicz, 2005). Such cells are characterized by clustering and posses short, stubby dendrites extending horizontally, in parallel to the hilar/GCL border (McDonald and Wojtowicz, 2005; Seki et al., 2007). More developed neurons with long dendrites are missing. In contrast, at 6 weeks the cells appear to include a normal range of shapes and sizes typical for the young neuronal population. At higher doses there is no rebound and ultimately the damage is permanent.

In summary, our results demonstrate the usefulness of the irradiation approach to studies of adult neurogenesis. With the targeted application of the radiation, the full dose was centered

in the 5 mm 5 mm 5 mm voxel of the brain tissue that comprised both hippocampi. There was an inevitable "spill-over" effect that included the surrounding brain tissue but the 80–60% isodose levels declined sharply within the approximate volume of 10 mm 10 mm 10 mm. The effects were dose-dependent and easily verifiable with *post hoc* immunohistochemistry. The effects of irradiation were uniform along the dorso-ventral axis of the hippocampus with equal effect on the number of BrdU+ cells in the dorsal, medial, and ventral regions. This result serves to verify the accuracy of our irradiation targeting procedure. The equal proportions of the CaBP/BrdU-labeled cells further show that the cells spared by irradiation develop normally according the same time line as that observed in control animals (**Figure 6**).

These results may be used in assessing possible collateral damage caused by radiotherapy and other types of treatment or imaging procedures involving radiation. It would appear that doses as small as 100 cGy (0.1 Gy) could cause noticeable damage in the neurogenic regions of the hippocampus. This in turn could cause deficits in learning and memory as well as possible changes in sensitivity of the subjects to antidepressants. Some aspects of depression, schizophrenia, and opioid-dependence have been linked to adult neurogenesis (Eisch et al., 2000; Santarelli et al., 2003; Reif et al., 2006; Canales, 2007). Reduced neurogenesis is expected to negatively affect the symptoms and treatment of these conditions. A proof of principle evidence has recently emerged from a study Dr. C. Menard and colleagues who reported memory deficits in patients undergoing radiation therapy at doses as low as 0.75 Gy (Bernard et al., 2010).

ACKNOWLEDGMENTS

We thank M. Khan, Y. Wang and J. Zhang for technical assistance in the study. Ms. Lulu Gao helped with immunohistochemical staining for microglia. This research was funded by operating grants from CIHR and NSERC.

REFERENCES

Barani, I. J., Benedict, S. H., and Lin, P.-S. (2007). Neural stem cells: implications for the conventional radiotherapy of central nervous system malignancies. *Int. J. Radiat. Oncol. Biol. Phys.* 68, 324–333.

Ben Abdallah, N. M.-B., Slomianka, L., and Lipp, H.-P. (2007). A reversible effect of X-irradiation on proliferation, neurogenesis and cell death in the dentate gyrus of adult mice. *Hippocampus* 17, 1230–1240.

Bernad, D., McAndrews, M., Kong, I., Becker, S., Shah, M., Wojtowicz, M., Cusimano, M., Laperriere, N., Mikulis, D., and Menard, C. (2010). The effects of low dose Hippocampal radiation exposure on memory in patients receiving stereotactic radiosurgery for benign neurological disorders. American Society for Radiation Oncology (ASTRO) Annual Meeting. *Int. J. Radiat. Oncol. Biol. Phys.* 78(Suppl. 3), 1066; S169.

Canales, J. J. (2007). Adult neurogenesis and the memories of drug addiction. *Eur. Arch. Psychiatry Clin. Neurosci.* 257, 261–270.

Cohen, N. J., and Eichenbaum, H. (1993). *Memory, Amnesia and the Hippocampal System.* Cambridge: The MIT Press.

Dash, P. K., Mach, S. A., and Moore, A. N. (2001). Enhanced neurogenesis in the rodent hippocampus following traumatic brain injury. *J. Neurosci. Res.* 63, 313–319.

Eisch, A. J., Barrot, M., Schad, C. A., Self, D. W., and Nestler, E. J. (2000). Opiates inhibit neurogenesis in the adult rat hippocampus. *Proc. Natl. Acad. Sci. U.S.A.* 97, 7579–7584.

Encinas, J. M., Vazquez, M. E., Switzer, R. C., Chamberland, D. W., Nick, H., Levine, H. G., Scarpa, P. J., Enikolopov, G., and Steindler, D. A. (2008). Quiescent adult neural stem cells are exceptionally sensitive to cosmic radiation. *Exp. Neurol.* 210, 274–279.

Hernandez-Rabaza, V., Llorens-Martin, M. V., Ferragud, A., Velazquez-Sanches, C., Arcusa, A., Gomez-Pinedo, U., Perez-Villalba, A., Rosello, J., Trejo, J. L., Barcia, J. A., and Canales, J. J. (2009). Inhibition of adult hippocampal neurogenesis disrupts contextual learning but spares spatial working memory, long-term conditional rule retention and spatial reversal. *Neuroscience* 159, 59–68.

Kee, N., Preston, E., and Wojtowicz, J. M. (2001). Enhanced neurogenesis after transient ischemia in the dentate gyrus of the rat. *Exp. Brain Res.* 136, 313–320.

Kee, N., Sivalingam, S., Boonstra, R., and Wojtowicz, J. M. (2002). The utility of Ki-67 and BrdU as proliferative markers of adult neurogenesis. *J. Neurosci. Methods* 115, 97–105.

Koh, E.-S., Laperriere, N., Bernstein, M., Jaffray, D., and Menard, C. (2006). Cranial stereotactic surgery: overview of current technology and clinical practice. *Oncol. Rounds* 6, 1–5.

Laack, N. N., and Brown, P. D. (2004). Cognitive sequelae of brain radiation in adults. *Semin. Oncol.* 31, 702–713.

McDonald, H. Y., and Wojtowicz, J. M. (2005). Dynamics of neurogenesis in the dentate gyrus of adult rats. *Neurosci. Lett.* 385, 70–75.

Mizumatsu, S., Monje, M. L., Morhardt, D. R., Rola, R., Palmer, T. D., and Fike, J. R. (2003). Extreme sensitivity of adult neurogenesis to low doses of X-irradiation. *Cancer Res.* 63, 4021–4027.

Monje, M. L., Mizumatsu, S., Fike, J. R., and Palmer, T. D. (2002). Irradiation induces neural precursor-cell dysfunction. *Nat. Med.* 8, 955–962.

Monje, M. L., and Palmer, T. D. (2003). Radiation injury and neurogenesis. *Curr. Opin. Neurol.* 16, 129–134.

Monje, M. L., Toda, H., and Palmer, T. D. (2003). Inflammatory blockade restores adult hippocampal neurogenesis. *Science* 302, 1760–1765.

Noonan, M. A., Bulin, S. E., Fuller, D. C., and Eisch, A. J. (2010). Reduction of adult hippocampal neurogenesis confers vulnerability in an animal model of cocaine addiction. *J. Neurosci.* 30, 304–315.

Peissner, W., Kocher, M., Treurer, H., and Gillardon, F. (1999). Ionizing radiation-induced apoptosis of proliferating stem cells in the dentate gyrus of the adult rat hippocampus. *Mol. Brain Res.* 71, 61–68.

Reif, A., Fritzen, S., Finger, M., Strobel, A., Lauer, M., Schmitt, A., and Lesch, K. P. (2006). Neural stem cell proliferation is decreased in schizophrenia, but not in depression. *Mol. Psychiatry* 11, 514–522.

Rola, R., Raber, J., Rizk, A., Otsuka, S., VandenBerg, S. R., Morhardt, D. R., and Fike, J. R. (2004). Radiation-induced impairment of hippocampal neurogenesis is associated with cognitive deficits in young mice. *Exp. Neurol.* 188, 316–330.

Santarelli, L., Saxe, M., Gross, C., Surget, A., Battaglia, F., Dulawa, S., Weisstaub, N., Lee, J., Duman, R. S., Arancio, O., Belzung, C., and Hen, R. (2003). Requirement of hippocampal neurogenesis for the behavioral effects of antidepressants. *Science* 301, 805–809.

Saxe, M. D., Battaglia, F., Wang, J.-W., Melleret, G., David, D. J., Monckton, J. E., Garcia, A. D. R., Sofroniev, M. V., Kandel, E. R., Santarelli, L., Hen, R., and Drew, M. R. (2006). Ablation of hippocampal neurogenesis impairs contextual fear conditioning and synaptic plasticity in the dentate gyrus. *Proc. Natl. Acad. Sci. U.S.A.* 103, 17501–17506.

Seki, T., and Arai, Y. (1993). Highly polysialylated neural cell adhesion molecule (NCAM-H) is expressed by newly generated granule cells in the dentate gyrus of the adult rat. *J. Neurosci.* 13, 2351–2358.

Seki, T., Namba, T., Mochizuki, H., and Onodera, M. (2007). Clustering, migration, and neurite formation of neural precursor cells in the adult rat hippocampus. *J. Comp. Neurol.* 502, 275–290.

Sharp, F. R., Liu, J., and Bernabeu, R. (2002). Neurogenesis following brain ischemia. *Dev. Brain Res.* 134, 23–30.

Snyder, J. S., Radik, R., Wojtowicz, J. M., and Cameron, H. A. (2008). Anatomical gradients of neurogenesis and activity: young neurons in the ventral dentate gyrus are activated by water maze training. *Hippocampus* 19, 360–370.

Tada, E., Parent, J. M., Lowenstein, D. H., and Fike, J. R. (2000). X-irradiation causes a prolonged reduction in cell proliferation in the dentate gyrus of adult rats. *Neuroscience* 99, 33–41.

Tan, Y.-F., Preston, E., and Wojtowicz, J. M. (2010). Enhanced postischemic neurogenesis in aging rats. *Front. Neurosci.* 4:163. doi: 10.3389/fnins.2010.00163

Winocur, G., Wojtowicz, J. M., Sekeres, M., Snyder, J. S., and Wang, S. (2006).

Inhibition of neurogenesis interferes with hippocampal-dependent memory function. *Hippocampus* 16, 296–304.

Wojtowicz, J. M. (2006). Irradiation as an experimental tool in studies of adult neurogenesis. *Hippocampus* 16, 261–266.

Wojtowicz, J. M., Askew, M. L., and Winocur, G. (2008). The effects of running and inhibiting adult neurogenesis on learning and memory in rats. *Eur. J. Neurosci.* 27, 1494–1502.

Wojtowicz, J. M., and Kee, N. (2006). BrdU assay for neurogenesis in rodents. *Nat. Protocols* 1, 1399–1405.

Conflict of Interest Statement: The authors declare that the research was conducted in the absence of any commercial or financial relationships that could be construed as a potential conflict of interest.

Received: 24 January 2011; accepted: 07 April 2011; published online: 21 April 2011.

*Citation: Tan Y.-F, Rosenzweig S, Jaffray D and Wojtowicz JM (2011) Depletion of new neurons by image guided irradiation. Front. Neurosci. **5**:59. doi: 10.3389/fnins.2011.00059*

This article was submitted to Frontiers in Neurogenesis, a specialty of Frontiers in Neuroscience.

frontiers in
NEUROSCIENCE

METHODS ARTICLE
published: 21 March 2011
doi: 10.3389/fnins.2011.00034

Analyzing dendritic growth in a population of immature neurons in the adult dentate gyrus using laminar quantification of disjointed dendrites

Shira Rosenzweig* and J. Martin Wojtowicz

Department of Physiology, University of Toronto, Toronto, ON, Canada

Edited by:
Silvia De Marchis, University of Turin, Italy

Reviewed by:
Heather A. Cameron, National Institutes of Health, USA
Sophie Tronel, Institut National de la Santé et de la Recherche Médicale, France

****Correspondence:***
Shira Rosenzweig, Department of Physiology, University of Toronto, 1 King's College Circle, Toronto, ON, Canada M5S 1A8.
e-mail: s.rosenzweig@utoronto.ca

In the dentate gyrus (DG) of the hippocampus, new granule neurons are continuously produced throughout adult life. A prerequisite for the successful synaptic integration of these neurons is the sprouting and extension of dendrites into the molecular layer of the DG. Thus, studies aimed at investigating the developmental stages of adult neurogenesis often use dendritic growth as an important indicator of neuronal health and maturity. Based on the known topography of the DG, characterized by distinct laminar arrangement of granule neurons and their extensions, we have developed a new method for analysis of dendritic growth in immature adult-born granule neurons. The method is comprised of laminar quantification of cell bodies, primary, secondary and tertiary dendrites separately and independently from each other. In contrast to most existing methods, laminar quantification of dendrites does not require the use of exogenous markers and does not involve arbitrary selection of individual neurons. The new method relies on immunohistochemical detection of endogenous markers such as doublecortin to perform a comprehensive analysis of a sub-population of immature neurons. Disjointed, "orphan" dendrites that often appear in the thin histological sections are taken into account. Using several experimental groups of rats and mice, we demonstrate here the suitable techniques for quantifying neurons and dendrites, and explain how the ratios between the quantified values can be used in a comparative analysis to indicate variations in dendritic growth and complexity.

Keywords: dendrites, adult neurogenesis, dentate gyrus, doublecortin, dendritic complexity

INTRODUCTION

Laminar arrangement of neuronal fields and axonal projections is a characteristic of the mammalian forebrain. This anatomical feature is particularly prominent in the dentate gyrus (DG) of the hippocampal formation, where incoming afferents make synaptic contacts with granule neurons within the three laminar regions of the molecular layer (ML; Ruth et al., 1982; Witter, 2007). In addition to the layering of the afferent inputs which has a well-known topographical and physiological significance, the cell bodies of the granule neurons are similarly arranged in layers and their position is related to their chronological formation (Wang et al., 2000). A consequence of such laminar arrangement is an intricate matrix of connections between the upstream entorhinal cortex and the first relay of the tri-synaptic circuit of the hippocampus.

Into this complex circuitry there is a continuous introduction of new neurons born in the sub-granular zone (SGZ) of the DG throughout adult life (Christie and Cameron, 2006). Since neuronal progenitors are mostly devoid of any neural processes, a fundamental milestone in the development of adult-born neurons is the extension of dendrites into the ML where the synaptic connections are formed (Carlen et al., 2002; Abrous et al., 2005). Because this progression is critical for successful neuronal integration and subsequent functionality, studies evaluating adult neurogenesis often include measurements of dendritic growth in developing neurons and use these measurements as indicators of the growth process (Eadie et al., 2005; Rao et al., 2005; Overstreet-Wadiche et al., 2006; Redila and Christie, 2006; Tronel et al., 2010; Ramirez-Rodriguez et al., 2011).

Most existing methods used to measure dendritic length and complexity require the complete visualization of isolated neurons and a subsequent tracing of their entire dendritic tree. In these instances the neurons are either loaded with a dye (e.g., Golgi staining) or induced to express a fluorescent protein which is introduced by a viral vector or through genetic manipulation (Zhao et al., 2006; Nishi et al., 2007; Ide et al., 2008; Ambrogini et al., 2010; Winner et al., 2011). While these methods produce an accurate analysis on a single-cell resolution, extrapolating the acquired data to a larger neuronal population might prove inaccurate if the staining technique selectively labels only specific neurons. Additional selection bias might also occur in these cases if the researcher chooses to measure "convenient" cells which are visualized more clearly and without overlap with other neurons.

To overcome such problems we delineate here a new approach for analyzing dendritic growth in a sub-population of adult-born neurons in the DG. We demonstrate how laminar quantification of disjointed dendrites accurately represents all the cells in the population and does not require the use of exogenous markers or dyes. The neurons are identified by their expression of endogenous

Abbreviations: DCX, doublecortin; DG, dentate gyrus; GCL, granule cell layer; GFP, green fluorescent protein; ML, molecular layer; SGZ, sub-granular zone.

markers such as doublecortin (DCX) or PSA-NCAM, which are well-established and frequently used in neurogenesis research to identify and quantify immature neurons.

Doublecortin is a microtubule-associated protein required for neuronal migration and differentiation (Gleeson et al., 1999). In the adult DG DCX is expressed throughout the soma and neurites of immature neurons residing in the SGZ and inner granule cell layer (GCL). DCX expression begins shortly after the neurons are born, persists for approximately 2 weeks in rats and 3 weeks in mice, and then gradually declines as the neurons continue to mature (Rao and Shetty, 2004; Snyder et al., 2009). Due to a similar expression pattern in the DG, this marker can be complemented or interchanged by PSA-NCAM, a polysialylated form of the neural cell adhesion molecule which has been shown to be involved in the regulation of myelination in the central nervous system as well as axonal guidance and synapse formation (Seki and Arai, 1999; Nguyen et al., 2003).

While both markers are expressed throughout the cell bodies and neurites, it is often difficult to visualize the cells that express them in their entirety due to overlap between adjacent cells. This may prevent the researcher from accurately discerning which dendrites originate from which cells. In addition, neurites are often separated from their cell bodies when the tissue is sectioned, resulting in either "orphaned" dendrites or cell bodies that appear to have no dendrites, but actually have well-developed dendritic trees which now reside in an adjacent section.

These pitfalls have minimal or no effect when using laminar quantification of disjointed dendrites, because this method does not require the visualization of any vertical connections (i.e., between cell bodies and dendrites, or primary dendrites and secondary/tertiary dendrites). Instead, the method relies on the known alignment of immature neurons in the DG (cell bodies in the SGZ, dendrites extended vertically toward the ML, see **Figure 1**) to quantify cell bodies and dendrites in a disjointed manner – separately and independently from each other. The ratios between the acquired numbers can be used in a comparative analysis to indicate changes in the number of cells and the extent of dendritic arborization in the population. We explain here how several visualization techniques can be used to quantify cells and dendrites with or without the acquisition of high-resolution stack confocal images, and demonstrate how the calculated ratios change between several experimental groups. In order to highlight the advantages of our method, we also compare it to the more commonly used tracing technique.

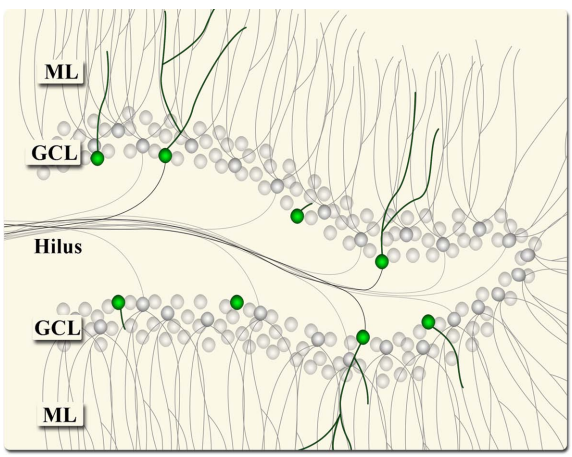

FIGURE 1 | Illustration of the structural arrangement of granule neurons in the dentate gyrus – cell bodies in the granule cell layer (GCL), dendrites extended into the molecular layer (ML), and axons extended into the hilus (toward CA3). The green cells represent immature, DCX-positive adult-born neurons.

MATERIALS AND METHODS

ANIMALS AND TREATMENTS

For demonstration purposes we used tissue taken from two groups of 4-months-old male Sprague-Dawley rats (Charles River, Quebec), and two groups of 3-months-old male mice. Each of the rat groups included four animals: the experimental (treated) group was administered seven daily injections (intra-peritoneal) of a drug known to modulate GABA-ergic neurotransmission, while the control group was injected with saline. The animals were sacrificed 2 weeks after the last injection. One additional group of 3-months-old rats (Sprague-Dawley) was used for retrovirus-mediated green fluorescent protein (GFP) labeling. The mouse groups were consisted of four wild-type C57BL/6J mice (WT group), and four knock-out mice lacking a specific ionotropic GABA receptor subunit (KO group). All animal procedures conformed to animal health and welfare guidelines of the University of Toronto.

RETROVIRUS-MEDIATED LABELING OF NEW NEURONS IN RATS

The animals were anesthetized using intra-peritoneal injection of ketamine/xylazine (85/5 mg/kg), and then placed in a stereotaxic device. A retroviral vector expressing GFP was originally donated by Dr. F. Gage's laboratory (Salk Inst., San Diego; van Praag et al., 2002) with additional batches of the virus produced locally at the University of Toronto in collaboration with Dr. C. Morshead (Medicine). A concentrated solution of the virus (>10^8 infectious units/ml) was prepared and injected into the DG at the following coordinates (two sites in each DG, 1.5 µl/site): AP: −3.3, ML: ±1.5, DV: −4.4, and AP: −4.3, ML: ±2.6, DV: −4. The animals were sacrificed 2 weeks after the injection.

IMMUNOHISTOCHEMISTRY

Animals were perfused intracardially with phosphate-buffered saline followed by 4% paraformaldehyde. The brains were removed and fixed in 4% paraformaldehyde for 24 h at 4°C. Hemispheres were sectioned using a vibratome into 40 µm coronal sections, yielding approximately 100 sections along the hippocampus in rats and 60 in mice. For DCX immunostaining, nine sections were sampled at fixed intervals from each animal. Free-floating sections were incubated with a primary goat anti-DCX antibody (1:200, Santa Cruz Biotechnology, 24 h at 4°C), followed by Alexa 488 donkey anti-goat secondary antibody (1:200; Invitrogen; 2 h at RT). All antibodies were diluted in phosphate-buffered saline containing 0.03% Triton X-100.

IMAGING AND TRACING OF GFP-POSITIVE NEURONS

Sections from animals injected with GFP-expressing retrovirus were imaged with a Leica TCS-SL confocal microscope (Leica Microsystems) using a 40× oil immersion objective lens. The

analysis of GFP-positive neurons was performed in maximum-intensity projection of a *z*-series stack acquired at 0.8 μm intervals throughout 40 μm thick sections. For the demonstrated comparison we chose stacks that contained no GFP-positive cell bodies within 10 μm of the surface of the section, to minimize the inclusion of cells with cut-off dendritic trees. The dendrites in the image were traced using NeuronJ (Meijering et al., 2004) and the number of branching points was counted manually from the same image. Similar technique has been described previously in numerous studies (Overstreet-Wadiche et al., 2006; Zhao et al., 2006; Winner et al., 2011).

IMAGING AND QUANTIFICATION OF DCX-POSITIVE CELLS AND DENDRITES

The analysis of dendrites in DCX-positive cells was performed both under a fluorescent microscope (Nikon Optiphot-2) using a 40× objective lens and in images obtained with a Leica TCS-SL confocal microscope (Leica Microsystems) using a 40× oil immersion objective lens. Each image was constructed from a maximum-intensity projection of a *z*-series stack acquired at 0.8 μm intervals throughout 40 μm thick sections. While it is not necessary to reconstruct an entire section into a single image for the quantification, the DG area should be imaged with minimum gaps or overlap while making sure the gain settings remain constant between images.

The typical arrangement of DCX-positive cells in the DG (as illustrated in **Figure 1**), mandates that the cell bodies be counted in the SGZ and inner GCL, the primary dendrites counted in the middle of the GCL, secondary dendrites counted along the external edge of the GCL and tertiary branches counted in the ML. The cell bodies and dendrites are quantified separately and several independent values are obtained. The first value (*a*) represents the number of DCX-positive cells and is traditionally obtained by visualizing and counting the cell bodies under a fluorescent microscope, a technique which can be employed in this case as well. Alternatively, when confocal stack images are obtained for further dendritic analysis, the cell bodies can be quantified as they appear in the images. For example, the estimated number of cells in **Figure 2A** is 10.

The next several values (*b*, *c*, *d*) represent the number of dendrites at distinct spans from the cell bodies layer. Theoretically, while three values may be sufficient, if additional values are collected more information can be inferred regarding the dendritic complexity of the cells. The first value in this series (*b*) should represent the number of primary dendrites and thus be measured just above the cell bodies of DCX-positive cells (approximately in the middle of the GCL). Line 1 in **Figure 2A** demonstrates the correct area for the quantification of *b*. The dendrites along the line can be quantified by manually tracing the line and marking any dendrites along its path, or by using image processing software such as ImageJ (NIH) to plot a profile of the intensity of the signal along the line. The profile of line 1 is displayed in **Figure 2B**, and a threshold of 7 was set to yield a correct estimation of 13 dendrites (peaks). The same threshold was subsequently used for the next two values in the series; however, since the brightness of tertiary dendrites may differ from that of primary dendrites, and the levels of background "noise" may differ between the GCL and ML, a different threshold will occasionally have to be set for each measurement line.

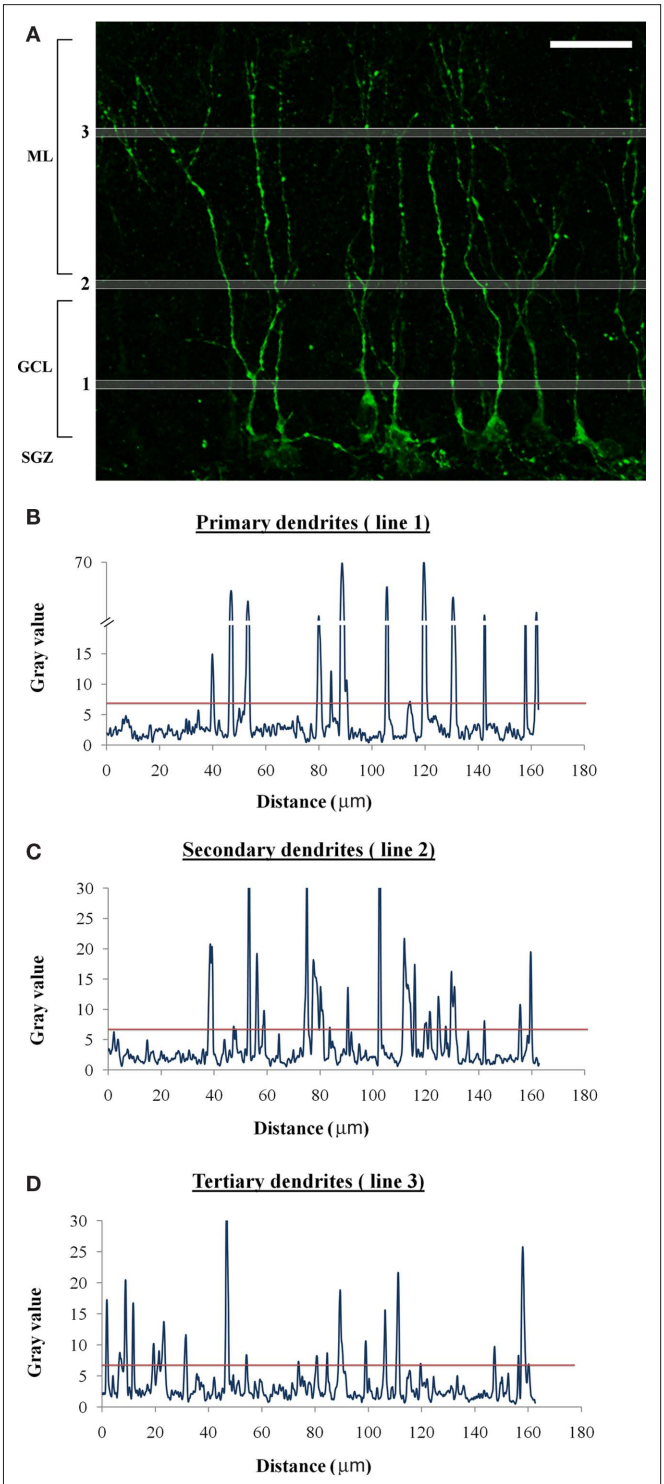

FIGURE 2 | Example of dendritic quantification. (A) High-resolution confocal stack image of a section through the DG immunostained for DCX. DCX-positive cell bodies are arranged along or just above the SGZ, primary dendrites are quantified along line 1 in the middle of the GCL, secondary dendrites are quantified along line 2 on the outer edge of the GCL and tertiary dendrites are quantified along line 3 in the ML. Scale bar = 20 μm. **(B–D)** plot profiles for lines 1–3 obtained using ImageJ software. The red line indicates the threshold (set for 7) and all the peaks that cross it are counted.

The value *c* represents secondary dendrites and is measured along the outer edge of the GCL (line 2 in **Figure 2A**). The number of dendrites "encountered" along the line is measured similarly to line 1. The profile of line 2 is displayed in **Figure 2C** and indicates 22 secondary dendrites for a threshold of 7. The next value (*d*) represents tertiary branches and will be measured in the same fashion in the ML (line 3 in **Figure 2A**). The profile of line 3 is displayed in **Figure 2D** and indicates 22 dendrites for a threshold of 7. The locations of the three lines demonstrated here can be shifted according to the specific requirements of the experiment, and additional values/lines can be added if needed.

While this technique provides consistent results, it is also possible to perform dendritic measurements under a fluorescent microscope in the same manner as when cell bodies are conventionally counted. The three lines – middle GCL, outer edge of the GCL, and middle ML can be visualized and separately "traced" by the investigator, and any "encounter" with dendrites along the lines counted. This technique is significantly less time-consuming because it does not require the imaging of entire sections; however, the accuracy and consistency of the results may vary considerably according to the investigator's experience and skill.

ANALYSIS

Changes in the number of DCX-positive cells (*a*) provide important information regarding variations in the rate of adult neurogenesis between different experimental groups. However, changes in the values representing dendrites (*b*, *c*, and *d*) become indicative of variations in dendritic complexity only when the ratios between the values are calculated and compared across experimental groups. For instance, a decrease in the number of primary dendrites (*b*) would be a given in a case where the total number of cell bodies (*a*) is decreased, because primary dendrites originate directly from the cell bodies. As long as the ratio *b*/*a* is unchanged, the decrease in the number of primary dendrites would not be a sign of diminished dendritic growth. However, a decrease in the number of primary dendrites with no change in the number of cells (i.e., *b*/*a* is lower), might indicate a reduction in the initial ability of young neurons to sprout dendrites. In that case the number of secondary dendrites (*c*) might be reduced as well (because secondary dendrites originate directly from primary dendrites), but if the effect on primary sprouting does not extend to more developed neurons (those that have already extended secondary dendrites), the ratio between tertiary and secondary dendrites (*d*/*c*) will remain unchanged.

Thus, the relevant parameters are:

N_n: Number of neurons (*a*).

N_p: The level of primary dendrite sprouting (*b*/*a*).

N_s: The level of secondary branching (*c*/*b*).

N_t: The level of tertiary branching from secondary dendrites (*d*/*c*).

A comparative analysis of dendritic complexity will be based on these four parameters, calculated for each experimental group.

RESULTS

COMPARATIVE ANALYSIS OF DENDRITIC GROWTH IN MICE AND RATS

We tested the laminar quantification of disjointed dendrites method in two experiments, as part of a comprehensive assessment of variations in adult neurogenesis between different groups of animals. In experiment 1 we compared the treated rat group to the control group and in experiment 2 we compared KO mice to WT mice. Nine sections were sampled from each animal, imaged using a confocal microscope or analyzed using a fluorescent microscope. Only minor differences were observed between the two imaging techniques and the data displayed were obtained using the former. The number of cell bodies (*a*), primary dendrites (*b*) secondary dendrites (*c*), and tertiary dendrites (*d*) were quantified along 1 mm stretch in individual sections, and averaged for each animal and then for each group. **Table 1** displays the averaged values *a*, *b*, *c*, and *d* as well as the calculated ratios N_p, N_s, and N_t for each group.

The number of DCX-positive cells (N_n) was significantly higher in the treated rat group compared to the control group, as well as in KO mice compared to WT mice ($p < 0.01$, $n = 4$ for both rats and mice). The values *b*, *c*, and *d* were significantly higher in the treated group and KO mice compared to the control group and WT mice, respectively [experiment 1 (rats): $p < 0.05$ for *b*, $p < 0.03$ for *c* and *d*, $n = 4$; experiment 2 (mice): $p < 0.03$ for *b* and *c*, $n = 4$], with one exception (*d* value in mice, $p > 0.07$, $n = 4$). However, the calculated values N_p, N_s, and N_t revealed that the effect on the treated group in experiment 1 (rats) was different from the effect on the KO mice in experiment 2.

In experiment 1, none of the three calculated ratios N_p, N_s, and N_t differed between the treated and control groups (**Figure 3A**, $p > 0.3$, $n = 4$). This indicates that while the experiment induced an increase in the total number of DCX-positive cells in both species it did not affect the dendritic complexity in rats. Conversely, in experiment 2 the parameters N_s and N_t were significantly lower in the KO mice compared to the WT mice (**Figure 3B**, $p < 0.05$, $n = 4$). This indicates that the experiment induced an increase in the total number of DCX-positive cells but decreased the relative number of secondary and tertiary dendrites (even though the absolute number of secondary and tertiary dendrites, represented by the values *c* and *d*, was higher or unchanged in the KO group – see **Table 1**).

COMPARISON WITH THE TRACING METHOD

In order to demonstrate the advantages of the new method over existing methods, we compared it to the commonly used dendritic tracing technique. Tracing is often used in conjunction with GFP-expressing retrovirus injection, because this labeling strategy permits better iden-

Table 1 | Summary of the data obtained for the four groups in experiments 1 and 2.

	Rats control	Rats treated	Mice WT	Mice KO
a (N_n)	84 ± 3	102 ± 4**	71 ± 4	108 ± 9**
b	88 ± 5	112 ± 7*	76 ± 6	117 ± 10*
c	121 ± 8	153 ± 9*	102 ± 6	131 ± 8*
d	154 ± 8	183 ± 8*	127 ± 13	132 ± 12
N_p	1.048 ± 0.072	1.098 ± 0.085	1.070 ± 0.064	1.083 ± 0.058
N_s	1.375 ± 0.109	1.366 ± 0.116	1.342 ± 0.049	1.120 ± 0.061*
N_t	1.273 ± 0.097	1.196 ± 0.101	1.245 ± 0.052	1.008 ± 0.066*

The values a–d represent the number of cells or dendrites along 1 mm stretch. Each value is presented as an average of four animals ± SE. The ratios N_p, N_s, and N_t were calculated for each animal and averaged for each group as well.
**p<0.05, **p<0.01.*

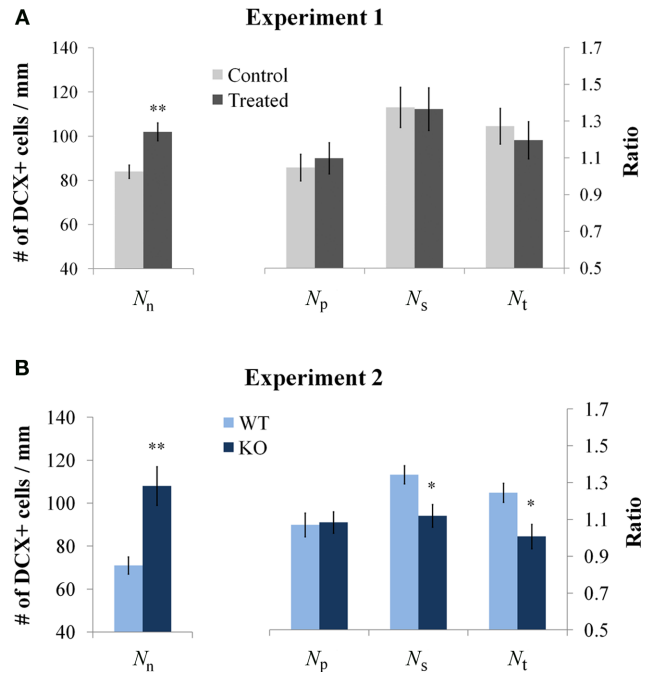

FIGURE 3 | Comparison between animal groups. (A) In experiment 1 the number of DCX-positive neurons was increased in the treated rat group with no change in dendritic complexity. **(B)** In experiment 2 the number of DCX-positive neurons was increased in the KO mice but secondary and tertiary branching were reduced.

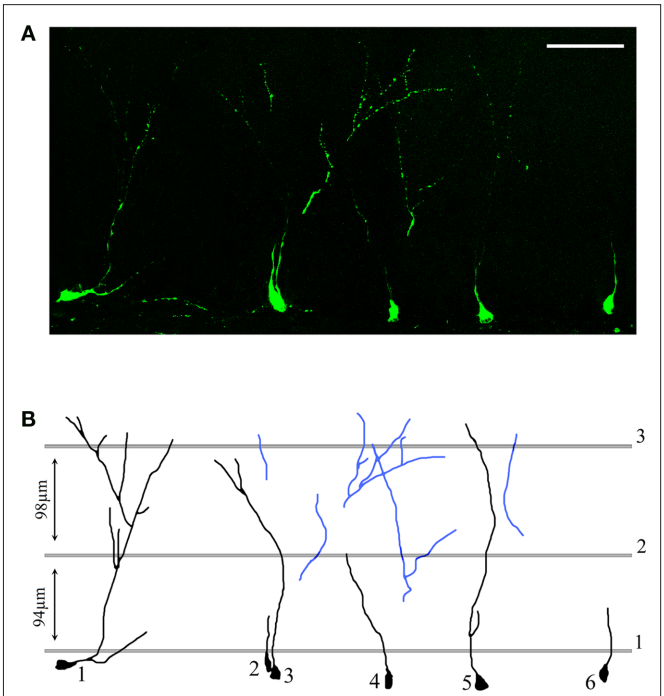

C

Tracing

Neuron #	Dendritic length (µm)	Branching points
1	594	8
2	38	0
3	233	1
4	113	0
5	251	1
6	53	0
Avg	214	1.67

Laminar quantification

a	6
b (line 1)	7
c (line 2)	9
d (line 3)	11

FIGURE 4 | Comparison between dendritic tracing and laminar quantification methods. (A) High-resolution confocal (collapsed stack) image of a section through the DG, showing neurons expressing GFP 14 days post-injection. Scale bar = 60 µm. **(B)** Tracings of six GFP-positive dendrites and measurement lines for the quantification of primary (1), secondary (2), and tertiary (3) dendrites. The blue dendrites were considered "disjointed" and were only included in the laminar quantification. **(C)** Values obtained using both methods.

tification and visualization of single-cells. (Ge et al., 2006; Zhao et al., 2006). We imaged GFP-labeled neurons in the rat DG 2 weeks after a GFP-expressing retrovirus was injected. A segment containing six GFP-positive neurons was selected for the demonstration (**Figure 4A**) and the dendrites in the image were analyzed using the tracing technique as well as the new laminar quantification method.

When the new method was used, "orphan" dendrites were included in the analysis (**Figure 4B**, blue dendrites). These dendrites were excluded during the tracing because their origin (cell body) could not be visualized. The length of the dendrites that could be traced from soma to tip (**Figure 4B**, black dendrites) was measured directly using the tracing method, and the complexity of the dendritic tree was evaluated by counting the number of branching points. The individual measurements as well as the averages are summarized in **Figure 4C** (left).

These values are different from the ones obtained using the laminar quantification method (number of neurons – *a*, primary dendrites – *b*, secondary dendrites – *c*, tertiary dendrites – *d*, **Figure 4C** – right), but an estimation of the average dendritic length and the average number of branching points can be calculated as follows:

$$\begin{aligned}\text{Dendritic length} &= (c \quad \text{distance between line 1 and 2}) \\ &\quad + (d \quad \text{distance between line 2 and 3}) \\ &= (9 \quad 94 \quad \text{m}) + (11 \quad 98 \quad \text{m}) \\ &= 1924 \quad \text{m}/6 \text{ neurons} = 321 \quad \text{m/neuron}\end{aligned}$$

$$\text{Branching points} = (c+d)/a = (9+11)/6 = 3\tfrac{1}{3}$$

In both cases the calculated values (321 µm, 3 1/3) are higher than the ones obtained using the tracing method (214 µm, 1.67, **Figure 4C**) due to the additional dendrites that were included in the analysis ("extra" three secondary dendrites and six tertiary dendrites). Still, these values are an underestimation since some dendrites extend beyond line 3 or begin and end between the lines. A higher degree of accuracy can be achieved by adding more measurement lines at shorter intervals.

DISCUSSION

We have demonstrated here how a series of simple measurements can be used to detect subtle changes in dendritic growth in a subpopulation of adult-born neurons. Quantifying dendrites at vary-

ing distances from the cell bodies in a disjointed manner enabled us to incorporate many cells and dendrites that would otherwise be excluded from the analysis based on their discontinuous visualization. The result was a comprehensive data set offering an informative representation of the DCX-positive neuronal population in the DGs of studied animals.

ANALYSIS OF THE DATA SET

Analysis of the rat tissue in experiment 1 revealed an increase in the number of DCX-positive neurons in the treated rat group with no accompanying changes in the ratios representing dendritic branching. This suggests that while the size of the DCX-positive neuronal population was increased, its composition (in terms of the level of development of the neurons comprising it) remained unchanged (**Figures 5A,B**). This result would be expected when the overall rate of neurogenesis (i.e., production and retention of new neurons) is increased. Such increase can be verified directly using standard immunohistochemical markers. Traditionally, measurements of proliferation and survival of adult-born neurons in the DG are performed using the proliferative marker BrdU and the endogenous Ki-67 (Kee et al., 2002; Wojtowicz and Kee, 2006).

In experiment 2, the decrease in the ratios representing secondary and tertiary branching (N_s and N_t) suggests that a different process is taking place in the KO mice. Not only the size of the DCX-positive neuronal population is changed, but also the relative level of development of the neurons comprising it. In this case, the lack of change in primary sprouting (N_p) may indicate that only the more mature cells are affected. This result might also suggest that the higher number of DCX-positive cells in the KO mice is not due to an increase in the rate of neurogenesis, but due to a delay in neuronal development which causes neurons to express the marker DCX for a longer period of time (the capacity of the neurons to develop beyond the DCX-expressing stage is diminished). In this case, the "extra" DCX-positive neurons are derived from accumulation of neurons in a relatively early developmental stage – neurons that only have short primary dendrites (**Figures 5A,C**). This interpretation conforms to the results obtained from the analysis of DCX-positive cells, but other explanations cannot be ruled out without additional complementary experiments. For example, measurements showing that proliferation and/or survival are unchanged (using BrdU and Ki-67) will further support this interpretation. Generally, analysis of DCX-positive cells and dendritic complexity is only one part of the study, and is combined with additional approaches to provide a more comprehensive view (Gao et al., 2007; Wang et al., 2008; Revest et al., 2009).

Thus, laminar quantification of disjointed dendrites effectively detects developmental changes within the DCX-positive neuronal population, but a range of interpretations must be considered for the results and further analysis using additional tools and markers is required in order to place the changes in the context of a general effect on neurogenesis. It should be noted that different experiments were performed on mice and rats. Hence, the different effects observed here are likely due to the experimental design and not necessarily due to species differences.

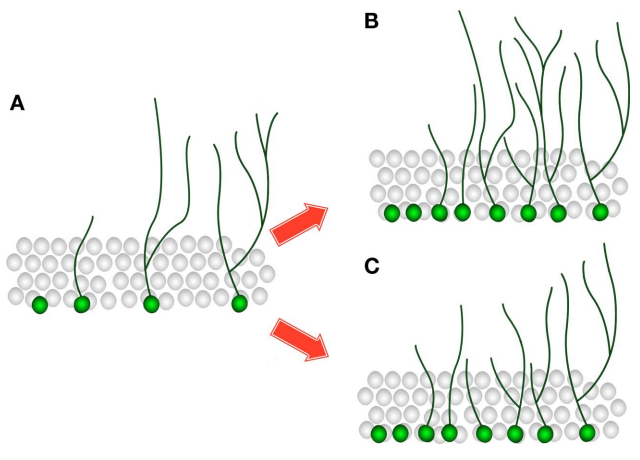

FIGURE 5 | Differential effects on dendritic growth in experiments 1 and 2. In both the treated rat group and KO mice **(B,C)** the number of DCX-positive neurons is increased compared to the control rat group and WT mice **(A)**. However, the relative level of development of the neurons comprising the DCX-positive population is unchanged in experiment 1, as evident by a similar portion of cells that have no dendrites, have only primary dendrites or have secondary/tertiary dendrites in the treated group **(B)** compared to the control group **(A)**. In experiment 2 there is a larger portion of neurons with only primary dendrites and a smaller portion on neurons that have tertiary dendrites in the KO mice **(C)** compared to the WT mice **(A)**, thus the overall dendritic complexity in the KO mice is decreased.

COMPARISON WITH OTHER METHODS

One of the main advantages of the method is the use of endogenous markers such as DCX or PSA-NCAM. Several previous studies have attempted to use endogenous markers for dendritic analysis (Rao and Shetty, 2004; Gao et al., 2007; Wang et al., 2008; Revest et al., 2009); however, some problems become apparent when the techniques used in some of those studies are examined in depth. For instance, Revest et al. (2009) included an analysis of dendritic morphology as part of the characterization of adult neurogenesis in a transgenic mouse model. In that study, specific DCX-positive neurons were selected on the basis of their general morphology (i.e., cells that exhibited vertically orientated dendrites that extended into the ML) and minimal overlap with the dendrites of adjacent cells which allowed the authors to unambiguously trace the entire dendritic tree. While this method provided an accurate estimation of the dendritic structure in the analyzed neurons, it is difficult to determine whether the neurons selected for analysis accurately represented the relevant neuronal population.

Another study by Gao et al. (2007) attempted a different approach. They classified the majority of the DCX-positive cells into two developmental stages: A – cells with bipolar short process, located adjacent to the SGZ with the axis of cell body parallel to SGZ, and B – Cells with long dendrites projecting close to or crossing the ML, with axis of cell body perpendicular to SGZ. In this case the relevant neuronal population was more adequately represented, but the resolution of the analysis was low – only two categories of cells were defined, providing minimal data regarding dendritic arborization.

Our intention was to develop a method that achieves both an adequate representation of the entire DCX-positive population and detailed information regarding the length and complexity of the dendritic tree. A direct comparison between our new method and

the commonly used dendritic tracing method revealed that when the same segment is analyzed by both methods, the data obtained from laminar quantification is comparable in detail and accuracy to the data obtained by tracing, but is more representative of the examined population due to the inclusion of "disjointed" dendrites. Depending on the resolution required for a specific experiment, the new method can be adjusted and additional measurement lines can be inserted to yield better accuracy.

It is interesting to note that while all six neurons in the imaged sample segment were traced for demonstration purposes, most studies using the tracing technique mention the selection of specific neurons for analysis (Ge et al., 2006; Winner et al., 2011). These neurons, chosen at the discretion of the researcher, are considered representative of the studied neuronal population. An examination of the neurons in the sample segment (**Figure 4**) reveals why this type of subjective selection may pose a problem. While the average length of traced dendrites per neuron was found to be 214 μm, the lengths of the six individual dendritic trees ranged between 38 and 594 μm. This variation extended to branching points as well. Therefore, it is likely that an inference based on analysis of specific neurons over others will vary considerably based on the individual neurons that make up the selected cohort.

CRITIQUE

When using this method it is important to consider its limitations which arise from the basic assumptions the method relies on. For instance, laminar quantification relies on the relatively uniform arrangement of cell bodies along the SGZ and the vertical extension of dendrites toward the ML. This arrangement is only consistent in neurons within a certain range of developmental stages. Therefore, only endogenous markers which are expressed during those stages (and those stages alone) can be used. More advanced neuronal markers are expressed in neurons which have migrated further into the GCL. Once the neurons are no longer arranged along the SGZ it becomes impossible to quantify primary and secondary dendrites in the GCL. However, the basic concept of the method can still be implemented to quantify proximal and distal dendrites in the ML, and this type of analysis may have significant implications for synaptic transmission and connectivity in the DG.

Another important assumption the method relies on is the polarity of young granule neurons. It is important to remember that if the alignment and directionality of the dendrites in the experimental group is affected, the results might not accurately reflect dendritic complexity (because some dendrites will be detected in the "wrong" location or altogether missed).

The use of endogenous markers presents additional limitations. For instance, the expression of DCX persists for up to 3 weeks, thus the exact age of the analyzed cells is unknown. This may become significant in experiments testing the acute effects of certain treatments. Furthermore, an effect on the expression of the endogenous marker itself (e.g., a treatment which reduces the amount of DCX expression in dendrites) might also affect the accuracy of the results.

CONCLUSION

We have developed an alternative method for measurement and analysis of dendritic growth in a sub-population of DG granule neurons. The main advantage over the pre-existing methods is the improved, unbiased sampling. The method may yield new, alternate data which would be missed with the traditional techniques. Although we focused on the young, adult-generated subpopulation, the technique is also suitable for analysis of other, more mature neuronal populations within the DG. The laminar arrangement of the afferent synaptic inputs suggests specialized functions for each layer of the dendritic tree. Given the dynamic changes within the DG in response to various physiological and pathological manipulations (Jessberger and Gage, 2008; van Praag, 2008; Schaeffer et al., 2009), these functions can now be further examined using dendritic analysis.

ACKNOWLEDGMENTS

We thank Michael Vu for his help with confocal imaging and analysis. This work was supported by operating grants from CIHR and NSERC.

REFERENCES

Abrous, D. N., Koehl, M., and Le Moal, M. (2005). Adult neurogenesis: from precursors to network and physiology. *Physiol. Rev.* 85, 523–569.

Ambrogini, P., Cuppini, R., Lattanzi, D., Ciuffoli, S., Frontini, A., and Fanelli, M. (2010). Synaptogenesis in adult-generated hippocampal granule cells is affected by behavioral experiences. *Hippocampus* 20, 799–810.

Carlen, M., Cassidy, R. M., Brismar, H., Smith, G. A., Enquist, L. W., and Frisen, J. (2002). Functional integration of adult-born neurons. *Curr. Biol.* 12, 606–608.

Christie, B. R., and Cameron, H. A. (2006). Neurogenesis in the adult hippocampus. *Hippocampus* 16, 199–207.

Eadie, B. D., Redila, V. A., and Christie, B. R. (2005). Voluntary exercise alters the cytoarchitecture of the adult dentate gyrus by increasing cellular proliferation, dendritic complexity, and spine density. *J. Comp. Neurol.* 486, 39–47.

Gao, X., Arlotta, P., Macklis, J. D., and Chen, J. (2007). Conditional knockout of beta-catenin in postnatal-born dentate gyrus granule neurons results in dendritic malformation. *J. Neurosci.* 27, 14317–14325.

Ge, S., Goh, E. L., Sailor, K. A., Kitabatake, Y., Ming, G. L., and Song, H. (2006). GABA regulates synaptic integration of newly generated neurons in the adult brain. *Nature* 439, 589–593.

Gleeson, J. G., Lin, P. T., Flanagan, L. A., and Walsh, C. A. (1999). Doublecortin is a microtubule-associated protein and is expressed widely by migrating neurons. *Neuron* 23, 257–271.

Ide, Y., Fujiyama, F., Okamoto-Furuta, K., Tamamaki, N., Kaneko, T., and Hisatsune, T. (2008). Rapid integration of young newborn dentate gyrus granule cells in the adult hippocampal circuitry. *Eur. J. Neurosci.* 28, 2381–2392.

Jessberger, S., and Gage, F. H. (2008). Stem-cell-associated structural and functional plasticity in the aging hippocampus. *Psychol. Aging* 23, 684–691.

Kee, N., Sivalingam, S., Boonstra, R., and Wojtowicz, J. M. (2002). The utility of Ki-67 and BrdU as proliferative markers of adult neurogenesis. *J. Neurosci. Methods* 115, 97–105.

Meijering, E., Jacob, M., Sarria, J. C., Steiner, P., Hirling, H., and Unser, M. (2004). Design and validation of a tool for neurite tracing and analysis in fluorescence microscopy images. *Cytometry A* 58, 167–176.

Nguyen, L., Rigo, J. M., Malgrange, B., Moonen, G., and Belachew, S. (2003). Untangling the functional potential of PSA-NCAM-expressing cells in CNS development and brain repair strategies. *Curr. Med. Chem.* 10, 2185–2196.

Nishi, M., Usuku, T., Itose, M., Fujikawa, K., Hosokawa, K., Matsuda, K. I., and Kawata, M. (2007). Direct visualization of glucocorticoid receptor positive cells in the hippocampal regions using green fluorescent protein transgenic mice. *Neuroscience* 146, 1555–1560.

Overstreet-Wadiche, L. S., Bromberg, D. A., Bensen, A. L., and Westbrook, G. L. (2006). Seizures accelerate functional integration of adult-generated granule cells. *J. Neurosci.* 26, 4095–4103.

Ramirez-Rodriguez, G., Ortiz-Lopez, L., Dominguez-Alonso, A., Benitez-King, G. A., and Kempermann, G. (2011). Chronic treatment with melatonin stimulates dendrite maturation and complexity in adult hippocampal neurogenesis of mice. *J. Pineal Res.* 50, 29–37.

Rao, M. S., Hattiangady, B., Abdel-Rahman, A., Stanley, D. P., and Shetty, A. K. (2005). Newly born cells in the ageing dentate gyrus display normal migration, survival and neuronal fate choice but endure retarded early maturation. *Eur. J. Neurosci.* 21, 464–476.

Rao, M. S., and Shetty, A. K. (2004). Efficacy of doublecortin as a marker to analyse the absolute number and dendritic growth of newly generated neurons in the adult dentate gyrus. *Eur. J. Neurosci.* 19, 234–246.

Redila, V. A., and Christie, B. R. (2006). Exercise-induced changes in dendritic structure and complexity in the adult hippocampal dentate gyrus. *Neuroscience* 137, 1299–1307.

Revest, J. M., Dupret, D., Koehl, M., Funk-Reiter, C., Grosjean, N., Piazza, P. V., and Abrous, D. N. (2009). Adult hippocampal neurogenesis is involved in anxiety-related behaviors. *Mol. Psychiatry* 14, 959–967.

Ruth, R. E., Collier, T. J., and Routtenberg, A. (1982). Topography between the entorhinal cortex and the dentate septotemporal axis in rats: I. Medial and intermediate entorhinal projecting cells. *J. Comp. Neurol.* 209, 69–78.

Schaeffer, E. L., Novaes, B. A., da Silva, E. R., Skaf, H. D., and Mendes-Neto, A. G. (2009). Strategies to promote differentiation of newborn neurons into mature functional cells in Alzheimer brain. *Prog. Neuropsychopharmacol. Biol. Psychiatry* 33, 1087–1102.

Seki, T., and Arai, Y. (1999). Temporal and spacial relationships between PSA-NCAM-expressing, newly generated granule cells, and radial glia-like cells in the adult dentate gyrus. *J. Comp. Neurol.* 410, 503–513.

Snyder, J. S., Choe, J. S., Clifford, M. A., Jeurling, S. I., Hurley, P., Brown, A., Kamhi, J. F., and Cameron, H. A. (2009). Adult-born hippocampal neurons are more numerous, faster maturing, and more involved in behavior in rats than in mice. *J. Neurosci.* 29, 14484–14495.

Tronel, S., Fabre, A., Charrier, V., Oliet, S. H., Gage, F. H., and Abrous, D. N. (2010). Spatial learning sculpts the dendritic arbor of adult-born hippocampal neurons. *Proc. Natl. Acad. Sci. U.S.A.* 107, 7963–7968.

van Praag, H. (2008). Neurogenesis and exercise: past and future directions. *Neuromolecular Med.* 10, 128–140.

van Praag, H., Schinder, A. F., Christie, B. R., Toni, N., Palmer, T. D., and Gage, F. H. (2002). Functional neurogenesis in the adult hippocampus. *Nature* 415, 1030–1034.

Wang, J. W., David, D. J., Monckton, J. E., Battaglia, F., and Hen, R. (2008). Chronic fluoxetine stimulates maturation and synaptic plasticity of adult-born hippocampal granule cells. *J. Neurosci.* 28, 1374–1384.

Wang, S., Scott, B. W., and Wojtowicz, J. M. (2000). Heterogeneous properties of dentate granule neurons in the adult rat. *J. Neurobiol.* 42, 248–257.

Winner, B., Melrose, H. L., Zhao, C., Hinkle, K. M., Yue, M., Kent, C., Braithwaite, A. T., Ogholikhan, S., Aigner, R., Winkler, J., Farrer, M. J., and Gage, F. H. (2011). Adult neurogenesis and neurite outgrowth are impaired in LRRK2 G2019S mice. *Neurobiol. Dis.* 41, 706–716.

Witter, M. P. (2007). The perforant path: projections from the entorhinal cortex to the dentate gyrus. *Prog. Brain Res.* 163, 43–61.

Wojtowicz, J. M., and Kee, N. (2006). BrdU assay for neurogenesis in rodents. *Nat. Protoc.* 1, 1399–1405.

Zhao, C., Teng, E. M., Summers, R. G. Jr., Ming, G. L., and Gage, F. H. (2006). Distinct morphological stages of dentate granule neuron maturation in the adult mouse hippocampus. *J. Neurosci.* 26, 3–11.

Conflict of Interest Statement: The authors declare that the research was conducted in the absence of any commercial or financial relationships that could be construed as a potential conflict of interest.

Received: 15 December 2010; accepted: 02 March 2011; published online: 21 March 2011.

Citation: Rosenzweig S and Wojtowicz JM (2011) Analyzing dendritic growth in a population of immature neurons in the adult dentate gyrus using laminar quantification of disjointed dendrites. Front. Neurosci. ***5****:34. doi: 10.3389/fnins.2011.00034*

This article was submitted to Frontiers in Neurogenesis, a specialty of Frontiers in Neuroscience.

frontiers in
NEUROSCIENCE

METHODS ARTICLE
published: 13 May 2011
doi: 10.3389/fnins.2011.00070

Combining confocal laser scanning microscopy with serial section reconstruction in the study of adult neurogenesis

***Federico Luzzati*[1,2]*, *Aldo Fasolo*[1] *and Paolo Peretto*[1,2]**

[1] *Department of Animal and Human Biology, University of Turin, Turin, Italy*
[2] *Neuroscience Institute Cavalieri Ottolenghi, Orbassano, Italy*

Edited by:
Silvia De Marchis, University of Turin, Italy

Reviewed by:
Vincent Prevot, INSERM, France
Joao R. L. Menezes, Universidade Federal do Rio de Janeiro, Brazil

***Correspondence:**
Federico Luzzati, Neuroscience Institute Cavalieri Ottolenghi, Regione Gonzole, 10, 10043 Orbassano, Turin, Italy.
e-mail: federico.luzzati@unito.it

Current advances in imaging techniques have extended the possibility of visualizing small structures within large volumes of both fixed and live specimens without sectioning. These techniques have contributed valuable information to study neuronal plasticity in the adult brain. However, technical limits still hamper the use of these approaches to investigate neurogenic regions located far from the ventricular surface such as parenchymal neurogenic niches, or the scattered neuroblasts induced by brain lesions. Here, we present a method to combine confocal laser scanning microscopy (CLSM) and serial section reconstruction in order to reconstruct large volumes of brain tissue at cellular resolution. In this method a series of thick sections are imaged with CLSM and the resulting stacks of images are registered and 3D reconstructed. This approach is based on existing freeware software and can be performed on ordinary laboratory personal computers. By using this technique we have investigated the morphology and spatial organization of a group of doublecortin (DCX)+ neuroblasts located in the lateral striatum of the late post-natal guinea pig. The 3D study unraveled a complex network of long and poorly ramified cell processes, often fascicled and mostly oriented along the internal capsule fiber bundles. These data support CLSM serial section reconstruction as a reliable alternative to the whole mount approaches to analyze cyto-architectural features of adult germinative niches.

Keywords: neurogenesis, striatum, whole mount, confocal laser scanning microscopy, serial section reconstruction

INTRODUCTION

Newly generated neuronal cells are constantly added to the mammalian olfactory bulb (OB) and dentate gyrus (DG) during adult life (Kriegstein and Alvarez-Buylla, 2009). Comparative analyses in different mammalian species either in physiologic or pathologic conditions, indicate that neurogenesis can also occur in other brain regions (Lindsey and Tropepe, 2006; Gould, 2007). Nonetheless, out of the OB and DG neurogenic niches, most of adult-generated neurons show short survival life span and elusive identity. In this context, a detailed description of newborn neurons morphology and neuroanatomical organization in both physiological and pathological conditions is a fundamental step to understand their identity and function.

The study of neuroanatomy has been classically carried out through histological sections cut with different orientations and thickness. Although stereological methods contribute much information on the intact 3D structures, the global architecture is mostly lost in sectioned samples. To retrieve information over this higher anatomical level, the structures of interest must be either entirely imaged or reconstructed from serially sectioned material. Recent advances in light microscopy and in molecular and genetic manipulations have greatly extended the possibility of imaging large volumes of both fixed and live neural tissue at cellular resolution, enabling the visualization of complex 3D objects such as neuronal or vascular networks (Mizrahi, 2007; Lu et al., 2009; Tsai et al., 2009; Wilt et al., 2009; Khairy and Keller, 2011). These imaging techniques represent a pivotal innovation for multiple neuroanatomical fields ranging from the definition of comprehensive maps of neuronal connections, the so called "connectome," to the study of neuronal plasticity (Hofer et al., 2009; DeFelipe, 2010). Nonetheless, the relatively limited depth at which objects can be observed with conventional microscopy, and the difficulties of using immunohistochemistry in large tissue volumes, still hamper a general use of these techniques among brain regions and animal species. Given the periventricular location of the subventricular zone (SVZ) neurogenic niche, whole mount preparations have been used in mice to deal with several architectural aspects of this germinative region, ranging from the orientation of the chains of migrating neuroblasts to the spatial organization of progenitor cells (Doetsch and Alvarez-Buylla, 1996; Tavazoie et al., 2008; Mirzadeh et al., 2010). However, the whole mount preparation is less suitable to study neurogenic regions located far from the ventricular surface such as parenchymal neurogenic niches (Luzzati et al., 2006, 2007), or scattered neuroblasts induced by a brain lesion (Arvidsson et al., 2002; Parent et al., 2002). In these latter cases, reconstruction from serial sections represents a reliable alternative. In the classic version of this technique, supported by several commercial and freeware software, planar images are taken from an ordered series of sections and digitally registered. Individual structures can be then converted into virtual 3D objects through different segmentation methods (Fiala, 2005; Cardona et al., 2010). A major drawback of reconstructing from serial sections is that since each slice is represented by a single image, the *z*-axis resolution directly depends on the slice thickness. Accordingly, serial section reconstruction at cellular or sub-cellular resolution is usually performed by registering electron microscopy (EM) images (Fiala, 2005; Cardona et al., 2010). This technique

provided much information on the composition of SVZ and DG adult germinative niches (Doetsch et al., 1997; Seri et al., 2004) and on the organization of chains of neuroblasts in the rabbit brain parenchyma (Luzzati et al., 2003). However, limiting the section thickness critically increases the number of sections to acquire and register, and thus it considerably lengthens the reconstruction of a given volume (Cardona et al., 2010). A possible implementation of this approach can be obtained matching the use of laser scanning confocal microscopy (CLSM) to serial section reconstruction, thus allowing the use of thick sections without losing resolution along the *z*-axis. To date, only a few attempts have been made to use CLSM stacks instead of planar images in serial section reconstructions but they were not employed to perform reconstructions at cellular resolution (Capek et al., 2009).

Here, we describe a new method in which serial section reconstruction is combined to CLSM in order to produce multi scale 3D reconstructions of large volumes of brain tissue at cellular resolution. The *in silico* part of the analysis is performed on standard laboratory personal computers (PC) and it is based on the use of freeware software including: serial section editors, volume integration of tiled optical sections, image analysis and object tracing in large confocal data sets. In this paper, we apply this method to characterize the morphology and the organization of a population of DCX+ neuroblasts located in the ventro-lateral caudate putamen complex of the guinea pig. The obtained results support the CLSM serial section reconstruction method as a useful tool to analyze neuroanatomical features of adult germinative niches.

MATERIALS AND METHODS

Experiments were conducted in accordance with current European Union and Italian law, under authorization of the Italian Ministry of Health number 66/99-A. All experiments were designed to minimize the numbers of animals used and their discomfort.

Results and data-analyses here presented were obtained from two female albino Dunkin-Hartley guinea pig (*Cavia porcellus*) 50 days old that was purchased from a local breeder. The animal was deeply anesthetized with a ketamine/xylazine solution (100 and 33 mg/kg body weight, respectively) and transcardially perfused with ice-cold saline solution (0.9% NaCl), followed by a freshly prepared solution of 4% paraformaldehyde (PFA) plus 2% picric acid in 0.1 M sodium phosphate buffer, pH 7.4. Brains were then postfixed overnight, cryoprotected, frozen at −80°C, and cryostat 40 μm sectioned along a coronal plane in four series.

Free-floating sections were incubated for 48 h at 4°C in a solution of 0.01 M PBS, pH 7.4, containing 1% Triton X-100, normal horse serum and either anti-DCX antibody 1:500 (goat polyclonal sc-8066; Santa Cruz Biotechnology, Santa Cruz, CA, USA) or myelin associated glycoprotein (MAG; mouse monoclonal, Chemicon international, Billerica, MA, USA). After rinsing in PBS solution, sections were incubated with an anti-goat or anti-mouse cyanine 3 (Cy3)-conjugated (1:800; Jackson ImmunoResearch, West Grove, PA, USA). Sections were then coverslipped with antifade mounting medium Dabco (Sigma) and analyzed with a laser scanning Olympus Optical (Milan, Italy) Fluoview confocal system (Olympus Optical). In one series of sections the anti-DCX antibodies were revealed with biotin–avidin system. In this case sections were rinsed in PBS, incubated with the anti-goat biotinylated secondary antibody for 1 h (1:250; Vector Laboratories, Burlingame, CA, USA), rinsed, and incubated in avidin–biotin complex (1:400; Vector Laboratories). The reaction product was visualized with 0.15 mg/ml 3,3-diaminobenzidine (DAB) in PBS with 0.01% H_2O_2. Sections were then serially mounted onto Superfrost Plus slides (Fisher Scientific, Pittsburgh, PA, USA), air dried, dehydrated in graded alcohols, cleared in xylenes, and coverslipped using DPX mounting medium (Aldrich, Milwaukee, WI, USA).

Images (1024 × 1024) were taken with the following objectives (4×, NA 0.13; 10×, NA 0.3; 20×, NA 0.7; 100×, NA 1.3). The actual value of *z* in the voxel size of 20× and 100× CLSM reconstruction was calculated *a posteriori* by dividing the number of the optical planes for the total length along the *z*-axis. Considering that the *z*-step used for the acquisition of the 20× and 100× images were 2 and 0.7 μm respectively, we can calculate slice shrinkage of 66% along the *z*-axis.

Image analyses were conducted on a laptop DELL Vostro, Intel Core i5 M 520 2.40 GHz × 4, 5.87 GB RAM and running 64 bit version of Windows 7. General adjustments to color, contrast, and brightness were made with Adobe Photoshop 7.0 (Adobe Systems, San Jose, CA, USA).

RESULTS

In the brain of 2-month-old guinea pigs several doublecortin (DCX+) positive newborn neurons were identified along the central part of the external capsule (EC) and in surrounding regions of the lateral striatum (LS; **Figure 1** and data not shown). These cells spanned about two millimeters along the antero-posterior axis, however most of them were found at the level of the decussation of the anterior commissure. At this level, the DCX+ cells occupied the entire dorso-ventral extent of the LS, while at more rostral and caudal positions they were restricted to the ventral EC.

A time course analysis with BrdU indicated that these cells were newly generated (data not shown).

In coronal sections containing the LS, the DCX immunostaining identified cells organized as cluster or individual elements (**Figures 1D,E**). Clustered elements were restricted to the ventral end of the EC, while individual elements were scattered along the EC and in the surrounding striatal parenchyma (**Figures 1D,E**). The cell processes of the individual elements were often fascicled and closely associated with the internal capsule fiber bundles (arrow in **Figures 1E,F–F"**). This neurogenic system, which will be described in detail in a separate study (Luzzati et al., unpublished results), offers a good opportunity to show how the method of CLSM serial section reconstruction we developed is suitable to investigate the distribution, organization, and morphological features of immunolabeled newborn neurons located deep within the brain parenchyma.

CHOOSING THE SECTION THICKNESS AND CUTTING PLANE

When planning a serial section reconstruction, firstly the section thickness must be chosen. The use of thick sections (60–100 μm) reduces the number of gaps in the reconstruction, as well as the number of sections to acquire and register. This leads to a more uniform and quickly performed reconstruction. At the same time, thick sections tend to deform after drying, especially near cavities

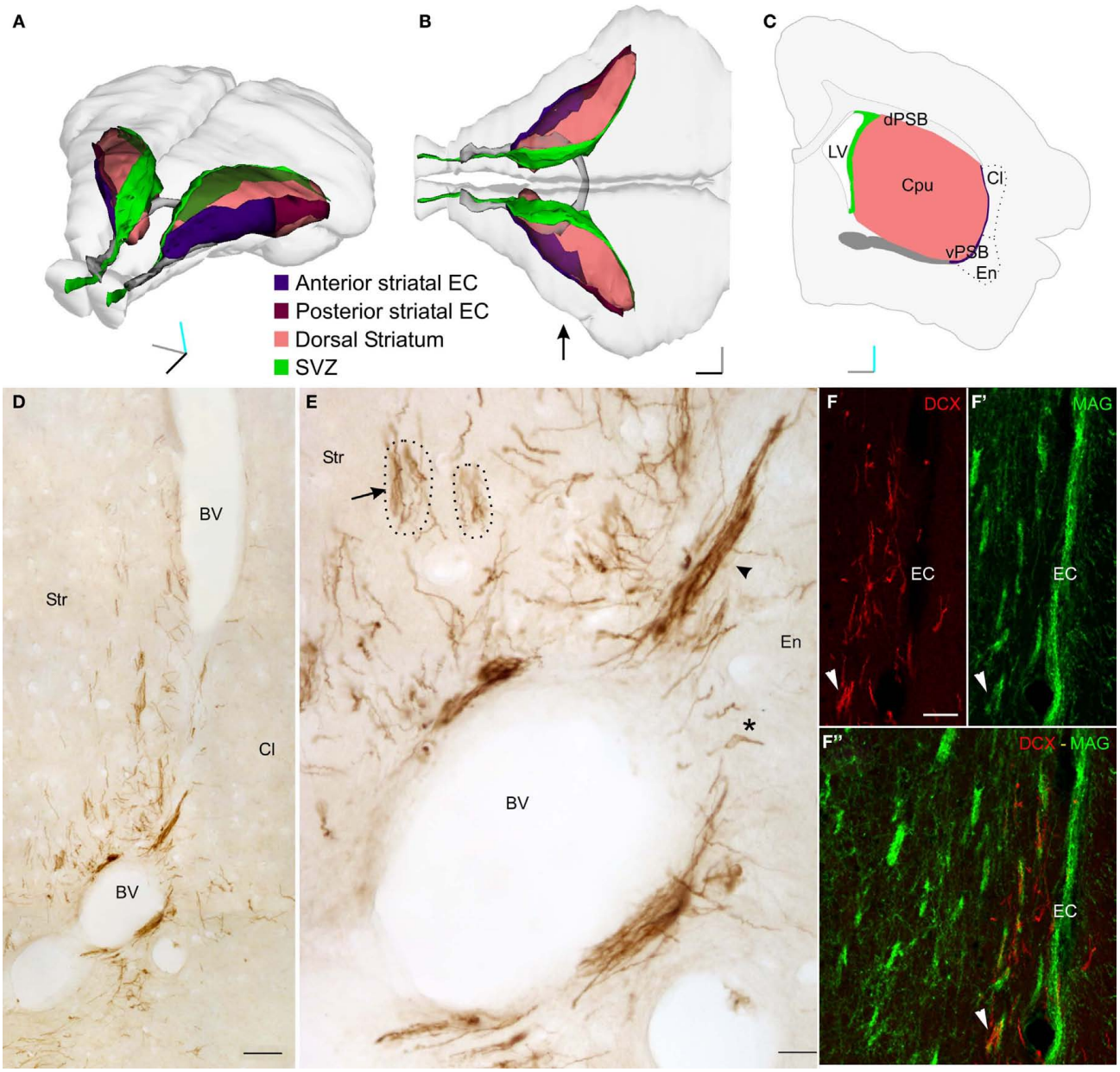

FIGURE 1 | Dcx+ cells in the lateral striatum (LS). (A–B) Perspective **(A)** and top **(B)** views of a 3D reconstruction of the adult guinea pig brain showing the SVZ (green), the dorsal striatum (pink), the anterior commissure (gray), the striatal tract of the external capsule (anterior: violet; posterior: maroon). This reconstruction was produced with *Reconstruct* through coronal sections available from the University of Wisconsin and Michigan State Comparative Mammalian Brain Collections (www.brainmuseum.org). **(C)** Scheme of a single coronal section of the guinea pig brain, about 300 micrometer rostral to the decussation of the anterior commissure. **(D,E)** DCX staining in a coronal section of the LS. DCX positive cells can be organized either as individual (asterisk) or clustered (arrowheads) elements. In addition, several cell processes, often fascicled (arrow), can be observed. Dotted lines indicate the approximate limits of two internal capsule fiber bundles associated with fascicled DCX processes. **(F–F″)** Double labeling for MAG and DCX showing the close association between fascicles of DCX+ processes and internal capsule fiber bundles (arrowhead). Orientation Bars: Gray line: medial; cyan line: dorsal; dark line: rostral. BV: blood vessel; Cl: claustrum; dPSB: dorsal pallial subpallial boundary; vPSB: ventral pallial subpallial boundary; EC: external capsule; Str: Striatum; Scale bars: 80 μm in **(D)**; 20 μm in **(E)**; 50 μm in **(F–F″)**.

like the lateral ventricles or large blood vessels. Furthermore, section thickness must not exceed the penetration capacity of the antibodies and must be consistent with the optical properties of the used lenses.

In our specific case we found 40 μm thickness as the best compromise to obtain limited deformations after drying, good antibody penetration and high signal to noise ratio of the acquired images. In addition, in order to increase antibody penetration, and to enable a better control of section uniformity, immunohistochemistry was performed on free-floating sections.

Another important point to be considered in serial section studies regards the selection of the cutting plane. In the case of the current reconstruction, the minimum number of sections containing all the

DCX+ cells of the LS would be obtained by cutting parallel to the EC. However, by this way the fascicles of DCX+ processes would be nearly parallel to the slice surfaces, where small tissue loss and irregularities can occur. This increases the level of ambiguity in the identification of corresponding neurites in subsequent slices. Starting from these considerations, we chose to cut the brain along the coronal plane. This way, most of the DCX+ elements of the LS region were comprised within 25 coronal sections, covering a tract of 1 mm along the rostro-caudal axis.

ROUGH RECONSTRUCTION OF DCX STAINING IN THE LS BY CONVENTIONAL SERIAL SECTION RECONSTRUCTION (VOXEL SIZE: 1.4 μm × 1.4 μm × 40 μm)

Before producing high-resolution CSLM serial sections reconstructions, it is usually convenient to produce a *rough reconstruction* in order to map the region of interest and to control the slices order. This can be done by conventional serial section reconstruction, in which each slice is represented by a single image spanning its entire thickness (**Figures 2A,B**). In our material, the use of 40 μm thick slices resulted in a relatively low resolution along the *z*-axis. This resolution was only suitable to reconstruct large objects, having cross-sectional profiles comparable to the section thickness, such as large blood vessels (**Figure 3** gray and golden) or the DCX stained area as a whole (**Figure 3** violet and red).

This reconstruction was quickly performed in *Reconstruct*[1] (Fiala, 2005; Lu et al., 2009; see **Table 1**). This open source software was initially developed for EM serial section reconstruction, and subsequently implemented for light microscopy analyses. *Reconstruct* allows performing all the steps required for a serial section analysis: multi-fields montage (or stitching), section alignment (or registration), image segmentation and 3D representation as detailed below.

Multi-field montage

Bi-dimensional images of the full section thickness were acquired on a CLSM with a 10× objective (pixel size 1.4 pixel/μm; **Figure 2A**). Since the size of the LS was larger than the microscope field of view, we collected multiple images per slice at each magnification. The montage (or stitching) of multiple fields in a single mosaic image was automatically performed using the 2D/3D stitching plugins bundled with *Fiji*, an image-processing package based on *Image J*[2] (Preibisch et al., 2009). Alternatively, manual stitching can be performed directly in *Reconstruct*.

[1]http://tech.groups.yahoo.com/group/reconstruct_users
[2]http://pacific.mpi-cbg.de/wiki/index.php/Fiji

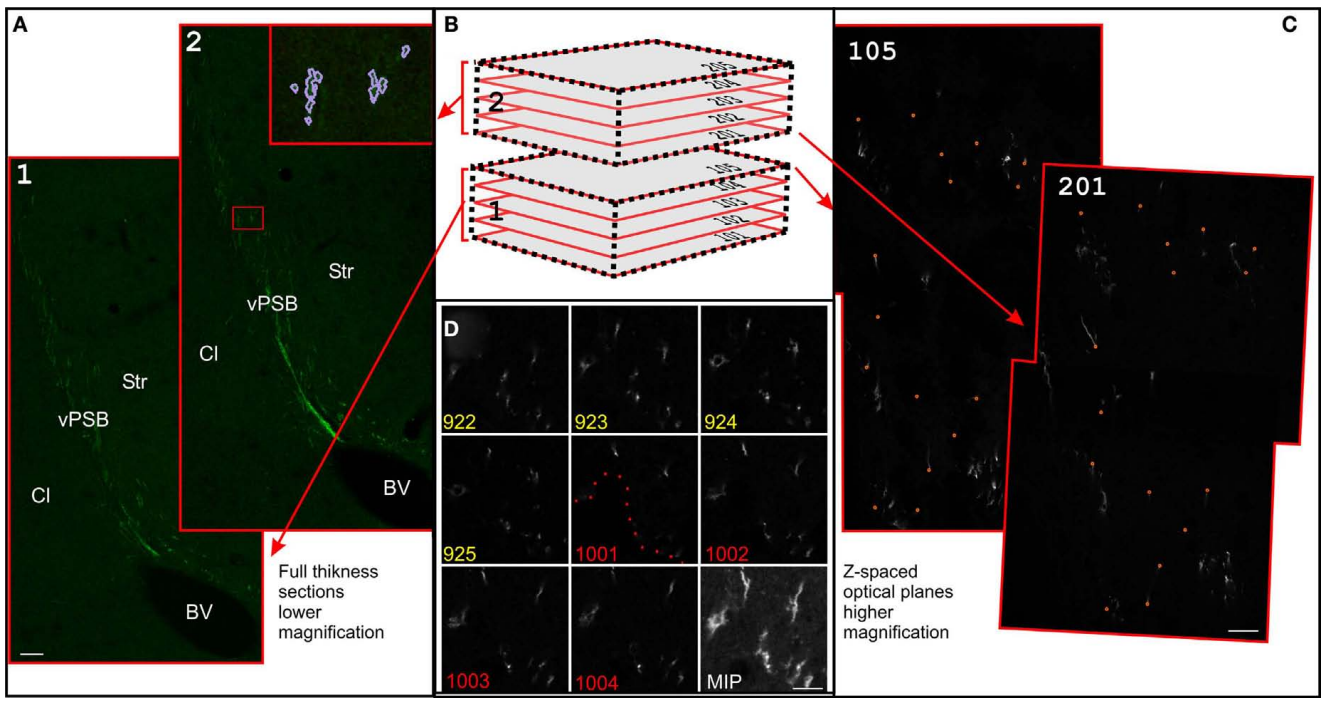

FIGURE 2 | Serial section reconstructions of thick sections. (A) Full thickness projection of the DCX staining in two subsequent slices at low magnification (1.2). In the inset in 2, *traces* made in *Reconstruct* around the DCX staining are shown (violet). The original *traces* were thickened for clarity. Slices 1 and 2 are respectively slices 13 and 12 of the reconstruction shown in **Figure 3**. **(B)** Scheme of two subsequent thick slices. This material can be either entirely imaged (left) or re-sampled with CLSM in *z*-spaced thin optical planes (right). In the CLSM reconstruction these optical planes are numbered with a first digit indicating the slice number and subsequent digits indicating the optical plane number within each slice (101–205). **(C)** Superficial optical planes at the surface of subsequent slices at high magnification. Corresponding fiducial marks used for alignment are shown with small orange circles. Optical planes 105 and 201 are respectively optical plane 829 and 901 of the reconstruction shown in **Figure 6**. **(D)** Detail of the last four optical planes of slice number 9 (922–925), and first four optical planes of slice number 10 (1001–1004) of the 100× reconstruction shown in **Figure 6**. Dotted line show the border of a hollow at the surface of the section number 10. Scale Bars: 80 μm in **(A)**; 7 μm in **(C)**; 10 μm in **(D)**.

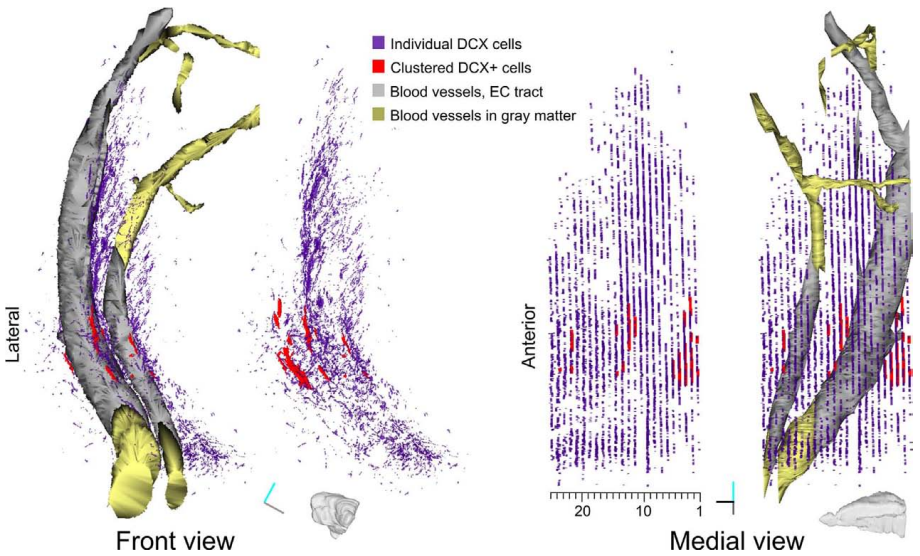

FIGURE 3 | Reconstruction of DCX staining distribution in LS. Front and medial views of a 3D model of DCX staining distribution in the LS of guinea pig. For both views the model is shown either with or without blood vessels. The model is about 30° rotated medially, to give a more comprehensive visualization on the medial view. This model is the result of the tracing of individual DCX+ cells and processes (violet), clustered DCX+ cells (red), blood vessels passing through the EC (gray and gold). Tracts of the blood vessels running in the EC or in the gray matter are depicted as separate *Boissonnat surfaces* colored in gray and golden respectively. Both DCX+ staining and clustered DCX+ cells are represented as traces slabs. A scale indicating the number of individual sections in the reconstruction is shown under the medial view of the model. Orientation Bars: gray line: medial; cyan line: dorsal; dark line: rostral.

Table 1 | Voxel size, number of slices, and optical planes, and approximate time required to perform stitching, alignment, and segmentation in each reconstruction described in this study.

	Voxel size (μm)	No. of slices	No. of optical planes	Time for stitching (min)	Time for alignment (min)	Time for segmentation (min)
Rough Rec (10×)	1.4 × 1.4 × 40	25	25 (4 fields)	15	20	45
20x Rec	0.7 × 0.7 × 4.5	9	79 (4 fields)	60	45	300
100x Rec	0.14 × 0.14 × 1.6	9	229 (2 fields)	45	45	45
100x Rec individual cells	0.14 × 0.14 × 1.6	9	229 (2 fields)	45	45	240

Section alignment

All stitched images were then imported in *Reconstruct*. In this software each image is represented as a *domain* that is part of a *section*. Each *section* has a specific number indicating its position into a *series* of *sections*. After importing, adjacent *sections* were randomly rotated and translated with respect to each other. *Reconstruct* offers several possibilities to perform section alignment, which include both rigid-body (translation, rotation) and non-linear transformations (slant, scaling, deformation, and bending). All these operations can be performed manually, or based on imposed fiducial marks.

Since each slice has its unique texture and is independently deformed by cutting, slide attachment and drying, during the alignment process there is a high risk of introducing biases by propagating deformations, shifts or distortions (Fiala, 2005; Capek et al., 2009). Here, due to the low number of slices, and to their good shape preservation, the alignment process was entirely performed with rigid-body transformations.

Image segmentation

Three-dimensional objects drawing requires the clustering of pixels into salient image regions, a process called image segmentation. The production of algorithms to automatically perform segmentation is constantly growing. However, one of the main limits of these algorithms lies in the difficulty to delineate an object without *a priori* knowledge of its possible form. In the next paragraphs we will briefly describe the use of some segmentation methods specifically designed for neuronal cells. For a more general discussion on segmentation the reader can refer to a recent review (Khairy and Keller, 2011).

For the rough 3D reconstruction of the LS, we applied a simple and flexible way to extract 3D object surfaces based on the manual or semi-automatic definition of the object contour in each section. In *Reconstruct* this segmentation method consists of drawing *traces* around the cross-section profiles of objects (inset in **Figure 2A**). The name applied to a specific *trace* defines the object to which the *trace* belongs. *Traces* can be drawn manually or semi-automatically

with the *wildfire* "region growing" tool, which identifies the object boundaries through user-defined constraints including: hue, saturation, brightness, minimum area and distance from other *traces*. An implementation of the *wildfire* uses *traces* drawn in one section to automatically seed a new "region growing" process in subsequent *sections* (Lu et al., 2009). This function enables to rapidly follow a given object through multiple *sections*. For the LS reconstruction we used this automatic *wildfire* tool to trace the blood vessels passing through the EC and having at least a 25-μm diameter. Two blood vessels were recognized without ambiguity throughout *sections*, thus we could define each of them as individual objects. For visualization purpose, the blood vessel tracts running through the EC or in the gray matter were kept as separate objects (**Figure 3** gray and golden respectively). By contrast, the relationships of the *traces* of DCX stained structures in adjacent slices could not be inferred; thus we collected all of them in two objects: (1) individual cells and processes, which were traced by using the conventional *wildfire* tool (**Figure 3**, violet), (2) clustered DCX+ cells, which were manually drawn (**Figure 3**, red).

3D representation

In *Reconstruct* traced objects can be 3D represented in multiple forms. Here, the blood vessels were represented as realistic 3D surfaces using the *Boissonnat surface* function (**Figure 3**). This function interpolates the object *traces* to create a 3D surface. This method is suitable to produce realistic representations of complex shapes, including branched structures. However, the *Boissonnat surface* was not appropriate for the 3D representation of the DCX staining, since the relationships between *traces* in adjacent sections were highly ambiguous. For this reason, the DCX staining was represented as *traces slabs* (**Figure 3**, violet and red). With this option *traces* are filled with color and extruded along the *z*-axis for a user-defined length. To more clearly discriminate between traces of clustered and individual DCX+ cells, the *traces slabs* of these objects were given different colors, transparency and extrusion thickness (**Figure 3**).

Overall, the rough reconstruction of the LS showed the clustered DCX+ cells were mostly restricted to the ventral EC, closely associated to two large caliber blood vessels, while the individual DCX+ cells and their processes were widely distributed in a strip of LS extending about 300 μm from the EC. Within the LS, a dense patch of DCX+ cells and processes stand out in the caudo-dorsal sector of the reconstructed volume (sections #4–12).

CLSM SERIAL SECTION RECONSTRUCTION OF THE SHAPE OF DCX+ CELLS

The main limit of the above described reconstruction concerns the low resolution along the *z*-axis (**Figure 3**). This results in a nearly complete loss of information about the 3D shape of the DCX-labeled cells. One possible way to circumvent this problem is the use of the CLSM. This implies the optical sectioning of a slice along the *z*-axis in series of images that can be processed to extract volume information.

Here, by using multiple available freeware software, we developed a procedure to use CLSM image stacks in serial section reconstructions (**Figures 2B,C**). Through this method we were able to obtain detailed 3D reconstructions of the DCX staining in the LS at cellular resolution.

Images acquisition and multi-fields montage

When planning a CLSM serial section reconstruction, firstly it is important to carefully evaluate the acquisition area and the voxel size, in order to use the minimum required data set. This will greatly improve data handling and interpretation.

To unravel the general 3D organization of the DCX staining in the LS, we selected, from the above described rough reconstruction, a sequence of nine sections in which a dense patch of DCX+ cells and processes, including numerous fiber fascicles, were found (**Figure 3**, sections #4–12).

A first set of images was acquired with a 20× objective along the entire dorso-ventral extent of the LS (4 fields/slice; voxel size 0.7 μm × 0.7 μm × 4.5 μm; **Figure 4**). Then, we acquired higher resolution images by using a 100× objective, to obtain a more detailed view of a selected group of DCX+ fascicles (2 field/slice; 229 optical planes; voxel size 0.14 μm × 0.14 μm × 1.6 μm; **Figure 5**). In both cases (20× and 100× reconstructions) acquisition of multiple fields-of-view and subsequent stitching of overlapping stacks was required. It is to note that although *Reconstruct* is able to import stacks, it is not suitable to stitch them. Mosaic montage of stacks can be performed with freeware tools, such as the 3D stitching plugins of *Fiji* (Preibisch et al., 2009), or *VIAS 2.4*[3] (Rodriguez et al., 2003). The 3D stitching plugins of *Fiji* operate with minimum user intervention and are also designed to work with tile scans. However, in our study, we preferred *VIAS 2.4* since with this software overlapping stacks are montaged either manually or semi-automatically. This helps to maintain the superficial planes of the resulting mosaic stack as flat as possible. This is particularly important when large numbers of stacks are used. In addition, in the *VIAS* workspace only projections of the stacks on the *x*–*y*, *y*–*z*, and *x*–*z* planes are imported, thus reducing memory requirement and enabling a more fluid image manipulation. The output of *VIAS* is a sequence of mosaic optical planes defining a single volume (**Figures 2D and 4A**). If correctly numbered the sequences of optical sections derived from all the physical slices can be directly imported in *Reconstruct* for alignment. The numbering of slices must be consistent with the direction of the reconstruction so that the last optical plane of a slice is followed by the first optical plane of the next slice (**Figures 2B,D**).

Alignment

Superficial optical planes of subsequent slices had very similar staining patterns, thus they were appropriate for alignment based on imposed *fiducial marks*. In this procedure, three or more couples of corresponding points are marked in two adjacent sections and used as reference to perform registration (**Figure 2C**). As previously mentioned, this procedure can involve rigid-body or non-linear transformations. In *Reconstruct* transformations applied to the superficial optical plane of a slice needs to be manually propagated to the others. This can be done through the command *Propagate* from the sub-menu *Movement* of the menu *Section*. It is to note that the slice surface is rarely planar and occasionally corresponding points must be searched in deeper optical planes, particularly at higher magnification (**Figure 2D**). Overall for both the 20× and 100× reconstructions, the alignment procedure was performed trough 8 rigid-body transformations, resulting in two series of 79 and 229 aligned optical planes respectively.

[3]http://research.mssm.edu/

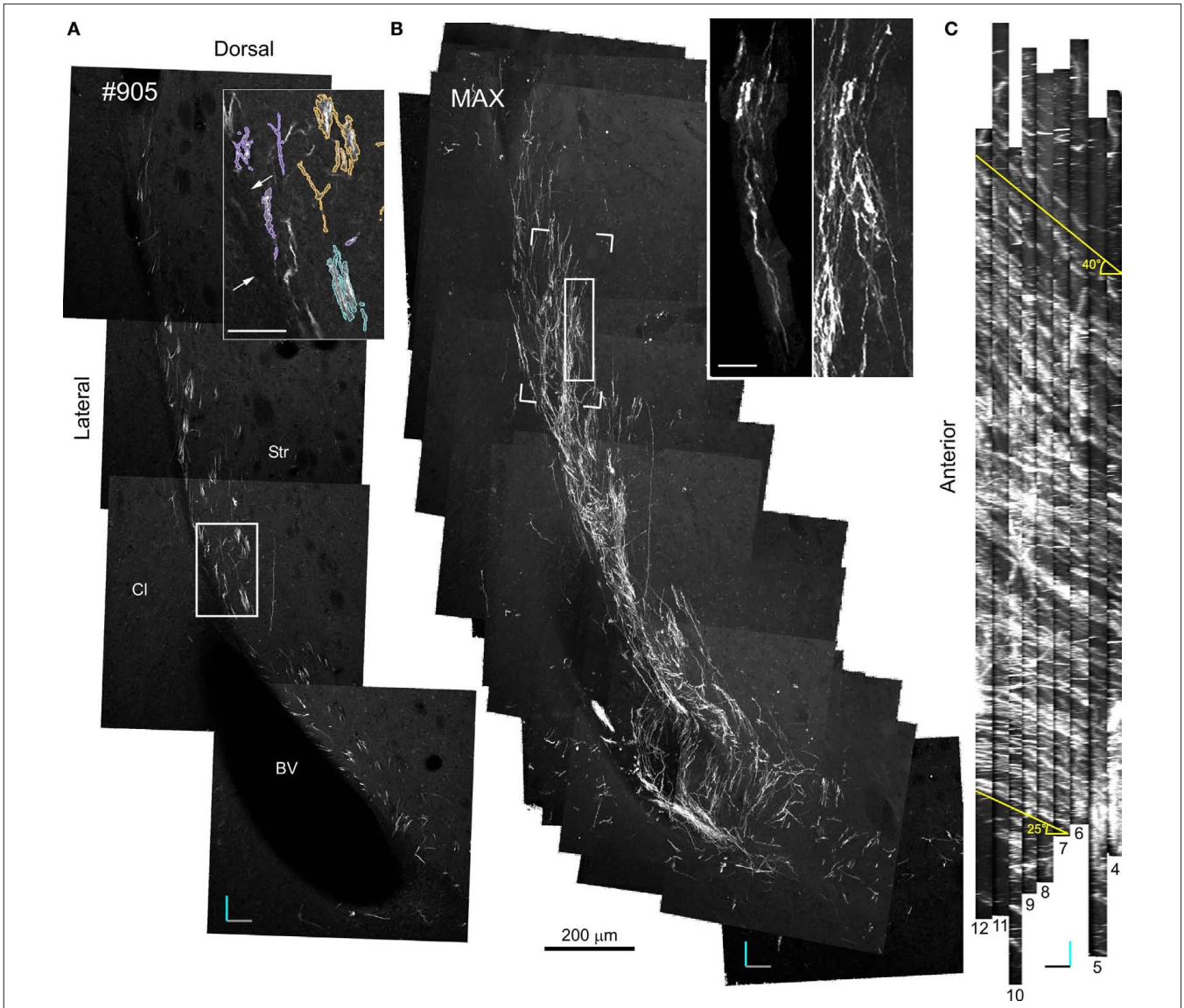

FIGURE 4 | 20× Confocal laser scanning microscopy serial section reconstruction. (A) Image of the fifth optical plane of section #9 in the 20× CLSM serial section reconstruction. Note that this image is the result of four separate fields-of-view stitched together with *Vias*. In the inset, DCX+ processes belonging to distinct fascicles are outlined by differently colored *traces*. **(B)** Maximal intensity projections (MIP) along the *z*-axis of 79 optical planes taken from nine subsequent sections (#4–12). In the inset: on the right a magnified view of the area outlined by a continuous line in the main image, on the left a DCX+ cell in a fascicle (the pink fascicle of **Figures 5 and 7**) within the same area after a manual cut-off of the unwanted parts section by section. The open box indicates the position of the reconstruction shown in **Figures 6 and 7**. **(C)** MIP along the *y*-axis, note the numerous parallel fascicles of DCX+ processes. The slope of these fascicles on the rostro-caudal axis is indicated. Orientation Bars: gray line: medial; cyan line: dorsal; dark line: rostral; Scale bars: 50 μm in the inset in A; 25 μm in the inset in B.

SEGMENTATION AND 3D REPRESENTATION OF 20× CLSM SERIAL SECTION RECONSTRUCTION: SPATIAL ORGANIZATION OF THE FASCICLES OF DCX+ CELLS (VOXEL SIZE 0.7 μm × 0.7 μm × 4.5 μm)

Specific aim of the 20× CLSM reconstruction was to unravel the general 3D organization of the DCX staining in the LS, focusing on the fiber fascicles (**Figures 4 and 5**). The voxel size of this reconstruction (0.7 μm × 0.7 μm × 4.5 μm) was adequate to recognize DCX+ cell bodies and processes when isolated. By contrast, within fascicles DCX labeled structures were often too close to be resolved (**Figure 4A**). To visualize the entire data set as a single volume, the aligned Reconstruct *series* of images was exported and assembled in a 570-MB 8-bit stack (2104 × 3596 × 79 pixels) using *Image J*. As for any CLSM stacks, this data set can be visualized in several ways such as cross-sectional views, maximal intensity projections (MIP) or alpha bending. All these type of visualization are supported by freeware software packages such as the volume viewer of *Image J* or *V3D Neuron*[4] (Peng et al., 2010). The MIP projection on the *y*, *z* plane of the entire 20× reconstruction stack showed that the DCX+ fascicles had a slope gradually increasing from 25° ventrally to 40° dorsally, in respect to the rostro-caudal axis (**Figure 4C**). This

[4]http://penglab.janelia.org/proj/v3d

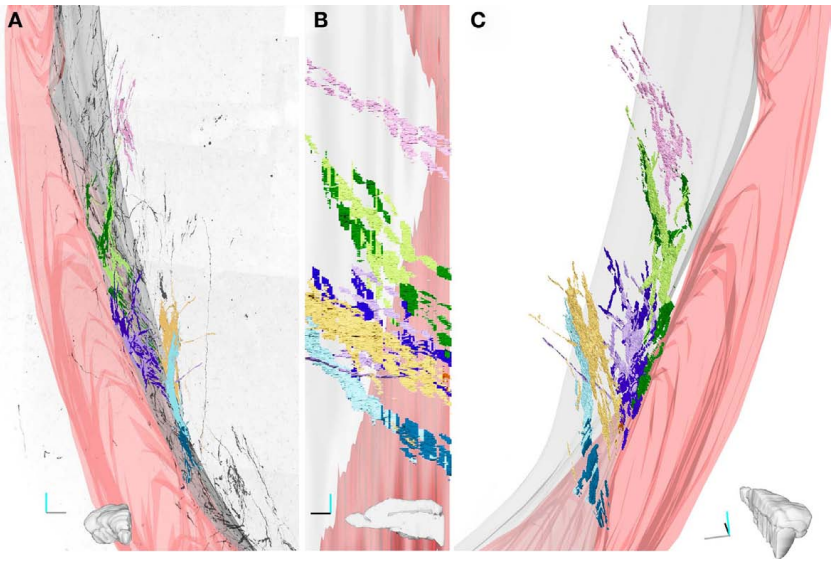

FIGURE 5 | Three-dimensional reconstruction of four fascicles of DCX+ processes. (A–C). Four fascicles of DCX+ processes were traced in the stack shown in **Figure 4**. Each fascicles is represented by a different color and its tracts running within the EC are in darker colors. The 3D model was rendered in Blender (www.blender.org). In A the front view of the 3D model is superposed to an inverted image of the MIP of the stack along the *z*-axis. **(B)** medial view. **(C)** Caudal view slightly rotated medially. Only one fascicle (pink) runs exclusively in the striatal parenchyma, while the others run partly inside the EC. The Lilac and green fascicle extend always close to the EC, while the yellow and cyan contact the EC caudally and then turn medially within the striatal parenchyma. The medial surface of the EC is in gray; the surface of a big blood vessel running through the EC is in pink. Orientation Bars: gray line: medial; cyan line: dorsal; dark line: caudal.

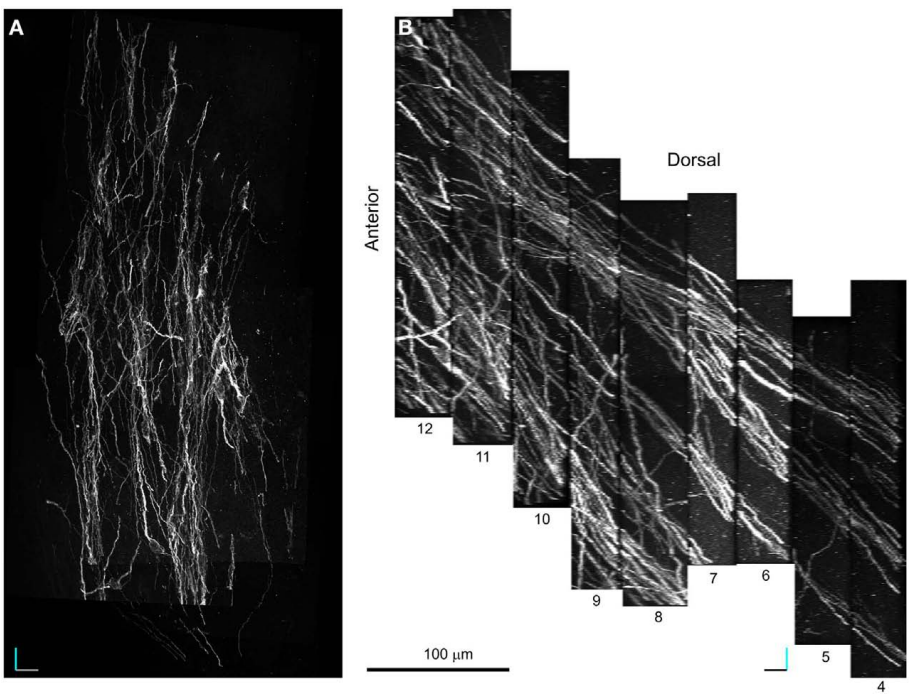

FIGURE 6 | 100× Confocal laser scanning microscopy serial section reconstruction. (A–B) MIP along the *z* **(A)** and *y* **(B)** axis of a stack of 229 optical planes taken from nine subsequent optical slices (voxel size is 0.14 µm × 0.14 µm × 1.6 µm). This volume includes four fascicles of DCX+ processes one of which is the pink colored fascicle shown in **Figure 5**. The position of the reconstructed volume relative to the 20× reconstruction is indicated by the open box in **Figure 4B**. Note that fascicles of DCX+ processes extend parallel in the rostro-caudal direction within a network of less densely packed cell processes more randomly oriented. Orientation Bars: gray line: medial; cyan line: dorsal; dark line: caudal.

specific organization is closely reminding that of internal capsule fibers bundles (**Figure A1** in Appendix). For more in depth observation of the 3D stack we used V3D Neuron. This latter software has a user-friendly interface that easily enables the rotation, zoom and volume cut of image stacks. In particular, volume cut is useful to analyze individual structures, since it reduces the visualized area allowing a better discrimination of small objects within a large volume (**Figures 4B,C**). Nonetheless, since volume-cut acts along a fixed plane, it can be inadequate for the analysis of highly convoluted and densely packed objects. In this case, it is possible to manually cut-off the unwanted parts of the image stack, section by section (compare right and left insets in **Figure 4B**). Alternatively, since this procedure can be relatively time consuming, it might be preferable to highlight the structures of interest through *image segmentation*. In the 20× reconstruction we used *image segmentation* to track the pathway of five fascicles of DCX+ cell processes. To this aim, the fascicles contour in each optical plane was traced with the *wildfire* tool of *Reconstruct* (inset in **Figure 4A**). The drawn traces were represented as differently colored *traces slabs* in the 3D environment (**Figure 5**). The parts of the DCX+ fascicles running within the EC were rendered in darker colors. We did not need to counter stain the tissue in order to identify the EC, since it appeared as a darker region in the background (arrows in **Figure 4A**). Four of the reconstructed DCX+ fascicles run partly inside the EC and partly in the striatal parenchyma. In particular, the two more ventral fascicles (yellow and cyan, **Figure 5**) contacted the EC caudally, then proceeding dorsally into the striatal parenchyma.

Although the slope and curvature of these fascicles are reminding those of internal capsule fibers bundles (**Figure 5**; **Figure A1** in Appendix), these latter proceed in an opposite direction (rostral-to-ventral) from their EC origin. It is thus possible that these DCX+ fascicles entered within an internal capsule fiber bundle originating more rostrally and then followed it backward (ventral-to-rostral).

Overall, the 20× reconstruction indicates the 3D organization of the DCX+ fiber fascicles is closely reminding that of the internal capsule fiber bundles, with which they are closely associated.

SEGMENTATION AND 3D REPRESENTATION OF THE 100× CLSM SERIAL SECTION RECONSTRUCTION: ORGANIZATION OF DCX+ CELLS WITHIN AND AMONG FASCICLES. (VOXEL SIZE 0.14 μm × 0.14 μm × 1.6 μm)

The purpose of the 100× CLSM reconstruction was to obtain a more detailed representation of the morphology of the DCX+ cells in the LS, and in parallel to understand the organization of cell processes within and among the DCX+ fascicles.

The acquired volume laid in the dorsal LS (**Figure 4B**) and included four fascicles of DCX+ processes, one of which was previously reconstructed at lower resolution (**Figure 5**, pink). To visualize the entire data set as a single volume, the aligned Reconstruct *series* of images was exported and assembled into a 991-MB 8-bit stack (1516 × 2995 × 229 pixels) using *Image J*. In the reconstructed volume four main parallel fascicles of DCX+ processes extended in the rostro-caudal direction within a network of less densely packed cell processes showing variable orientation (**Figure 5**). The resolution of this reconstruction (voxel size: 0.14 μm × 0.14 μm × 1.6 μm) enabled a detailed discrimination of both isolated and fascicled DCX+ cell processes. Nonetheless, the definition of clean-cut boundaries between individual DCX+ cells was not always possible since in regions of close proximity (that likely include cell contacts), the fluorescence of different processes tended to amalgamate.

For this reason, to reconstruct the path of the DCX+ processes, within and among fascicles, we traced the DCX+ processes of each fascicles as a unique network. To this aim we used *Neuronstudio 0.9.92*[5] (Rodriguez et al., 2003), a freeware software specifically designed to automatically trace neuronal elements. Starting from seeding points, the medial axis of a neuritic process is automatically skeletonized as a chain of nodes, and the diameter of each node is computed using the *Rayburst sampling algorithm* (Rodriguez et al., 2006). Using *Neuronstudio* we produced separate groups of tracings for each of the four fascicles that were comprised in the acquired volume. Often, from single seeding points, the growing algorithm trace spreads to multiple cells of the same fascicle and occasionally it extended also to other fascicles. In this latter case, bridging processes were manually interrupted at the first contacting point with the un-traced fascicles.

Digital reconstructions of the four fascicles were stored as *.swc* files (Cannon et al., 1998), imported in *V3D neuron*, and differently colored. As visible in **Figures 7A–C**, these fascicles run mostly independently, being interconnected only by a few DCX+ processes coursing in the mediolateral plane. Processes interconnecting multiple fascicles could be recognized because they were labeled in multiple colors.

Given that *Neuronstudio* works optimally only when the fluorescence completely fill the cell, and that DCX staining does not satisfy this pre-requisite, to entirely reconstruct individual DCX+ cells we switched to a manual tracing method. To this aim we used *Neuromantic 1.7.5*[6], a freeware software that is specifically designed for manual or semi-automatic tracing of neuronal cells. In this software neuronal cells are traced accordingly with the .swc file format, in which traces are made by cylindrical segments of specific length and diameter. *Neuromantic* has several advantages for manual tracing over *Neuronstudio* including: the selective visualization of traced neuronal segments close to the focal plane, the possibility to color segments differentially by depth and to automatically focus at specific segments. Due to the above mentioned resolution limits of our data set, only a few DCX+ cells could be entirely reconstructed. In **Figure 7** the reconstruction of seven cells is illustrated. The cell bodies of these cells were recognized as cytoplasmic swellings with a superficial DCX staining. Four of the reconstructed DCX+ cells were part of the pink colored fascicle shown in **Figure 4** (**Figures 7E,F** pink), while the others were not associated to any fiber fascicles (**Figures 7E,F** cyan). The reconstructed cells showed mostly a bipolar morphology, consistent with that of immature or migrating neuroblasts. Nonetheless, one cell showed two very long opposing processes, suggesting it was at a more differentiated stage (**Figures 7E,F**). It is to note that the reconstructed cells represent a biased sample of the entire population, since they were chosen among the more isolated DCX+ cells. Overall, the 100× reconstruction unveils that the fiber fascicles were made by long and poorly ramified processes, running mostly within the same fascicle, but occasionally interconnecting distinct fascicles.

[5]http://research.mssm.edu/

[6]http://bit.ly/buYykd

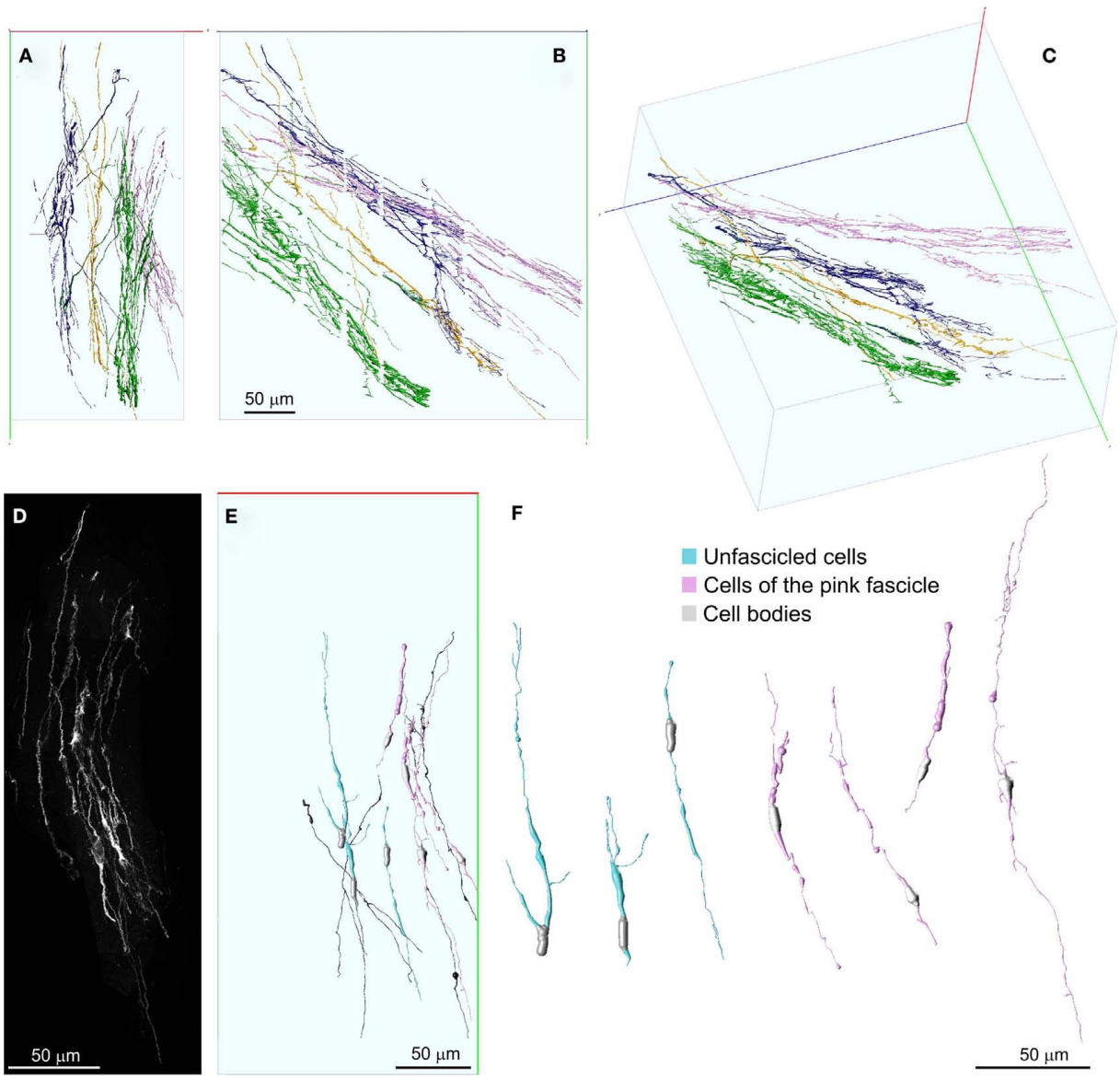

FIGURE 7 | Detailed 3D representation of DCX+ cells and processes within and among fascicles. (A–C) Front **(A)**, lateral **(B)**, and perspective **(C)** views of DCX+ processes within and among four separate fascicles, represented in different colors. Fascicles were automatically segmented in *Neuronstudio* and rendered in *V3D neuron*. No manual editing has been performed in order to connect corresponding processes at the inter-slice gaps. The numerous small orthogonal branches in **(B)** are artifacts of the automatic tracing algorithm. **(D)** MIP of the DCX+ processes composing the pink colored fascicle after a manual cut-off of surrounding areas section by section. **(E,F)** 3D reconstructions of individual DCX+ cells isolated (cyan) or being part of the pink colored fascicle (pink). Some individual DCX+ process, whose cell body was not included in the reconstructed volume, are also shown (dark) in **(E)**. These cells were reconstructed in *Neuromantic* and rendered in *V3D neuron*. Note these cells are mostly bipolar and show long and poorly ramified processes. Orientation Bars: gray line: medial; cyan line: dorsal; dark line: caudal.

DISCUSSION

Newborn neuronal cells have been described in the mature striatum of different mammalian species, raising hopes to exploit this neurogenic activity for brain repair (Arvidsson et al., 2002; Bedard et al., 2002; Luzzati et al., 2006, 2007). However, much information is still lacking regarding the identity and function of newborn striatal cells (Liu et al., 2009; Kernie and Parent, 2010). Detailed neuroanatomical analyses of the newly formed elements regarding their spatial organization and relationships with specific circuits, can help to unravel the role of these cells both in physiological and pathological conditions.

In the present paper we describe a method to combine CLSM with serial section reconstruction, in order to obtain 3D reconstructions of large tissue volumes at cellular resolution. Through this method we provided the first description of the morphology and neuroanatomical organization of a population of newborn

neuroblasts occurring in the mammalian striatum. Data obtained from this study indicate that newborn cells in LS of the guinea pig are mostly bipolar elements, showing poorly ramified processes that organize to form long fascicles. Interestingly, these fascicles follow the path of the fiber bundles of the internal capsule, suggesting newborn cells may play a role within this striatal compartment. Given that only very few DCX+ cells and no DCX+ bundle can be entirely included in a single 40 μm thick section, the use of classical anatomical approaches to describe this system would have required much more time (to find the right planes of sectioning, to look for the right section), and would have led to a less precise and complete picture.

Current advances in two-photon excitation microscopy allow the visualization of large tissue volumes at cellular resolution within the living brain (Sigler and Murphy, 2010). Although this technique represents a pivotal innovation for the study of neuroanatomy and neuronal plasticity, it has been little used in studies of adult neurogenesis (Mizrahi, 2007). A major limiting factor is that two-photon microscopy can image only within a few hundred micrometers of depth (Sigler and Murphy, 2010), confining the analyses to relatively superficial regions, such as the mice neocortex or the OB (Mizrahi, 2007). *Ex vivo* whole mount preparation of both fixed and living specimens is a possible approach to overcome depth limits. This approach has been successfully used to study the periventricular SVZ and it could be potentially extended to other brain regions (Tavazoie et al., 2008; Tsai et al., 2009; Lacar et al., 2010). Nonetheless, besides superficial regions such as the SVZ, the specimen thickness in whole mount preparations can be too large for the penetration capacity of most histological staining methods, in particular for immunofluorescence labeling. This can be a major limiting factor, especially in mammalian species in which genetically labeled models are not currently available. The DCX+ neuroblasts in the LS of the guinea pig represent a good example of a cell population that cannot be visualized through current whole mount approaches since these cells are scattered over a large area, and require immunohistochemistry to be labeled.

The serial section reconstruction represents a reliable alternative to visualize at cellular resolution large volumes of tissue, independently from depth and from the staining method. The main drawback of the classic version of this technique is that an inverse relationship exists between *z*-axis resolution and section thickness. Although much effort has been devoted to the automation of image acquisition and registration, serial section reconstruction at cellular resolution is a considerable time-consuming approach (Fiala, 2005; Cardona et al., 2010).

Here, we present an implementation of the serial section reconstruction method in which CLSM stacks of images are registered in order to use thick slices to produce reconstructions at cellular resolution. The basic idea behind this method is to fragment the region of interest in the minimum number of slices enabling their staining and high-resolution imaging. These slices are then optically sectioned with CLSM and virtually stitched along the *z*-axis using a serial section reconstruction editor. The reduction in the number of slices per volume consistently speed up image acquisition and registration. Moreover, the intrinsic registration of the optical planes within each slice and the need of less transformations per volume, increase also the reliability of the reconstruction. Indeed, this reduces the risks of introducing biases during slice registration by propagating deformations, shifts or distortions (Fiala, 2005; Capek et al., 2009). The good shape preservation of the thick slices further contribute to the precision of the reconstruction. Overall, the advantages of our implementation of serial section reconstruction are well demonstrated by the 100× reconstruction in which we obtained a series of 229 aligned optical sections by using only eight rigid-body transformations.

The main drawback of CLSM serial section reconstruction in respect to whole mount imaging is the occurrence of small gaps within the reconstructed volume. These gaps lie between slices and are the result of tissue loss during cutting and further tissue processing. The impact of these superficial artifacts has been extensively evaluated for stereological methods, and it has been shown to be strongly dependent on tissue quality, cutting angle, and embedding media (Baryshnikova et al., 2006). In the context of CLSM serial section reconstruction, slice surface artifacts cause a variable reduction of the actual resolving power at the inter-slice interface. Depending on dimensions, orientation and density of the structures of interest, inter-slice gaps differentially hamper the identification of corresponding structures between consecutive slices. In particular, tiny structures running parallel to the cutting plane are more likely to be affected by slice surface artifacts. In such cases, the identification of corresponding structures between subsequent slices will be strongly dependent on their density. In general since multiple factors influence the reconstruction of specific objects, the impact of slice surface artifacts should be determined case by case. In the present paper we were able to reconstruct a network of fascicled DCX+ processes that were relatively densely packed, taking advantage from their straight orientation and choosing a perpendicular cutting plane. This minimized the effects of surface artifacts.

It is to note that despite the periodic drop of the resolving power between slices, the resolution within slices obtained with CLSM serial section reconstruction can be higher than in whole mount imaging. Indeed, since the signal to noise ratio suffers from considerable degradation with depth, the resolution limit of light microscopes is higher for slice than for whole mount imaging (Wilt et al., 2009; Sigler and Murphy, 2010). Moreover, since our method is compatible with virtually any stack-based microscopy technique, it can be adapted for the recently developed super-resolution fluorescence microscopy that can resolve particles separated by few tens of nanometers (Schermelleh et al., 2010). Considering that these applications so far efficiently work only within a limited depth range, stack-based serial sections reconstruction might increase the volume that can be visualized with these methods (Schermelleh et al., 2010).

A direct demonstration of the resolution capacity of CLSM serial section reconstruction was not the specific aim of the present study. Accordingly, the resolution used here does not represent the maximum resolution of CLSM, but rather the minimal resolution required to reconstruct the network of DCX+ processes within and among fascicles. The reconstruction of individual elements within this network was often impaired by the presence of close contacts between their processes. Indeed, in contrast to the EM, closely apposed membranes cannot be resolved with CSLM without specific markers. For analyses at sub-cellular resolution, higher

resolving power can be achieved even with ordinary CLSM in example through higher NA of the objective, closer optical planes, or the use of image deconvolution.

Confocal laser scanning microscopy serial section reconstruction is a modification of both whole mount imaging and classic serial section reconstruction and accordingly it takes advantage from diverse software developed for these two methods. Although here we used specific sets of software, we would like to emphasize that other applications can be used to perform the stitching, registration and segmentation of series of CLSM stacks. In example, a method of CLSM serial section reconstruction has been recently proposed by Capek et al. (2009) by using the unreleased software *Rapid 3D*. This method has been designed to reconstruct large volumes such as entire brains or embryos, and to date it has been used only for low magnification reconstructions. Nonetheless, it should be interesting to test *Rapid 3D* to produce reconstructions at cellular resolution. In addition, several useful stitching, registration and segmentation plugins are bundled with the free software package *Fiji*. Among them, *TrakEM2* is a powerful *Image J* plugin that is closely related to *Reconstruct*[7] (Cardona et al., 2010).

In conclusion, we showed that LSCM serial section reconstruction is a profitable effective way to analyze diverse architectural aspects of the adult brain. In particular, we propose it is suitable to investigate neuroanatomical features of adult neurogenic niches. Future development of this method may include imaging at higher resolution, within larger volumes and using multiple wavelengths.

ACKNOWLEDGMENTS

Supports Contributed by Compagnia di San Paolo (NEUROTRANSPLANT 2004.2019; 2008.2192); Università di Torino 2007; PRIN 2007; Regione Piemonte – Ricerca Sanitaria Finalizzata (2009).

[7]http://www.ini.uzh.ch/~acardona/trakem2.html

REFERENCES

Arvidsson, A., Collin, T., Kirik, D., Kokaia, Z., and Lindvall, O. (2002). Neuronal replacement from endogenous precursors in the adult brain after stroke. *Nat. Med.* 8, 963–970.

Baryshnikova, L. M., Von Bohlen Und Halbach, O., Kaplan, S., and Von Bartheld, C. S. (2006). Two distinct events, section compression and loss of particles ("lost caps"), contribute to z-axis distortion and bias in optical disector counting. *Microsc. Res. Tech.* 69, 738–756.

Bedard, A., Cossette, M., Levesque, M., and Parent, A. (2002). Proliferating cells can differentiate into neurons in the striatum of normal adult monkey. *Neurosci. Lett.* 328, 213–216.

Cannon, R. C., Turner, D. A., Pyapali, G. K., and Wheal, H. V. (1998). An online archive of reconstructed hippocampal neurons. *J. Neurosci. Methods* 84, 49–54.

Capek, M., Bruza, P., Janacek, J., Karen, P., Kubinova, L., and Vagnerova, R. (2009). Volume reconstruction of large tissue specimens from serial physical sections using confocal microscopy and correction of cutting deformations by elastic registration. *Microsc. Res. Tech.* 72, 110–119.

Cardona, A., Saalfeld, S., Preibisch, S., Schmid, B., Cheng, A., Pulokas, J., Tomancak, P., and Hartenstein, V. (2010). An integrated micro- and macroarchitectural analysis of the Drosophila brain by computer-assisted serial section electron microscopy. *PLoS Biol.* 8, e1000502. doi: 10.1371/journal.pbio.1000502

DeFelipe, J. (2010). From the connectome to the synaptome: an epic love story. *Science* 330, 1198–1201.

Doetsch, F., and Alvarez-Buylla, A. (1996). Network of tangential pathways for neuronal migration in adult mammalian brain. *Proc. Natl. Acad. Sci. U S A.* 93, 14895–14900.

Doetsch, F., Garcia-Verdugo, J. M., and Alvarez-Buylla, A. (1997). Cellular composition and three-dimensional organization of the subventricular germinal zone in the adult mammalian brain. *J. Neurosci.* 17, 5046–5061.

Fiala, J. C. (2005). Reconstruct: a free editor for serial section microscopy. *J. Microsc.* 218, 52–61.

Gould, E. (2007). How widespread is adult neurogenesis in mammals? *Nat. Rev. Neurosci.* 8, 481–488.

Hofer, S. B., Mrsic-Flogel, T. D., Bonhoeffer, T., and Hübener, M. (2009). Experience leaves a lasting structural trace in cortical circuits. *Nature* 457, 313–317.

Kernie, S. G., and Parent, J. M. (2010). Forebrain neurogenesis after focal Ischemic and traumatic brain injury. *Neurobiol. Dis.* 37, 267–274.

Khairy, K., and Keller, P. J. (2011). Reconstructing embryonic development. *Genesis.* 1–26.

Kriegstein, A., and Alvarez-Buylla, A. (2009). The glial nature of embryonic and adult neural stem cells. *Annu. Rev. Neurosci.* 32, 149–184.

Lacar, B., Young, S. Z., Platel, J. C., and Bordey, A. (2010). Imaging and recording subventricular zone progenitor cells in live tissue of postnatal mice. *Front. Neurosci.* 4:43. doi: 10.3389/fnins.2010.00043

Lindsey, B. W., and Tropepe, V. (2006). A comparative framework for understanding the biological principles of adult neurogenesis. *Prog. Neurobiol.* 80, 281–307.

Liu, F., You, Y., Li, X., Ma, T., Nie, Y., Wei, B., Li, T., Lin, H., and Yang, Z. (2009). Brain injury does not alter the intrinsic differentiation potential of adult neuroblasts. *J. Neurosci.* 29, 5075–5087.

Lu, J., Fiala, J. C., and Lichtman, J. W. (2009). Semi-automated reconstruction of neural processes from large numbers of fluorescence images. *PLoS ONE* 4, e5655. doi: 10.1371/journal.pone.0005655

Luzzati, F., De Marchis, S., Fasolo, A., and Peretto, P. (2006). Neurogenesis in the caudate nucleus of the adult rabbit. *J. Neurosci.* 26, 609–621.

Luzzati, F., De Marchis, S., Fasolo, A., and Peretto, P. (2007). Adult neurogenesis and local neuronal progenitors in the striatum. *Neurodegener. Dis.* 4, 322–327.

Luzzati, F., Peretto, P., Aimar, P., Ponti, G., Fasolo, A., and Bonfanti, L. (2003). Glia-independent chains of neuroblasts through the subcortical parenchyma of the adult rabbit brain. *Proc. Natl. Acad. Sci. U.S.A.* 100, 13036–13041.

Mirzadeh, Z., Doetsch, F., Sawamoto, K., Wichterle, H., and Alvarez-Buylla, A. (2010). The subventricular zone en-face: wholemount staining and ependymal flow. *J. Vis. Exp.* 39, pii: 1938.

Mizrahi, A. (2007). Dendritic development and plasticity of adult-born neurons in the mouse olfactory bulb. *Nat. Neurosci.* 10, 444–452.

Parent, J. M., Vexler, Z. S., Gong, C., Derugin, N., and Ferriero, D. M. (2002). Rat forebrain neurogenesis and striatal neuron replacement after focal stroke. *Ann. Neurol.* 52, 802–813.

Peng, H., Ruan, Z., Long, F., Simpson, J. H., and Myers, E. W. (2010). V3D enables real-time 3D visualization and quantitative analysis of large-scale biological image data sets. *Nat. Biotechnol.* 28, 348–353.

Preibisch, S., Saalfeld, S., and Tomancak, P. (2009). Globally optimal stitching of tiled 3D microscopic image acquisitions. *Bioinformatics* 25, 1463–1465.

Rodriguez, A., Ehlenberger, D., Kelliher, K., Einstein, M., Henderson, S. C., Morrison, J. H., Hof, P. R., and Wearne, S. L. (2003). Automated reconstruction of three-dimensional neuronal morphology from laser scanning microscopy images. *Methods* 30, 94–105.

Rodriguez, A., Ehlenberger, D. B., Hof, P. R., and Wearne, S. L. (2006). Rayburst sampling, an algorithm for automated three-dimensional shape analysis from laser scanning microscopy images. *Nat. Protoc.* 1, 2152–2161.

Schermelleh, L., Heintzmann, R., and Leonhardt, H. (2010). A guide to super-resolution fluorescence microscopy. *J. Cell Biol.* 190, 165–175.

Seri, B., Garcia-Verdugo, J. M., Collado-Morente, L., McEwen, B. S., and Alvarez-Buylla, A. (2004). Cell types, lineage, and architecture of the germinal zone in the adult dentate gyrus. *J. Comp. Neurol.* 478, 359–378.

Sigler, A., and Murphy, T. H. (2010). In vivo 2-photon imaging of fine structure in the rodent brain: before, during, and after stroke. *Stroke* 41, S117–S123.

Tavazoie, M., Van der Veken, L., Silva-Vargas, V., Louissaint, M., Colonna, L., Zaidi, B., Garcia-Verdugo, J. M., and Doetsch, F. (2008). A special-

ized vascular niche for adult neural stem cells. *Cell Stem Cell* 3, 279–288.

Tsai, P. S., Kaufhold, J. P., Blinder, P., Friedman, B., Drew, P. J., Karten, H. J., Lyden, P. D., and Kleinfeld, D. (2009). Correlations of neuronal and microvascular densities in murine cortex revealed by direct counting and colocalization of nuclei and vessels. *J. Neurosci.* 29, 14553–14570.

Wilt, B. A., Burns, L. D., Wei Ho, E. T., Ghosh, K. K., Mukamel, E. A., and Schnitzer, M. J. (2009). Advances in light microscopy for neuroscience. *Annu. Rev. Neurosci.* 32, 435–506.

Conflict of Interest Statement: The authors declare that the research was conducted in the absence of any commercial or financial relationships that could be construed as a potential conflict of interest.

Received: 23 February 2011; accepted: 03 May 2011; published online: 13 May 2011.

*Citation: Luzzati F, Fasolo A and Peretto P (2011) Combining confocal laser scanning microscopy with serial section reconstruction in the study of adult neurogenesis. Front. Neurosci. **5**:70. doi: 10.3389/fnins.2011.00070*

This article was submitted to Frontiers in Neurogenesis, a specialty of Frontiers in Neuroscience.

APPENDIX

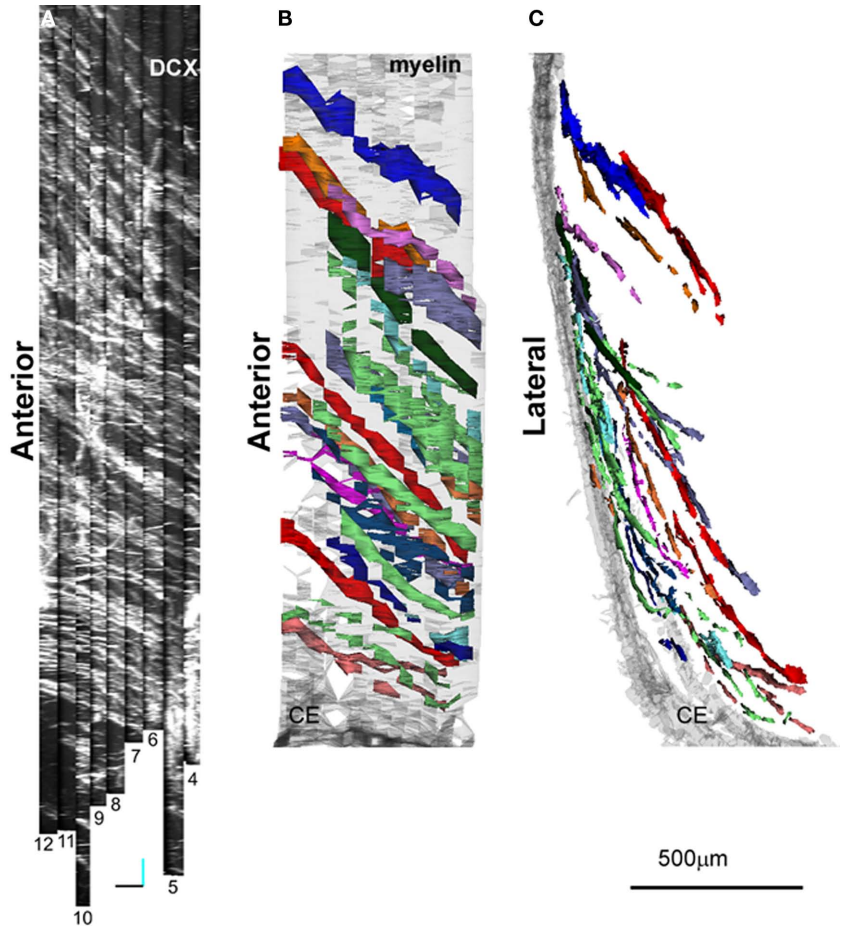

FIGURE A1 | Comparison between the orientation of DCX+ fascicles and internal capsule fiber bundles. In **(A)** MIP along the *y*-axis of the 20× reconstruction as shown in **Figure 4C**. In **(B,C)** lateral and caudal views, respectively, of a rough 3D reconstruction of part of the internal capsule fiber bundles (stained with MAG) running through the LS. The reconstruction has been obtained from 15 subsequent 40 μm thick sections and has been rendered in Reconstruct.

frontiers in
NEUROSCIENCE

REVIEW ARTICLE
published: 21 March 2011
doi: 10.3389/fnins.2011.00030

Subventricular zone cell migration: lessons from quantitative two-photon microscopy

Rachel James[1], Yongsoo Kim[2], Philip E. Hockberger[3] and Francis G. Szele[1]*

[1] *Department of Physiology, Anatomy and Genetics, University of Oxford, Oxford, UK*
[2] *Cold Spring Harbor Laboratory, Cold Spring Harbor, New York, NY, USA*
[3] *Department of Physiology, Feinberg School of Medicine, Northwestern University, Chicago, IL, USA*

Edited by:
Silvia De Marchis, University of Turin, Italy

Reviewed by:
Angelique Bordey, Yale University School of Medicine, USA
Dennis Steindler, McKnight Brain Institute of the University of Florida, USA

****Correspondence:***
Francis G. Szele, Department of Physiology, Anatomy and Genetics, Le Gros Clark Building, University of Oxford, South Parks Road, Oxford OX1 3QS, UK.
e-mail: francis.szele@dpag.ox.ac.uk

Neuroblasts born in the adult subventricular zone (SVZ) migrate long distances in the rostral migratory stream (RMS) to the olfactory bulbs where they integrate into circuitry as functional interneurons. As very little was known about the dynamic parameters of SVZ neuroblast migration, we used two-photon time-lapse microscopy to analyze migration in acute slices. This involved analyzing 3D stacks of images over time and uncovered several novel aspects of SVZ migration: chains remain stable, cells can be immotile for extensive periods, morphology does not necessarily correlate with motility, neuroblasts exhibit local exploratory motility, dorsoventral migration occurs throughout the striatal SVZ, and neuroblasts turn at distinctive angles. We investigated these novel findings in the SVZ and RMS from the population to the single cell level. In this review we also discuss some technical considerations when setting up a two-photon microscope imaging system. Throughout the review we identify several unsolved questions about SVZ neuroblast migration that might be addressed with current or emerging techniques.

Keywords: migration, neuroblast, multiphoton, subependymal zone, subependymal layer

SVZ NEUROBLASTS MIGRATE THROUGH THE ROSTRAL MIGRATORY STREAM TO THE OLFACTORY BULBS

The subventricular zone (SVZ) lining the lateral ventricles is one of the two largest neurogenic areas within the adult mouse brain. The predominant model of the SVZ delineates three neurogenic cell-types: glial fibrillary acidic protein (GFAP+) stem cells, epidermal growth factor receptor (EGFr+) transit amplifying cells, and doublecortin (Dcx+) neuroblasts. Slowly dividing stem cells generate more rapidly dividing transit amplifying progenitor cells which in turn give rise to postmitotic migratory neuroblasts (Doetsch et al., 1999). Every day tens of thousands of these immature neurons migrate anteriorly along the rostral migratory stream (RMS) to their final destination in the olfactory bulb (OB; Morshead and van der Kooy, 1992; Luskin, 1993; Lois and Alvarez-Buylla, 1994; Carleton et al., 2003). SVZ neuroblasts move at a distance of 5–8 mm through the RMS making it the longest migratory pathway in the developing or adult brain. They can take 2–6 days to traverse this length and as will be discussed below it is thus far not possible to follow an individual cell during its entire trajectory. Upon arrival in the OB, these immature neurons migrate into the granular and periglomerular layers and differentiate into a variety of interneurons that integrate into the existing neuronal circuitry (Doetsch and Alvarez-Buylla, 1996; Belluzzi et al., 2003; Carleton et al., 2003).

Throughout development immature neurons tend to migrate in two distinct ways. Radial migration depends upon radial glia acting as a guiding structure. This is typified by excitatory neuron movement from the ventricular zone out to the upper layers of the cerebral cortex. The second type is tangential migration which is in some ways opposite to the classical radial migration of immature neurons. Tangential migration is defined by movement across rather than along radial glia, it covers a longer distance and is not limited to postmitotic neurons (Luskin, 1993; Menezes et al., 1995; Kriegstein and Alvarez-Buylla, 2009). Neuroblast migration from the SVZ to the OB is thought to have features of both of these: tangential migration occurs from the SVZ through the RMS, then there is a switch to migrating radially outward into the OB layers even though this radially oriented migration does not depend on radial glia.

During the tangential migration through the RMS, migrating neuroblasts make cell–cell contacts through neuronophilic interactions and organize themselves into long contiguous arrays of cells (Lois et al., 1996). The combination of individual arrays produces a large scale network of longitudinal "chain migration" that feeds into the RMS and is contiguous with the SVZ. In this homotypic migration cells use each other as a migratory substrate where one cell extends a process that the following cells can use to guide and direct their migration. It seems to follow that if all cells were moving simultaneously as the term chain migration implies, they would have no traction on each other. In fact, as elaborated below a significant portion of neuroblasts in the chain are stationary at any given time (Wichterle et al., 1997; Nam et al., 2007), giving their neighbors substrates for adhesion. Direct cell–cell contact between neuroblasts is crucial for migration, of which the originally studied mediator the polysialylated form of neural cell adhesion molecule is expressed at high levels in the SVZ (PSA–NCAM; Szele et al., 1994; Rousselot et al., 1995; Szele and Chesselet, 1996). PSA residues allow the migration of cells by binding to NCAM and reducing cell adhesion (Sadoul et al., 1983). Removal of PSA–NCAM either by enzymes (Ono et al., 1994) or genetic deletion (Tomasiewicz et al., 1993; Cremer et al., 1994) severely disrupts neuronal migration to the OB (Chazal et al., 2000; Hu, 2000).

The neuroblasts in the chains migrate rostrally though the SVZ and the RMS to the OB ensheathed by a network of astrocytic processes that form "glial tubes." Ensheathment by the glial tubes does not occur until the third postnatal week before which there is a more homogenous network of glial processes (Peretto et al., 1997, 2005). The exact function of glial tubes is currently unknown as chain migration can occur in the absence of glia (Wichterle et al., 1997). High levels of GFAP and vimentin are expressed by these astrocytes which also secret large amounts of extracellular matrix (ECM) proteins such as tenascin and chondroitin sulfate proteoglycan (Gates et al., 1995; Jankovski and Sotelo, 1996; Thomas et al., 1996). ECM cell surface integrin receptors are present on neuroblasts which interact with laminin to guide migration (Murase and Horwitz, 2002; Emsley and Hagg, 2003), in particular β1 integrin promotes the formation of chains (Belvindrah et al., 2007). RMS astrocytes have been proposed to serve both as a physical barrier, preventing dispersion into surrounding parenchyma and as a guidance system for tangential neuroblast migration (Jankovski and Sotelo, 1996; Thomas et al., 1996; Peretto et al., 1997; Kaneko et al., 2010).

The study of SVZ neuroblast migration is important for three major reasons. First it is a convenient system within which to study patterns of cell migration and the molecular mechanisms that regulate them. It eliminates difficult *exo utero* surgeries, comprises an anatomically defined migratory pathway and shares features of healthy embryonic as well as pathological adult migration (i.e., cancer metastasis). Features of typical embryonic migration that SVZ cells share include lamellipodia, nucleokinesis, and chemotaxis. Cell proliferation during migration occurs in SVZ neuroblasts and during interneuron migration to the cerebral cortex. On the other hand SVZ migration has some unusual features only exhibited by a small number of other migratory events. For example chain migration is unusual but is also seen in neural crest cells. Another reason to study SVZ migration is that SVZ cells may become therapeutically relevant and thus understanding the factors that normally keep them in the RMS in healthy brains or that beckon them toward brain injuries is essential. Finally, migration is a fundamental component of postnatal and adult SVZ neurogenesis. Its proper regulation is as important as cell cycle kinetics, differentiation, and survival in maintaining basal rates of neurogenesis.

TWO-PHOTON TIME-LAPSE MICROSCOPY: DYNAMIC STUDIES OF SVZ MIGRATION

Many studies have used static histologic sections to infer migration routes and behavior of migrating cells. This is clearly not ideal and more direct analyses are favored since one snapshot of a migrating cell can not reveal its dynamic behavior. Other work has relied on confocal microscopy to generate single optical sections over time. For example, studies on SVZ neuroblast migration from the Goldman lab revealed many interesting aspects of SVZ migration, see history of SVZ imaging below and references (Kakita and Goldman, 1999; Kakita, 2001; Suzuki and Goldman, 2003).

Two-photon microscopy offers an alternative approach to confocal microscopy with several inherent advantages. The technique was first reported by Denk et al. (1990) and has become the preferred method for imaging the dynamic properties of living tissue (Denk and Svoboda, 1997; Zipfel et al., 2003; Svoboda and Yasuda, 2006). The two key advantages of this approach are the small excitation volume (typically on the order of 1 μm^3) and the long excitation wavelengths that facilitate deep tissue imaging, reduced photobleaching of the fluorophore, and reduced phototoxicity of cells. In short, two-photon microscopy enables long-term imaging of fluorescently labeled neurons deep within tissues and is ideal for fast moving cells.

One of the major obstacles to performing two-photon microscopy is cost. The main difference in cost between confocal and two-photon microscopy is the laser. Whereas confocal lasers are relatively inexpensive, ranging from $5 to $50 K for suitable visible lasers, two-photon lasers are more complex and thus more expensive. Two-photon microscopy requires pulsed infrared lasers with a minimum output power of roughly 500 mW for adequate tissue penetration. Such lasers cost $100 K or more especially if you want higher output power (up to 3 W).

Another obstacle is that custom built two-photon systems are not as turn-key as commercially available confocal microscopes. In particular, changing objectives is straight-forward using confocal microscopy, whereas it requires some technical expertise to change objectives in two-photon microscopy, i.e., if you want to maintain excitation and collection efficiencies. While not an insurmountable obstacle, this generally requires some knowledge of optics, lasers, and beam alignment. For a more detailed description of our two-photon system, please consult (Nam et al., 2007).

TECHNICAL CONSIDERATIONS WHEN SETTING UP A TWO-PHOTON MICROSCOPIC IMAGING SYSTEM

1 *General microscope setup.* There are several commercial suppliers of two-photon microscopes, but they are quite expensive due mostly to development costs. If you have the expertise, then building a custom microscope is not difficult and less costly. Either way, you will need an upright microscope and water-dipping objectives to image tissue slices. The type of microscope is less important and more dependent upon your personal preferences and experience. All commercial suppliers make water-dipping objectives.

2 *Objective choice.* The most important factor in deciding which water-dipping objective to use is deciding how large a surface area you would like to measure and the level of resolution required. This is determined by the magnification of the lens and the numerical aperture, respectively. We use 20× and 40× lenses with high N.A. (0.95 and 0.8, respectively). The high N.A. maximized our excitation and collection efficiencies. A large diameter back aperture was also preferred as this enabled greater laser beam throughput and greater laser power at the sample which facilitated deeper imaging.

3 *Laser choice.* You need a tunable, pulsed Ti-Sapphire laser with output ranging from at least 800–900 nm (most fluorophores are excited within this range). The pulse repetition rate should be at least 75 MHz to maximize the energy per pulse and increase the probability that a fluorophore will absorb two-photons nearly simultaneously (in less than 10^{-15} s). Such short pulses also minimize heating of the water in the tissue and surrounding areas that occur at these wavelengths. The latter can become a problem when the laser power at the sample exceeds 50 mW.

4 *Scanners, detector, filters.* Since two-photon microscopy is essentially a confocal microscope with a different laser, the need for scanners, detectors, and filters is identical. Since the excitation volume is restricted in two-photon microscopy (due to the low probability of a two-photon absorption event), one does not need to restrict the emission through a pinhole as in confocal microscopy. All of the excitation that reaches the detector can be assumed to arise from the excitation volume. Thus, deeper tissue imaging is possible even though the emitted photons are scattered within the tissue on their way to the detector.
5 *Acquisition speed.* The speed of acquisition is limited by the amount of fluorophore, its excitation properties (dye cross-section), laser power at the sample, and the efficiency of detection. In our experience, GFP-labeled SVZ cells can be easily visualized using a dwell time of 4 μs per pixel (the time the laser remains in that location), 800 nm excitation, 5–10 mW, and internal PMT detectors. At this scanning speed, we routinely collect 40–60 Z-planes every 3 min for 4 h and even up to 20 h with no evidence of photobleaching or phototoxicity. Excitation and collection efficiency could be improved with longer wavelength excitation (900 nm) and use of external detectors.
6 *Tissue preparation and plane of sectioning.* Acute tissue slices can be a very important tool for examining structural and physiological properties of cells both in imaging and electrophysiological studies. They have several advantages as they are relatively easy to prepare and largely maintain the cytoarchitecture of the tissue. Briefly, the brain is dissected from the skull and chilled in oxygenated artificial cerebrospinal fluid (aCSF). Chilling of the tissue is important as it improves the ease of sectioning and reduces stress to the tissue. Sections of 300 μm in thickness are then cut at low speed using a vibratome, followed by incubation in 37°C oxygenated aCSF for at least 1 h then back to room temperature until imaging commences. For multiphoton imaging, and indeed confocal imaging, there are two main planes of section for acute slices that are commonly used: coronal and sagittal. The plane of sectioning for imaging is not always obvious and there are many factors to be considered. Coronal slicing allows limited view of the RMS but may be better for imaging migration out of the SVZ. Cutting tissue coronally results in severing of rostral migration, which may scramble neuroblast migration or cause them to migrate out of the slice. Sagittal slices allow visualization of large portions of the RMS especially if they are angled such that they follow the natural course of the SVZ/RMS. To capture most of the RMS in one slice, we cut the rostral portion of the slice slightly more medially than the caudal. Slicing this way also keeps the OB attached, theoretically maintaining OB chemoattractants. While we find acute slices one of the best methods to preserve tissue integrity without wide spread apoptosis they are short-lived preparations that we have only used experimentally for up to 24 h. Even when the slice preparation and two-photon microscope are optimal, the experimenter has to continuously monitor the automated image capture for slice drift, computer freezes, etc.

For longer experiments organotypic slice culture may prove a better alternative. However, this method should be approached with some caution if it is to be used to address questions about how certain molecules may influence migration patterns. Bonfanti and colleagues have shown that culturing of SVZ containing coronal sections results in significant disruption of slice cytoarchitecture and cell death over the first several days (Armentano et al., 2011). As a consequence of this loss of 3D structure, neuroblasts disaggregate at the top and bottom of the slice. Long-term culture is also accompanied by astrocytosis and microgliosis. De Marchis et al. (2001) noted the presence of macrophage-like cells in 3 day old organotypic slices (20%) that was associated with fragility of the slice. As SVZ/RMS cells can express chemokine and cytokine receptors activation of these inflammatory cells may affect migration (Kokovay et al., 2010).

IMAGE ACQUISITION AND IMAGE ANALYSIS

The first issue is that the slice must always be immersed in solution to prevent damage to the tissue. Second, while making time-lapse movies, the focus may change due to downward drift in the z dimension that can occur due to the weight of the C ring used to hold it in place (**Figure 1A**). Third, drift of the slice may occur in the direction of the perfusion flow. Both drift issues can be prevented or significantly decreased by properly anchoring the slice with a C ring (**Figure 1A**) and by leaving the slice in the perfusion chamber for 1 h before acquiring movies so that the slice has time to adhere to the top of the platform. Most z drift occurs during this 1 h time period which also allows acclimatization of the slice to the aCSF and the temperature. We routinely look for drift during the preincubation period by rapidly using a 5× objective lens to visualize GFP+ cells

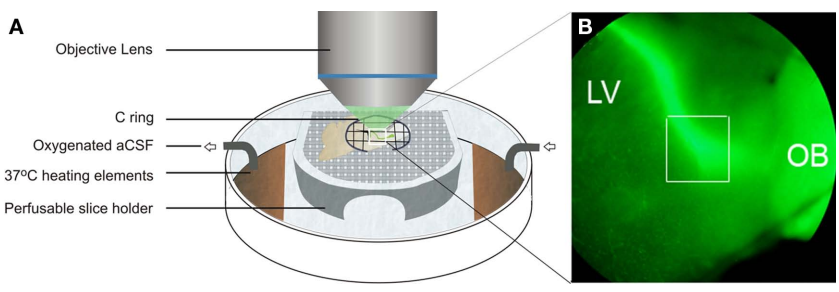

FIGURE 1 | Depiction of a GFP+ slice in the imaging chamber. (A) The slice rests on a perfusable platform and is held in place by the weight of a C ring. **(B)** Low magnification image of a nestin-GFP slice showing labeled cells migrating from the SVZ above the lateral ventrical (LV) through the RMS (boxed area) into the olfactory bulb (OB). Adapted from Kim et al. (2009).

(**Figure 1B**). Temperature control is an important parameter since fluctuations in the temperature can cause expansion and contraction of the tissue and thus unnecessary loss of focus. Several stage and objective warmers are available, but we have primarily used a Bioptechs chamber (**Figure 1A**). This chamber utilizes current resistance in a thin metallic film across the bottom to generate heat that is easily regulated. Oxygenated aCSF is then rapidly (1 ml/min) perfused over and under the slice which is held in place with a simple C ring fashioned from tungsten wire and cross-hatched with nylon fibers. Once the slice is in place we search for optimal fields with a 5× lens and then switch to 40× and confirm that sufficient signal to noise ratios can be attained.

We have used Olympus Confocal software (Fluoview) to capture images (**Figure 2A**). Fluoview is rather easy to use and allows control over the number of optical slices, the distance between slices, the digital zoom and initial Kallman filtering. Once the time-lapse is completed files are imported into Volocity (Improvision) software and are rendered into 3D images (**Figure 2B**). Although Volocity can run into $10–30K depending on the suite of modules one chooses, we have found it ideal for subsequent filtering (**Figure 2C**) and especially for tracking and quantifying cells in 3D. Although the program requires a high-performance computer with large memory capacity, the computer should still only amount to 10–20% of cost of the image analysis system. We have found it extremely useful to routinely convert movies from Volocity into Quicktime files for archiving, rapid examination of parameters and for presentations (**Figure 2D**). To image the tracks taken by migrating cells we frequently export data to Graphis (Kylebank Software) which is convenient for visualizing the pathways from multiple angles (**Figure 2E**).

A BRIEF HISTORY OF SVZ NEUROBLAST TIME-LAPSE IMAGING

Studies by Joseph Altman in the 1960s using tritiated thymidine clearly delineated separate proliferative and migratory cells in the SVZ and RMS (Altman, 1962, 1969). It was not until the 1990s that live imaging of SVZ neuroblast migration was achieved. Kakita and Goldman labeled early postnatal rat SVZ cells with GFP encoding retroviruses and used confocal time-lapse microscopy to image their migration in the SVZ and into adjacent nuclei (Kakita and Goldman, 1999; Kakita, 2001). The majority of these cells were glial progenitors and interestingly they took many dramatic turns, similar to those we have subsequently observed in mouse neuroblasts (Martinez-Molina et al., 2010). The turns could result from *de novo* growth of processes or from bending of pre-existing processes (Kakita, 2001). Furthermore, the authors noted significant dorsoventral movements within the wall of the lateral ventricle, a behavior we have also documented and which suggests that significant intermixing of SVZ lineages could take place. Subsequent studies from the Goldman lab used similar techniques and directly visualized rostral migration of SVZ neuroblasts to the OB, contrasting that route with migration of SVZ glioblasts to the corpus callosum, cerebral cortex, and striatum (Suzuki and Goldman, 2003). Remarkably many neuroblasts could reverse their direction by 180°, even though the large majority eventually migrate from the SVZ to the OB. In that study, the authors also noted obvious boundaries to migration of neuroblasts into the adjacent structures that glial precursors readily moved into (Suzuki and Goldman, 2003). To this day it is unclear what the molecular basis of such different behaviors may be.

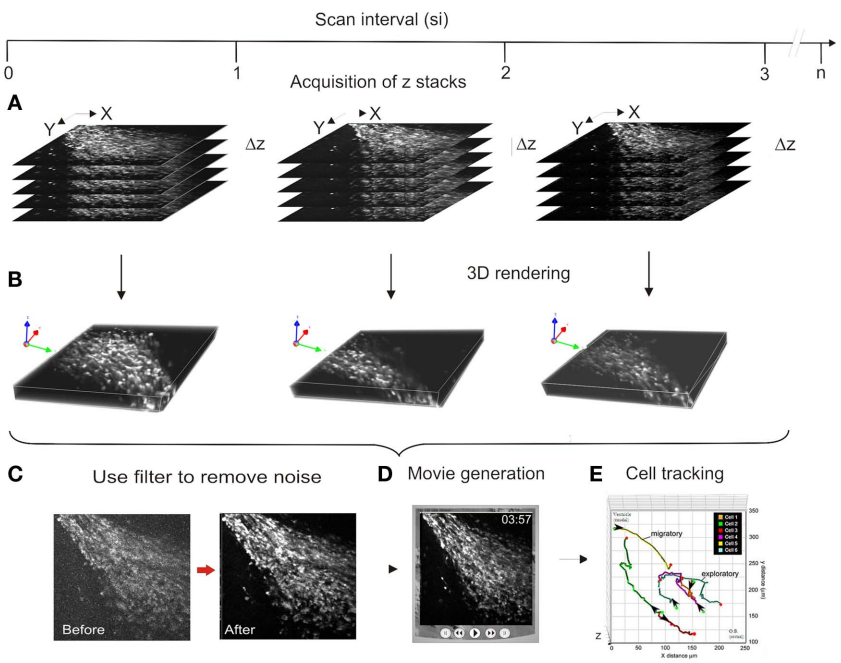

FIGURE 2 | Flow chart of image analysis. (A) Raw z-stacks are captured with Fluoview software over time. Three actual stacks collected at 3 min scan intervals. We typically collect 50 Z optical sections whereas only five are illustrated for simplicity. **(B)** Images are imported into Volocity and rendered into 3D. **(C)** Images filtered in Volocity. **(D)** Quicktime movies are generated. **(E)** Cell positions are tracked in Volocity and exported to Graphis for illustration.

Later dynamic imaging studies of neuroblasts by Puche and colleagues involved injecting a fluorescent dye called cell tracker green (CTG) into the lateral ventricles (De Marchis et al., 2001, 2004a). This dye is able to diffuse though the wall of the ventricle and label migratory cells within the SVZ, irrespective of their location in the SVZ. As the CTG does not passively spread into the RMS any cells labeled cells found in the RMS after several days can only have migrated there from the SVZ (Kim et al., 2009). CTG is enzymatically modified upon entry is rendered impermeable to the plasma membrane and thus becomes trapped in the cell. CTG fills the cytoplasm of cells allowing visualization of morphology such as leading and trailing processes and their dynamic changes during migration. Using this method, De Marchis et al. (2001) showed it is possible to track SVZ neuroblasts along the RMS to the OB using confocal microscopy. They also identified a second ventrocaudal migratory stream originating at the elbow between the vertical and horizontal limbs of the RMS that is present during the first postnatal week (De Marchis et al., 2004a). While the CTG technique has several obvious strengths it also has some inherent problems. In order to study specific SVZ populations cell subtypes need to be identified after dynamic imaging with *post hoc* immunohistochemistry as the dye does not label specific cells. Another important consideration is that CTG is not water soluble and requires dimethyl sulfoxide (DMSO) as a carrier. Although few signs of toxicity have been reported (De Marchis et al., 2001), it cannot be ruled out that DMSO induces changes within the SVZ molecular niche. In our laboratory limiting the concentration of CTG and the volume of DMSO injected were both essential to avoid periventricular degeneration (Kim et al., 2009).

One of the central difficulties in studying the SVZ is distinguishing the multiple cell types found in it and in the RMS (**Figure 3A**). Recently several lines of transgenic mice have become available in which fluorescent proteins are expressed under the control of cell-type specific promoters (**Figure 3B**), for an excellent review see Lacar et al. (2010). These mouse lines have opened up the ability to ask specific questions about migration and motility of distinct SVZ/RMS cell populations. Two main lines are available for neuroblasts: Dcx-eGFP mice and Gad65-eGFP mice (**Figure 3B**; Nam et al., 2007). Dcx is expressed by SVZ neuroblasts and is a microtubule-associated protein necessary for their migration (Koizumi et al., 2006; Ocbina et al., 2006). The Dcx-GFP mouse by Gensat (Gong et al., 2003) clearly shows chains and for the first time allowed visualization of migration within the entire array of cells (Nam et al., 2007). However, since SVZ cell density is very high it is difficult to discern individual cells. Gad65, the 65-kDa isoform of glutamic acid decarboxylase (Gad) is expressed by a subset of neuroblasts as they migrate through the SVZ and RMS (De Marchis et al., 2004b; Hamilton et al., 2008). In Gad65-eGFP mice this subset of Dcx+ and PSA–NCAM+ neuroblasts probably represents the more mature cells. By labeling individual cells within arrays this facilitates morphological and quantitative analyses.

Several nestin-eGFP lines have been generated that label similar precursor cell populations (**Figure 3B**; Yamaguchi et al., 2000; Kawaguchi et al., 2001; Mignone et al., 2004; Walker et al., 2011). Nestin is an intermediate filament protein widely used to identify neural stem and progenitor cells (Lendahl et al., 1990; Thomas et al., 1996; Doetsch et al., 1997). These nestin-GFP lines label various subsets of all SVZ and RMS cells. We have used a particularly bright nestin-eGFP mouse that clearly labels individual neuroblasts (**Figure 3B**; Nam et al., 2007; Walker et al., 2011). This can be advantageous insofar as individual fluorescent cells can be clearly visualized making it easy to track them in 3D, frame by frame. Another very useful line is from the Enikolopov laboratory at Cold Spring Harbor, we have it termed "CSH-Nestin-GFP" (Mignone et al., 2004). In these mice, GFAP+ stem-like cells and transit amplifying cells in the SVZ are labeled with bright GFP and neuroblasts with dim GFP (**Figure 3B**) allowing them to be distinguished in the same slice (Kim et al., 2009).

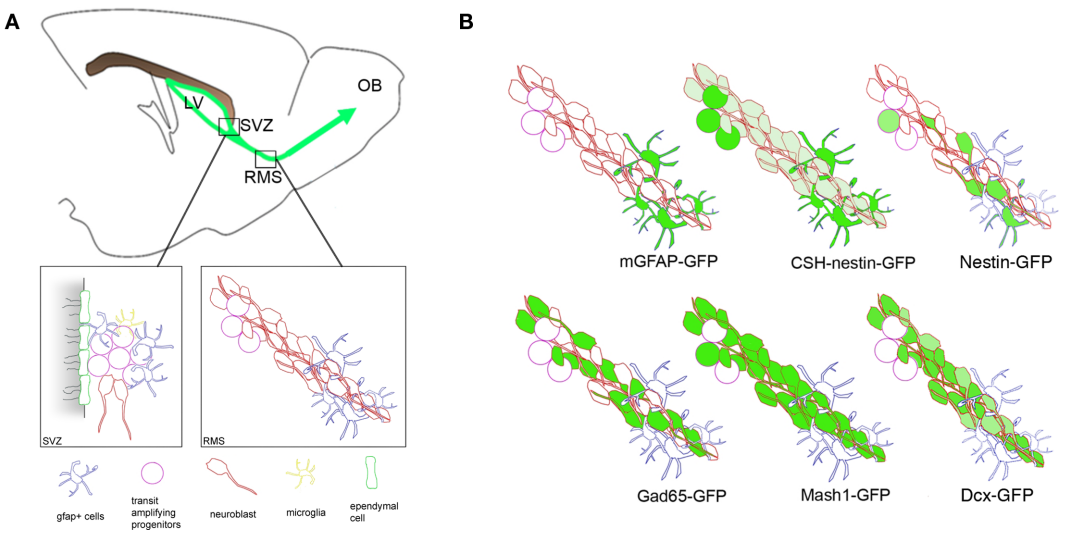

FIGURE 3 | Schematic of the SVZ, RMS, and cell subtypes labeled in different transgenic lines. (A) Low magnification view of a sagittal section showing location of the SVZ, RMS, and OB. SVZ cell subpopulations are depicted by different shapes and colors. Boxed areas show cytoarchitectural organization of the SVZ (left, coronal plane) and RMS (right, sagittal plane). **(B)** Examples of mouse lines used to label SVZ subpopulations. Green indicates SVZ cell subtypes labeled as well as the relative intensity of GFP fluorescence. (Modified from Nam et al., 2007 and Kim et al., 2009).

VISUALIZING CHAIN MIGRATION

The SVZ/RMS pathway contains a diverse and unique molecular environment with the presence of soluble, ECM and adhesion molecules (Thomas et al., 1996; Conover et al., 2000; Hedin-Pereira et al., 2000). Currently we have little understanding of how these molecules coordinate to regulate chemoattraction, chemorepulsion, motogenesis, speed, detachment from chains and cell adhesion. The RMS has no clear anatomical guidance structure so how do these cells orientate and navigate through this complex environment? One of the main goals of using two-photon imaging is to understand the fundamental rules and factors involved in governing these subcomponents of cell motility.

The first studies using dynamic imaging to demonstrate homotypic or chain migration cultured SVZ explants and produced time-lapse movies of the outgrowth of chains (Wichterle et al., 1997). Interestingly, this study demonstrated that chains formed and neuroblasts migrated without the ensheathing glial tubes seen in the RMS, suggesting astrocytic tubes may not be necessary for chain formation and RMS migration. Neuroblasts leap-frogged over each other while a certain percentage were stationary, similar to what our 2-P time-lapse studies subsequently showed in slices (Nam et al., 2007). Although cell culture and tissue explants are important tools for studying the mechanisms of cell migration and differentiation, these models involve significant alterations to the normal anatomical and functional relationships of the cellular elements in the SVZ, RMS, and OB. Conclusions drawn from these may not represent the *in vivo* situation.

By using time-lapse two-photon imaging it is possible to study these chains at the population level and image these arrays for up to 24 h. Using the Dcx-GFP mouse which labels all neuroblasts (**Figure 3B**), movies can be taken that allow the arrays to be visualized in their entirety. Imaging reveals that the arrays have the appearance of cells streaming along clearly delineated, well defined pathways in which the direction of migration closely matches the orientation of the array. *In vitro* studies suggest that these chains are not stable but change shape by dissipating and reforming (Wichterle et al., 1997). However, our *ex vivo* studies suggest that this does not seem to be the case as the chains remain very stable over hours of imaging and cells very rarely err from the SVZ/RMS pathway into the surrounding tissue. This may be due to contact-mediated inhibition with neurons and oligodendrocytes in the striatum and corpus callosum that induce lamellipodial collapse.

The large numbers of cells born in the SVZ migrate rostrally through the RMS to the OB. As expected, imaging shows that neuroblast arrays are oriented rostrocaudally immediately under the corpus callosum, in the dorsal SVZ, and the majority of rostral migration probably occurs in this subregion (Nam et al., 2007). It is currently unknown what sets up this rostral direction of migration but it has been suggested it may be diffusible chemoattractants secreted by the OB (Liu and Rao, 2003; Ng et al., 2005) and chemorepellents from the caudal septum (Hu and Rutishauser, 1996) working in combination. Other studies however have shown that these long distance cues may not be required as rostral migration continues in the absence of the OB (Jankovski and Sotelo, 1996; Kirschenbaum et al., 1999). We have also observed that removal of the OB before imaging does not change the migration or motility of neuroblasts within the RMS (Szele Laboratory, unpublished observations).

Ependymal ciliary beating has been proposed to set up the flow of CSF around the ventricles and thereby establish caudal to rostral chemotactic gradients of factors secreted by the choroid plexus that can direct SVZ migration (Sawamoto et al., 2006). Loss of this flow in Tg737orpk mice with defective cilia results in neuroblast chain disorientation and a loss of their longitudinal arrangement. In the slice preparations used for two-photon imaging this seems unlikely to explain migration guidance as constant perfusion of aCSF would dissipate any gradient. Also, the direction of aCSF flow from experiment to experiment had no obvious effect on migration direction. It is more likely that gradients of factors such as Slit2 (Sawamoto et al., 2006) are important during developmental stages when morphogenic gradients have to be established across shorter distances, but are not vital for rostral migration throughout adulthood.

While migration in the dorsal SVZ occurs largely in the rostral direction, evidence suggests that the orientation of migration may be different in other regions of the SVZ. Previous studies have shown that in the ventral portions of the SVZ Dcx+ arrays are orientated dorsoventrally (Yang et al., 2004; Nam et al., 2007) and ventral migration may occur into the anterior striatal SVZ (Sawamoto et al., 2006). Using two-photon time-lapse to visualize dorsoventral migration, we showed that it occurs throughout the entire striatal SVZ and not only in the anterior subregion (Nam et al., 2007). The ventral SVZ is characterized by radial glia like cells whose processes fan out into the ventral forebrain regions (Sundholm-Peters et al., 2004). In neonatal, and to a lesser extent adult mice, Dcx+ cells may use these radial processes to emigrate dorsoventrally to the ventral forebrain and produce neurons in the olfactory tubercles, islands of Calleja and nucleus accumbens (De Marchis et al., 2004a; Sundholm-Peters et al., 2004; Yang et al., 2004). Our finding of this widespread dorsoventral migration raises several interesting questions regarding differences between dorsal and ventral SVZ cells. Do dorsal and ventral cells intermix or are they two distinct populations? Are there differences in the molecular mechanisms that create the varying array orientation and motility directions? Future imaging studies may reveal different migration mechanisms in SVZ subregions.

MORPHOLOGY AND MOTILITY OF SVZ NEUROBLASTS

A large amount of what is known about the SVZ has been inferred from histological studies including several ideas about neuroblast migration. Many studies performing static studies have identified migrating cells by using a common "migratory morphology" represented by unipolar or bipolar cells that display a leading process and trailing edge (De Marchis et al., 2001). Leading process orientation is often used as a sole indicator of directionality of cell migration (Szele and Cepko, 1996; Sawamoto et al., 2006). It has long been assumed that there is a strict relationship between this morphology and motility without direct evidence to prove this is the case. A major impetus for conducting time-lapse imaging studies was to directly study this relationship between morphology and motility.

Time-lapse confocal studies examining the migration of CTG labeled cells (De Marchis et al., 2001; Bovetti et al., 2007a) demonstrate that many migratory neurons exhibit a long leading process with a short trailing process. As described above, these studies have difficulties in resolving the processes as intensity and exposure time have to be kept short to prevent phototoxicity. The use of

confocal for studying migration is limited as images can only be taken on average every 10–15 min over a limited period of time (De Marchis et al., 2001; Bovetti et al., 2007a) and pathways of migration between these imaging frames may not be observed. Furthermore, by examining CTG+ cells that have migrated from the SVZ into the RMS imaging is biased toward cells that have migrated long distances and may not accurately represent local migration.

We took z-stacks every 3 min with two-photon time-lapse providing much greater temporal resolution than confocal time-lapse. 3 min intervals were necessary to raster in the *XY* dimension across 512 × 512 pixels (0.125 mm^2) in 50 optical sections (Z dimension; Nam et al., 2007). However in preparations that label large number of cells smaller volumes and shorter time intervals between 3D frames should be very possible. Using two-photon imaging of nestin-eGFP mice we unexpectedly found that many cells that had typical migratory morphology were in fact stationary in the RMS (19%), with an even larger percentage stationary in the SVZ (40%) (Nam et al., 2007; Kim et al., 2009). Imaging over several hours showed that these stationary cells could have stable cell bodies but dynamic processes that changed in length, orientation, or disappeared completely. Alternatively, the processes remained stable but the cell bodies exhibit subtle morphological changes. It is possible that these cells represent SVZ GFAP+ astrocytes and the dynamic processes interacted directly with the motile cells. While many cells with "migratory morphology" were indeed motile more surprising was the presence of motile cells that had no processes or were multipolar. This was particularly important as close to half of the cells in the RMS were motile (Nam et al., 2007) and would have been classed as stationary using histological methods.

SPEED OF SVZ NEUROBLAST MIGRATION

A fundamental feature of migration is the average speed at which cells travel, as speed must be well regulated throughout the RMS to synchronize cell production in the SVZ with integration in the OB. Any changes in this speed can have dramatic effects, as is shown when PSA is removed from NCAM reducing migration speeds so cells accumulate in the RMS and the size of the OB diminishes (Chazal et al., 2000). The earliest studies on neuroblast migratory speed used retroviral lineage tracers in rats and calculated speed by measuring the distance between a cell's point of origin and its final destination after a certain time (Luskin and Boone, 1994). These studies calculated average speed to be around 20–30 μm/h. These are inherently inaccurate measurements, as they make the assumption that cells move in a straight line and at constant velocity. Measurements of neuroblast migration from SVZ explants show a much higher speed of migration, around 122 μm/h (Wichterle et al., 1997). This is most probably due to the lack of complex cytoarchitecture that cells have to migrate through *in situ*. Also, there are no glial tubes in the *in vitro* system, suggesting that astrocytes may slow migration speed.

Migrating cells within the RMS use 3D and often very complex pathways which cannot be fully appreciated using standard confocal methodology. Analysis of confocal and early two-photon movies (Koizumi et al., 2006) was achieved by collapsing the z-stack to produce a 2D image, meaning that the path taken by the cell appears much shorter and may have lead to underestimations of speeds. By using two-photon imaging, cell migration can be tracked in 3D by recording the *X*, *Y*, and *Z* coordinates over time as described above. Using this method we were able to show that by examining complex 3D movements, speed can be calculated with more accuracy (Nam et al., 2007; Kim et al., 2009). Generally average speeds measured using two-photon were faster than those reported using confocal due to the larger distance measured as traveled. Interestingly, Gad65-GFP cells migrated at a faster speed (71 μm/h) than nestin-eGFP+ cells (52 μm/h). Gad65+ neuroblasts are thought to be relatively differentiated in comparison to nestin+ cells (De Marchis et al., 2001). This raised an intriguing possibility that older neuroblasts may be distinguished from younger ones by using speed as a phenotypic characterization.

Studies using confocal imaging of organotypic slices allowed the first dynamic imaging of neuroblast migration *in situ* in the RMS and show that cells migrate in a saltatory manner representative of nucleokinesis (Kakita and Goldman, 1999; Suzuki and Goldman, 2003). This movement is characterized by elongation of the leading process followed by translocation of the nucleus (Nadarajah et al., 2003; Tsai and Gleeson, 2005) resulting in alternating periods of higher and lower migration rates when based on cell body movement. There is large variation in measured average migration speeds for different confocal studies (De Marchis et al., 2001; Bovetti et al., 2007b; Platel et al., 2008). Some of this may be due to different ages of the animals with some focusing on neonates and other using adult animals. Alternatively speeds may be affected by temperature, a correlation that we have not examined since we always work at physiological temperatures. Many changes occur in the SVZ during the first postnatal week with retraction of radial glial processes as they differentiate into SVZ astrocytes and ependymal cells (Merkle et al., 2004). Bovetti et al. (2007b) report that cells migrate quicker at P21 than at P5 and that younger mice lack defined glial tubes (Peretto et al., 1997, 2005) and chains and migrate more as individual cells.

SVZ NEUROBLASTS DISPLAY COMPLEX MOTILITY PATTERNS

The detailed information that can be gathered using two-photon methods means that fundamental but previously undetected motility behaviors can be detected and studied. One approach to this is to use a "migratory index" which is a simple indication of motility complexity that is independent of speed (MI = net distance/total distance). By grouping cells based on migratory index we found the RMS is comprised of at least three distinct subpopulations of cells: migratory, exploratory, and intermediate (Nam et al., 2007). The migratory cells have fairly direct, straight migration pathways with little deviation. In contrast exploratory cells move in a local exploratory fashion.

It is possible that exploratory behavior may be an epiphenomenon within the *ex vivo* environment caused by the disruption of molecular gradients. We think this is unlikely, and that exploratory motility is not due to unhealthy slices or unusual mouse strains because it is consistently observed in all slices and in different transgenic lines. In addition, multipolar migration in the embryonic cortex (Tabata and Nakajima, 2003) closely resembles exploratory behavior. However that work was also performed in cultured slices, which may cause loss of local diffusion factors and thereby induce these behaviors. If exploratory motility does also occur *in vivo* what is its function? One possibility is it serves as a prelude to injury induced emigration from the SVZ/RMS into surrounding tissues (Goings et al., 2004; Sundholm-Peters et al., 2005; Dizon

et al., 2006) as our observations suggest that exploratory behavior increases after cortical injury (Szele laboratory, unpublished observations). Exploratory behavior may provide a means of sampling the environment to receive molecular cues. Further studies are required to see if migratory and exploratory cells express different cell surface signaling molecules, allowing intrinsic regulation of motility in a given microenvironment. It is important to point out that neuroblasts could switch behaviors from exploratory to migratory. Although we have yet to perform a thorough analysis of these switches thus far it seems that they are random.

Using two-photon time-lapse our laboratory has also found that EGFr signaling may be another mechanism controlling neuroblast motility. Neuroblasts that expressed low levels of EGFr tended to move in exploratory patterns. Neuroblasts show an inverse correlation between EGFr and Dcx/PSA–NCAM/bIII-tubulin expression, suggesting that EGFr is gradually lost as neuroblasts mature. Epidermal growth factor (EGF) regulates cell division in the SVZ *in vivo* (Reynolds and Weiss, 1992; Kuhn et al., 1997; Gritti et al., 1999) and is important for neurosphere generation *in vitro*. In the presence of transforming growth factor alpha (TGFa), an EGFr-selective agonist the percentage of motile cells decreased by approximately 40% (Kim et al., 2009). A very important consequence of this finding is with regards to the use of organotypic slices to measure aspects of motility as EGF is sometimes included as a constituent of culture media (Zhang et al., 2009).

SVZ NEUROBLASTS EXHIBIT STEREOTYPIC BEHAVIORS

Previous reports in rats had documented cells migrating countercurrent to each other within the chains, with some cells migrating caudally (Kakita and Goldman, 1999; Suzuki and Goldman, 2003). In both Gad65-GFP and nestin-GFP mice around 25% of cells turned and migrated caudally. Interestingly there was no difference in average speeds of cells that migrated caudally compared to cells that migrated only rostrally (Nam et al., 2007). These changes in direction were accompanied by complex and dynamic movements of the leading process and lamellipodium. Kakita and Goldman (1999) described how glia progenitors changed direction by branching and curving of the leading process or growth of a new process at the opposite pole of the cell body. Using two-photon time-lapse we show that neuroblasts could change direction by either polarity reversal or sequential bending of the leading process as previously described or by a newly observed method of branching of the leading process (Martinez-Molina et al., 2010).

During forward migration cells also exhibited complex methods of turning even in the absence of direction changes. Most cells deviated from straight paths through bending of the leading process close to the cell body (47% of turns), we termed this P-bending. We also observed bending of the distal leading process (30% of turns) or branching of the leading process (23% of turns). Remarkably, the angle of bending (128°) and of branching (101°) was very consistent from cell to cell, which may imply that similar molecular mechanisms control these movements regardless of the direction of movement or type of turn (Martinez-Molina et al., 2010).

The SVZ is a mosaic of cells of different lineages which raises the possibility they exhibit different patterns of motility (Merkle et al., 2007; Young et al., 2007). Interestingly, individual neuroblasts do not seem to be restricted to a specific type of turning behavior. Indeed, the same cell can not only switch between exploratory and migratory behaviors but can also change direction in multiple patterns. This suggests that certain behaviors are not specific to different lineages. As behaviors are not cell specific does one type of behavior predict or preclude another? What remains to be answered are the specific sequences and molecular mechanisms that govern neuroblast turning.

Given that neuroblast chains are largely established through neuronophilic interactions neural progenitor cells may influence each other's motility to maintain chain migration. Within the interior of chains, neuroblasts form contacts with each other, while on the exterior, cells encounter astrocytes forming the glial tube in addition to other neuroblasts. It is currently unknown whether *in vivo* cells are able to switch chain position and shift between the interior and exterior. Further analysis of cell migration patterns may reveal whether individual turning behaviors are associated with the cell's position in the interior versus exterior of the chain. For example, neuroblasts that stop movement in the interior of the chains may be carried along with the other cells, while on the exterior neuroblasts may be able to form stable contacts with glial tubes that anchor them in a stationary position. Contact with astrocytes may then induce turning or direction reversal through contact inhibition as seen in other systems. *In vitro* experiments have shown that SVZ neuroblasts repel astrocytes via Slit/Robo signaling in dissociated cells (Kaneko et al., 2010). However, in SVZ explants which lack ensheathing glial tubes a cell moving in a chain may become stationary, and by changing the orientation of its leading process begin to move in the opposite direction (Wichterle et al., 1997). Furthermore, the addition of striatal, septal, or OB explants alongside SVZ explants does not influence the direction of migration (Jankovski et al., 1998). Together this would suggest that extrinsic directional cues may not be required for cell turning patterns but that turning is regulated by mechanisms that are intrinsic to the neuronal progenitors.

NEUROBLAST DIVISION AND TRANSIT AMPLIFYING PROGENITOR MIGRATION

An essential feature of SVZ biology which has been largely neglected in most dynamic migration studies is the interaction between proliferation and cell motility. During tangential migration through the RMS, cells continue to divide and initiate neuronal maturation (Menezes et al., 1995; Coskun et al., 2007). Retroviral studies demonstrate that cells dividing in the RMS have a much longer cell cycle time than those dividing in the SVZ (Smith and Luskin, 1998). It will be interesting to study whether daughter cells pause during or after division or whether daughter cells migrate immediately. It is also unknown if sibling cells share the same migratory behaviors.

Recent evidence suggested that some SVZ progenitor cells may be motile (Aguirre et al., 2004, 2005). If multipotent stem cells or rapidly dividing progenitor cells have migratory potential they may be able to migrate to injury sites. Since they are not as fate-restricted as neuroblasts, they may be more reparative. We found motile nestin-GFP+ cells that did not express Dcx, suggesting stem cells or progenitor SVZ cells could be motile (Nam et al., 2007) since Dcx is thought to be expressed only in SVZ neuroblasts. In addition, cells with SVZ progenitor cell characteristics emigrated to the striatum in a model of injury supplemented with growth factor infusion (de Chevigny et al., 2008).

To directly address whether SVZ stem or progenitor cells could be migratory we performed two-photon imaging using the CSH-nestin-GFP mouse. To further distinguish between the stem and progenitor cells two-photon movies were made with the mGFAP-GFP mouse which labels a subset of SVZ astrocytes (**Figure 3B**; Kuzmanovic et al., 2003; Kim et al., 2009). After examination of over 800 CSH-Nestin-GFP^{bright} and 65 mGFAP-GFP+ cells none moved suggesting that GFAP+ astrocyte-like stem cells are normally static within the SVZ (Kim et al., 2009).

To examine the progenitor population we imaged the Nestin-GFP mouse and immediately after imaging the tissue was fixed and followed by *post hoc* double immunohisotchemistry for Dcx and Mash1. Mash1 is a transcription factor characteristic of SVZ transit amplifying progenitors which can be easily co-localized with GFP *post hoc*. The confocal image of the immunohistochemistry was matched with the last frame of the two-photon movie and Mash1+/GFP+ cells that were identified as being Dcx-negative identified. By following the movies backward the motility of these cells could be tracked. We never saw any motile Mash1+ cells implying that Mash1+ progenitor cells do not migrate from the SVZ into the RMS. Currently there are no transgenic lines that are specific to the transit amplifying progenitor cells. The Rockefeller Gensat Project have produced a Mash1-GFP mouse but immunostaining showed that the GFP expression pattern did not mirror that of the endogenous Mash1 protein (**Figure 3B**), but more represented that of Dcx labeling of the neuroblast population (Kim et al., 2009).

In summary we have learned much about cellular patterns of SVZ neuroblast migration and the mechanisms that regulate them. We contend that use of two-photon time-lapse microscopy to study this fascinating migratory system is still in its early days. Several emerging strategies may further harness the deep potential of two-photon microscopy. These include time-lapse of whole mount preparations to study migration at the population level and intravital microscopy using a variety of lenses (Flusberg et al., 2008; Barretto et al., 2009). The latter will be important to confirm current findings from slice preparations *in vivo*.

ACKNOWLEDGMENTS

We would like to thank members of the Szele lab and M. Majumdar for reading and suggestions on the manuscript. Francis G. Szele supported by NIH RO1 NS-42253. Rachel James supported by a Wellcome Trust studentship.

REFERENCES

Aguirre, A., Rizvi, T. A., Ratner, N., and Gallo, V. (2005). Overexpression of the epidermal growth factor receptor confers migratory properties to nonmigratory postnatal neural progenitors. *J. Neurosci.* 25, 11092–11106.

Aguirre, A. A., Chittajallu, R., Belachew, S., and Gallo, V. (2004). NG2-expressing cells in the subventricular zone are type C-like cells and contribute to interneuron generation in the postnatal hippocampus. *J. Cell Biol.* 165, 575–589.

Altman, J. (1962). Are new neurons formed in the brains of adult mammals? *Science* 135, 1127–1128.

Altman, J. (1969). Autoradiographic and histological studies of postnatal neurogenesis. IV. Cell proliferation and migration in the anterior forebrain, with special reference to persisting neurogenesis in the olfactory bulb. *J. Comp. Neurol.* 137, 433–457.

Armentano, M., Canalia, N., Crociara, P., and Bonfanti, L. (2011). Culturing conditions remarkably affect viability and organization of mouse subventricular zone in ex vivo cultured forebrain slices. *J. Neurosci. Methods* (In Press).

Barretto, R. P., Messerschmidt, B., and Schnitzer, M. J. (2009). In vivo fluorescence imaging with high-resolution microlenses. *Nat. Methods* 6, 511–512.

Belluzzi, O., Benedusi, M., Ackman, J., and LoTurco, J. J. (2003). Electrophysiological differentiation of new neurons in the olfactory bulb. *J. Neurosci.* 23, 10411–10418.

Belvindrah, R., Hankel, S., Walker, J., Patton, B. L., and Muller, U. (2007). Beta1 integrins control the formation of cell chains in the adult rostral migratory stream. *J. Neurosci.* 27, 2704–2717.

Bovetti, S., Bovolin, P., Perroteau, I., and Puche, A. C. (2007a). Subventricular zone-derived neuroblast migration to the olfactory bulb is modulated by matrix remodelling. *Eur. J. Neurosci.* 25, 2021–2033.

Bovetti, S., Hsieh, Y. C., Bovolin, P., Perroteau, I., Kazunori, T., and Puche, A. C. (2007b). Blood vessels form a scaffold for neuroblast migration in the adult olfactory bulb. *J. Neurosci.* 27, 5976–5980.

Carleton, A., Petreanu, L. T., Lansford, R., Alvarez-Buylla, A., and Lledo, P. M. (2003). Becoming a new neuron in the adult olfactory bulb. *Nat. Neurosci.* 6, 507–518.

Chazal, G., Durbec, P., Jankovski, A., Rougon, G., and Cremer, H. (2000). Consequences of neural cell adhesion molecule deficiency on cell migration in the rostral migratory stream of the mouse. *J. Neurosci.* 20, 1446–1457.

Conover, J. C., Doetsch, F., Garcia-Verdugo, J. M., Gale, N. W., Yancopoulos, G. D., and Alvarez-Buylla, A. (2000). Disruption of Eph/ephrin signaling affects migration and proliferation in the adult subventricular zone. *Nat. Neurosci.* 3, 1091–1097.

Coskun, V., Falls, D. L., Lane, R., Czirok, A., and Luskin, M. B. (2007). Subventricular zone neuronal progenitors undergo multiple divisions and retract their processes prior to each cytokinesis. *Eur. J. Neurosci.* 26, 593–604.

Cremer, H., Lange, R., Christoph, A., Plomann, M., Vopper, G., Roes, J., Brown, R., Baldwin, S., Kraemer, P., Scheff, S., Barthels, D., Rajewsky, K., and Wille, W. (1994). Inactivation of the N-CAM gene in mice results in size reduction of the olfactory bulb and deficits in spatial learning. *Nature* 367, 455–459.

de Chevigny, A., Cooper, O., Vinuela, A., Reske-Nielsen, C., Lagace, D. C., Eisch, A. J., and Isacson, O. (2008). Fate mapping and lineage analyses demonstrate the production of a large number of striatal neuroblasts after transforming growth factor alpha and noggin striatal infusions into the dopamine-depleted striatum. *Stem Cells* 26, 2349–2360.

De Marchis, S., Fasolo, A., and Puche, A. C. (2004a). Subventricular zone-derived neuronal progenitors migrate into the subcortical forebrain of postnatal mice. *J. Comp. Neurol.* 476, 290–300.

De Marchis, S., Temoney, S., Erdelyi, F., Bovetti, S., Bovolin, P., Szabo, G., and Puche, A. C. (2004b). GABAergic phenotypic differentiation of a subpopulation of subventricular derived migrating progenitors. *Eur. J. Neurosci.* 20, 1307–1317.

De Marchis, S., Fasolo, A., Shipley, M., and Puche, A. (2001). Unique neuronal tracers show migration and differentiation of SVZ progenitors in organotypic slices. *J. Neurobiol.* 49, 326–338.

Denk, W., Strickler, J. H., and Webb, W. W. (1990). Two-photon laser scanning fluorescence microscopy. *Science* 248, 73–76.

Denk, W., and Svoboda, K. (1997). Photon upmanship: why multiphoton imaging is more than a gimmick. *Neuron* 18, 351–357.

Dizon, M. L., Shin, L., Sundholm-Peters, N. L., Kang, E., and Szele, F. G. (2006). Subventricular zone cells remain stable in vitro after brain injury. *Neuroscience* 142, 717–725.

Doetsch, F., and Alvarez-Buylla, A. (1996). Network of tangential pathways for neuronal migration in adult mammalian brain. *Proc. Natl. Acad. Sci. U.S.A.* 93, 14895–14900.

Doetsch, F., Garcia-Verdugo, J. M., and Alvarez-Buylla, A. (1997). Cellular composition and three-dimensional organization of the subventricular germinal zone in the adult mammalian brain. *J. Neurosci.* 17, 5046–5061.

Doetsch, F., Garcia-Verdugo, J. M., and Alvarez-Buylla, A. (1999). Regeneration of a germinal layer in the adult mammalian brain. *Proc. Natl. Acad. Sci. U.S.A.* 96, 11619–11624.

Emsley, J. G., and Hagg, T. (2003). Alpha6beta1 integrin directs migration of neuronal precursors in adult mouse forebrain. *Exp. Neurol.* 183, 273–285.

Flusberg, B. A., Nimmerjahn, A., Cocker, E. D., Mukamel, E. A., Barretto, R. P., Ko, T. H., Burns, L. D., Jung, J. C., and Schnitzer, M. J. (2008). High-speed, miniaturized fluorescence microscopy in freely moving mice. *Nat. Methods* 5, 935–938.

Gates, M. A., Thomas, L. B., Howard, E. M., Laywell, E. D., Sajin, B., Faissner, A., Gotz, B., Silver, J., and Steindler, D. A. (1995). Cell and molecular analysis of

the developing and adult mouse subventricular zone of the cerebral hemispheres. *J. Comp. Neurol.* 361, 249–266.

Goings, G. E., Sahni, V., and Szele, F. G. (2004). Migration patterns of subventricular zone cells in adult mice change after cerebral cortex injury. *Brain Res.* 996, 213–226.

Gong, S., Zheng, C., Doughty, M. L., Losos, K., Didkovsky, N., Schambra, U. B., Nowak, N. J., Joyner, A., Leblanc, G., Hatten, M. E., and Heintz, N. (2003). A gene expression atlas of the central nervous system based on bacterial artificial chromosomes. *Nature* 425, 917–925.

Gritti, A., Frolichsthal-Schoeller, P., Galli, R., Parati, E. A., Cova, L., Pagano, S. F., Bjornson, C. R., and Vescovi, A. L. (1999). Epidermal and fibroblast growth factors behave as mitogenic regulators for a single multipotent stem cell-like population from the subventricular region of the adult mouse forebrain. *J. Neurosci.* 19, 3287–3297.

Hamilton, K. A., Parrish-Aungst, S., Margolis, F. L., Erdelyi, F., Szabo, G., and Puche, A. C. (2008). Sensory deafferentation transsynaptically alters neuronal GluR1 expression in the external plexiform layer of the adult mouse main olfactory bulb. *Chem. Senses* 33, 201–210.

Hedin-Pereira, C., deMoraes, E. C., Santiago, M. F., Mendez-Otero, R., and Lent, R. (2000). Migrating neurons cross a reelin-rich territory to form an organized tissue out of embryonic cortical slices. *Eur. J. Neurosci.* 12, 4536–4540.

Hu, H. (2000). Polysialic acid regulates chain formation by migrating olfactory interneuron precursors. *J. Neurosci. Res.* 61, 480–492.

Hu, H., and Rutishauser, U. (1996). A septum-derived chemorepulsive factor for migrating olfactory interneuron precursors. *Neuron* 16, 933–940.

Jankovski, A., Garcia, C., Soriano, E., and Sotelo, C. (1998). Proliferation, migration and differentiation of neuronal progenitor cells in the adult mouse subventricular zone surgically separated from its olfactory bulb. *Eur. J. Neurosci.* 10, 3853–3868.

Jankovski, A., and Sotelo, C. (1996). Subventricular zone-olfactory bulb migratory pathway in the adult mouse: cellular composition and specificity as determined by heterochronic and heterotopic transplantation. *J. Comp. Neurol.* 371, 376–396.

Kakita, A. (2001). Migration pathways and behavior of glial progenitors in the postnatal forebrain. *Hum. Cell* 14, 59–75.

Kakita, A., and Goldman, J. E. (1999). Patterns and dynamics of SVZ cell migration in the postnatal forebrain: monitoring living progenitors in slice preparations. *Neuron* 23, 461–472.

Kaneko, N., Marin, O., Koike, M., Hirota, Y., Uchiyama, Y., Wu, J. Y., Lu, Q., Tessier-Lavigne, M., Alvarez-Buylla, A., Okano, H., Rubenstein, J. L., and Sawamoto, K. (2010). New neurons clear the path of astrocytic processes for their rapid migration in the adult brain. *Neuron* 67, 213–223.

Kawaguchi, A., Miyata, T., Sawamoto, K., Takashita, N., Murayama, A., Akamatsu, W., Ogawa, M., Okabe, M., Tano, Y., Goldman, S. A., and Okano, H. (2001). Nestin-EGFP transgenic mice: visualization of the self-renewal and multipotency of CNS stem cells. *Mol. Cell. Neurosci.* 17, 259–273.

Kim, Y., Comte, I., Szabo, G., Hockberger, P., and Szele, F. G. (2009). Adult mouse subventricular zone stem and progenitor cells are sessile and epidermal growth factor receptor negatively regulates neuroblast migration. *PLoS ONE* 4, e8122. doi: 10.1371/journal.pone.0008122

Kirschenbaum, B., Doetsch, F., Lois, C., and Alvarez-Buylla, A. (1999). Adult subventricular zone neuronal precursors continue to proliferate and migrate in the absence of the olfactory bulb. *J. Neurosci.* 19, 2171–2180.

Koizumi, H., Higginbotham, H., Poon, T., Tanaka, T., Brinkman, B. C., and Gleeson, J. G. (2006). Doublecortin maintains bipolar shape and nuclear translocation during migration in the adult forebrain. *Nat. Neurosci.* 9, 779–786.

Kokovay, E., Goderie, S., Wang, Y., Lotz, S., Lin, G., Sun, Y., Roysam, B., Shen, Q., and Temple, S. (2010). Adult SVZ Lineage cells home to and leave the vascular niche via differential responses to SDF1/CXCR4 signaling. *Cell Stem Cell* 7, 163–173.

Kriegstein, A., and Alvarez-Buylla, A. (2009). The glial nature of embryonic and adult neural stem cells. *Annu. Rev. Neurosci.* 32, 149–184.

Kuhn, H. G., Winkler, J., Kempermann, G., Thal, L. J., and Gage, F. H. (1997). Epidermal growth factor and fibroblast growth factor-2 have different effects on neural progenitors in the adult rat brain. *J. Neurosci.* 17, 5820–5829.

Kuzmanovic, M., Dudley, V. J., and Sarthy, V. P. (2003). GFAP promoter drives Muller cell-specific expression in transgenic mice. *Invest. Ophthalmol. Vis. Sci.* 44, 3606–3613.

Lacar, B., Young, S. Z., Platel, J. C., and Bordey, A. (2010). Imaging and recording subventricular zone progenitor cells in live tissue of postnatal mice. *Front. Neurosci.* 4:43. doi: 10.3389/fnins.2010.00043

Lendahl, U., Zimmerman, L. B., and McKay, R. D. (1990). CNS stem cells express a new class of intermediate filament protein. *Cell* 60, 585–595.

Liu, G., and Rao, Y. (2003). Neuronal migration from the forebrain to the olfactory bulb requires a new attractant persistent in the olfactory bulb. *J. Neurosci.* 23, 6651–6659.

Lois, C., and Alvarez-Buylla, A. (1994). Long-distance neuronal migration in the adult mammalian brain. *Science* 264, 1145–1148.

Lois, C., Garcia-Verdugo, J. M., and Alvarez-Buylla, A. (1996). Chain migration of neuronal precursors. *Science* 271, 978–981.

Luskin, M. B. (1993). Restricted proliferation and migration of postnatally generated neurons derived from the forebrain subventricular zone. *Neuron* 11, 173–189.

Luskin, M. B., and Boone, M. S. (1994). Rate and pattern of migration of lineally-related olfactory bulb interneurons generated postnatally in the subventricular zone of the rat. *Chem. Senses* 19, 695–714.

Martinez-Molina, N., Kim, Y., Hockberger, P., and Szele, F. G. (2010). Rostral migratory stream neuroblasts turn and change directions in stereotypic patterns. *Cell Adh. Migr.* 5, 83–95.

Menezes, J. R., Smith, C. M., Nelson, K. C., and Luskin, M. B. (1995). The division of neuronal progenitor cells during migration in the neonatal mammalian forebrain. *Mol. Cell. Neurosci.* 6, 496–508.

Merkle, F. T., Mirzadeh, Z., and Alvarez-Buylla, A. (2007). Mosaic organization of neural stem cells in the adult brain. *Science* 317, 381–384.

Merkle, F. T., Tramontin, A. D., Garcia-Verdugo, J. M., and Alvarez-Buylla, A. (2004). Radial glia give rise to adult neural stem cells in the subventricular zone. *Proc. Natl. Acad. Sci. U.S.A.* 101, 17528–17532.

Mignone, J. L., Kukekov, V., Chiang, A. S., Steindler, D., and Enikolopov, G. (2004). Neural stem and progenitor cells in nestin-GFP transgenic mice. *J. Comp. Neurol.* 469, 311–324.

Morshead, C. M., and van der Kooy, D. (1992). Postmitotic death is the fate of constitutively proliferating cells in the subependymal layer of the adult mouse brain. *J. Neurosci.* 12, 249–256.

Murase, S., and Horwitz, A. F. (2002). Deleted in colorectal carcinoma and differentially expressed integrins mediate the directional migration of neural precursors in the rostral migratory stream. *J. Neurosci.* 22, 3568–3579.

Nadarajah, B., Alifragis, P., Wong, R. O. L., and Parnavelas, J. G. (2003). Neuronal migration in the developing cerebral cortex: observations based on real-time imaging. *Cereb. Cortex* 13, 607–611.

Nam, S. C., Kim, Y., Dryanovski, D., Walker, A., Goings, G., Woolfrey, K., Kang, S. S., Chu, C., Chenn, A., Erdelyi, F., Szabo, G., Hockberger, P., and Szele, F. G. (2007). Dynamic features of postnatal subventricular zone cell motility: a two-photon time-lapse study. *J. Comp. Neurol.* 505, 190–208.

Ng, K. L., Li, J. D., Cheng, M. Y., Leslie, F. M., Lee, A. G., and Zhou, Q. Y. (2005). Dependence of olfactory bulb neurogenesis on prokineticin 2 signaling. *Science* 308, 1923–1927.

Ocbina, P. J., Dizon, M. L., Shin, L., and Szele, F. G. (2006). Doublecortin is necessary for the migration of adult subventricular zone cells from neurospheres. *Mol. Cell. Neurosci.* 33, 126–135.

Ono, K., Tomasiewicz, H., Magnuson, T., and Rutishauser, U. (1994). N-CAM mutation inhibits tangential neuronal migration and is phenocopied by enzymatic removal of polysialic acid. *Neuron* 13, 595–609.

Peretto, P., Giachino, C., Aimar, P., Fasolo, A., and Bonfanti, L. (2005). Chain formation and glial tube assembly in the shift from neonatal to adult subventricular zone of the rodent forebrain. *J. Comp. Neurol.* 487, 407–427.

Peretto, P., Merighi, A., Fasolo, A., and Bonfanti, L. (1997). Glial tubes in the rostral migratory stream of the adult rat. *Brain Res. Bull.* 42, 9–21.

Platel, J. C., Heintz, T., Young, S., Gordon, V., and Bordey, A. (2008). Tonic activation of GLUK5 kainate receptors decreases neuroblast migration in whole-mounts of the subventricular zone. *J. Physiol.* 586, 3783–3793.

Reynolds, B. A., and Weiss, S. (1992). Generation of neurons and astrocytes from isolated cells of the adult mammalian central nervous system. *Science* 255, 1707–1710.

Rousselot, P., Lois, C., and Alvarez-Buylla, A. (1995). Embryonic (PSA) N-CAM reveals chains of migrating neuroblasts between the lateral ventricle and the olfactory bulb of adult mice. *J. Comp. Neurol.* 351, 51–61.

Sadoul, R., Hirn, M., Deagostini-Bazin, H., Rougon, G., and Goridis, C. (1983). Adult and embryonic mouse neural cell adhesion molecules have different binding properties. *Nature* 304, 347–349.

Sawamoto, K., Wichterle, H., Gonzalez-Perez, O., Cholfin, J. A., Yamada, M., Spassky, N., Murcia, N. S., Garcia-Verdugo, J. M., Marin, O., Rubenstein, J. L., Tessier-Lavigne, M., Okano, H., and Alvarez-Buylla, A. (2006). New neurons follow the flow of cerebrospinal fluid in the adult brain. *Science* 311, 629–632.

Smith, C. M., and Luskin, M. B. (1998). Cell cycle length of olfactory bulb neuronal progenitors in the rostral migratory stream. *Dev. Dyn.* 213, 220–227.

Sundholm-Peters, N. L., Yang, H. K., Goings, G. E., Walker, A. S., and Szele, F. G. (2004). Radial glia-like cells at the base of the lateral ventricles in adult mice. *J. Neurocytol.* 33, 153–164.

Sundholm-Peters, N. L., Yang, H. K., Goings, G. E., Walker, A. S., and Szele, F. G. (2005). Subventricular zone neuroblasts emigrate toward cortical lesions. *J. Neuropathol. Exp. Neurol.* 64, 1089–1100.

Suzuki, S. O., and Goldman, J. E. (2003). Multiple cell populations in the early postnatal subventricular zone take distinct migratory pathways: a dynamic study of glial and neuronal progenitor migration. *J. Neurosci.* 23, 4240–4250.

Svoboda, K., and Yasuda, R. (2006). Principles of two-photon excitation microscopy and its applications to neuroscience. *Neuron* 50, 823–839.

Szele, F. G., and Cepko, C. L. (1996). A subset of clones in the chick telencephalon arranged in rostrocaudal arrays. *Curr. Biol.* 6, 1685–1690.

Szele, F. G., and Chesselet, M. F. (1996). Cortical lesions induce an increase in cell number and PSA-N-CAM expression in the subventricular zone of adults rats. *J. Comp. Neurol.* 368, 439–454.

Szele, F. G., Dowling, J. J., Gonzales, C., Theveniau, M., Rougon, G., and Chesselet, M. F. (1994). Pattern of expression of highly polysialylated neural cell adhesion molecule in the developing and adult rat striatum. *Neuroscience* 60, 133–144.

Tabata, H., and Nakajima, K. (2003). Multipolar migration: the third mode of radial neuronal migration in the developing cerebral cortex. *J. Neurosci.* 23, 9996–10001.

Thomas, L. B., Gates, M. A., and Steindler, D. A. (1996). Young neurons from the adult subependymal zone proliferate and migrate along an astrocyte, extracellular matrix-rich pathway. *Glia* 17, 1–14.

Tomasiewicz, H., Ono, K., Yee, D., Thompson, C., Goridis, C., Rutishauser, U., and Magnuson, T. (1993). Genetic deletion of a neural cell adhesion molecule variant (N-CAM-180) produces distinct defects in the central nervous system. *Neuron* 11, 1163–1174.

Tsai, L. H., and Gleeson, J. G. (2005). Nucleokinesis in neuronal migration. *Neuron* 46, 383–388.

Walker, A., Goings, G., Kim, Y., Miller, R. J., Chen, A., Szele, F. (2011). Nestin reporter transgene labels multiple central nervous system precursor cells. *Neural Plast.* 2010, Article ID 894374.

Wichterle, H., Garcia-Verdugo, J. M., and Alvarez-Buylla, A. (1997). Direct evidence for homotypic, glia-independent neuronal migration. *Neuron* 18, 779–791.

Yamaguchi, M., Saito, H., Suzuki, M., and Mori, K. (2000). Visualization of neurogenesis in the central nervous system using nestin promoter-GFP transgenic mice. *Neuroreport* 11, 1991–1996.

Yang, H. K., Sundholm-Peters, N. L., Goings, G. E., Walker, A. S., Hyland, K., and Szele, F. G. (2004). Distribution of doublecortin expressing cells near the lateral ventricles in the adult mouse brain. *J. Neurosci. Res.* 76, 282–295.

Young, K. M., Fogarty, M., Kessaris, N., and Richardson, W. D. (2007). Subventricular zone stem cells are heterogeneous with respect to their embryonic origins and neurogenic fates in the adult olfactory bulb. *J. Neurosci.* 27, 8286–8296.

Zhang, R. L., Chopp, M., Gregg, S. R., Toh, Y., Roberts, C., Letourneau, Y., Buller, B., Jia, L., Davarani, S. P. N., and Zhang, Z. G. (2009). Patterns and dynamics of subventricular zone neuroblast migration in the ischemic striatum of the adult mouse. *J. Cereb. Blood Flow Metab.* 29, 1240–1250.

Zipfel, W. R., Williams, R. M., and Webb, W. W. (2003). Nonlinear magic: multiphoton microscopy in the biosciences. *Nat. Biotechnol.* 21, 1369–1377.

Conflict of Interest Statement: The authors declare that the research was conducted in the absence of any commercial or financial relationships that could be construed as a potential conflict of interest.

Received: 26 January 2011; accepted: 24 February 2011; published online: 21 March 2011.

Citation: James R, Kim Y, Hockberger PE and Szele FG (2011) Subventricular zone cell migration: lessons from quantitative two-photon microscopy. Front. Neurosci. ***5****:30. doi: 10.3389/fnins.2011.00030*

This article was submitted to Frontiers in Neurogenesis, a specialty of Frontiers in Neuroscience.

frontiers in
NEUROSCIENCE

REVIEW ARTICLE
published: 09 May 2011
doi: 10.3389/fnins.2011.00067

In vivo monitoring of adult neurogenesis in health and disease

Sebastien Couillard-Despres[1], Ruth Vreys[2], Ludwig Aigner[1] and Annemie Van der Linden[2]*

[1] *Institute of Molecular Regenerative Medicine, Paracelsus Medical University, Salzburg, Austria*
[2] *Bio-Imaging Lab, Department of Biomedical Sciences, University of Antwerp, Antwerp, Belgium*

Edited by:
Silvia De Marchis, University of Turin, Italy

Reviewed by:
Jason Lerch, Toronto Center for Phenogenomics, Canada
Maurice Curtis, Auckland University, New Zealand

****Correspondence:***
Annemie Van der Linden, Bio-Imaging Lab, University of Antwerp, Universiteitsplein 1, B-2610 Antwerpen (Wilrijk), Belgium.
e-mail: annemie.vanderlinden@ua.ac.be

Adult neurogenesis, i.e., the generation of new neurons in the adult brain, presents an enormous potential for regenerative therapies of the central nervous system. While 5-bromo-2′-deoxyuridine labeling and subsequent histology or immunohistochemistry for cell-type-specific markers is still the gold standard in studies of neurogenesis, novel techniques, and tools for *in vivo* imaging of neurogenesis have been recently developed and successfully applied. Here, we review the latest progress on these developments, in particular in the area of magnetic resonance imaging (MRI) and optical imaging. *In vivo in situ* labeling of neural progenitor cells (NPCs) with micron-sized iron oxide particles enables longitudinal visualization of endogenous progenitor cell migration by MRI. The possibility of genetic labeling for cellular MRI was demonstrated by using the iron storage protein ferritin as the MR reporter-gene. However, reliable and consistent results using ferritin imaging for monitoring endogenous progenitor cell migration have not yet been reported. In contrast, genetic labeling of NPCs with a fluorescent or bioluminescent reporter has led to the development of some powerful tools for *in vivo* imaging of neurogenesis. Here, two strategies, i.e., viral labeling of stem/progenitor cells and transgenic approaches, have been used. In addition, the use of specific promoters for neuronal progenitor cells such as doublecortin increases the neurogenesis-specificity of the labeling. Naturally, the ultimate challenge will be to develop neurogenesis imaging methods applicable in humans. Therefore, we certainly need to consider other modalities such as positron emission tomography and proton magnetic resonance spectroscopy (^{1}H-MRS), which have already been implemented for both animals and humans. Further improvements of sensitivity and neurogenesis-specificity are nevertheless required for all imaging techniques currently available.

Keywords: neurogenesis, MRI, MRS, PET, bioluminescence, fluorescence, optical imaging, MPIO

INTRODUCTION

The existence of adult neurogenesis in the mammalian brain has been demonstrated almost half of a century ago (Altman and Das, 1965), nevertheless, broad attention to this process only arose after the discovery of pools of neural stem-like cells residing in discrete brain regions (Reynolds and Weiss, 1992). In most adult mammals, proliferating neural stem cells can be detected in two neurogenic niches, the subventricular zone (SVZ) of the lateral ventricle wall and the subgranular zone (SGZ) of the hippocampal dentate gyrus (see Ma et al., 2009 for a recent review). The SVZ constitutes the most active site of neurogenesis (Conover and Allen, 2002). Young neural progenitor cells (NPCs), also known as neuroblasts, are generated throughout the entire SVZ and subsequently migrate along the rostral migratory stream (RMS) into the olfactory bulb (OB) where they differentiate into new interneurons (Lois and Alvarez-Buylla, 1994). In the SGZ, neurogenesis occurs at a lower rate compared to the SVZ (Altman and Das, 1965; Cameron et al., 1993) and, in contrast to the SVZ-derived neuroblasts, new neurons of the SGZ migrate only short distances into the overlying granule cell layer (Stanfield and Trice, 1988; Markakis and Gage, 1999). Great hope followed the discovery that active populations of neural stem cells also generate new neurons within the adult human brain (Eriksson et al., 1998). Endogenous stem cell-based therapy for neuroregeneration after brain injury appeared suddenly nearer.

Clinical and preclinical studies have shown that adult neurogenesis is altered in response to brain insults with neuronal death. For example, ischemic lesions stimulate cell proliferation in the SVZ and the SGZ (Parent et al., 1997; Liu et al., 1998; Jin et al., 2001; Zhang et al., 2001; Arvidsson et al., 2002). Furthermore, it has been reported that new neurons migrate to non-neurogenic regions lining the ischemic lesion sites (Magavi et al., 2000; Arvidsson et al., 2002; Parent et al., 2002).

Postmortem studies on patients suffering from Huntington's disease (HD) demonstrated increased cell proliferation in the neurogenic regions (Curtis et al., 2003, 2005). Nonetheless, failure of the reparative process has been observed in animal models of HD (Lazic et al., 2004; Gil et al., 2005; Kohl et al., 2007; Kandasamy et al., 2010). Impaired neurogenesis was also found in several other neurodegenerative disorder models, such as models of Parkinson's disease and Alzheimer's disease (Haughey et al., 2002; Hoglinger et al., 2004; Wen et al., 2004; Donovan et al., 2006; Winner et al., 2008). In addition to modulating cell proliferation, pathological conditions might severely compromise the survival capacity of newly generated neurons. Recent studies have indicated a decrease of the long-term survival chance of newborn neurons by more than 80% (Winner et al., 2004, 2008; Kohl et al., 2007; Marxreiter et al., 2009; Kandasamy et al., 2010). These observations underscore the incapacity of the endogenous mechanisms to achieve

brain repair after injuries of the central nervous system. Our understanding of neurogenesis and its potential for functional brain repair still remain rudimentary.

A significant fraction of our knowledge of adult neurogenesis has been gained so far from static analyses. For example, the most prevailing technique to assess neurogenesis consists in injecting the thymidine analog 5-bromo-2′-deoxyuridine (BrdU), which integrate in newly synthesized DNA of proliferating cells. As further immunohistological analyses are required for the detection and phenotyping of cells labeled with BrdU, neurogenesis measurements are restricted to a single time point per individual. In order to understand the functional relevance of neurogenesis modulation and its potential role in the etiology of neurological and psychiatric disorders, it is required to assess neurogenesis repeatedly in a fashion as minimally invasive as possible. Consequently, over the past years sustained effort has been dedicated to develop imaging techniques to monitor adult neurogenesis *in vivo*.

From a clinical perspective, it would be advantageous to develop imaging procedures based on the use of currently available equipment, i.e., magnetic resonance imaging (MRI) and positron emission tomography (PET), as it could be more readily implanted in the clinics. Yet, for preclinical research, the exorbitant costs associated with these imaging devices limit their accessibility. The development of optical imaging procedures and devices partially filled the needs for low-cost imaging alternatives. This review summarizes the recent progress made in the field of *in vivo* imaging of neurogenesis and points to the strengths and weaknesses of the various strategies (**Table 1**).

IN VIVO IMAGING OF NEUROGENESIS WITH MAGNETIC RESONANCE IMAGING AND SPECTROSCOPY

The main advantage of MRI is its high spatial resolution that results in clear anatomical information. MRI uses a high magnetic field to align the nuclear magnetization of hydrogen atoms, or protons, of water in the body. Submitting a radio frequency pulse at the resonance frequency of these protons will cause the net magnetic vector to turn over into the plane perpendicular with the magnetic field. The oscillation of this net magnetic vector about the main magnetic field will induce an electromotive force in the radio frequent (RF) antenna, i.e., the MR signal. Depending on the applied MRI pulse sequence, a specific MRI parameter will dominate the contrast in the images (i.e., contrast weighting). For most clinical examinations both T_1-weighted and T_2-weighted images are acquired for observation of white and gray matter brain structures. Other types of MRI contrast correlate with the diffusion of water molecules (i.e., Brownian motion) in biological tissues (Le Bihan et al., 1986) and are quite valuable in studying neuropathology related changes in intra/extracellular water balance and subcellular structural changes (Gass et al., 2001).

Magnetic resonance imaging contrast can be improved by applying contrast agents based on relaxivity (e.g., gadolinium chelates) or magnetic susceptibility (e.g., iron oxide particles, iron containing proteins). When placed in a magnetic field, iron oxide particles have been shown to induce local field inhomogeneities. These inhomogeneities shorten the T_2 relaxation time of protons within a large perimeter, which results in hypointense (dark) signals in conventional T_2/T_2*-weighted imaging and therefore iron oxide particles are referred to as MRI-negative contrast agents (Norman et al., 1992; Bulte et al., 1999).

DIRECT LABELING USING IRON OXIDE PARTICLES

In order to enable cellular MRI, cells of interest have to be labeled with MR contrast agents. One of the options is the use of exogenous contrast agents. Numerous reports have demonstrated that iron oxide particles (from nanometer to micrometer size range) could be readily engulfed *in vitro* by cells of various origins, including neural stem and progenitor cells (for excellent reviews see Bulte et al., 2002; Bulte and Kraitchman, 2004; Frank et al., 2004; Modo et al., 2005). This approach constitutes an efficient strategy to label cells for detection as negative contrast. Results from agar phantoms containing iron oxide particle-labeled cells at various densities suggested that detection down to a single cell might be possible using high-resolution MRI (Kustermann et al., 2008). Previous studies

Table 1 | Comparison of various imaging methods for *in vivo* monitoring of adult neurogenesis.

Technique	**Optical Imaging**	**PET**	**MRI**			
Resolution	Low	Low	High			
Sensitivity	Limited depth penetration	High	High			
Human applicability	No	Yes	Yes			
Method	**Fluorescence-based imaging**	**Bioluminescence-based imaging**	**Isotope-labeled molecules**	**Iron oxide particles**	**MR reporter-genes**	**MR spectroscopy**
Technique	Genetic labeling	Genetic labeling	Direct labeling	Direct labeling	Genetic labeling	/
Neurogenesis-specificity	High with use of specific promoters	High with use of specific promoters	Low	Low	High with use of specific promoters	Low
Toxicity	No	No	?	Yes	?	No
Cell-viability	Yes	Yes	Yes	No	Yes	Yes
Limitations	Signal scatter, background fluorescence	Signal scatter	Exposure to radiation	Inhomogeneity artifact, contrast dilution upon cell division	Low detection-sensitivity	Partial volume artifact

? = remains to be determined; / = no labeling required.

have also shown that MRI is a useful tool to follow labeled, transplanted cell migration in the brain (Hoehn et al., 2002; Jendelova et al., 2003; Ben-Hur et al., 2007; Cohen et al., 2010).

Based on the observations that neural stem and progenitor cells could be loaded with iron oxide particles *in vitro*, various groups intended to label these cell populations by injecting iron oxide particles directly into the lateral ventricles (Shapiro et al., 2006a; Panizzo et al., 2009; Sumner et al., 2009; Vreys et al., 2010) or in the subventricular regions (Nieman et al., 2010; Vreys et al., 2010). This *in situ* labeling strategy proved to be successful, as a fraction of the injected particles were taken up by neuroblasts and carried away toward the OB (**Figure 1**). Hence permitting to follow neuronal migration along the RMS and into the OB as a read-out for neurogenesis and/or cell survival and migration.

Despite the valuable information on cell localization and migration dynamics, studies based on iron oxide labeled cells have several intrinsic limitations, with the most relevant one being the fact that iron oxide particles are passive contrast agents. The detected contrast on MR images refers only to the particle, and does not give any information on the cell-type or viability of the labeled cells, which leads to the possibility of non-specific findings (Slotkin et al., 2007; Schafer, 2010). Considering that more than half of the newly generated neurons die as they fail to integrate in their target regions (Winner et al., 2002; Kempermann et al., 2003), the extensive release of confounding particles arising from this cellular pruning would be far from incidental. Following death of the former carrier-cells, intracellular contrast particles will simply get deposited extracellular. These particles could be taken up by surrounding cells, such as microglia, and be carried away in an absolutely neurogenesis-independent fashion. Moreover, extracellular particles can be transported on cell surfaces and thereby migrate away from the injection site. Vreys et al. (2011) investigated the ability of magnetoliposomes (MLs) to label endogenous NPCs after direct injection into the adult mouse brain. Whereas MRI revealed contrast relocation toward the OB, the relocation was found to be independent of the migration of endogenous NPCs and represented background migration of MLs along white matter tracts. It was suggested that the small size of the MLs intrinsically limits their potential for *in situ* labeling of NPCs (Vreys et al., 2011).

Another limitation of particle-based cell labeling is the progressive dilution of the contrast medium with cell division. Cellular uptake of iron oxide particles occurs through endocytosis, which results in the accumulation of particles in the cytoplasm. As a result, the concentration of iron oxide particles halves with every cell division, leading to a progressive decrease in sensitivity to detect labeled cells (Magnitsky et al., 2005). While the use of micron-sized iron oxide particles (MPIOs) allows visualization of cells containing a single particle (Shapiro et al., 2006b), cell progeny after further proliferation of the cells will not be labeled with contrast particles. This dilution effect upon cell division is a major drawback for the longitudinal follow-up of highly proliferating cells.

In case of direct *in situ* labeling, the labeling efficiency is quite low and only a small fraction of targeted cells will be labeled with the contrast agent (Sumner et al., 2009; Nieman et al., 2010). In addition, the engulfment of iron oxide particles is rather unspecific. For example, immunohistochemistry and electron microscopy showed that after direct injection of MPIOs in the lateral ventricle, contrast particles were not only located inside the targeted cell-type, i.e., neural stem and progenitor cells, but also in ependymal cells, microglia, and oligodendrocyte progenitor cells (Shapiro et al., 2006a; Sumner et al., 2009). Careful analysis of the nature of labeled cells suggests that the site of injection is defining the subpopulation of cells labeled with the contrast particles (Nieman et al., 2010). The fact that the phenotype of cells internalizing the particles can only be determined *a posteriori* by histological analysis, is particularly troublesome for longitudinal studies, taken that labeled neural stem and progenitor cells are multipotent and may undergo extensive differentiation processes comprising multiple transient maturation stages.

Currently, the use of *in situ* labeling of endogenous neural stem and progenitor cells is restricted to the neurogenic niche of the SVZ. The reason for this restriction is that the amount of iron oxide particles required for *in situ* labeling generates substantial

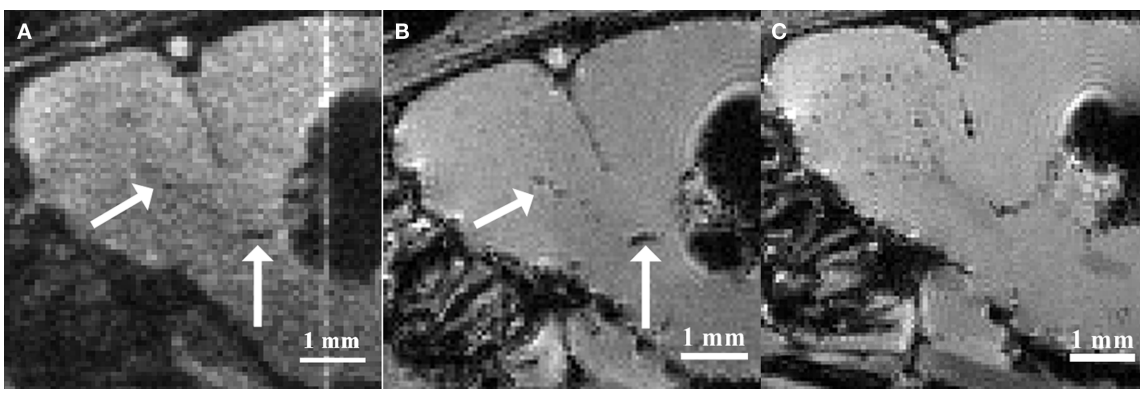

FIGURE 1 | Magnetic resonance imaging of *in situ* labeled neural precursor cell migration. (A) *In vivo* MRI of a mouse injected with micron-sized iron oxide particles in the lateral ventricle at 3 weeks post-injection. **(B)** *Ex vivo* MRI of the same mouse at 3 weeks post-injection. **(C)** *Ex vivo* MRI of a mouse injected with micron-sized iron oxide particles in the lateral ventricle at 8 weeks post-injection. Arrows indicate corresponding hypointense contrast on the *in vivo* and *ex vivo* MRI of the same mouse (Adapted and reproduced from Vreys et al., 2010).

image distortion, i.e., susceptibility inhomogeneity, at the site of injection (Shapiro et al., 2006a; Vreys et al., 2010). As neuroblasts from the SGZ migrate into the directly overlying granule cell layer, the susceptibility inhomogeneity would hamper the visualization of the labeled cell migration.

Cell labeling using non-degradable iron oxide particles, such as MPIOs, is permanent, and careful evaluation of long-term toxicity caused by labeling compounds becomes critical. Although limited toxicity has been demonstrated following *in vitro* labeling (Crabbe et al., 2010), studies on *in vivo* application of iron oxide particles have recently revealed decreased cell proliferation and migration, as well as signs of inflammation (Schafer, 2010; Vreys et al., 2010). Unfortunately, in most reports the assessments of the impact of iron oxide particles on gene expression and cell fate have remained cursory.

The majority of studies on MR imaging of endogenous neural stem and progenitor cells are performed so far in naive and healthy animals. A recent study showed that *in situ* labeling of endogenous neural stem and progenitors cells with MPIOs could reveal altered cell migration toward an hypoxic–ischemic insult using *in vivo* MRI (Yang et al., 2009). The proof-of-principle should now be extended to various disease models. Undoubtedly, the feasibility of iron oxide particle labeling for long-term imaging of neurogenesis in clinically relevant applications should be fully investigated. It is expected that the modified cell composition of the neurogenic niche (e.g., presence of reactive gliosis, macrophage infiltrations, etc.) as observed in pathological conditions as well as the possibility of reduced survival of new neurons induced by the pathological conditions, as mentioned earlier, would complicate neurogenesis-specific labeling and its intended imaging.

GENETIC LABELING USING MRI REPORTER-GENES

In order to overcome the disadvantages of iron oxide particle labeling, a new approach using MRI reporter-genes has recently been developed. Genetic reporters can be incorporated in gene delivery systems like viral vectors or in transgenic animals. This labeling approach solves the problem of contrast agent dilution and subsequent signal loss upon cell division. In addition, vector-mediated reporter-gene delivery holds the potential for specific labeling of neuroblasts by the use of specific promoters. Another advantage is that the transgene construct can be coupled with an additional transgene, for example a therapeutic one, or with other reporter-genes for multimodality imaging.

A promising reporter for MRI is ferritin, a ubiquitously expressed metalloprotein, assembled out of 24 light and heavy subunits (Cohen et al., 2005; Genove et al., 2005). Ferritin sequesters endogenous iron from the organism and stores it in a hydrated iron oxide (ferrihydrite) core that significantly affects the T_2 relaxation times of protons (Gossuin et al., 2004). The corresponding changes in contrast on T_2- and T_2*-weighted MR images could be a quantitative read-out for both neuronal proliferation and recruitment to the target region. Furthermore, the absence of image distortion (such as seen at the iron oxide particle injection area) would allow targeting the dentate gyrus of the hippocampus as well as the SVZ. To date, however, the low detection-sensitivity limits the use of current transgenic systems in cell tracking applications (Vande Velde et al., 2011). It was also reported that the viral vector systems used as delivery systems themselves can elicit ferritin-like hypointense contrast on MR images (Vande Velde et al., 2011). Enhancement of the sensitivity of MR reporter systems will remain a challenge and future studies should focus not only on optimization of the vector constructs for the delivery of MR reporter-genes, but also on improving the sensitivity to detect reporter-gene based contrast both at the acquisition and at the post-processing level.

Another MRI reporter candidate is *magA*, a gene known to be involved with iron transport in magnetotactic bacteria. Zurkiya et al. (2008) and Goldhawk et al. (2009) demonstrated that *magA* transfected mammalian cells formed *in vivo* magnetic iron oxide nanoparticles which allowed subsequent visualization of the cells with MRI (Zurkiya et al., 2008; Goldhawk et al., 2009). Whether *magA* is an appropriate MRI reporter-gene for endogenous stem cell labeling needs to be further investigated.

Although these approaches are attractive in that they combine the cell specificity of the transgenic system with the high-resolution of MR imaging, possible toxicity associated with the accumulation of iron in the cytoplasm must be carefully evaluated. Evidence for toxicity has been provided by recent reports demonstrating that in a transgenic model, long-term expression of elevated ferritin levels in neurons may lead to age-associated neurodegeneration (Kaur et al., 2007, 2009).

MAGNETIC RESONANCE SPECTROSCOPY

Magnetic resonance spectroscopy (MRS) is an MR technique that can measure brain biochemistry. In this way, it adds nicely to other MRI applications as it provides metabolic information in addition to anatomical, physiological, functional, or molecular imaging information. Localized ^{1}H-MRS currently allows for the quantification of more than 18 ^{1}H containing metabolites *in vivo* (Pfeuffer et al., 1999). The complexity of an MR spectrum can be appreciated in **Figure 2** in which a region of an MR spectrum

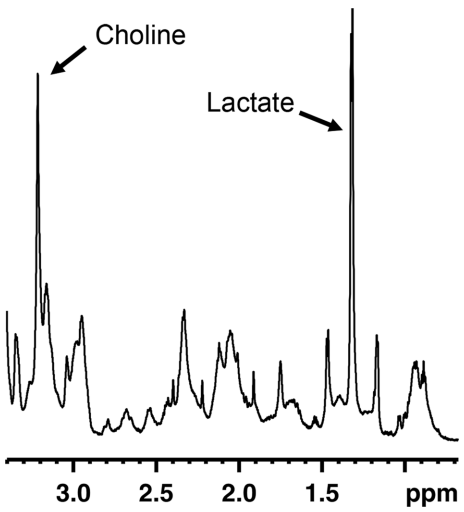

FIGURE 2 | Region of an MR spectrum generated from mouse fetal neural progenitor cells in culture. MRS reveals to complexity of metabolites found in these cells. Abundant molecules leading to strong signals, such as choline or lactate, can readily be identified.

measured on mouse fetal neural stem and progenitor cells is represented. Localized MRS techniques allow assessment of metabolites comprised in a well-defined volume/voxel within the brain and can return single-volume, or multi-volume information with microliter resolution. This constitutes an attractive strategy to appreciate the rate of neurogenesis in a non-invasive fashion. If there would be a molecule specific or enriched in the neurogenic niche, it would be theoretically possible to detect a spectroscopic signature proper to this molecule in voxels located within neurogenic regions. The intensity of the neurogenesis-associated peak would reveal the "concentration of neural stem or progenitor cells" within the voxel.

Manganas et al. (2007) reported the identification of an MRS peak, detected on the spectrum at 1.28 ppm, which seemed to correlate with the presence of neural stem/progenitor cells in the dentate gyrus of both humans and rats. *In vitro*, this peak was particularly abundant in undifferentiated neural stem cells, and appeared to be absent or weak in neurons, astrocytes, and oligodendrocytes. Interestingly, it was possible to detect and localize *in vivo* implanted neural stem cells in the cortex of rats, based on the 1.28-ppm peak. In addition, Manganas et al. (2007) demonstrated that in agreement with the expected age-related decrease of neurogenesis the intensity of the 1.28-ppm peak measured within the hippocampus was undergoing a dramatic decrease when comparing recordings performed in 8 to 10-year-old children with those of 30 to 35-year-old adults. Although the report from Manganas et al. (2007) promptly put MRS back into the limelight, several researchers question the specificity of the 1.28-ppm, as well as the capacity to detect the stem and progenitor cells using the equipment currently available (Friedman, 2008; Hoch et al., 2008; Jansen et al., 2008; Dong et al., 2009; Ramm et al., 2009). A recent study, which aimed to identify the origin of the 1.28-ppm peak, demonstrated that this spectroscopic signal correlates with the presence of mobile lipid droplets within cells (Ramm et al., 2009), a phenomenon observed during cell proliferation and apoptosis regardless of the cell-type (e.g., neural stem cells, COS7 cells, etc.). This may turn the 1.28-ppm signal into a correlated peak of the neurogenic niches rather than as a specific marker for neurogenesis *per se*.

The greatest advantage of MRS is the complete non-invasive nature of the protocol. For measurements in the SVZ, however, its close lining to the ventricles filled with cerebrospinal fluid constitutes an extra challenge. When an MRS voxel contains a mixture of tissue types the spectroscopic signal will also consist of signals from different tissues (i.e., a partial volume artifact). Since large voxel sizes are currently required to acquire sufficient signal-to-noise ratios, performing a reliable measurement of the SVZ is a difficult task. Further technical developments are warranted to reduce the voxel size targeted during spectroscopic analysis and to increase the sensitivity with the main objective to focus exclusively on neurogenic regions and thereby to increase the "stem cell concentration" and detectability.

IN VIVO IMAGING OF NEUROGENESIS WITH POSITRON EMISSION TOMOGRAPHY

Positron emission tomography might not have the resolution of MRI, however, it shows an extraordinary sensitivity, which is a powerful advantage considering the relatively scarceness of stem cells in the adult brain. PET relies on the administration of radioactive isotope-labeled molecules designed to bind to or concentrate themselves at the specified target sites. Positron-emitting radionuclides, such as [^{18}F] or [^{11}C], are selected for labeling since upon annihilation of a positron with an electron from the body, two gamma photons with an energy of 511 keV are emitted in diametrically opposite directions. Registration of these so-called coincident photons, i.e., pairs of photons reaching quasi simultaneously the sensitive photodetectors ringing the subject, allows for the computation of position and intensity of the emission source(s).

Rueger et al. (2010) recently reported the *in vivo* detection of cell proliferation within the rat neurogenic niches based on 3′-deoxy-3′-[^{18}F]fluoro-L-thymidine ([^{18}F]-FLT) signals (**Figure 3**). [^{18}F]-FLT is a thymidine analog and can be regarded as a PET equivalent to BrdU used in histological analysis. Even though Rueger et al. (2010) also reported that modulated proliferation rates following pharmacological or surgical interventions could be detected, [^{18}F]-FLT signal intensities emanating from the SVZ and SGZ appeared similar to each other although it is known that the magnitude of proliferation in the SVZ is from one to two orders higher than in the SGZ. Hence, these findings suggest that binding of [^{18}F]-FLT is determined by additional parameters than solely neural stem and progenitor cell proliferation. Thus, great care should be taken when comparing signals from different sources.

Furthermore, some other issues remain to be resolved before PET can be reliably used to monitor neurogenesis *in vivo*. For example, the identity of cells at the origin of the [^{18}F]-FLT signals cannot be inferred by this technique. This precludes the use of [^{18}F]-FLT for neurogenesis imaging under pathological conditions, since proliferation associated with reactive gliosis or immune cell infiltrations would be indistinguishable from neural stem/progenitor cell proliferation. Nonetheless, the work of Rueger et al. (2010) constitutes a valuable proof-of-principle that PET could be used for *in vivo* imaging of neurogenesis in the future. The development of neurogenesis-specific labeling compounds currently constitutes an important limiting step for this achievement.

IN VIVO IMAGING OF NEUROGENESIS WITH OPTICAL IMAGING

Over the last decade, optical imaging techniques became widespread in numerous preclinical research fields, including the study of neurogenesis. The possibility to combine several labels simultaneously, as well as the broad availability of current transgenic technologies, made optical imaging a very attractive method. Optical imaging can be based on the detection of fluorescent or bioluminescent signals, both bearing their strengths and limitations.

FLUORESCENCE-BASED IMAGING OF NEUROGENESIS

The simplicity of fluorescence-based imaging and the minimal requirement in equipment explain the extensive usage of this technique. The method is based on the capacity of some fluorescent molecules to reflect specific incident wavelengths with a red shift. The incident and reflected light can be separated using an appropriate sets of passfilters. Components for fluorescence imaging are frequently coupled with microscopes, resulting in an imaging resolution at the level of the cell and even subcellular elements (**Figure 4**). This high-resolution is an advantage for the study of neurogenesis, since not only the position and amount of cells, but

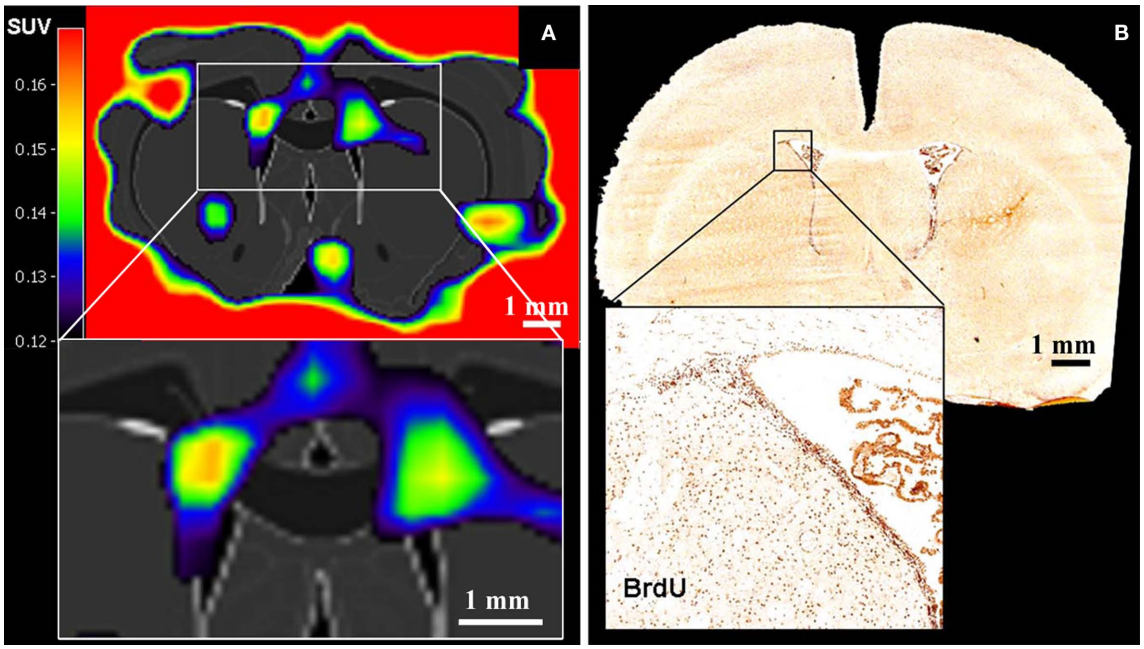

FIGURE 3 | Positron emission tomography imaging of neural stem cell proliferation ([18F]-FLT–PET matched on MRI-atlas of rat brain). (A) Increased [18F]-FLT signal was detected in the SVZ. **(B)** Location of BrdU-labeled proliferating cells in the SVZ corresponds well with the elevated [18F]-FLT signal in the SVZ **(A)** (Adapted from Rueger et al., 2010).

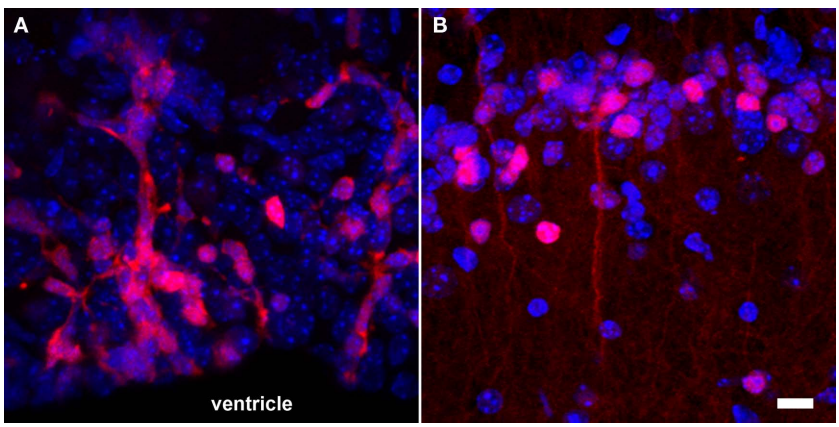

FIGURE 4 | Fluorescence-based imaging of neurogenesis using transgenic expression of DsRed under the control of the doublecortin promoter. (A) A large number of neuronal precursors (red) are generated in the SVZ and migrate in toward the olfactory bulb along the RMS; **(B)** once neuroblasts (red) reach the granular cell layer of the olfactory bulb, they start to functionally integrate and have a more complex cellular morphology. Nuclei appear in blue. Scale bar = 10 μm.

also the morphology and the integration of newly generated neurons are highly relevant. However, high-resolution fluorescence imaging can only be performed on relatively thin samples. As a result, neurogenesis is generally analyzed on acute brain slices, which can be maintained alive *in vitro* for only a few hours. In case of whole body *in vivo* imaging, where animals are placed in a dark chamber equipped with an illumination source and a sensitive photodetector system, the spatial resolution is rather low because the light reflected from deep structures is scattered before it reaches the body surface.

The use of fluorescent protein expression, such as the green fluorescent protein (GFP), was a breakthrough for *in vivo* imaging of biological processes (Heim et al., 1994). Fluorescent reporters have the advantage that once encoding transgenes have been introduced within the genome, fluorescent signals are generated throughout life without further need for additional labeling. Transgenic mouse and rat models for the analysis of neurogenesis have been generated over the last years using cell-type-specific promoters to control the expression of various fluorescent proteins. For example, transgenic models have been developed using the nestin and the doublecortin

promoters to detect neural stem and progenitor cells respectively (Yamaguchi et al., 2000; Karl et al., 2005; Couillard-Despres et al., 2006, 2008b; Ladewig et al., 2008). Besides the transgenic models, the delivery of retroviral vectors encoding fluorescent proteins to neurogenic regions has also been fruitfully exploited (Carleton et al., 2003; van Praag et al., 2005; Toni et al., 2008). Taking advantage of the proliferation capacity of neural stem and progenitor cells, it is possible to label a sub-population of these cells permanently and rather selectively using retroviral vectors. Moreover, using the fluorescent signal to target recording electrodes, synaptic integration of newly generated neurons can be investigated by electrophysiology (Carleton et al., 2003; Couillard-Despres et al., 2006; Toni et al., 2008).

One general concern for *in vivo* fluorescent imaging is the autofluorescence of biological tissues. In addition, the shallow tissue penetration at which high quality imaging is currently achievable by *in vivo* fluorescence imaging constitutes a major hindrance to the analysis of neurogenesis. Even in relatively small animals such as mice, the hippocampus and subventricular regions are too deep within the brain for conventional microscopy. Significant improvement has already been obtained using multiphoton confocal microscopy, which expands the observation window to a depth of approximately 500 μm (Fuhrmann et al., 2007), yet this is barely enough for the analysis of the mouse cerebral cortex. Furthermore, signal scattering will always be a limiting factor for accurate recording, especially when light is reflected from regions lying deep in tissues. Thus the cellular resolution of fluorescence imaging obtained *in vitro* using conventional microscopy is beyond the limits of current whole body *in vivo* imaging. Optical tomography, might significantly improve the quality and precision of fluorescence imaging, in a fashion similar to PET acquisitions (Garofalakis et al., 2007). To improve the detectability of fluorescent reporters, bright red-shifted fluorescent proteins, such as tdTomato, mCherry, mPlum, or Katushka have been developed over the last years to take advantage of a good light transmission window in the far-red region of the visible light spectrum, from approximately 600 to 850 nm (Shaner et al., 2004; Deliolanis et al., 2008).

BIOLUMINESCENCE-BASED IMAGING OF NEUROGENESIS

The use of various luciferase reporter-genes for bioluminescent optical imaging is another technique that has recently gained interest. Enzymes of the luciferase family are not evolutionary related, but they all cause photons to be emitted upon catalysis of their respective substrates. These photons can be acquired and processed for imaging purposes. The luciferase isolated from the firefly (*Photinus pyralis*) and the sea pansy (*Renilla reniformis*) are the most widely distributed among the various luciferases identified and cloned so far. However, the substrate catalyzed by the *Renilla* luciferase, i.e., coelenterazine, presents an imidazopyrazine structure that can promptly auto-oxidize. This auto-degradation process is further enhanced by the presence of albumin (Zhao et al., 2004). Thus, the structural instability of coelenterazine could lead to elevated background signals during *in vivo* imaging of weak reporter activities. In addition, coelenterazine can be re-transported out of cells by the multidrug resistance MDR1 P-glycoprotein (Pgp), which could generate unforeseen variability in signal intensities between various cell populations exposed to the same extracellular coelenterazine concentration (Pichler et al., 2004). Therefore, the firefly's luciferase is currently the most broadly used enzyme for *in vivo* bioluminescence imaging in mice and rats.

During *in vivo* bioluminescence imaging, animals are placed in a dark chamber equipped with an extremely sensitive photodetector system. In contrast to fluorescent imaging, the appropriate substrate (e.g., D-luciferin in the case of the firefly luciferase) needs to be injected shortly before recording in order to achieve a detectable bioluminescent signal. Since each organ or body compartment is supplied differently, the regional distribution, catalysis, and elimination kinetics of the substrate must be taken into account in the design and execution of the work (Lee et al., 2003).

The use of bioluminescence for imaging of neurogenesis resolves some problems discussed previously with the use of iron oxide particles in MRI. For example, bioluminescence recording guaranties viability of cells at the origin of the reporter signal since the generation of photons resulting from the catalysis of D-luciferin is ATP-dependent. In addition, there have been so far no reports on toxicity or inflammation elicited by the firefly's luciferase or its substrate d-luciferin. As a result, the impact on neurogenesis is assumed to be minimal. Nonetheless, this topic requires further investigation in order to fully verify this assumption.

Although the spatial resolution of bioluminescence imaging is similar to that of fluorescence imaging due to signal scatter from deep brain regions, it has one solid advantage over fluorescence-based imaging. The virtual absence of bioluminescence background from tissues allows for a greater sensitivity of detection, as required for neural stem and progenitor cells. Both grafting of transgenic neural stem cells and *in situ* retroviral labeling of endogenous neural stem cells in wild type mice have been shown to result in a very high signal/noise ratio (Couillard-Despres et al., 2008a; Reumers et al., 2008). The fate of a small group of transgenic neural stem cells implanted in the subventricular region of a wild type mouse could be followed over several days during their journey toward the OB (**Figure 5**). Moreover, the use of a neuronal precursor-specific promoter to drive luciferase expression, such as a doublecortin promoter, guarantees that the bioluminescence is neurogenesis-specific (Couillard-Despres et al., 2008a).

Even though the use of specific promoters can selectively target specific cell populations, such transgenic systems remain confined to preclinical research. Furthermore, given the large size of the

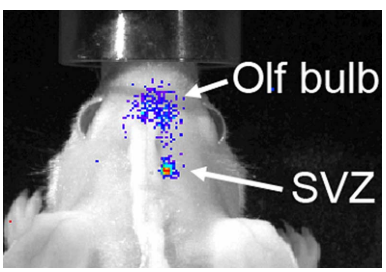

FIGURE 5 | Bioluminescence-based imaging of neurogenesis using grafted neural stem cells encoding a luciferase transgene under the control of the doublecortin promoter. Eight days after grafting in the SVZ of a wild type mouse, neuronal differentiation of implanted cells resulted into a strong bioluminescent signal. The latter partially spread from the site of graft toward the olfactory bulb as the transgenic neuroblasts migrated to their target.

human brain, it is unlikely that optical techniques will be suited for *in vivo* imaging of human neurogenesis. Nevertheless, optical imaging remains a powerful and valuable method in preclinical research for the *in vivo* imaging of neurogenesis.

CONCLUSION

Over the last decade, tremendous progress has been made in the development of strategies for *in vivo* imaging of neurogenesis. With the exception of MRS, all imaging modalities discussed in this review rely on either direct labeling (e.g., iron oxide particles, [^{18}F]-FLT) or indirect labeling (i.e., the use of reporter-genes) to achieve visualization of cells contributing to neurogenesis. Although both labeling strategies have shown their potentials for *in vivo* imaging, the major challenges to achieve are neurogenesis-specificity and detection-sensitivity for direct and indirect labeling respectively. Beside these challenges one must always carefully evaluate safety requirements. Therefore, the toxicity and interference associated with labels applied or genes expressed should be addressed with great care. Moreover, in cases of direct labeling, labels must not only be non-toxic, but in view of future clinical applications, should preferentially be biodegradable as well.

Although MRS does not encounter the problems related with cell labeling, proof of specific visualization of neurogenesis by this modality has still to be provided. Briefly, none of the imaging strategies has so far been able to fulfill all needs and expectations; they all have their advantages and disadvantages regarding sensitivity, tissue penetration, etc. Nonetheless, the different approaches available are rather to be considered as complementary.

Similar to the use of BrdU or tritiated-thymidine in the earlier neurogenesis studies, assessment of cell proliferation does not constitute a valid measurement of neurogenesis. At this time, improvement of the detection using direct or indirect labeling of neuronal precursors and young neurons, which reflects the rates of neurogenesis, constitutes the next challenge (Couillard-Despres et al., 2005). Finally, although preclinical settings offer the possibility to use transgenic reporter systems, which are powerful tools for the understanding of neurogenesis under physiological and pathological contexts, the development of neurogenesis imaging techniques applicable to human remains the ultimate goal.

ACKNOWLEDGMENTS

The authors are grateful to Paul Ramm for fruitful discussion and for providing graphical material. The authors also wish to thank Dr. Greetje Vande Velde for her help with the manuscript. This work was supported in part by the State Government of Salzburg (Austria), the Bavarian State Ministry of Sciences, Research and Arts (ForNeuroCell2 grant), Inter University Attraction Poles (IUAP-NIMI-P6/38), the Flemish institute supporting scientific-technological research in industry (IWT-60838 BRAINSTIM), the University of Antwerp (Concerted Research Actions funding), and the European Commission for EC-FP6 network DiMI (LSHB-CT-2005-512146).

REFERENCES

Altman, J., and Das, G. D. (1965). Autoradiographic and histological evidence of postnatal hippocampal neurogenesis in rats. *J. Comp. Neurol.* 124, 319–335.

Arvidsson, A., Collin, T., Kirik, D., Kokaia, Z., and Lindvall, O. (2002). Neuronal replacement from endogenous precursors in the adult brain after stroke. *Nat. Med.* 8, 963–970.

Ben-Hur, T., van Heeswijk, R. B., Einstein, O., Aharonowiz, M., Xue, R., Frost, E. E., Mori, S., Reubinoff, B. E., and Bulte, J. W. M. (2007). Serial in vivo MR tracking of magnetically labeled neural spheres transplanted in chronic EAE mice. *Magn. Reson. Med.* 57, 164–171.

Bulte, J. W., Brooks, R. A., Moskowitz, B. M., Bryant, L. H. Jr., and Frank, J. A. (1999). Relaxometry and magnetometry of the MR contrast agent MION-46L. *Magn. Reson. Med.* 42, 379–384.

Bulte, J. W., Duncan, I. D., and Frank, J. A. (2002). In vivo magnetic resonance tracking of magnetically labeled cells after transplantation. *J. Cereb. Blood Flow Metab.* 22, 899–907.

Bulte, J. W., and Kraitchman, D. L. (2004). Monitoring cell therapy using iron oxide MR contrast agents. *Curr. Pharm. Biotechnol.* 5, 567–584.

Cameron, H. A., Woolley, C. S., McEwen, B. S., and Gould, E. (1993). Differentiation of newly born neurons and glia in the dentate gyrus of the adult rat. *Neuroscience* 56, 337–344.

Carleton, A., Petreanu, L. T., Lansford, R., Alvarez-Buylla, A., and Lledo, P. M. (2003). Becoming a new neuron in the adult olfactory bulb. *Nat. Neurosci.* 6, 507–518.

Cohen, B., Dafni, H., Meir, G., Harmelin, A., and Neeman, M. (2005). Ferritin as an endogenous MRI reporter for noninvasive imaging of gene expression in C6 glioma tumors. *Neoplasia* 7, 109–117.

Cohen, M. E., Muja, N., Fainstein, N., Bulte, J. W. M., and Ben-Hur, T. (2010). Conserved fate and function of feruмoxides-labeled neural precursor cells in vitro and in vivo. *J. Neurosci. Res.* 88, 936–944.

Conover, J. C., and Allen, R. L. (2002). The subventricular zone: new molecular and cellular developments. *Cell. Mol. Life Sci.* 59, 2128–2135.

Couillard-Despres, S., Finkl, R., Winner, B., Ploetz, S., Wiedermann, D., Aigner, R., Bogdahn, U., Winkler, J., Hoehn, M., and Aigner, L. (2008a). In vivo optical imaging of neurogenesis: watching new neurons in the intact brain. *Mol. Imaging* 7, 28–34.

Couillard-Despres, S., Quehl, E., Altendorfer, K., Karl, C., Ploetz, S., Bogdahn, U., Winkler, J., and Aigner, L. (2008b). Human in vitro reporter model of neuronal development and early differentiation processes. *BMC Neurosci.* 9, 31. doi: 10.1186/1471-2202-9-31

Couillard-Despres, S., Winner, B., Karl, C., Lindemann, G., Schmid, P., Aigner, R., Laemke, J., Bogdahn, U., Winkler, J., Bischofberger, J., and Aigner, L. (2006). Targeted transgene expression in neuronal precursors: watching young neurons in the old brain. *Eur. J. Neurosci.* 24, 1535–1545.

Couillard-Despres, S., Winner, B., Schaubeck, S., Aigner, R., Vroemen, M., Weidner, N., Bogdahn, U., Winkler, J., Kuhn, H. G., and Aigner, L. (2005). Doublecortin expression levels in adult brain reflect neurogenesis. *Eur. J. Neurosci.* 21, 1–14.

Crabbe, A., Vandeputte, C., Dresselaers, T., Sacido, A. A., Verdugo, J. M. G., Eyckmans, J., Luyten, F. P., Van Laere, K., Verfaillie, C. M., and Himmelreich, U. (2010). Effects of MRI contrast agents on the stem cell phenotype. *Cell Transplant.* 19, 919–936.

Curtis, M. A., Penney, E. B., Pearson, A. G., van Roon-Mom, W. M., Butterworth, N. J., Dragunow, M., Connor, B., and Faull, R. L. (2003). Increased cell proliferation and neurogenesis in the adult human Huntington's disease brain. *Proc. Natl. Acad. Sci. U.S.A.* 100, 9023–9027.

Curtis, M. A., Penney, E. B., Pearson, J., Dragunow, M., Connor, B., and Faull, R. L. (2005). The distribution of progenitor cells in the subependymal layer of the lateral ventricle in the normal and Huntington's disease human brain. *Neuroscience* 132, 777–788.

Deliolanis, N. C., Kasmieh, R., Wurdinger, T., Tannous, B. A., Shah, K., and Ntziachristos, V. (2008). Performance of the red-shifted fluorescent proteins in deep-tissue molecular imaging applications. *J. Biomed. Opt.* 13, 044008.

Dong, Z., Dreher, W., Leibfritz, D., and Peterson, B. S. (2009). Challenges of using MR spectroscopy to detect neural progenitor cells in vivo. *AJNR Am. J. Neuroradiol.* 30, 1096–1101.

Donovan, M. H., Yazdani, U., Norris, R. D., Games, D., German, D. C., and Eisch, A. J. (2006). Decreased adult hippocampal neurogenesis in the PDAPP mouse model of Alzheimer's disease. *J. Comp. Neurol.* 495, 70–83.

Eriksson, P. S., Perfilieva, E., Bjork-Eriksson, T., Alborn, A. M., Nordborg, C., Peterson, D. A., and Gage, F. H. (1998). Neurogenesis in the adult human hippocampus. *Nat. Med.* 4, 1313–1317.

Frank, J. A., Anderson, S. A., Kalsih, H., Jordan, E. K., Lewis, B. K., Yocum, G. T., and Arbab, A. S. (2004). Methods for magnetically labeling

stem and other cells for detection by in vivo magnetic resonance imaging. *Cytotherapy* 6, 621–625.

Friedman, S. D. (2008). Comment on "magnetic resonance spectroscopy identifies neural progenitor cells in the live human brain." *Science* 321, 640.

Fuhrmann, M., Mitteregger, G., Kretzschmar, H., and Herms, J. (2007). Dendritic pathology in prion disease starts at the synaptic spine. *J. Neurosci.* 27, 6224–6233.

Garofalakis, A., Zacharakis, G., Meyer, H., Economou, E. N., Mamalaki, C., Papamatheakis, J., Kioussis, D., Ntziachristos, V., and Ripoll, J. (2007). Three-dimensional in vivo imaging of green fluorescent protein-expressing T cells in mice with noncontact fluorescence molecular tomography. *Mol. Imaging* 6, 96–107.

Gass, A., Niendorf, T., and Hirsch, J. G. (2001). Acute and chronic changes of the apparent diffusion coefficient in neurological disorders-biophysical mechanisms and possible underlying histopathology. *J. Neurol. Sci.* 186(Suppl. 1), S15–S23.

Genove, G., DeMarco, U., Xu, H., Goins, W. F., and Ahrens, E. T. (2005). A new transgene reporter for in vivo magnetic resonance imaging. *Nat. Med.* 11, 450–454.

Gil, J. M., Mohapel, P., Araujo, I. M., Popovic, N., Li, J. Y., Brundin, P., and Petersen, A. (2005). Reduced hippocampal neurogenesis in R6/2 transgenic Huntington's disease mice. *Neurobiol. Dis.* 20, 744–751.

Goldhawk, D. E., Lemaire, C., McCreary, C. R., McGirr, R., Dhanvantari, S., Thompson, R. T., Figueredo, R., Koropatnick, J., Foster, P., and Prato, F. S. (2009). Magnetic resonance imaging of cells overexpressing MagA, an endogenous contrast agent for live cell imaging. *Mol. Imaging* 8, 129–139.

Gossuin, Y., Muller, R. N., and Gillis, P. (2004). Relaxation induced by ferritin: a better understanding for an improved MRI iron quantification. *NMR Biomed.* 17, 427–432.

Haughey, N. J., Nath, A., Chan, S. L., Borchard, A. C., Rao, M. S., and Mattson, M. P. (2002). Disruption of neurogenesis by amyloid beta-peptide, and perturbed neural progenitor cell homeostasis, in models of Alzheimer's disease. *J. Neurochem.* 83, 1509–1524.

Heim, R., Prasher, D. C., and Tsien, R. Y. (1994). Wavelength mutations and posttranslational autoxidation of green fluorescent protein. *Proc. Natl. Acad. Sci. U.S.A.* 91, 12501–12504.

Hoch, J. C., Maciejewski, M. W., and Gryk, M. R. (2008). Comment on "magnetic resonance spectroscopy identifies neural progenitor cells in the live human brain." *Science* 321, 640.

Hoehn, M., Kustermann, E., Blunk, J., Wiedermann, D., Trapp, T., Wecker, S., Focking, M., Arnold, H., Hescheler, J., Fleischmann, B. K., Schwindt, W., and Buhrle, C. (2002). Monitoring of implanted stem cell migration in vivo: a highly resolved in vivo magnetic resonance imaging investigation of experimental stroke in rat. *Proc. Natl. Acad. Sci. U.S.A.* 99, 16267–16272.

Hoglinger, G. U., Rizk, P., Muriel, M. P., Duyckaerts, C., Oertel, W. H., Caille, I., and Hirsch, E. C. (2004). Dopamine depletion impairs precursor cell proliferation in Parkinson disease. *Nat. Neurosci.* 7, 726–735.

Jansen, J. F., Gearhart, J. D., and Bulte, J. W. (2008). Comment on "Magnetic resonance spectroscopy identifies neural progenitor cells in the live human brain." *Science* 321, 640.

Jendelova, P., Herynek, V., DeCroos, J., Glogarova, K., Andersson, B., Hajek, M., and Sykova, E. (2003). Imaging the fate of implanted bone marrow stromal cells labeled with superparamagnetic nanoparticles. *Magn. Reson. Med.* 50, 767–776.

Jin, K., Minami, M., Lan, J. Q., Mao, X. O., Batteur, S., Simon, R. P., and Greenberg, D. A. (2001). Neurogenesis in dentate subgranular zone and rostral subventricular zone after focal cerebral ischemia in the rat. *Proc. Natl. Acad. Sci. U.S.A.* 98, 4710–4715.

Kandasamy, M., Couillard-Despres, S., Raber, K. A., Stephan, M., Lehner, B., Winner, B., Kohl, Z., Rivera, F. J., Nguyen, H. P., Riess, O., Bogdahn, U., Winkler, J., von Horsten, S., and Aigner, L. (2010). Stem cell quiescence in the hippocampal neurogenic niche is associated with elevated transforming growth factor-beta signaling in an animal model of Huntington disease. *J. Neuropathol. Exp. Neurol.* 69, 717–728.

Karl, C., Couillard-Despres, S., Prang, P., Munding, M., Kilb, W., Brigadski, T., Plotz, S., Mages, W., Luhmann, H., Winkler, J., Bogdahn, U., and Aigner, L. (2005). Neuronal precursor-specific activity of a human doublecortin regulatory sequence. *J. Neurochem.* 92, 264–282.

Kaur, D., Rajagopalan, S., and Andersen, J. K. (2009). Chronic expression of H-ferritin in dopaminergic midbrain neurons results in an age-related expansion of the labile iron pool and subsequent neurodegeneration: implications for Parkinson's disease. *Brain Res.* 1297, 17–22.

Kaur, D., Rajagopalan, S., Chinta, S., Kumar, J., Di Monte, D., Cherny, R. A., and Andersen, J. K. (2007). Chronic ferritin expression within murine dopaminergic midbrain neurons results in a progressive age-related neurodegeneration. *Brain Res.* 1140, 188–194.

Kempermann, G., Gast, D., Kronenberg, G., Yamaguchi, M., and Gage, F. H. (2003). Early determination and long-term persistence of adult-generated new neurons in the hippocampus of mice. *Development* 130, 391–399.

Kohl, Z., Kandasamy, M., Winner, B., Aigner, R., Gross, C., Couillard-Despres, S., Bogdahn, U., Aigner, L., and Winkler, J. (2007). Physical activity fails to rescue hippocampal neurogenesis deficits in the R6/2 mouse model of Huntington's disease. *Brain Res.* 1155, 24–33.

Kustermann, E., Himmelreich, U., Kandal, K., Geelen, T., Ketkar, A., Wiedermann, D., Strecker, C., Esser, J., Arnhold, S., and Hoehn, M. (2008). Efficient stem cell labeling for MRI studies. *Contrast Media Mol. Imaging* 3, 27–37.

Ladewig, J., Koch, P., Endl, E., Meiners, B., Opitz, T., Couillard-Despres, S., Aigner, L., and Brustle, O. (2008). Lineage selection of functional and cryopreservable human embryonic stem cell-derived neurons. *Stem Cells* 26, 1705–1712.

Lazic, S. E., Grote, H., Armstrong, R. J., Blakemore, C., Hannan, A. J., van Dellen, A., and Barker, R. A. (2004). Decreased hippocampal cell proliferation in R6/1 Huntington's mice. *Neuroreport* 15, 811–813.

Le Bihan, D., Breton, E., Lallemand, D., Grenier, P., Cabanis, E., and Laval-Jeantet, M. (1986). MR imaging of intravoxel incoherent motions: application to diffusion and perfusion in neurologic disorders. *Radiology* 161, 401–407.

Lee, K. H., Byun, S. S., Paik, J. Y., Lee, S. Y., Song, S. H., Choe, Y. S., and Kim, B. T. (2003). Cell uptake and tissue distribution of radioiodine labelled D-luciferin: implications for luciferase based gene imaging. *Nucl. Med. Commun.* 24, 1003–1009.

Liu, J., Solway, K., Messing, R. O., and Sharp, F. R. (1998). Increased neurogenesis in the dentate gyrus after transient global ischemia in gerbils. *J. Neurosci.* 18, 7768–7778.

Lois, C., and Alvarez-Buylla, A. (1994). Long-distance neuronal migration in the adult mammalian brain. *Science* 264, 1145–1148.

Ma, D. K., Bonaguidi, M. A., Ming, G. L., and Song, H. (2009). Adult neural stem cells in the mammalian central nervous system. *Cell Res.* 19, 672–682.

Magavi, S. S., Leavitt, B. R., and Macklis, J. D. (2000). Induction of neurogenesis in the neocortex of adult mice. *Nature* 405, 951–955.

Magnitsky, S., Watson, D. J., Walton, R. M., Pickup, S., Bulte, J. W., Wolfe, J. H., and Poptani, H. (2005). In vivo and ex vivo MRI detection of localized and disseminated neural stem cell grafts in the mouse brain. *Neuroimage* 26, 744–754.

Manganas, L. N., Zhang, X., Li, Y., Hazel, R. D., Smith, S. D., Wagshul, M. E., Henn, F., Benveniste, H., Djuric, P. M., Enikolopov, G., and Maletic-Savatic, M. (2007). Magnetic resonance spectroscopy identifies neural progenitor cells in the live human brain. *Science* 318, 980–985.

Markakis, E. A., and Gage, F. H. (1999). Adult-generated neurons in the dentate gyrus send axonal projections to field CA3 and are surrounded by synaptic vesicles. *J. Comp. Neurol.* 406, 449–460.

Marxreiter, F., Nuber, S., Kandasamy, M., Klucken, J., Aigner, R., Burgmayer, R., Couillard-Despres, S., Riess, O., Winkler, J., and Winner, B. (2009). Changes in adult olfactory bulb neurogenesis in mice expressing the A30P mutant form of alpha-synuclein. *Eur. J. Neurosci.* 29, 879–890.

Modo, M., Hoehn, M., and Bulte, J. W. (2005). Cellular MR imaging. *Mol. Imaging* 4, 143–164.

Nieman, B. J., Shyu, J. Y., Rodriguez, J. J., Garcia, A. D., Joyner, A. L., and Turnbull, D. H. (2010). In vivo MRI of neural cell migration dynamics in the mouse brain. *Neuroimage* 50, 456–464.

Norman, A. B., Thomas, S. R., Pratt, R. G., Lu, S. Y., and Norgren, R. B. (1992). Magnetic resonance imaging of neural transplants in rat brain using a superparamagnetic contrast agent. *Brain Res.* 594, 279–283.

Panizzo, R. A., Kyrtatos, P. G., Price, A. N., Gadian, D. G., Ferretti, P., and Lythgoe, M. F. (2009). In vivo magnetic resonance imaging of endogenous neuroblasts labelled with a ferumoxide-polycation complex. *Neuroimage* 44, 1239–1246.

Parent, J. M., Vexler, Z. S., Gong, C., Derugin, N., and Ferriero, D. M. (2002). Rat forebrain neurogenesis and striatal neuron replacement after focal stroke. *Ann. Neurol.* 52, 802–813.

Parent, J. M., Yu, T. W., Leibowitz, R. T., Geschwind, D. H., Sloviter, R. S., and Lowenstein, D. H. (1997). Dentate granule cell neurogenesis is increased by seizures and contributes to aberrant network reorganization in the adult rat hippocampus. *J. Neurosci.* 17, 3727–3738.

Pfeuffer, J., Tkac, I., Provencher, S. W., and Gruetter, R. (1999). Toward an in vivo neurochemical profile: quantification of 18 metabolites in short-echo-time

(1)H NMR spectra of the rat brain. *J. Magn. Reson.* 141, 104–120.

Pichler, A., Prior, J. L., and Piwnica-Worms, D. (2004). Imaging reversal of multidrug resistance in living mice with bioluminescence: MDR1 P-glycoprotein transports coelenterazine. *Proc. Natl. Acad. Sci. U.S.A.* 101, 1702–1707.

Ramm, P., Couillard-Despres, S., Plotz, S., Rivera, F. J., Krampert, M., Lehner, B., Kremer, W., Bogdahn, U., Kalbitzer, H. R., and Aigner, L. (2009). A nuclear magnetic resonance biomarker for neural progenitor cells: is it all neurogenesis? *Stem Cells* 27, 420–423.

Reumers, V., Deroose, C. M., Krylyshkina, O., Nuyts, J., Geraerts, M., Mortelmans, L., Gijsbers, R., Van den Haute, C., Debyser, Z., and Baekelandt, V. (2008). Noninvasive and quantitative monitoring of adult neuronal stem cell migration in mouse brain using bioluminescence imaging. *Stem Cells* 26, 2382–2390.

Reynolds, B. A., and Weiss, S. (1992). Generation of neurons and astrocytes from isolated cells of the adult mammalian central nervous system. *Science* 255, 1707–1710.

Rueger, M. A., Backes, H., Walberer, M., Neumaier, B., Ullrich, R., Simard, M. L., Emig, B., Fink, G. R., Hoehn, M., Graf, R., and Schroeter, M. (2010). Noninvasive imaging of endogenous neural stem cell mobilization in vivo using positron emission tomography. *J. Neurosci.* 30, 6454–6460.

Schafer, R. (2010). Labeling and imaging of stem cells – promises and concerns. *Transfus. Med. Hemother.* 37, 85–89.

Shaner, N. C., Campbell, R. E., Steinbach, P. A., Giepmans, B. N., Palmer, A. E., and Tsien, R. Y. (2004). Improved monomeric red, orange and yellow fluorescent proteins derived from *Discosoma* sp. red fluorescent protein. *Nat. Biotechnol.* 22, 1567–1572.

Shapiro, E. M., Gonzalez-Perez, O., Garcia-Verdugo, J. M., Alvarez-Buylla, A., and Koretsky, A. P. (2006a). Magnetic resonance imaging of the migration of neuronal precursors generated in the adult rodent brain. *Neuroimage* 32, 1150–1157.

Shapiro, E. M., Sharer, K., Skrtic, S., and Koretsky, A. P. (2006b). In vivo detection of single cells by MRI. *Magn. Reson. Med.* 55, 242–249.

Slotkin, J. R., Cahill, K. S., Tharin, S. A., and Shapiro, E. M. (2007). Cellular magnetic resonance imaging: nanometer and micrometer size particles for noninvasive cell localization. *Neurotherapeutics* 4, 428–433.

Stanfield, B. B., and Trice, J. E. (1988). Evidence that granule cells generated in the dentate gyrus of adult rats extend axonal projections. *Exp. Brain Res.* 72, 399–406.

Sumner, J. P., Shapiro, E. M., Maric, D., Conroy, R., and Koretsky, A. P. (2009). In vivo labeling of adult neural progenitors for MRI with micron sized particles of iron oxide: quantification of labeled cell phenotype. *Neuroimage* 44, 671–678.

Toni, N., Laplagne, D. A., Zhao, C., Lombardi, G., Ribak, C. E., Gage, F. H., and Schinder, A. F. (2008). Neurons born in the adult dentate gyrus form functional synapses with target cells. *Nat. Neurosci.* 11, 901–907.

van Praag, H., Shubert, T., Zhao, C., and Gage, F. H. (2005). Exercise enhances learning and hippocampal neurogenesis in aged mice. *J. Neurosci.* 25, 8680–8685.

Vande Velde, G., Raman Rangarajan, J., Toelen, J., Dresselaers, T., Ibrahimi, A., Krylychkina, O., Vreys, R., Van der Linden, A., Maes, F., Debyser, Z., Himmelreich, U., and Baekelandt, V. (2011). Evaluation of the specificity and sensitivity of ferritin as an MRI reporter gene in mouse brain using lentiviral and adeno-associated viral vectors. *Gene Ther.* [Epub ahead of print].

Vreys, R., Soenen, S. J., De, C. M., and Van der Linden, A. (2011). Background migration of USPIO/MLs is a major drawback for in situ labeling of endogenous neural progenitor cells. *Contrast Media Mol. Imaging* 6, 1–6.

Vreys, R., Vande Velde, G., Krylychkina, O., Vellema, M., Verhoye, M., Timmermans, J. P., Baekelandt, V., and Van der Linden, A. (2010). MRI visualization of endogenous neural progenitor cell migration along the RMS in the adult mouse brain: validation of various MPIO labeling strategies. *Neuroimage* 49, 2094–2103.

Wen, P. H., Hof, P. R., Chen, X., Gluck, K., Austin, G., Younkin, S. G., Younkin, L. H., DeGasperi, R., Gama Sosa, M. A., Robakis, N. K., Haroutunian, V., and Elder, G. A. (2004). The presenilin-1 familial Alzheimer disease mutant P117L impairs neurogenesis in the hippocampus of adult mice. *Exp. Neurol.* 188, 224–237.

Winner, B., Cooper-Kuhn, C. M., Aigner, R., Winkler, J., and Kuhn, H. G. (2002). Long-term survival and cell death of newly generated neurons in the adult rat olfactory bulb. *Eur. J. Neurosci.* 16, 1681–1689.

Winner, B., Lie, D. C., Rockenstein, E., Aigner, R., Aigner, L., Masliah, E., Kuhn, H. G., and Winkler, J. (2004). Human wild-type alpha-synuclein impairs neurogenesis. *J. Neuropathol. Exp. Neurol.* 63, 1155–1166.

Winner, B., Rockenstein, E., Lie, D. C., Aigner, R., Mante, M., Bogdahn, U., Couillard-Despres, S., Masliah, E., and Winkler, J. (2008). Mutant alpha-synuclein exacerbates age-related decrease of neurogenesis. *Neurobiol. Aging* 29, 913–925.

Yamaguchi, M., Saito, H., Suzuki, M., and Mori, K. (2000). Visualization of neurogenesis in the central nervous system using nestin promoter-GFP transgenic mice. *Neuroreport* 11, 1991–1996.

Yang, J., Liu, J., Niu, G., Chan, K. C., Wang, R., Liu, Y., and Wu, E. X. (2009). In vivo MRI of endogenous stem/progenitor cell migration from subventricular zone in normal and injured developing brains. *Neuroimage* 48, 319–328.

Zhang, R. L., Zhang, Z. G., Zhang, L., and Chopp, M. (2001). Proliferation and differentiation of progenitor cells in the cortex and the subventricular zone in the adult rat after focal cerebral ischemia. *Neuroscience* 105, 33–41.

Zhao, H., Doyle, T. C., Wong, R. J., Cao, Y., Stevenson, D. K., Piwnica-Worms, D., and Contag, C. H. (2004). Characterization of coelenterazine analogs for measurements of *Renilla* luciferase activity in live cells and living animals. *Mol. Imaging* 3, 43–54.

Zurkiya, O., Chan, A. W., and Hu, X. (2008). MagA is sufficient for producing magnetic nanoparticles in mammalian cells, making it an MRI reporter. *Magn. Reson. Med.* 59, 1225–1231.

Conflict of Interest Statement: The authors declare that the research was conducted in the absence of any commercial or financial relationships that could be construed as a potential conflict of interest.

Received: 25 January 2011; accepted: 27 April 2011; published online: 09 May 2011.
*Citation: Couillard-Despres S, Vreys R, Aigner L and Van der Linden A (2011) In vivo monitoring of adult neurogenesis in health and disease. Front. Neurosci. **5**:67. doi: 10.3389/fnins.2011.00067*
This article was submitted to Frontiers in Neurogenesis, a specialty of Frontiers in Neuroscience.

frontiers in
NEUROSCIENCE

REVIEW ARTICLE
published: 04 April 2011
doi: 10.3389/fnins.2011.00047

Adult human neurogenesis: from microscopy to magnetic resonance imaging

Amanda Sierra*, Juan M. Encinas and Mirjana Maletic-Savatic*

Department of Pediatrics, Baylor College of Medicine, Jan and Dan Duncan Neurological Research Institute at Texas Children's Hospital, Houston, TX, USA

Edited by:
Silvia De Marchis, University of Turin, Italy

Reviewed by:
Adam C. Puche, University of Maryland, USA
Nader Sanai, Barrow Neurological Institute, USA

****Correspondence:***
Mirjana Maletic-Savatic and Amanda Sierra, Department of Pediatrics, Baylor College of Medicine, Neurological Research Institute, 1250 Morsund St, MS NR1250.01, Houston, TX 77030, USA.
e-mail: maletics@bcm.edu; amanda.sierrasaavedra@gmail.com

Neural stem cells reside in well-defined areas of the adult human brain and are capable of generating new neurons throughout the life span. In rodents, it is well established that the new born neurons are involved in olfaction as well as in certain forms of memory and learning. In humans, the functional relevance of adult human neurogenesis is being investigated, in particular its implication in the etiopathology of a variety of brain disorders. Adult neurogenesis in the human brain was discovered by utilizing methodologies directly imported from the rodent research, such as immunohistological detection of proliferation and cell-type specific biomarkers in postmortem or biopsy tissue. However, in the vast majority of cases, these methods do not support longitudinal studies; thus, the capacity of the putative stem cells to form new neurons under different disease conditions cannot be tested. More recently, new technologies have been specifically developed for the detection and quantification of neural stem cells in the living human brain. These technologies rely on the use of magnetic resonance imaging, available in hospitals worldwide. Although they require further validation in rodents and primates, these new methods hold the potential to test the contribution of adult human neurogenesis to brain function in both health and disease. This review reports on the current knowledge on adult human neurogenesis. We first review the different methods available to assess human neurogenesis, both *ex vivo* and *in vivo* and then appraise the changes of adult neurogenesis in human diseases.

Keywords: adult, neurogenesis, neural stem cells, human, methods, BrdU, cerebral blood volume, metabolomics

INTRODUCTION: A BRIEF HISTORY OF THE ADULT MAMMALIAN NEUROGENESIS DISCOVERY

The discovery of adult neurogenesis crushed the century-old dogma that no new neurons are formed in the mammalian brain after birth. However, this finding and its acceptance by the scientific community did not happen without hurdles. At the beginning of the last century, based on detailed observations of the brain anatomy reported by Santiago Ramon y Cajal and others, it was established that the human nervous system develops *in utero* (Colucci-D'Amato et al., 2006). In adult brains, it was thought, no more neurons could be generated, as the brain is grossly incapable of regenerating after damage (for a more detailed historical report see Watts et al., 2005; Whitman and Greer, 2009). This dogma was deeply entrenched in the Neuroscience community, and Altman's (1962) discovery of newborn cells in well-defined areas of the adult rodent brain was largely ignored. The phenomenon was reexamined in the 1970–1980s, when Michael Kaplan (Kaplan and Hinds, 1977) and Fernando Nottebohm (Goldman and Nottebohm, 1983) demonstrated the presence of newborn cells in the adult brain of mice and canaries, respectively, and showed that these cells had ultrastructural characteristics of neurons. However, such findings could not be repeated in adult rhesus monkeys, where proliferating cells appeared to be glial and endothelial cells and not neurons (Rakic, 1985; Eckenhoff and Rakic, 1988). Thus, neurogenesis seemed to be absent in adult primates (Eckenhoff and Rakic, 1988).

The field of adult neurogenesis finally took off in the 1990s with the development of new technologies. First, the use of ^{3}H-thymidine, a radioactive nucleotide used to study proliferation when incorporated into the cells during the S phase of the cell cycle, was replaced by its analog, bromodeoxyuridine (BrdU), which could be detected by a specific antibody. Utilization of the BrdU for labeling of newborn cells via immunohistochemistry allowed their further studies by co-labeling with specific neuronal markers (Miller and Nowakowski, 1988). Further, it was shown that neuroprogenitor cells (NPCs), isolated from adult mouse brains, proliferated and differentiated into neurons and astrocytes *in vitro* (Reynolds and Weiss, 1992). In addition, NPCs labeled with viral vectors were able to migrate and differentiate into neurons in the adult mouse brain (Lois and Alvarez-Buylla, 1993), demonstrating

Abbreviations: 1H-MRS, proton magnetic resonance spectroscopy; AD, Alzheimer's disease; ANPs, amplifying neuroprogenitors; APP, amyloid precursor protein; BBB, blood–brain barrier; BrdU, bromodeoxyuridine; CBF, cerebral blood flow; CBV, cerebral blood volume; DCX, doublecortin; DG, dentate gyrus; DISC1, disrupted-in-schizophrenia 1; EGFR, epidermal growth factor receptor; FACS, fluorescence-activated cell sorting; FDA, Food and Drug Administration; FFT, Fourier-fast transform; FID, free-induction decay; GFAP, glial fibrillary acidic protein; GFP, green fluorescent protein; HD, Huntington's disease; MCAO, medial cerebral artery occlusion; MCM2, minichromosome maintenance protein; MDD, major depressive disorder; MR, magnetic resonance; MRI, magnetic resonance imaging; NAA, *N*-acetylaspartate; NBs, neuroblasts; NeuN, neuronal nuclei; NMR, nuclear magnetic resonance; NPCs, neuroprogenitor cells; NSE, neuronal specific enolase; OB, olfactory bulb; PCNA, proliferating cell nuclear antigen; PD, Parkinson's disease; ppm, parts per million; PS1, presenilin 1; QNPs, quiescent neuroprogenitors; RMS, rostral migratory stream; SGZ, subgranular zone; SN, substantia nigra; SSRIs, selective serotonin reuptake inhibitors; SVZ, subventricular zone; TCAs, tricyclic antidepressants; TLE, temporal lobe epilepsy; TOAD-64, turned on after division 64.

that the adult neurogenesis was functional in rodents. Finally, the existence of adult neurogenesis in humans was firmly established when, in 1998, Gage and colleagues demonstrated for the first time that new neurons were produced in the adult hippocampus (Eriksson et al., 1998).

Currently, adult neurogenesis is one of the hot topics in Neuroscience especially because of the new opportunities it may bring for treatments of neurodegenerative diseases, either by harnessing resident progenitors to regenerate the lost tissue (Sohur et al., 2006) or by cell transplantation therapies (Goldman and Windrem, 2006). The field is currently on the rise, as shown by the exponential growth of publications with the key words "adult" AND "neurogenesis OR neural stem cells" (PubMed search up to December 31, 2010): a total of 6,437 papers have been published, of which 57% (3,695 papers) was published in the last 5 years (**Figure 1**). However, only 8% of published papers (530 papers) deal with human data (search including the term "human" in the title), suggesting that the research on adult neurogenesis in humans is still in its infancy. Thus, the actual knowledge on adult human neurogenesis is limited and in many cases, data is directly extrapolated from the rodent literature. Herein, we review the methodologies used to assess adult human neurogenesis and its status in several neuropsychiatric disorders.

METHODS TO ASSESS NEUROGENESIS IN HUMANS

The extent of our knowledge on adult human neurogenesis directly correlates with the type of available techniques that can be applied to human brain tissue research. Several methodologies exist, but each method yields different sensitivity, specificity, and ultimately different units of quantification, thus rendering it difficult to compare different studies. In addition, some methodologies can assess only proliferation (NPCs or total proliferating cells) while others can provide the data on neurogenesis [neuroblasts (NBs, neuronal committed cells) or newborn neurons]. Herein, we review the advantages and disadvantages of methods used to assess adult human neurogenesis both *ex vivo* and *in vivo*.

METHODS TO ASSESS NEUROGENESIS ON POSTMORTEM AND BIOPSIED TISSUE

The majority of the methodologies used to study neurogenesis *ex vivo* have been inherited from the rodent literature, where they have been thoroughly validated (**Figure 2**). These techniques require brain tissue that is obtained postmortem, either frozen fresh immediately after death or, more frequently, fixed and stored in brain tissue banks. In both cases, it is important to note that the cause of death, presence of brain and/or systemic illnesses, age of death, and postmortem interval (the time from death to tissue fixation) may be confounding factors when interpreting the results (Boldrini et al., 2009). Alternatively, brain tissue can also be obtained from biopsies or surgical resections, such as in temporal lobectomy due to intractable epilepsy.

Bromodeoxyuridine labeling

Bromodeoxyuridine is widely used in animal models to quantify the number of dividing cells in a tissue and to trace their progeny. When administered systemically, it is incorporated into the DNA during the S phase of the cell cycle and is transmitted to the daughter cells, as long as it is not diluted through many rounds of proliferation (Karpowicz et al., 2005). Using a variety of specific anti-BrdU antibodies, it can be detected by immunohistochemistry. Although it can be mutagenic (Rakic, 2002a), BrdU was approved in 1995 by the Food and Drug Administration (FDA) to be used in humans under the commercial name of Broxine/Neomark as a radiation sensitizer in the treatment of primary brain tumors[1]. Furthermore, BrdU is currently used in several clinical trials to measure cell cycle kinetics in patients with hematologic malignancies, to study white blood cell replication and survival in patients with human immunodeficiency virus, and to assess the degree of tumor proliferation in biopsies as well as to treat patients with pancreatic tumors as an antineoplastic agent[2]. It was the treatment with BrdU of patients who suffered from larynx, pharynx, or tongue cancers that enabled the detection of proliferating NPCs in the hippocampus (Eriksson et al., 1998), the discovery which paved the way for further investigations of adult neurogenesis in the human brain.

The major advantage of BrdU labeling is its sensitivity to detect proliferating cells compared to other immunohistological methods. For instance, neurogenesis in adult rhesus monkeys was only detected using BrdU (Kornack and Rakic, 1999) but not

[1]http://www.fda.gov/ohrms/dockets/dailys/00/mar00/030100/lst0094.pdf\
[2]http://clinicaltrials.gov/ct2/result?intr=bromodeoxyuridine

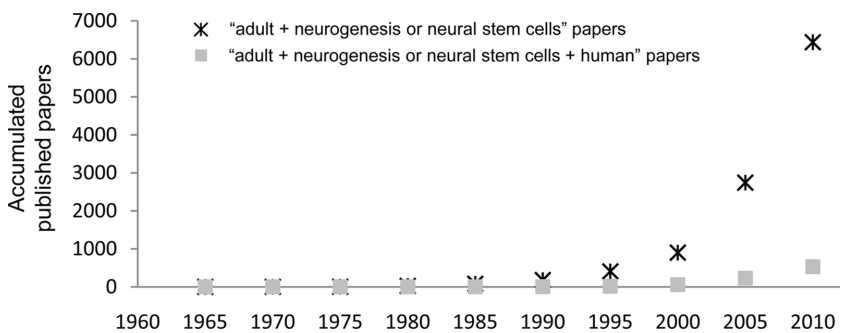

FIGURE 1 | Published papers on adult neurogenesis per quinquennium. The graph shows the accumulated papers published from 1960 onward, searched in PubMed with the search terms "adult" AND ("neurogenesis" OR "stem cells"). The asterisks show the total number of papers, and the filled squares show those papers with the term "human" in their title.

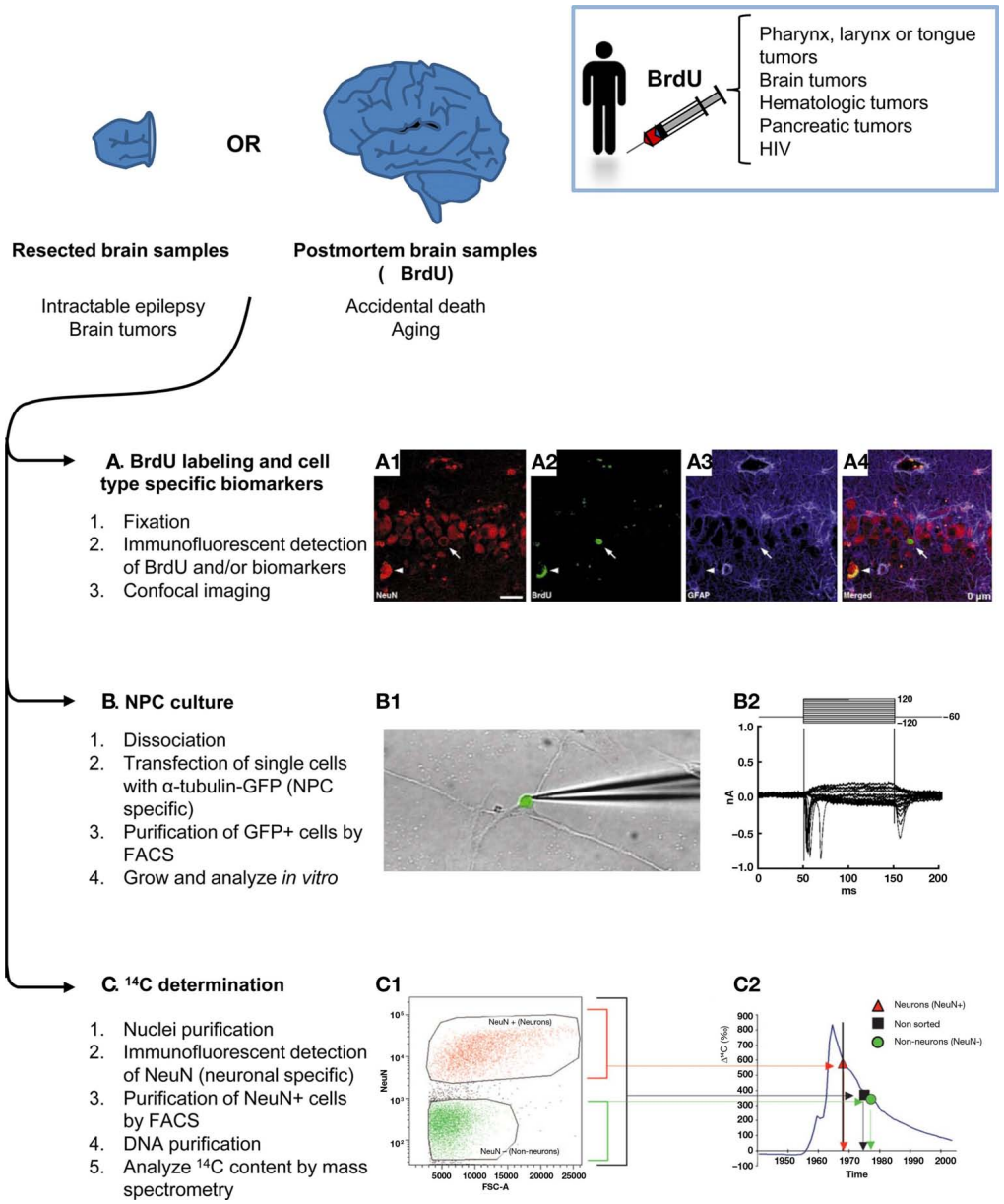

FIGURE 2 | Methods to assess adult human neurogenesis in resected or postmortem brain samples. Brain samples from live individuals can be obtained by surgical resection of the focus of the seizures in intractable epilepsy or brain tumors. Alternatively, bank tissues store frozen or fixed brain samples from accidental deaths and aging individuals, some of which may have been treated with BrdU. Once the tissue is obtained, three main methods can be applied to study neurogenesis: **(A)** Immunodetection of BrdU and/or proliferation and cell-type specific biomarkers in fixed tissue, followed by analysis by confocal analysis. An example of new born neurons in the SGZ of the hippocampus of an aging patient is shown in **(A1)** NeuN+ neurons (red), **(A2)** BrdU labeling (green), **(A3)** GFAP+ astrocytes (blue), **(A4)** merged image showing one newborn neuron labeled with BrdU and NeuN, but not with GFAP (arrow); and non-specific fluorescence emission due to lipofuscin accumulation in old tissue (arrowhead). Scale bar is 25 μm. **(B)** Culture of NPCs. In this case, the fresh tissue is dissociated and transfected with a reporter gene (GFP) driven by aTα1 tubulin promoter, an early neuronal regulatory gene. The transfected cells are then purified by FACS and cultured *in vitro*. The grown cells differentiate into fully functional neurons which when patch-clamped in a voltage-clamped configuration **(B1)** show typical depolarizations of the voltage-gated sodium currents measured in nanoAmperes (nA) over a time course of milliseconds (ms) **(B2)**. **(C)** Determination of the ^{14}C content. Cell nuclei from prefrontal cortex samples are purified by density gradients, labeled with NeuN and purified by FACS. Next, their DNA is purified and the ^{14}C content is analyzed by mass spectrometry. **(C1)** FACS plot showing the expression of NeuN (vertical axis) versus the area of the forward scatter (FSC-A, which is considered a measure of the particle size). The neuronal nuclei (NeuN+, orange) are separated from the rest of the nuclei (NeuN–, green). **(C2)** ^{14}C content of the sorted nuclei ($\Delta^{14}C$, given in relation to a universal standard and corrected for radioactive decay) compared to the atmosphere ^{14}C content (blue line) and the age of the individual (vertical black line). Neuronal nuclei (orange triangles) have a ^{14}C content that indicates that their age is coincident with that of the individual. Non-neuronal nuclei (green circles) are younger than the individual, making the non-sorted (black squares) cells younger than the individual in average as well. Figures **(A1–A4)** and **(B1–B2)** are reprinted by permission from Macmillan Publishers Ltd: Nature Medicine, Eriksson et al. (1998), copyright 1998; and Roy et al. (2000), copyright 2000, respectively. Figures **(C1–C2)** are reprinted by permission from Bhardwaj et al. (2006), copyright 2006, National Academy of Sciences, U.S.A.

H^3-thymidine, which also incorporates into the DNA of dividing cells (Rakic and Nowakowski, 1981). In addition, proliferation in the adult human hippocampus was found using BrdU (Eriksson et al., 1998), but not other markers of proliferation such as MiB-1 (Seress et al., 2001). Another advantage of BrdU labeling is utilization of pulse-and-chase analysis, which enables studies of both proliferation (hours after the BrdU injection) and differentiation (days or months after the BrdU injection). Such studies may ultimately be used to distinguish between neurogenesis and gliogenesis, a particularly significant feature in human brain diseases.

Despite its wide use, BrdU labeling has some drawbacks. For instance, BrdU does not diffuse freely through the blood–brain barrier (BBB), but rather, it likely uses the deoxythymidine transporters (Spector and Johanson, 2007). Therefore, conditions that disrupt the BBB, such as inflammation, irradiation, status epilepticus, trauma, etc., may lead to different BrdU availability which, in turn, leads to labeling of different number of cells without actual changes in proliferation (von Bohlen Und Halbach, 2007). To overcome this possible cause of misinterpretation of the data, it is particularly important to determine the integrity of the BBB when comparing neurogenesis in healthy and diseased individuals. Furthermore, BrdU can label phenomena other than proliferation, such as DNA turnover or repair, or abortive reentry in the cell cycle during apoptosis (Rakic, 2002a,b). Finally, some dividing cells may preferentially use *de novo* synthesis of deoxythymidine rather than the salvage enzymes which phosphorylate existing deoxynucleotides (including BrdU) to generate the deoxynucleotides for DNA synthesis during the S phase (Spector and Johanson, 2007). In such cases, BrdU labeling will not correlate with the proliferative activity of the cells. Thus, while it has revolutionized the studies of neurogenesis, BrdU labeling should be meticulously analyzed to avoid possible misinterpretations as noted above.

Expression of cell-specific biomarkers

Particular cell types and particular stages of the cell cycle of dividing cells can be assessed by specific antibodies. When utilizing these reagents for immunostaining of the human tissue, it is important to take into account antigenicity, which can be affected by the delayed fixation of the postmortem tissue (Boekhoorn et al., 2006; Liu et al., 2008) and the specificity of the antibodies, which may be related to a particular species (for example, antibodies which work for rodent tissue may not work for human tissue). Ideally, quantification of cells expressing the biomarker of interest should be obtained using unbiased stereology, such as the optical dissector method (Lemmens et al., 2010), although in human samples this goal can be difficult to achieve due to the low number of proliferating cells (Liu et al., 2008).

Proliferation biomarkers are expressed while cells are cycling (**Table 1**), such as *Ki-67* (Hall and Woods, 1990; Yerushalmi et al., 2010) and *MCM2* (Stoeber et al., 2001; Bailis and Forsburg, 2004). Ki-67 immunolabeling relies heavily on pH (Boekhoorn et al., 2006); thus other antibodies against the Ki67 antigen, such as *MIB-1*, have been developed for different tissue conditions (Cattoretti et al., 1992). Another widely used marker is *PCNA* (Takasaki et al., 1981), although it is also expressed by some non-proliferating cells (Rakic, 2002a). Compared to BrdU, these markers offer the advantage of not requiring a priori administration of the label, thus increasing the number of samples that can be studied. However, these markers only label proliferating cells and cannot be used to trace their fate or to assess actual neurogenesis. Importantly, proliferation biomarkers in neurogenic regions are usually assumed to label NPCs, but it is also possible that they label proliferating astrocytes, oligoprogenitors, or endothelial cells. Gliogenesis should be ruled out by double-labeling with specific glial biomarkers.

Cell-specific biomarkers can also be detected using specific antibodies (thoroughly reviewed by von Bohlen Und Halbach, 2007; Encinas and Enikolopov, 2008). The most common cell biomarkers used for studies of the human tissue are described in **Table 1**: *Nestin* (Lendahl et al., 1990), *GFAP* (Doetsch et al., 1997), *Vimentin* (Doetsch et al., 1997), *EGFR* (Danilov et al., 2009), *Musashi* (Sakakibara and Okano, 1997), *PSA-NCAM* (Doetsch et al., 1997), *Doublecortin* (DCX; des Portes et al., 1998), *NeuroD* (Miyata et al., 1999), *TOAD-64* (Minturn et al., 1995), *NeuN* (Mullen et al., 1992; Kim et al., 2009), NSE (Kaiser et al., 1989), and β*III-Tubulin* (Encinas and Enikolopov, 2008). However, caution must be observed when using these antibodies to assign the cell identity. For instance, apart from labeling migrating NBs, PSA-NCAM is also involved in synaptic plasticity (Dityatev et al., 2004) and is expressed in non-neurogenic areas in rodents (Nacher et al., 2002). In addition, the specificity of DCX as a marker for neurogenesis has been recently challenged, as it has been found in mature astrocytes in the human neocortex in patients suffering from neurodegeneration (Verwer et al., 2007). Finally, some authors (Boekhoorn et al., 2006), but not others (Liu et al., 2008), find that DCX immunolabeling is very sensitive to postmortem delay, an important confounding factor when comparing human postmortem samples.

NPC culture

Human NPCs have been isolated and cultured *in vitro*. Originally, Steindler and colleagues were able to grow NPCs from the temporal lobe tissue extracted from patients with intractable epilepsy. These NPCs proliferated *in vitro* in the form of neurospheres and differentiated into neurons and astrocytes (Johansson et al., 1999; Kukekov et al., 1999). Later on, Goldman and colleagues refined the technique and were able to specifically isolate the NPCs (Roy et al., 2000). They transfected cells from mixed brain cultures with viral constructs expressing a humanized green fluorescent protein (GFP) under regulatory elements of the nestin or the early neuronal Tα1 tubulin genes, and then purified the NPCs based on the expression of the transgene by fluorescence-activated cell sorting (FACS). The isolated NPCs divided in culture and gave rise to physiologically active neurons (Roy et al., 2000). This technique was not designed for quantification purposes and, thus, cannot be used to assess the degree of neurogenesis in different disorders or after different treatments. Nonetheless, it has generated a great excitement because it was seen as the first serious step toward cell replacement therapies for human neurological diseases by transplantation of either precursors or already differentiated cells (Antel et al., 2000).

^{14}C retrospective labeling

Similar to the ^{14}C-dating used in archeology, this method uses the ^{14}C-content to assess the average age of the cells present in a particular tissue (Spalding et al., 2005; Bhardwaj et al., 2006). Due to

Table 1 | Proliferation and cell-type specific biomarkers commonly used in human neurogenesis studies.

Antigen	Function	Expression	References
PROLIFERATION BIOMARKERS			
Ki67	Unknown	Expression during G1-M	Del Bigio (1999), Blumcke et al. (2001), Bedard and Parent, (2004), Sanai et al. (2004), Boekhoorn et al. (2006), Jin et al. (2006), Macas et al. (2006), Reif et al. (2006), Ziabreva et al. (2006), Fahrner et al. (2007), Shen et al. (2008), Boldrini et al. (2009), Mattiesen et al. (2009), Knoth et al. (2010), Marti-Fabregas et al. (2010)
PCNA	Proliferating cell nuclear antigen, a co-factor of DNA-Polδ	Synthesized during S phase	Bernier et al. (2000), Curtis et al. (2003, 2005a,b), Bedard and Parent (2004), Hoglinger et al. (2004), Crespel et al. (2005), Jin et al. (2006), Liu et al. (2008), Shen et al. (2008), Gerber et al. (2009), Kam et al. (2009), Mattiesen et al. (2009), Knoth et al. (2010)
MCM2	Minichromosome maintenance protein 2, a DNA helicase	Throughout cell cycle	Jin et al. (2006), Liu et al. (2008), Shen et al. (2008), Knoth et al. (2010)
CELL-SPECIFIC BIOMARKERS			
Nestin	An intermediate filament	NPC, astrocytes, radial glia, perivascular cells	Arnold and Trojanowski (1996), Blumcke et al. (2001), Bedard and Parent (2004), Hoglinger et al. (2004), Crespel et al. (2005), Jin et al. (2006), Macas et al. (2006), Ziabreva et al. (2006), Boldrini et al. (2009), Mattiesen et al. (2009), Knoth et al. (2010), Marti-Fabregas et al. (2010)
EGFR	Epidermal growth factor receptor	C cells, A cells	Weickert et al. (2000), Hoglinger et al. (2004)
GFAP	Glial fibrillary acidic protein, an intermediate filament	Quiescent NPCs, B cells, radial glia, astrocytes	Eriksson et al. (1998), Del Bigio (1999), Bernier et al. (2000), Weickert et al. (2000), Blumcke et al. (2001), Curtis et al. (2003), Hoglinger et al. (2004), Sanai et al. (2004), Crespel et al. (2005), Boekhoorn et al. (2006), Macas et al. (2006), Fahrner et al. (2007), Shen et al. (2008), Boldrini et al. (2009), Gerber et al. (2009), Kam et al. (2009), Mattiesen et al. (2009), Knoth et al. (2010), Marti-Fabregas et al. (2010)
Vimentin	An intermediate filament	Quiescent NPCs, B cells, astrocytes	Arnold and Trojanowski (1996), Curtis et al. (2003, 2005a), Crespel et al. (2005), Fahrner et al. (2007), Mattiesen et al. (2009)
Musashi	An RNA-binding protein	NPC, astrocytes	Crespel et al. (2005), Macas et al. (2006), Ziabreva et al. (2006), Shen et al. (2008), Mattiesen et al. (2009)
PSA-NCAM	Polysialylated cell adhesion molecule, involved in cell migration	Migrating neuroblasts	Mikkonen et al. (1998), Bernier et al. (2000), Weickert et al. (2000), Bedard and Parent (2004), Hoglinger et al. (2004), Crespel et al. (2005), Curtis et al. (2005b), Boekhoorn et al. (2006), Macas et al. (2006), Liu et al. (2008), Kam et al. (2009), Marti-Fabregas et al. (2010)
DCX	Doublecortin, promotes microtubule proliferation	Neuroblasts and neurons	Bedard and Parent (2004), Crespel et al. (2005), Boekhoorn et al. (2006), Jin et al. (2006), Fahrner et al. (2007), Liu et al. (2008), Shen et al. (2008), Gerber et al. (2009)
NeuroD	A transcription factor, involved in neuronal commitment	Neuroblasts and neurons	Bedard and Parent (2004), Knoth et al. (2010)

(Continued)

Table 1 | Continued

Antigen	Function	Expression	References
TOAD64	Turned on after division 64, a membrane associated protein from the TUC4 family involved in axonal growth	Neuroblasts	Jin et al. (2006), Shen et al. (2008), Gerber et al. (2009), Mattiesen et al. (2009), Knoth et al. (2010)
NeuN	A splicing factor of the Fox-3 family	Neurons	Eriksson et al. (1998), Weickert et al. (2000), Blumcke et al. (2001), Curtis et al. (2003), Crespel et al. (2005), Fahrner et al. (2007), Liu et al. (2008), Boldrini et al. (2009), Knoth et al. (2010),
βIII-Tubulin	A microtubule	Neurons	Arnold and Trojanowski (1996), Bernier et al. (2000), Weickert et al. (2000), Blumcke et al. (2001), Curtis et al. (2003, 2005b), Bedard and Parent (2004), Hoglinger et al. (2004), Jin et al. (2006), Macas et al. (2006), Liu et al. (2008), Shen et al. (2008), Knoth et al. (2010)
NSE	Neuron specific enolase	Neurons	Eriksson et al. (1998), Del Bigio (1999)

The function and expression of the different markers and the papers in which they were used are shown.

the extensive testing of nuclear weapons in the 1950–1960s, large quantities of ^{14}C were generated; since then, the ^{14}C levels in the biosphere have decayed at a known rate. This ^{14}C incorporates into the cells, matching the ^{14}C levels in the atmosphere. The exception is genomic DNA because the molecular composition of DNA is stable after the last cell division (except in case of DNA repair). The DNA ^{14}C-content reflects the age of the cell and not the atmospheric levels (Spalding et al., 2005; Bhardwaj et al., 2006). Thus, the strategy devised by the Jonas Frisen's group was to isolate cell nuclei from fresh or frozen brain autopsy specimens and label them with NeuN. Next, neuronal nuclei (NeuN+) were sorted by FACS, their DNA purified and the ^{14}C-content measured by accelerator mass spectrometry (Spalding et al., 2005; Bhardwaj et al., 2006). Using this technique, it was shown that neurogenesis in the adult neocortex is absent or very limited because the age of the neurons matched the age of the individual and had ^{14}C levels similar to atmospheric levels at the time when the individual was born (Bhardwaj et al., 2006). On the contrary, NeuN-nuclei, including glial cells which are known to have a higher turnover rate, showed an average age several years younger than the age of the individual, suggesting that those were cells born during adulthood (Bhardwaj et al., 2006). This method yields high sensitivity as it has been estimated that it detects newborn cells down to 1% of the population (Bhardwaj et al., 2006). However, it only provides the average age of the neurons in the tissue and does not allow dating or tracing of individual cells. Surprisingly, this method has not yet been used to test adult neurogenesis in the hippocampus or the olfactory bulb (OB), the two major areas of adult neurogenesis.

METHODS TO ASSESS NEUROGENESIS *IN VIVO*

More recently, methods have been specifically designed to detect neurogenesis in live human brain by means of magnetic resonance imaging (MRI; **Figure 3**). In the MRI scanner, the subjects are exposed to a harmless magnetic field that aligns the magnetic spin of all the protons in the tissue in a low energy configuration; next, the subjects receive radiofrequency electrical stimulation, which excites the spins out of equilibrium. The spins then naturally relax back to their original conformation with time constants T1 (spin–lattice relaxation time, for longitudinal magnetization) and T2 (spin–spin relaxation time, for transversal magnetization; Maletic-Savatic et al., 2008). The difference in relaxation times of different molecules, such as water and fat, is used to generate detailed MRI images of the brain. In addition, further information can be extracted from these constants, and different MR modalities have been adapted to study neurogenesis (Modo and Bulte, 2011).

The major advantage of MR-based methods is that they are performed in live individuals with no side effects, supporting repeated measures and longitudinal studies. Thus, these methods allow a more controlled experimental design, and variables such as the cause or age of death no longer have to be taken into account. Nonetheless, these methods rely on correlations to indirectly quantify neurogenesis, and extensive validation in both rodents and humans is required to demonstrate that they are specific for neurogenesis. More importantly, it is essential to determine whether the data correlate with the number of NPCs, proliferating NPCs (versus other cell types that proliferate), or newborn neurons. Another major advantage of MRI-based methods is that MRI scanners are widely available in hospitals and research centers worldwide. Thus, these methods could be easily implemented in many labs and offer a unique research opportunity to increase our understanding of the role of adult neurogenesis in humans.

Cerebral blood volume measurements

Cerebral blood volume (CBV) can be measured by several methods, one of which is MRI. In MR-based CBV measurements, the contrast agent gadolinium is injected systemically. The chelated gadolinium used is a non-toxic highly lipophobic agent, thus restricted to the intravascular space when the BBB is not challenged (Zaharchuk, 2007). Due to its paramagnetic properties, it creates variations in the local magnetic field which lead to decreased T1 signal intensity. These changes can be used to generate maps of the CBV and cerebral blood flow (CBF) by an array of computational methods (reviewed in Zaharchuk, 2007). Among these, the steady-state T1

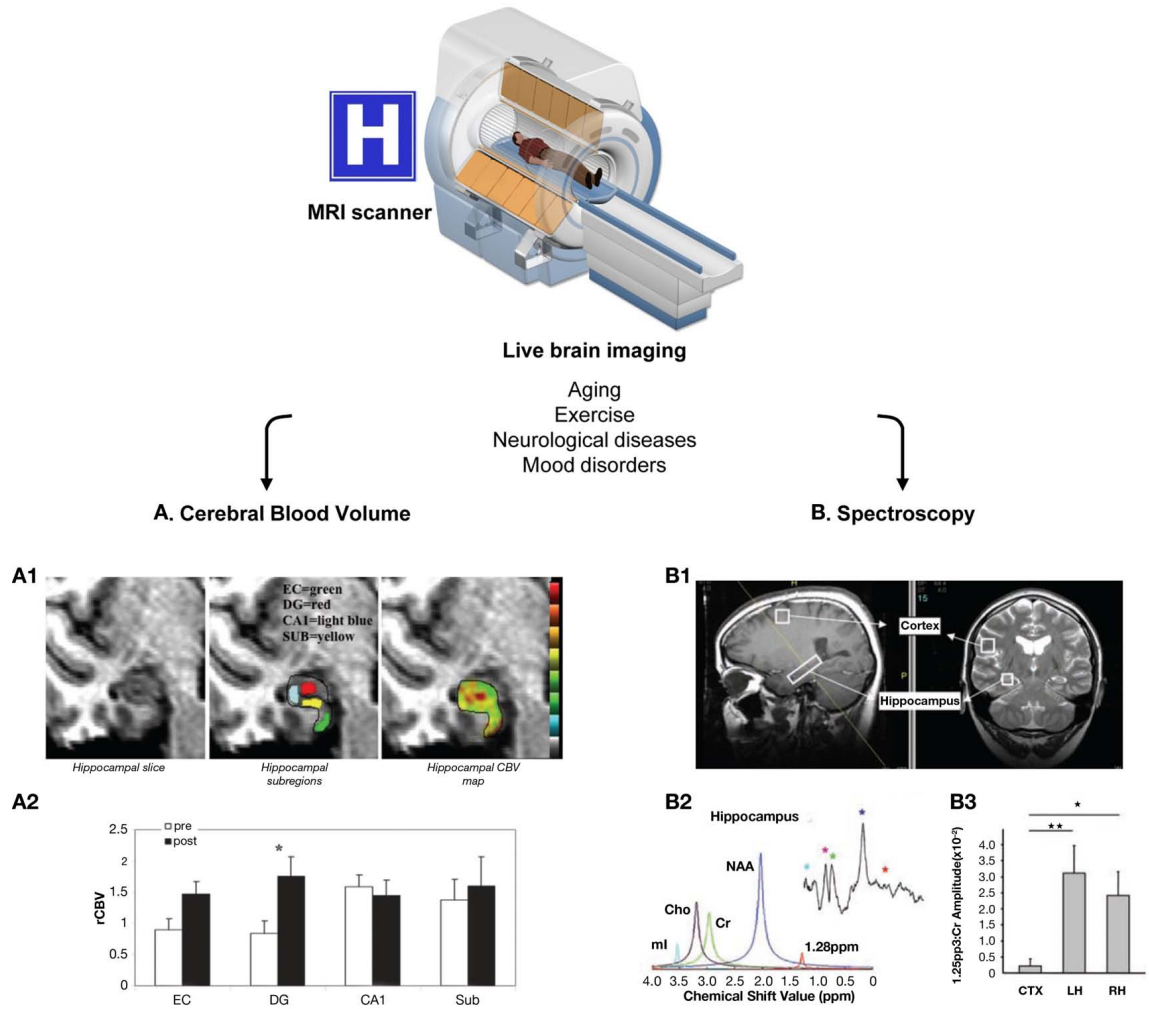

FIGURE 3 | Live methods to assess adult human neurogenesis. These methods are based on magnetic resonance, using MRI scanners available in hospitals worldwide. Because there are no side effects, both healthy and diseased people can be re-scanned throughout aging, before and after exercise, to follow-up the effect of pharmacological interventions, etc. Two main methods have been developed to indirectly quantify adult human neurogenesis using different MR modalities: **(A)** CBV measurement. The dentate gyrus CBV is a proxy for neurogenesis in physical exercise paradigms. This method is based on the consecutive correlation of neurogenesis–angiogenesis, and angiogenesis–CBV. **(A1)** High resolution MRI slice of the adult human hippocampus (right panel), showing the different hippocampal subregions (entorhinal cortex, EC, green; dentate gyrus, DG, red; cornu ammonis 1, CA1, light blue; and subiculum, SUB, yellow; central panel) and a typical hippocampal CBV map (warmer colors indicate higher CBV). **(A2)** Quantification of the mean relative hippocampal CBV (rCBV), before (white bars) and after (black bars) exercise in healthy humans. As in mice, physical exercise resulted in a significant increase in CVB only in the DG (asterisk). **(B)** Spectroscopy. A lipidic metabolite resonating at 1.28 ppm was identified as a marker of rodent NPCs. **(B1)** Positioning of the voxel of interest in the cortex and the hippocampus of a healthy person. **(B2)** Spectroscopic analysis of the metabolite content in the hippocampal voxel using SVD and FFT (small upper insert). Identified metabolites are myolnositol (mI, light blue), choline (Cho, purple), creatine (green), *N*-acetylaspartate (NAA, dark blue), and the 1.28 ppm metabolite (red). **(B3)** Quantification of the abundance of the 1.28 ppm metabolite in the cortical (CTX) and hippocampal voxels (LH and RH for left and right hippocampus, respectively), normalized over the amplitude of the creatine peak. The hippocampi had much higher content of the 1.28 ppm metabolite than the cortex. The MRI cutaway is printed from permission from the National High Magnetic Field Lab website (http://www.magnet.fsu.edu/education /tutorials/magnetacademy/mri/). Figures **(A1–A2)** are reprinted by permission from Pereira et al. (2007), copyright 2007, National Academy of Sciences, U.S.A. Figures **(B1–B3)** are from Manganas et al. (2007) and are reprinted with permission from AAAS.

method is based on the assumption that the MRI signal derives from two separate compartments – intravascular (vessels) and extravascular (brain parenchyma; Lin et al., 1999). When gadolinium is administered, only the T1 signal from the intravascular compartment will decrease, assuming the BBB is intact. Then, the difference between pre-contrast and post-contrast images normalized over a voxel that contains only blood, such as the sagittal sinus, is used to generate the CBV map (Lin et al., 1999). The main advantage of the steady-state T1 method, compared to other methods such as bolus tracking (also called dynamic imaging), is that it renders absolute estimations of the CBV, supporting longitudinal studies of brain perfusion, and has high spatial resolution. This method has been validated through correlation with estimations of gray matter CBV using other imaging modalities. However, it requires

longer acquisition time and has lower signal-to-noise ratio than bolus tracking (Lin et al., 1999). Nevertheless, the steady-state T1 method is well-established for determining CBV (Zaharchuk, 2007) and has been recently used by the group of Scott Small to indirectly assess changes in adult human neurogenesis (Pereira et al., 2007).

The basis for the CBV studies of neurogenesis is the correlation between angiogenesis and neurogenesis. Increased cortical CBV correlates with angiogenesis in ischemia (Lin et al., 2002; Seevinck et al., 2010) and gliomas (Aronen et al., 2000; Cha et al., 2003). In turn, angiogenesis occurs in the hippocampal neurogenic niche (Palmer et al., 2000), and both angiogenesis and neurogenesis are elevated in the hippocampus following physical exercise (van Praag et al., 2005; Van der Borght et al., 2009). Thus, because of the correlation of CBV–angiogenesis and angiogenesis–neurogenesis, the CBV might provide an indirect measure of neurogenesis in the adult human hippocampus (Pereira et al., 2007). In fact, the CBV increased selectively in the human dentate gyrus (DG, where NPCs reside) after a 12-week exercise paradigm, and this increase correlated with cognitive performance, such as declarative memory but not delayed recognition (Pereira et al., 2007). As a validation experiment, the authors showed that in running mice, the CBV increased in the DG and not in other hippocampal areas, and this increase correlated with the number of 1- to 3-week-old BrdU+ cells (Pereira et al., 2007). More recently, others have demonstrated increased number of micro-vessels occurring in parallel to increased proliferation (Ki67+ cells) and the number of newborn cells committed to the neuronal lineage (DCX+ cells) after 10 days of running (Van der Borght et al., 2009). However, it remains to be elucidated if the angiogenesis–neurogenesis coupling occurs in conditions other than exercise, which would render the CBV measurements for assessments of human neurogenesis more widely applicable.

Spectroscopic biomarker of NPCs

Here, the MRI modality used is proton magnetic resonance spectroscopy (^{1}H-MRS), which exploits the magnetic properties of different protons to detect an array of small metabolites in the living tissue. Some protons of some metabolites are mobile in the magnetic field, and the relaxation of their spins can be detected by MR. This relaxation is observed as a sinusoid wave of decay in the time domain (free-induction decay, or FID), which is conventionally transformed into a function in the frequency domain (Fourier-fast transform, or FFT; Maletic-Savatic et al., 2008). The FFT is usually plotted as a graph of peaks representing the proton content of different metabolites. The *x*-axis represents the resonant frequency of each particular metabolite (in parts per million or ppm); and the *y*-axis represents the intensity of the signal, so that the integrated area under each peak is a readout of the amount of protons that contribute to that particular signal (Sibtain et al., 2007). Using this conventional signal analysis, a few relevant metabolites can be detected (Soares and Law, 2009): *N-acetylaspartate* (NAA), a marker of neurons whose major peak resonates at 2.02 ppm; *Creatine*, resonating at 3.02 ppm, an energy metabolite considered to be stable and thus used as a house-keeping metabolite for normalization; and *Myoinositol*, a marker of astrocytes which resonates at 3.56 ppm. Other metabolites commonly analyzed include choline, alanine, lactate, glutamate, glutamine, glucose, and some macromolecular proteins and lipids (Soares and Law, 2009). Using the ^{1}H-MRS, our group recently identified a metabolite with main resonance at 1.28 ppm, which was enriched in rodent NPCs and was used to indirectly quantify adult human neurogenesis (Manganas et al., 2007).

This metabolite was initially discovered in rodent NPCs, grown as embryonically derived neurospheres, by high-field nuclear magnetic resonance (NMR; Manganas et al., 2007; Ma et al., 2011), although it had not been previously found in NPCs differentiated in culture from embryonic stem cells (ESCs; Jansen et al., 2006). Its association with neurogenesis *in vivo* was validated by microMR spectroscopy, which detected it in the rodent hippocampus, as well as in the cortex after NPC transplantation (Manganas et al., 2007). Furthermore, the amount of the metabolite detected by microMR spectroscopy correlated with the number of BrdU+ cells in the hippocampus following an electroconvulsive shock-induced increase in endogenous neurogenesis. These studies further led to imaging of the human hippocampus, where this metabolite was expressed in very small amounts and was not detectable using conventional signal processing. Thus, to extract it from the human ^{1}H-MRS, Manganas et al. (2007) utilized singular value decomposition (SVD), a parametric method which models metabolite signals as decaying complex sinusoids in the time domain. The validity and reliability of SVD to quantify the 1.28 ppm signal encountered criticisms mostly due to potential overfitting of the data (Friedman, 2008; Hoch et al., 2008; Jansen et al., 2008; Dong et al., 2009). However, most of these issues were addressed using simulated and semi-simulated data showing that the rate of false positives was less than 5% for the range of signal-to-noise ratios found in the initial studies (under −20 dB), and thus that the estimations of human NPCs based on the 1.28 ppm peak were reliable (Djuric et al., 2008). Overall, these issues have been considered a matter of optimization of the technique rather than a fundamental problem in the methodology (Romer et al., 2008; Dong et al., 2009), with the agreement that more research is necessary to unequivocally establish the 1.28 ppm spectral peak as a marker of neurogenesis with clinical value (Djuric et al., 2008; Romer et al., 2008; Dong et al., 2009).

The identity of the 1.28 ppm metabolite remains unknown. Although it most likely contains a lipid component (Manganas et al., 2007), its exact molecular nature has not yet been determined and its functional significance for neurogenesis awaits further studies. Recent reports indicate that the 1.28 ppm and adjacent resonances may also be associated with apoptosis. A similar lipidic peak resonating at 1.30 ppm has been also reported in apoptotic rat gliomas *in vivo* (Liimatainen et al., 2008), and more recent studies have found that the 1.28 ppm peak in cultured NPC increased during conditions that favored quiescence and apoptosis (Ramm et al., 2009). Apoptosis is common in the hippocampal neurogenic niche, as vast amounts of newborn cells die (Sierra et al., 2010). Thus, whether the 1.28 ppm peak detected in living brains originates from living or apoptotic NPCs remains to be determined.

SITES OF NEUROGENESIS IN THE ADULT HUMAN BRAIN

Nowadays, the consensus is that adult neurogenesis occurs in two main areas of the brain: the subgranular zone (SGZ) of the DG of the hippocampus, where new granule neurons are locally produced and have been associated with learning and memory, and

mood disorders; and the subventricular zone (SVZ), from where newborn cells migrate through the rostral migratory stream (RMS) and give rise to neurons in the OB, related to olfaction (Ma et al., 2009). Additionally, there are recent reports of adult neurogenesis in the neocortex, as well as the striatum, amygdala, substantia nigra (SN), and a few other areas in the rodent brain, as reviewed by Gould (2007). In humans, multipotent progenitors have been isolated from the temporal and frontal cortex, as well as the amygdala from patients undergoing brain resection due to epilepsy, trauma, or dysplasia (Arsenijevic et al., 2001). However, studies in healthy humans have suggested that neocortical neurogenesis is restricted to the perinatal period or, at least, that the contribution of adult-born neurons to the total cortical population is extremely small and undetectable by ^{14}C methods (Spalding et al., 2005; Bhardwaj et al., 2006).

NEUROGENESIS IN THE ADULT HUMAN HIPPOCAMPUS

In rodents, the hippocampal neurogenic cascade starts with the quiescent neuroprogenitors (QNPs; type-1 cells; radial glia), which reside in the SGZ. QNPs proliferate, giving rise to a transient population, the amplifying neuroprogenitors (ANPs; type-2a cells) which in turn proliferate and differentiate into neuronal-committed NBs (type-2b and type-3 cells). Finally, at the end of a 4-week period, the surviving NBs become mature neurons integrated into the circuitry (reviewed by Kempermann et al., 2004; Encinas and Enikolopov, 2008).

In humans, adult hippocampal neurogenesis was demonstrated by analysis of postmortem tissue of cancer patients (Eriksson et al., 1998), and changes in it under different conditions such as physical exercise and aging have been observed indirectly using CBV (Pereira et al., 2007) and ^{1}H-MRS (Manganas et al., 2007) in healthy adults *in vivo*. The presence of functional NPCs in the adult human hippocampus was further demonstrated by culture, expansion, and differentiation of human NPCs *in vitro* (Kukekov et al., 1999; Roy et al., 2000; Moe et al., 2005). A recent study has shown that the adult human SGZ contains DCX-expressing cells that co-localize both with markers of proliferation (MCM2, Ki67, PCNA) and mature neurons (NeuN, β-III-tubulin), supporting the existence of NBs throughout the human lifespan (Knoth et al., 2010).

Other studies, however, failed to detect NPCs or proliferating cells in the adult hippocampus of epileptic patients using immunohistochemical methods, such as expression of nestin, vimentin, or Ki67 (Arnold and Trojanowski, 1996; Del Bigio, 1999; Blumcke et al., 2001; Seress et al., 2001; Fahrner et al., 2007). This conflicting literature can be explained by different sensitivities of the particular method used in each study. Overall, future work is needed to determine all components of the hippocampal neurogenic niche and the cellular types that comprise human neurogenic cascade.

NEUROGENESIS IN THE ADULT SVZ

In rodents, the stem cells of the SVZ are specialized astrocytes called B cells. These cells proliferate and give rise to C cells, the transient amplifying population of the system (Doetsch et al., 1999). These C cells generate NBs or A cells, which form chains of proliferating cells that migrate ensheathed by astrocytes forming the RMS toward the OB, where they differentiate into granule cells and periglomerular interneurons (Lois et al., 1996). In non-human primates, the structure is notably similar, with astrocytic-like precursors in the SVZ that generate chains and honeycomb-like structures of migrating NBs that reach the OB through the RMS (Kornack and Rakic, 2001; Pencea et al., 2001).

In humans, proliferating BrdU+ cells were found in the SVZ, but they did not co-localize with either GFAP or NeuN (Eriksson et al., 1998). Similarly to human SGZ NPCs, the functional NPCs from the human SVZ were grown *in vitro* (Kukekov et al., 1999) and, more recently, isolated from the healthy and diseased elderly SVZ (Leonard et al., 2009). Further studies showed the presence of proliferating putative NPCs, labeled with nestin and PCNA (Bernier et al., 2000), as well as putative NBs, labeled with PSA-NCAM, in the human SVZ (Weickert et al., 2000). However, only recently was the human SVZ niche thoroughly described. First, a well-defined astrocytic ribbon formed by the B cells was observed in the SVZ, similarly to rodent SVZ, but no evidence of cells migrating in an organized RMS was found (Sanai et al., 2004). The human RMS remained elusive, until a report that it was organized around the lateral ventricular extension which reached the OB (Curtis et al., 2007b). This report was criticized by Alvarez-Buylla and colleagues, who claimed that it had not unquestionably proved the existence of an olfactory ventricle and the migrating, proliferating NBs in the RMS (Sanai et al., 2007). Further study then showed scarce cells that co-expressed markers of proliferation (PCNA) and NBs (PSA-NCAM), but no clear evidence of migration (Kam et al., 2009). In addition, it appears that the human RMS consists of four layers, similar to the SVZ (Kam et al., 2009), which prompted others to suggest that the human RMS may be a rostral extension of the proliferative zone, rather than the migratory pathway as found in rodents and non-human primates (Whitman and Greer, 2009). Nonetheless, there is no consensus in the literature on whether the SVZ/RMS are actively providing a source of newborn neurons to the human OB throughout adulthood.

Finally, the human OB hosts NPCs, which have been isolated from patients undergoing neurosurgery and grown in culture, where they differentiated into neurons, astrocytes, and oligodendrocytes (Pagano et al., 2000). In agreement, new neurons seem to be produced locally in the human OB, as shown by co-localization with Ki67 and NeuroD (Bedard and Parent, 2004). However, the significance of local neurogenesis in the adult human OB is still debatable.

RELEVANCE OF ADULT NEUROGENESIS TO HUMAN DISEASE

The majority of studies on human neurogenesis compare findings in healthy people to those in patients with a variety of neurological diseases. A summary comparing the alteration in neurogenesis in rodent models of disease and human patients is shown in **Table 2**. These studies use immunohistochemistry to detect biomarkers of proliferation or specific cell-types, and thus are only able to report differences in proliferation and putative NPCs and NBs (pNPCs, pNBs), but not actual neurogenesis (i.e., formation of new neurons). Thus, we label these detected cells "putative" because none of the studies demonstrated that proliferating cells differentiated into mature, functional neurons. To directly reach the conclusion that neurogenesis is occurring lineage tracing using BrdU or analogs is required.

EPILEPSY

Epilepsy is a common human disease that affects more than 50 million people worldwide (Kuruba et al., 2009). One of the most intractable forms is temporal lobe epilepsy (TLE), characterized by altered

Table 2 | Adult neurogenesis during disease.

Disease	Area	Rodent data	Human data
Epilepsy	Hippo.	Acute increase in proliferation	Increase in pNPCs and proliferation in pediatric patients
		Acute increase in neurogenesis	Increase or no change in proliferation in adult patients
		Aberrant and ectopic new neurons Chronic depletion	Decrease, no changed or increase in pNBs in adult patients
Huntington's disease	SVZ	Increased or unchanged SVZ proliferation migration of new neurons into the striatum	Increase in proliferation; thicker SVZ increase in pNPCs and pNBs
Alzheimer's disease	SVZ	Decrease in proliferation Decrease in differentiation	Decrease in proliferation Increase in pNPCs
	Hippo.	Increase, no change or decrease in proliferation Increase in neurogenesis Decrease in differentiation and survival of newborn neurons	No change in proliferation Increase in pNBs
Parkinson's disease	SVZ	Decrease in proliferation Transient decrease in OB neurogenesis Increase in OB neurogenesis and total neurons	Decrease in proliferation Decrease in putative OB progenitors Increase in OB neurogenesis and DA neurons
	Hippo.	Decrease in proliferation	Decrease in pNPCs
	S. nigra	No proliferation or NPCs Induction of neurogenesis	No proliferation or pNPCs
Stroke	SVZ	Increase in proliferation Increase in neurogenesis	NR
	Hippo.	Increase in proliferation Increase in neurogenesis	NR
	Striatum	Induction of neurogenesis from SVZ progenitors	NR
	Cortex	Induction of neurogenesis from SVZ progenitors	Increase in proliferation Increase in pNBs
Depression	Hippo.	Antidepressants increase proliferation and neurogenesis	Increase or no changes in proliferation
			Increase in pNPCs in patients treated with antidepressants

This table summarizes the major changes in neurogenesis in human neurological and psychiatric disorders. For details and references, see main text. Hippo., hippocampus; S. nigra, substantia nigra; NR, non-reported.

electrical activity, aberrant synaptic reorganization and neurodegeneration in the hippocampus, as well as development of depression and impairments in learning and memory (Kuruba et al., 2009).

In rodents, there is abundant literature reporting that hippocampal neurogenesis increases in models of acute seizures, either by administration of glutamate receptors agonists such as kainic acid, or by electrical stimulation of the hippocampus or the piriform cortex. In these models an increment in the proliferation of the hippocampal NPCs results in a concomitant increase in the number of newborn neurons (reviewed by Parent, 2002; Curtis et al., 2007a; Kuruba et al., 2009). However, the newborn neurons are located ectopically (in the hilus and the molecular layer of the dentate gyrus) and display aberrant connectivity and morphology (Parent et al., 1997; Scharfman et al., 2000). The seizure-induced abnormal neurogenesis may have detrimental consequences and contribute to aberrant synaptic reorganization (Parent, 2002). In contrast, in models of chronic epilepsy, neurogenesis seems to return to basal levels or even to be downregulated as compared to control animals (Kuruba et al., 2009).

Several studies have reported changes in adult neurogenesis in patients with TLE, who were all pharmacoresistant and had to undergo temporal lobectomy, providing the source for studies of neurogenesis. Utilizing Ki67 labeling the initial study showed no evidence of proliferation in the adult epileptic SGZ, since the number of Ki67+ cells was not significantly larger compared to other DG regions (Del Bigio, 1999). In addition, the number of pNBs (PSA-NCAM+ cells) was smaller in TLE patients than in age-matched controls (Mikkonen et al., 1998). Further comparison of adult TLE patients and controls showed similar levels of proliferation, measured by the number of Ki67+ and MCM2+ cells, as well as DCX protein expression and the number of DCX+ cells (Fahrner et al., 2007). In contrast, pediatric (<19 months of age) TLE patients had

increased number of proliferating pNPCs, labeled with nestin and Ki67 (Blumcke et al., 2001). More recent studies, however, contradict the previous literature. One study described a not quantified increase in proliferating cells (PCNA+ cells), and pNPCs (vimentin, musashi+ cells) in the SGZ and SVZ of adult TLE patients compared to controls (Crespel et al., 2005), while another reported augmented DCX protein and gene expression and number of pNBs (DCX+ cells) in TLE patients in the hippocampus and other temporal cortical regions (Liu et al., 2008). In these patients the DCX+ cells expressed markers of the neuronal lineage, such as PSA-NCAM or NeuN, but the authors did not provide the rationale for their findings contradicting previous literature and only noted that the effect of TLE on human neurogenesis was not as "dramatic" as in animal models of epilepsy (Liu et al., 2008). Finally, although many *ex vivo* studies showed the presence of functional NPCs in the epileptic hippocampus (Kukekov et al., 1999; Roy et al., 2000; Moe et al., 2005), it has been recently shown that their proliferative and multipotential properties *in vitro* depend on disease duration and were almost absent in epileptic patients with mesial temporal sclerosis, a late consequence of TLE (Paradisi et al., 2010). In conclusion, in infants, epilepsy is associated with increased proliferation in the hippocampus, but whether this proliferation leads to an increase of newborn neurons remains unknown. In adults, reports are controversial and most likely reflect a wide range of disease duration, which apparently affects NPCs (Paradisi et al., 2010). Whether changes in neurogenesis also relate to the changes in mood and cognitive performance observed in TLE patients remains to be determined.

Epilepsy also alters SVZ neurogenesis. In rats, pilocarpin-induced status epilepticus produced an increased proliferation of SVZ NPCs as well as an expansion of the RMS, which contained more proliferating cells and NBs (Parent et al., 2002). In addition, some cells in the RMS were found to migrate ectopically into the surrounding cortical parenchyma, although the majority of these ectopic cells did not survive (Parent et al., 2002). In human, increased proliferation, ectopic parenchymal migration, and neuronal differentiation were also found using organotypic slice preparations from tissue resected from patients with a variety of intractable cortical seizures (Gonzalez-Martinez et al., 2007). The functional significance of increased neurogenesis and ectopic migration of SVZ precursors induced by SE in rodents and humans remains to be established.

HUNTINGTON'S DISEASE

Huntington's disease (HD) is caused by expanded CAG repeats in the huntingtin gene, which leads to protein accumulation and neurodegeneration in the striatum, a brain area that lies below the SVZ. In transgenic mice models of HD, in which little striatal neurodegeneration occurs, neurogenesis in the SVZ remains unaltered; whereas in rat models of striatal degeneration an increased SVZ proliferation is observed (reviewed by Curtis et al., 2007a). Interestingly, some of the newly generated cells are able to migrate into the damaged striatum, where they express neuronal markers (Tattersfield et al., 2004), although it is unknown whether they are functionally mature neurons. These results suggested an endogenous regeneration potential in HD because the new born neurons would take long time to develop huntingtin inclusions and in the meanwhile could contribute to maintaining the striatal circuitry (Curtis et al., 2007a).

Studies of HD patients have shown increased intensity of PCNA staining in the SVZ lining of the striatum compared to age-matched controls, suggesting an increase in SVZ proliferation. Additionally, the expression levels of PCNA correlated with the number of CAG repeats in these patients. The proliferating cells expressed markers of glia (GFAP) and neurons (β-III-Tubulin), suggesting the presence of putative B and A cells, respectively (Curtis et al., 2003). Further, the SVZ was thicker due to an increase in the number of B cells, identified by cellular morphology, and the number of dividing cells, labeled with PCNA, in HD patients compared to age-matched controls (Curtis et al., 2005a,b). Unexpectedly, some of the proliferating PCNA+ cells expressed markers of mature neurons such as βIII-Tubulin and this was interpreted as increased neurogenesis in HD patients (Curtis et al., 2005a). However, it takes days, if not weeks, for newborn cells to express markers of mature neurons. Therefore, an aberrant expression of PCNA in mature neurons or an aberrant expression of βIII-Tubulin in dividing cells in the SVZ of HD patients cannot be ruled out. Finally, migration of the newborn cells from the SVZ into the damaged human striatum and their neuronal differentiation has not been described yet and, thus, it remains unknown if the endogenous SVZ cells can be harnessed for repair in HD patients.

ALZHEIMER'S DISEASE

Alzheimer's disease (AD) is characterized by accumulation of β-amyloid and neurofibrillary tangles containing hyperphosphorylated tau protein throughout the cortex and the hippocampus, resulting in progressive dementia (Curtis et al., 2007a). Some pathological features of AD can be modeled in transgenic mice overexpressing amyloid precursor protein and presenilin 1 (APP/PS1). In these mice, memory impairment and increased hippocampal proliferation and neurogenesis were observed at 9, but not 3 months of age (Yu et al., 2009). However, earlier works showed that 6-month-old APP/PSE1 mice have unaltered proliferation and short-term survival (1–13 days), whereas they have a significant reduction of long-term survival (30–42 days) and differentiation (Verret et al., 2007). In addition, other transgenic mouse models of AD have shown otherwise. For instance, in triple transgenic mice (APP/PSE1/Tau) there is a gradual decrease in SGZ proliferation starting at 6 months of age (Rodriguez et al., 2008). On the other hand, 3-month-old mice expressing mutated APP have increased proliferation (Jin et al., 2004a) although this increase was reverted to control levels in older animals (Lopez-Toledano and Shelanski, 2007). Finally, in 6-week-old transgenic mouse expressing human APP showed decreased proliferation in control housing conditions as well as a decreased 4-week survival in enriched environment conditions (Naumann et al., 2010). In postmortem hippocampal samples from patients with advanced AD, an increased expression of NB proteins (DCX, PSA-NCAM, and NeuroD) compared to age-matched controls was reported, suggesting increased neurogenesis perhaps as a compensatory mechanism to cope with the AD-related cognitive impairment (Jin et al., 2004b). However, a more recent study of presenile AD patients failed to demonstrate increased proliferation in the DG, whereas it showed an increased proliferation (Ki67+ cells) associated with gliogenesis and angiogenesis in other hippocampal regions. Further, the same study attributed changes in DCX immunolabeling to postmortem

breakdown (Boekhoorn et al., 2006). Thus, it is clear that more comprehensive studies are needed to clarify the changes in SGZ neurogenesis in AD. Furthermore, the relation between potentially altered neurogenesis and the cognitive impairments observed in AD remains to be elucidated (Lazarov et al., 2010).

Subventricular zone neurogenesis is also altered in mouse AD-models. For instance, transgenic APP or PSE1 mice as well as wild-type mice infused in the lateral ventricles with βA peptide had reduced SVZ proliferation compared to control mice (Haughey et al., 2002; Rodriguez et al., 2009; Veeraraghavalu et al., 2010). Decreased proliferation and neuronal differentiation were also observed in cultured NPCs isolated from PSE1 mutant SVZ (Veeraraghavalu et al., 2010) and from APP/PS1 mutant SVZ (Demars et al., 2010). In human AD patients, decreased proliferation (Ki67+ cells) accompanied by a puzzling increase in nestin expression was observed in postmortem sections (Ziabreva et al., 2006). In agreement, cultured embryonic human NPC had decreased proliferation and increased apoptosis when treated with Aβ peptide compared to control NPCs treated with vehicle (Haughey et al., 2002). Thus, there are consistently lower levels in SVZ neurogenesis in AD patients as well as in and rodent AD models, prompting the suggestion that impaired SVZ neurogenesis may have functional consequences in AD (Curtis et al., 2007a). For instance, olfactory deficits significantly predict development of AD in patients with mild cognitive impairment (Devanand et al., 2000), although whether these olfactory deficits are related to decreased SVZ neurogenesis remains unknown.

PARKINSON'S DISEASE

The major hallmark of the Parkinson's disease (PD) is the death of dopaminergic neurons in the SN, with consequent impairment of movement control, mood, and motivation (Hoglinger et al., 2004). In animal models of PD, a reduced proliferation in the SVZ overlaying the striatum is observed. C and A cells in the SVZ receive dopaminergic fibers from the SN (Hoglinger et al., 2004). In rodents, this dopaminergic innervation controls the proliferation of these two cell types, because the injection of a toxic dopamine analog (6-hydroxydopamine) in the nigrostriatal pathway dennervates both the striatum and the SVZ and results in decreased SVZ proliferation (Hoglinger et al., 2004), resulting in a transient decrease of newborn neurons in the OB granule cell layer (Hoglinger et al., 2004; Winner et al., 2006). In the lesioned mice, administration of a dopaminergic precursor (levodopa) partially recovered SVZ proliferation close to control levels (Hoglinger et al., 2004). Similar results were obtained in PD patients. The number of SVZ proliferating cells, labeled with PCNA, as well as OB pNPCs (nestin+ cells) was reduced compared to age-matched controls (Hoglinger et al., 2004), although no changes in the number of cells in the OB granule cell layer have been reported.

Interestingly, in the OB glomerule cell layer there is an increase in the number of newborn as well as total dopaminergic cells, expressing the synthesizing enzyme tyrosine hydroxylase, both in rodents whose nigrostriatal pathway was lesioned with 6-hydroxydopamine (Winner et al., 2006) and in PD patients (Huisman et al., 2004). This increase in dopaminergic cells remains unexplained and it is unexpected in the light of the decreased SVZ proliferation. Nonetheless, because dopamine inhibits olfactory transmission, it has been suggested that the increase in OB dopaminergic neurons could explain the hyposmia (Huisman et al., 2004) that occurs in up to 95% of PD patients prior to the onset of other clinical symptoms (Haehner et al., 2009). Dopaminergic innervation may also regulate neurogenesis in the hippocampus. In rodents, lesions of the nigrostriatal pathway decrease hippocampal proliferation (Hoglinger et al., 2004; Suzuki et al., 2010), and in the hippocampus of PD patients, less pNPCs (nestin+ cells) are observed compared to age-matched controls (Hoglinger et al., 2004). While initial reports suggested the neurogenesis was induced in the SN in rodent models of PD (Zhao et al., 2003), later studies, however, showed no evidences of proliferation or NPCs in the SN either in rodent models of PD (Frielingsdorf et al., 2004; Yoshimi et al., 2005) nor in PD patients (Yoshimi et al., 2005).

STROKE/ISCHEMIA

A stroke, or cerebrovascular accident, results from occlusion of cerebral arteries leading to decreased local blood flow (ischemia) or from a hemorrhage. In the stroked tissue, two areas of injury can be discriminated: the core infarcted area, where neurons die of necrosis and very little, if any, regeneration is possible; and the penumbra area, which surrounds the infarcted area, is perfused by collateral arteries, and is not irreversibly damaged. Given that the ischemic stroke is the third most frequent cause of mortality in industrialized countries, major scientific efforts have been directed toward discoveries of therapies to facilitate recovery from the insult.

In rodent and non-human primate models of stroke, such as occlusion of the medial cerebral artery occlusion (MCAO), adult neurogenesis is up-regulated both in the SVZ–RMS–OB and the hippocampus (Jin et al., 2001; Zhang et al., 2001; Koketsu et al., 2006; Lledo et al., 2006). In addition, stroke also induces ectopic neurogenesis in penumbra areas, such as the striatum, due to atypical migration of SVZ newborn cells (Arvidsson et al., 2002). Cortical neurogenesis in the penumbra area in rodent models of stroke has been found by some (Gu et al., 2000; Jin et al., 2003) but not by others (Arvidsson et al., 2002). Interestingly, the newborn cells differentiated into striatal neurons and acquired the same phenotype of the neurons which had died as a consequence of the stroke, suggesting that neuronal replacement can occur in the stroked striatum (Arvidsson et al., 2002). Although the vast majority of the striatal newborn cells died, possibly due to an unfavorable environment (Arvidsson et al., 2002), stroke-induced striatal neurogenesis seems to have functional consequences in rodents, since it has been shown that the transgenic ablation of the NB protein DCX prevented stroke-induced neurogenesis and worsened the sensorimotor and behavioral deficits after MCAO (Jin et al., 2010).

This research indicated that harnessing aberrant striatal neurogenesis in stroke may be useful to reduce the neurological deficits in patients (reviewed in Zhang and Chopp, 2009). The patients who suffered the ischemic, middle cerebral artery stroke showed increased proliferation of putative B cells (Ki67, GFAP+ cells) and putative C cells (PSA-NCAM+ cells), in the ipsilateral SVZ compared to the contralateral side of the stroke (Marti-Fabregas et al., 2010). In addition, there were traces of ectopic neurogenesis not in the striatum, but in the cortex. A significant increase in proliferating Ki67+ cells and pNBs (PSA-NCAM+ cells) was found in the cortical penumbra region of ischemic stroke patients compared to age-matched controls (Jin et al., 2006; Macas et al., 2006) as well

as in perihematomal regions in patients with intracerebral hemorrhage (Shen et al., 2008). The relevance of this increase in cortical neurogenesis in stroke patients remains to be investigated, but the phenomena certainly raise the hope that neurogenesis might be harnessed as a possible treatment for stroke patients.

MOOD DISORDERS

Depression, or major depressive disorder (MDD), is characterized by anhedonia and the absence of positive affect (Craske et al., 2009). MDD is thought to be caused by an imbalance in the levels of monoamines, such as serotonin and noradrenalin, as formulated in the "monoamine hypothesis of depression" (Duman et al., 2000; Wong and Licinio, 2001). This hypothesis is strongly supported by the ability of antidepressant drugs, such as selective serotonin reuptake inhibitors (SSRIs) or tricyclic antidepressants (TCAs), to improve the symptomatology by increasing synaptic levels of monoamines (Wong and Licinio, 2001). However, while antidepressant drugs modify monoamine levels within hours, it takes weeks of daily treatments to observe the behavioral effects, indicating that long-term changes underlie the effects of antidepressant therapies (Wong and Licinio, 2001). Structural changes in the cortex and hippocampus, such as alterations in neuronal morphology, synaptic plasticity, and cell survival, may also be part of the disease (Duman et al., 2000). For instance, MDD patients may have hippocampal atrophy (Sheline et al., 1996), which correlates with poor cognitive performance in these patients (Frodl et al., 2006). In addition, MDD patients have decreased pyramidal neuronal soma size and higher density of glial, pyramidal, and granule cells in the hippocampus compared to age-matched controls (Stockmeier et al., 2004). Together, these results suggest a significant reduction in the neuropil (glial and neuronal processes) in MDD patients (Stockmeier et al., 2004). While the absolute numbers of glia and neurons in the hippocampus of MDD patients are unknown (Stockmeier et al., 2004), small increases in hippocampal apoptosis in MDD patients have been reported (Lucassen et al., 2001).

The hippocampal pathology in MDD has led to the "neurogenesis hypothesis of depression." Postulated by Drew and Hen (2007), the hypothesis states that altered levels of adult hippocampal neurogenesis may underlie the pathology of depression as well as the behavioral effects of antidepressants. This hypothesis is based on several lines of evidence showing that in rodents, chronic antidepressant treatments increase hippocampal neurogenesis (Malberg et al., 2000) and that, conversely, hippocampal neurogenesis is necessary for the behavioral effects of antidepressant drugs (Santarelli et al., 2003). The main caveat of this hypothesis is that neurogenesis seems not to be sufficient to cause depression, because decreased neurogenesis does not always induce depressive behaviors, and vice versa, depressive behaviors can be induced in experimental paradigms that do not affect neurogenesis (Vollmayr et al., 2007). To further complicate the interpretation of the data, the depression-induced morphological alterations, including those in neurogenesis, have generally been blamed on depression-related stress (Duman et al., 2000).

Stress, or more properly, the failure to adapt to stressful situations, is a shared symptom of depression and other mood disorders, such as anxiety and fear disorders (Craske et al., 2009), although is still under debate whether it is a concurrent epiphenomenon or an actual pathological state (Wong and Licinio, 2001). The connection of stress, anxiety, and MDD is not trivial, because the most commonly utilized rodent models of depression, such as learned helplessness, chronic mild stress, and chronic psychosocial stress induce depressive behaviors by increasing stress levels (Vollmayr et al., 2007; Pryce and Seifritz, 2011). Stress, through the actions of glucocorticoids, reduces adult hippocampal neurogenesis (Mirescu and Gould, 2006), produces dendritic atrophy (McEwen, 2001), and leads to decreased hippocampal volume (Tata and Anderson, 2010). From the rodent literature, it is therefore difficult to extract a clear picture of whether the alterations in adult hippocampal neurogenesis are due to stress, anxiety, depression, or a combination of these factors.

In MDD patients, recent studies have shown alterations in adult hippocampal neurogenesis (Reif et al., 2006; Boldrini et al., 2009). An initial study on postmortem samples of a cohort of 15 MDD patients showed no alterations in proliferation (Ki67+ cells) compared to age-matched controls (Reif et al., 2006). In contrast, a more recent study of a cohort of 19 MDD patients treated with TCAs such as nortriptyline, showed a significant increase in proliferation (Ki67+ cells) compared to the untreated MDD patients. In addition, a significant increase in the number of pNPCs (nestin+ cells) was found in patients treated with TCAs or SSRIs such as fluoxetine, compared to the untreated MDD patients (Boldrini et al., 2009). Interestingly, and similar to the observation that decreased neurogenesis is not required to induce depression-like behavior in rodents (Vollmayr et al., 2007), there were no significant differences in the number of proliferative cells or pNPCs in MDD patients compared to age-matched controls (Boldrini et al., 2009). Several limitations where identified, such as the small sample size, the possibility that treated MDD patients had more severe symptoms than untreated patients (hence, the prescription of pharmacological treatment), and the high incidence of suicide in the untreated patients (Boldrini et al., 2009). Taken together, these data suggest that decreased neurogenesis is not causative for depressive symptoms; however, treatment with antidepressants does improve the symptoms while increasing neurogenesis in the adult hippocampus. Further research needs to test the correlations between neurogenesis, MDD, stress, and antidepressant drugs. In particular, methods to assess human neurogenesis *in vivo* are of particular importance for longitudinal studies in MDD patients, to quantify neurogenesis before and after the antidepressant treatment, and in correlation with the onset and/or improvement of depressive symptoms.

MISCELLANEA

Finally, there is also sporadic evidence that adult neurogenesis may be altered in other brain diseases. For instance, in *traumatic brain injury*, increased hippocampal proliferation has been reported in humans (Gerber et al., 2009) and mice (Yu et al., 2008). In patients with *hypoxic-ischemic encephalopathy,* which results in neuronal loss in the cortex and the hippocampus, there is a non-significant increase in PCNA labeled cells (Mattiesen et al., 2009). During *bacterial meningitis* an increase in hippocampal proliferation as well as the number of pNBs was observed (Gerber et al., 2009), although in mice inflammation results in decreased proliferation and neurogenesis (Monje et al., 2003). In patients with *subarachnoid hemorrhage*, increased mRNA and protein levels of vimentin, musashi, and nestin

were observed in the frontal lobe compared to control brains, while proliferating pNPCs (Ki67, nestin+ cells) were also found in the damaged frontal lobes (Sgubin et al., 2007). In *autism*, it has recently been suggested that neurogenesis may be altered because of the found increased thickness and dysplasia of the SVZ (Wegiel et al., 2010). In *schizophrenia*, decreased hippocampal proliferation (Ki67+ cells) has been reported (Reif et al., 2006), in agreement with the findings of decreased NPC proliferation (Mao et al., 2009) and aberrant morphology and excitability of the newborn neurons in mice with lower expression of disrupted-in-schizophrenia 1 (DISC1), a schizophrenia susceptibility gene (Duan et al., 2007). In *alcohol abuse* patients, no significant differences in hippocampal proliferation have been found (Reif et al., 2006), although chronic alcohol exposure decreases neurogenesis in rats (He et al., 2005).

CONCLUSION

Overall, studies of adult human neurogenesis, even though hampered by limitations of the available methodologies for both *ex vivo* and *in vivo* assessments, are promising. Development of new antibodies targeted to human antigens will certainly improve immunohistochemical data, but even then, such labeling will provide only putative information. It is in combination with BrdU labeling that the production of new neurons can be assessed and quantified. As more BrdU labeled tissue is generated, the changes in the neurogenic cascade that accompany brain disorders will be elucidated. However, several considerations need to be taken into account when studying postmortem human tissue, in particular the postmortem delay, the cause of death, and the age at the time of death. Thus, the future of adult human neurogenesis research and the prospects of harnessing its potential for treatments of brain disorders will heavily depend on the development and thorough validation of methods for *in vivo* assessments, as those offer unique opportunity for both cross-sectional and longitudinal studies of the neurogenic niches while they are intact within the living brain tissue.

ACKNOWLEDGMENTS

We would like to thank Juan J.P. Deudero, William T. Choi, and Fatih Semerci for their help during the preparation of this manuscript. This work was supported by the NIH Intellectual and Developmental Disabilities Research Grant (P30HD024064), the McKnight Endowment Fund, the DANA Foundation, and the Farish Foundation (Mirjana Maletic-Savatic).

REFERENCES

Altman, J. (1962). Are new neurons formed in the brains of adult mammals? *Science* 135, 1127–1128.

Antel, J. P., Nalbantoglu, J., and Olivier, A. (2000). Neuronal progenitors-learning from the hippocampus. *Nat. Med.* 6, 249–250.

Arnold, S. E., and Trojanowski, J. Q. (1996). Human fetal hippocampal development: II. The neuronal cytoskeleton. *J. Comp. Neurol.* 367, 293–307.

Aronen, H. J., Pardo, F. S., Kennedy, D. N., Belliveau, J. W., Packard, S. D., Hsu, D. W., Hochberg, F. H., Fischman, A. J., and Rosen, B. R. (2000). High microvascular blood volume is associated with high glucose uptake and tumor angiogenesis in human gliomas. *Clin. Cancer Res.* 6, 2189–2200.

Arsenijevic, Y., Villemure, J. G., Brunet, J. F., Bloch, J. J., Deglon, N., Kostic, C., Zurn, A., and Aebischer, P. (2001). Isolation of multipotent neural precursors residing in the cortex of the adult human brain. *Exp. Neurol.* 170, 48–62.

Arvidsson, A., Collin, T., Kirik, D., Kokaia, Z., and Lindvall, O. (2002). Neuronal replacement from endogenous precursors in the adult brain after stroke. *Nat. Med.* 8, 963–970.

Bailis, J. M., and Forsburg, S. L. (2004). MCM proteins: DNA damage, mutagenesis and repair. *Curr. Opin. Genet. Dev.* 14, 17–21.

Bedard, A., and Parent, A. (2004). Evidence of newly generated neurons in the human olfactory bulb. *Brain Res. Dev. Brain Res.* 151, 159–168.

Bernier, P. J., Vinet, J., Cossette, M., and Parent, A. (2000). Characterization of the subventricular zone of the adult human brain: evidence for the involvement of Bcl-2. *Neurosci. Res.* 37, 67–78.

Bhardwaj, R. D., Curtis, M. A., Spalding, K. L., Buchholz, B. A., Fink, D., Bjork-Eriksson, T., Nordborg, C., Gage, F. H., Druid, H., Eriksson, P. S., and Frisén, J. (2006). Neocortical neurogenesis in humans is restricted to development. *Proc. Natl. Acad. Sci. U.S.A.* 103, 12564–12568.

Blumcke, I., Schewe, J. C., Normann, S., Brustle, O., Schramm, J., Elger, C. E., and Wiestler, O. D. (2001). Increase of nestin-immunoreactive neural precursor cells in the dentate gyrus of pediatric patients with early-onset temporal lobe epilepsy. *Hippocampus* 11, 311–321.

Boekhoorn, K., Joels, M., and Lucassen, P. J. (2006). Increased proliferation reflects glial and vascular-associated changes, but not neurogenesis in the presenile Alzheimer hippocampus. *Neurobiol. Dis.* 24, 1–14.

Boldrini, M., Underwood, M. D., Hen, R., Rosoklija, G. B., Dwork, A. J., John Mann, J., and Arango, V. (2009). Antidepressants increase neural progenitor cells in the human hippocampus. *Neuropsychopharmacology* 34, 2376–2389.

Cattoretti, G., Becker, M. H., Key, G., Duchrow, M., Schluter, C., Galle, J., and Gerdes, J. (1992). Monoclonal antibodies against recombinant parts of the Ki-67 antigen (MIB 1 and MIB 3) detect proliferating cells in microwave-processed formalin-fixed paraffin sections. *J. Pathol.* 168, 357–363.

Cha, S., Johnson, G., Wadghiri, Y. Z., Jin, O., Babb, J., Zagzag, D., and Turnbull, D. H. (2003). Dynamic, contrast-enhanced perfusion MRI in mouse gliomas: correlation with histopathology. *Magn. Reson. Med.* 49, 848–855.

Colucci-D'Amato, L., Bonavita, V., and di Porzio, U. (2006). The end of the central dogma of neurobiology: stem cells and neurogenesis in adult CNS. *Neurol. Sci.* 27, 266–270.

Craske, M. G., Rose, R. D., Lang, A., Welch, S. S., Campbell-Sills, L., Sullivan, G., Sherbourne, C., Bystritsky, A., Stein, M. B., and Roy-Byrne, P. P. (2009). Computer-assisted delivery of cognitive behavioral therapy for anxiety disorders in primary-care settings. *Depress. Anxiety* 26, 235–242.

Crespel, A., Rigau, V., Coubes, P., Rousset, M. C., de Bock, F., Okano, H., Baldy-Moulinier, M., Bockaert, J., and Lerner-Natoli, M. (2005). Increased number of neural progenitors in human temporal lobe epilepsy. *Neurobiol. Dis.* 19, 436–450.

Curtis, M. A., Faull, R. L., and Eriksson, P. S. (2007a). The effect of neurodegenerative diseases on the subventricular zone. *Nat. Rev. Neurosci.* 8, 712–723.

Curtis, M. A., Kam, M., Nannmark, U., Anderson, M. F., Axell, M. Z., Wikkelso, C., Holtas, S., van Roon-Mom, W. M., Bjork-Eriksson, T., Nordborg, C., Frisén, J., Dragunow, M., Faull, R. L., and Eriksson, P. S. (2007b). Human neuroblasts migrate to the olfactory bulb via a lateral ventricular extension. *Science* 315, 1243–1249.

Curtis, M. A., Penney, E. B., Pearson, A. G., van Roon-Mom, W. M., Butterworth, N. J., Dragunow, M., Connor, B., and Faull, R. L. (2003). Increased cell proliferation and neurogenesis in the adult human Huntington's disease brain. *Proc. Natl. Acad. Sci. U.S.A.* 100, 9023–9027.

Curtis, M. A., Penney, E. B., Pearson, J., Dragunow, M., Connor, B., and Faull, R. L. (2005a). The distribution of progenitor cells in the subependymal layer of the lateral ventricle in the normal and Huntington's disease human brain. *Neuroscience* 132, 777–788.

Curtis, M. A., Waldvogel, H. J., Synek, B., and Faull, R. L. (2005b). A histochemical and immunohistochemical analysis of the subependymal layer in the normal and Huntington's disease brain. *J. Chem. Neuroanat.* 30, 55–66.

Danilov, A. I., Gomes-Leal, W., Ahlenius, H., Kokaia, Z., Carlemalm, E., and Lindvall, O. (2009). Ultrastructural and antigenic properties of neural stem cells and their progeny in adult rat subventricular zone. *Glia* 57, 136–152.

Del Bigio, M. R. (1999). Proliferative status of cells in adult human dentate gyrus. *Microsc. Res. Tech.* 45, 353–358.

Demars, M., Hu, Y. S., Gadadhar, A., and Lazarov, O. (2010). Impaired neurogenesis is an early event in the etiology of familial Alzheimer's disease in transgenic mice. *J. Neurosci. Res.* 88, 2103–2117.

des Portes, V., Pinard, J. M., Billuart, P., Vinet, M. C., Koulakoff, A., Carrie, A., Gelot, A., Dupuis, E., Motte, J., Berwald-Netter, Y., Catala, M., Kahn, A., Beldjord, C., and Chelly, J. (1998). A novel CNS gene required for neuronal migration and involved in X-linked subcortical laminar heterotopia and

lissencephaly syndrome. *Cell* 92, 51–61.

Devanand, D. P., Michaels-Marston, K. S., Liu, X., Pelton, G. H., Padilla, M., Marder, K., Bell, K., Stern, Y., and Mayeux, R. (2000). Olfactory deficits in patients with mild cognitive impairment predict Alzheimer's disease at follow-up. *Am. J. Psychiatry* 157, 1399–1405.

Dityatev, A., Dityateva, G., Sytnyk, V., Delling, M., Toni, N., Nikonenko, I., Muller, D., and Schachner, M. (2004). Polysialylated neural cell adhesion molecule promotes remodeling and formation of hippocampal synapses. *J. Neurosci.* 24, 9372–9382.

Djuric, P. M., Benveniste, H., Wagshul, M. E., Henn, F., Enikolopov, G., and Maletic-Savatic, M. (2008). Response to comments on "magnetic resonance spectroscopy identifies neural progenitor cells in the live human brain". *Science* 321, 640e.

Doetsch, F., Caille, I., Lim, D. A., Garcia-Verdugo, J. M., and Alvarez-Buylla, A. (1999). Subventricular zone astrocytes are neural stem cells in the adult mammalian brain. *Cell* 97, 703–716.

Doetsch, F., Garcia-Verdugo, J. M., and Alvarez-Buylla, A. (1997). Cellular composition and three-dimensional organization of the subventricular germinal zone in the adult mammalian brain. *J. Neurosci.* 17, 5046–5061.

Dong, Z., Dreher, W., Leibfritz, D., and Peterson, B. S. (2009). Challenges of using MR spectroscopy to detect neural progenitor cells in vivo. *AJNR Am. J. Neuroradiol.* 30, 1096–1101.

Drew, M. R., and Hen, R. (2007). Adult hippocampal neurogenesis as target for the treatment of depression. *CNS Neurol Disord Drug Targets* 6, 205–218.

Duan, X., Chang, J. H., Ge, S., Faulkner, R. L., Kim, J. Y., Kitabatake, Y., Liu, X. B., Yang, C. H., Jordan, J. D., Ma, D. K., Liu, C. Y., Ganesan, S., Cheng, H. J., Ming, G. L., Lu, B., and Song, H. (2007). Disrupted-in-schizophrenia 1 regulates integration of newly generated neurons in the adult brain. *Cell* 130, 1146–1158.

Duman, R. S., Malberg, J., Nakagawa, S., and D'Sa, C. (2000). Neuronal plasticity and survival in mood disorders. *Biol. Psychiatry* 48, 732–739.

Eckenhoff, M. F., and Rakic, P. (1988). Nature and fate of proliferative cells in the hippocampal dentate gyrus during the life span of the rhesus monkey. *J. Neurosci.* 8, 2729–2747.

Encinas, J. M., and Enikolopov, G. (2008). Identifying and quantitating neural stem and progenitor cells in the adult brain. *Methods Cell Biol.* 85, 243–272.

Eriksson, P. S., Perfilieva, E., Bjork-Eriksson, T., Alborn, A. M., Nordborg, C., Peterson, D. A., and Gage, F. H. (1998). Neurogenesis in the adult human hippocampus. *Nat. Med.* 4, 1313–1317.

Fahrner, A., Kann, G., Flubacher, A., Heinrich, C., Freiman, T. M., Zentner, J., Frotscher, M., and Haas, C. A. (2007). Granule cell dispersion is not accompanied by enhanced neurogenesis in temporal lobe epilepsy patients. *Exp. Neurol.* 203, 320–332.

Friedman, S. D. (2008). Comment on "magnetic resonance spectroscopy identifies neural progenitor cells in the live human brain". *Science* 321, 640; author reply 640.

Frielingsdorf, H., Schwarz, K., Brundin, P., and Mohapel, P. (2004). No evidence for new dopaminergic neurons in the adult mammalian substantia nigra. *Proc. Natl. Acad. Sci. U.S.A.* 101, 10177–10182.

Frodl, T., Schaub, A., Banac, S., Charypar, M., Jager, M., Kummler, P., Bottlender, R., Zetzsche, T., Born, C., Leinsinger, G., Reiser, M., Möller, H. J., and Meisenzahl, E. M. (2006). Reduced hippocampal volume correlates with executive dysfunctioning in major depression. *J. Psychiatry Neurosci.* 31, 316–323.

Gerber, J., Tauber, S. C., Armbrecht, I., Schmidt, H., Bruck, W., and Nau, R. (2009). Increased neuronal proliferation in human bacterial meningitis. *Neurology* 73, 1026–1032.

Goldman, S. A., and Nottebohm, F. (1983). Neuronal production, migration, and differentiation in a vocal control nucleus of the adult female canary brain. *Proc. Natl. Acad. Sci. U.S.A.* 80, 2390–2394.

Goldman, S. A., and Windrem, M. S. (2006). Cell replacement therapy in neurological disease. *Philos. Trans. R. Soc. Lond. B Biol. Sci.* 361, 1463–1475.

Gonzalez-Martinez, J. A., Bingaman, W. E., Toms, S. A., and Najm, I. M. (2007). Neurogenesis in the postnatal human epileptic brain. *J. Neurosurg.* 107, 628–635.

Gould, E. (2007). How widespread is adult neurogenesis in mammals? *Nat. Rev. Neurosci.* 8, 481–488.

Gu, W., Brannstrom, T., and Wester, P. (2000). Cortical neurogenesis in adult rats after reversible photothrombotic stroke. *J. Cereb. Blood Flow Metab.* 20, 1166–1173.

Haehner, A., Boesveldt, S., Berendse, H. W., Mackay-Sim, A., Fleischmann, J., Silburn, P. A., Johnston, A. N., Mellick, G. D., Herting, B., Reichmann, H., and Hummel, T. (2009). Prevalence of smell loss in Parkinson's disease – a multicenter study. *Parkinsonism Relat. Disord.* 15, 490–494.

Hall, P. A., and Woods, A. L. (1990). Immunohistochemical markers of cellular proliferation: achievements, problems and prospects. *Cell Tissue Kinet.* 23, 505–522.

Haughey, N. J., Liu, D., Nath, A., Borchard, A. C., and Mattson, M. P. (2002). Disruption of neurogenesis in the subventricular zone of adult mice, and in human cortical neuronal precursor cells in culture, by amyloid beta-peptide: implications for the pathogenesis of Alzheimer's disease. *Neuromol. Med.* 1, 125–135.

He, J., Nixon, K., Shetty, A. K., and Crews, F. T. (2005). Chronic alcohol exposure reduces hippocampal neurogenesis and dendritic growth of newborn neurons. *Eur. J. Neurosci.* 21, 2711–2720.

Hoch, J. C., Maciejewski, M. W., and Gryk, M. R. (2008). Comment on "magnetic resonance spectroscopy identifies neural progenitor cells in the live human brain". *Science* 321, 640; author reply 640.

Hoglinger, G. U., Rizk, P., Muriel, M. P., Duyckaerts, C., Oertel, W. H., Caille, I., and Hirsch, E. C. (2004). Dopamine depletion impairs precursor cell proliferation in Parkinson disease. *Nat. Neurosci.* 7, 726–735.

Huisman, E., Uylings, H. B., and Hoogland, P. V. (2004). A 100% increase of dopaminergic cells in the olfactory bulb may explain hyposmia in Parkinson's disease. *Mov. Disord.* 19, 687–692.

Jansen, J. F., Gearhart, J. D., and Bulte, J. W. (2008). Comment on "magnetic resonance spectroscopy identifies neural progenitor cells in the live human brain". *Science* 321, 640; author reply 640.

Jansen, J. F., Shamblott, M. J., van Zijl, P. C., Lehtimaki, K. K., Bulte, J. W., Gearhart, J. D., and Hakumaki, J. M. (2006). Stem cell profiling by nuclear magnetic resonance spectroscopy. *Magn. Reson. Med.* 56, 666–670.

Jin, K., Galvan, V., Xie, L., Mao, X. O., Gorostiza, O. F., Bredesen, D. E., and Greenberg, D. A. (2004a). Enhanced neurogenesis in Alzheimer's disease transgenic (PDGF-APPSw,Ind) mice. *Proc. Natl. Acad. Sci. U.S.A.* 101, 13363–13367.

Jin, K., Peel, A. L., Mao, X. O., Xie, L., Cottrell, B. A., Henshall, D. C., and Greenberg, D. A. (2004b). Increased hippocampal neurogenesis in Alzheimer's disease. *Proc. Natl. Acad. Sci. U.S.A.* 101, 343–347.

Jin, K., Minami, M., Lan, J. Q., Mao, X. O., Batteur, S., Simon, R. P., and Greenberg, D. A. (2001). Neurogenesis in dentate subgranular zone and rostral subventricular zone after focal cerebral ischemia in the rat. *Proc. Natl. Acad. Sci. U.S.A.* 98, 4710–4715.

Jin, K., Sun, Y., Xie, L., Peel, A., Mao, X. O., Batteur, S., and Greenberg, D. A. (2003). Directed migration of neuronal precursors into the ischemic cerebral cortex and striatum. *Mol. Cell. Neurosci.* 24, 171–189.

Jin, K., Wang, X., Xie, L., Mao, X. O., and Greenberg, D. A. (2010). Transgenic ablation of doublecortin-expressing cells suppresses adult neurogenesis and worsens stroke outcome in mice. *Proc. Natl. Acad. Sci. U.S.A.* 107, 7993–7998.

Jin, K., Wang, X., Xie, L., Mao, X. O., Zhu, W., Wang, Y., Shen, J., Mao, Y., Banwait, S., and Greenberg, D. A. (2006). Evidence for stroke-induced neurogenesis in the human brain. *Proc. Natl. Acad. Sci. U.S.A.* 103, 13198–13202.

Johansson, C. B., Svensson, M., Wallstedt, L., Janson, A. M., and Frisen, J. (1999). Neural stem cells in the adult human brain. *Exp. Cell Res.* 253, 733–736.

Kaiser, E., Kuzmits, R., Pregant, P., Burghuber, O., and Worofka, W. (1989). Clinical biochemistry of neuron specific enolase. *Clin. Chim. Acta* 183, 13–31.

Kam, M., Curtis, M. A., McGlashan, S. R., Connor, B., Nannmark, U., and Faull, R. L. (2009). The cellular composition and morphological organization of the rostral migratory stream in the adult human brain. *J. Chem. Neuroanat.* 37, 196–205.

Kaplan, M. S., and Hinds, J. W. (1977). Neurogenesis in the adult rat: electron microscopic analysis of light radioautographs. *Science* 197, 1092–1094.

Karpowicz, P., Morshead, C., Kam, A., Jervis, E., Ramunas, J., Cheng, V., and van der Kooy, D. (2005). Support for the immortal strand hypothesis: neural stem cells partition DNA asymmetrically in vitro. *J. Cell Biol.* 170, 721–732.

Kempermann, G., Jessberger, S., Steiner, B., and Kronenberg, G. (2004). Milestones of neuronal development in the adult hippocampus. *Trends Neurosci.* 27, 447–452.

Kim, K. K., Adelstein, R. S., and Kawamoto, S. (2009). Identification of neuronal nuclei (NeuN) as Fox-3, a new member of the Fox-1 gene family of splicing factors. *J. Biol. Chem.* 284, 31052–31061.

Knoth, R., Singec, I., Ditter, M., Pantazis, G., Capetian, P., Meyer, R. P., Horvat, V., Volk, B., and Kempermann, G. (2010). Murine features of neurogenesis in the human hippocampus across the lifespan from 0 to 100 years. *PLoS ONE* 5, e8809. doi: 10.1371/journal.pone.0008809

Koketsu, D., Furuichi, Y., Maeda, M., Matsuoka, N., Miyamoto, Y., and Hisatsune, T. (2006). Increased number of new neurons in the olfactory bulb and hippocampus of adult non-human primates after focal ischemia. *Exp. Neurol.* 199, 92–102.

Kornack, D. R., and Rakic, P. (1999). Continuation of neurogenesis in the hippocampus of the adult macaque monkey. *Proc. Natl. Acad. Sci. U.S.A.* 96, 5768–5773.

Kornack, D. R., and Rakic, P. (2001). The generation, migration, and differentiation of olfactory neurons in the adult primate brain. *Proc. Natl. Acad. Sci. U.S.A.* 98, 4752–4757.

Kukekov, V. G., Laywell, E. D., Suslov, O., Davies, K., Scheffler, B., Thomas, L. B., O'Brien, T. F., Kusakabe, M., and Steindler, D. A. (1999). Multipotent stem/progenitor cells with similar properties arise from two neurogenic regions of adult human brain. *Exp. Neurol.* 156, 333–344.

Kuruba, R., Hattiangady, B., and Shetty, A. K. (2009). Hippocampal neurogenesis and neural stem cells in temporal lobe epilepsy. *Epilepsy Behav.* 14(Suppl. 1), 65–73.

Lazarov, O., Mattson, M. P., Peterson, D. A., Pimplikar, S. W., and van Praag, H. (2010). When neurogenesis encounters aging and disease. *Trends Neurosci.* 33, 569–579.

Lemmens, M. A., Steinbusch, H. W., Rutten, B. P., and Schmitz, C. (2010). Advanced microscopy techniques for quantitative analysis in neuromorphology and neuropathology research: current status and requirements for the future. *J. Chem. Neuroanat.* 40, 199–209.

Lendahl, U., Zimmerman, L. B., and McKay, R. D. (1990). CNS stem cells express a new class of intermediate filament protein. *Cell* 60, 585–595.

Leonard, B. W., Mastroeni, D., Grover, A., Liu, Q., Yang, K., Gao, M., Wu, J., Pootrakul, D., van den Berge, S. A., Hol, E. M., and Rogers, J. (2009). Subventricular zone neural progenitors from rapid brain autopsies of elderly subjects with and without neurodegenerative disease. *J. Comp. Neurol.* 515, 269–294.

Liimatainen, T. J., Erkkila, A. T., Valonen, P., Vidgren, H., Lakso, M., Wong, G., Grohn, O. H., Yla-Herttuala, S., and Hakumaki, J. M. (2008). 1H MR spectroscopic imaging of phospholipase-mediated membrane lipid release in apoptotic rat glioma in vivo. *Magn. Reson. Med.* 59, 1232–1238.

Lin, T. N., Sun, S. W., Cheung, W. M., Li, F., and Chang, C. (2002). Dynamic changes in cerebral blood flow and angiogenesis after transient focal cerebral ischemia in rats. Evaluation with serial magnetic resonance imaging. *Stroke* 33, 2985–2991.

Lin, W., Celik, A., and Paczynski, R. P. (1999). Regional cerebral blood volume: a comparison of the dynamic imaging and the steady state methods. *J. Magn. Reson. Imaging* 9, 44–52.

Liu, Y. W., Curtis, M. A., Gibbons, H. M., Mee, E. W., Bergin, P. S., Teoh, H. H., Connor, B., Dragunow, M., and Faull, R. L. (2008). Doublecortin expression in the normal and epileptic adult human brain. *Eur. J. Neurosci.* 28, 2254–2265.

Lledo, P. M., Alonso, M., and Grubb, M. S. (2006). Adult neurogenesis and functional plasticity in neuronal circuits. *Nat. Rev. Neurosci.* 7, 179–193.

Lois, C., and Alvarez-Buylla, A. (1993). Proliferating subventricular zone cells in the adult mammalian forebrain can differentiate into neurons and glia. *Proc. Natl. Acad. Sci. U.S.A.* 90, 2074–2077.

Lois, C., Garcia-Verdugo, J. M., and Alvarez-Buylla, A. (1996). Chain migration of neuronal precursors. *Science* 271, 978–981.

Lopez-Toledano, M. A., and Shelanski, M. L. (2007). Increased neurogenesis in young transgenic mice overexpressing human APP(Sw, Ind). *J. Alzheimers Dis.* 12, 229–240.

Lucassen, P. J., Muller, M. B., Holsboer, F., Bauer, J., Holtrop, A., Wouda, J., Hoogendijk, W. J., De Kloet, E. R., and Swaab, D. F. (2001). Hippocampal apoptosis in major depression is a minor event and absent from subareas at risk for glucocorticoid overexposure. *Am. J. Pathol.* 158, 453–468.

Ma, D. K., Kim, W. R., Ming, G. L., and Song, H. (2009). Activity-dependent extrinsic regulation of adult olfactory bulb and hippocampal neurogenesis. *Ann. N. Y. Acad. Sci.* 1170, 664–673.

Ma, L. H., Li, Y., Djuric, P. M., and Maletic-Savatic, M. (2011). "Systems biology approach to imaging of neural stem cells," in *Magnetic Resonance Neuroimaging Methods and Protocols*, eds M. B. Modo and J. W. M. Bulte (New York: Springer), 421–435.

Macas, J., Nern, C., Plate, K. H., and Momma, S. (2006). Increased generation of neuronal progenitors after ischemic injury in the aged adult human forebrain. *J. Neurosci.* 26, 13114–13119.

Malberg, J. E., Eisch, A. J., Nestler, E. J., and Duman, R. S. (2000). Chronic antidepressant treatment increases neurogenesis in adult rat hippocampus. *J. Neurosci.* 20, 9104–9110.

Maletic-Savatic, M., Vingara, L. K., Manganas, L. N., Li, Y., Zhang, S., Sierra, A., Hazel, R., Smith, D., Wagshul, M. E., Henn, F., Krupp, L., Enikolopov, G., Benveniste, H., Djurić, P. M., and Pelczer, I. (2008). Metabolomics of neural progenitor cells: a novel approach to biomarker discovery. *Cold Spring Harb. Symp. Quant. Biol.* 73, 389–401.

Manganas, L. N., Zhang, X., Li, Y., Hazel, R. D., Smith, S. D., Wagshul, M. E., Henn, F., Benveniste, H., Djuric, P. M., Enikolopov, G., and Maletic-Savatic, M. (2007). Magnetic resonance spectroscopy identifies neural progenitor cells in the live human brain. *Science* 318, 980–985.

Mao, Y., Ge, X., Frank, C. L., Madison, J. M., Koehler, A. N., Doud, M. K., Tassa, C., Berry, E. M., Soda, T., Singh, K. K., Biechele, T., Petryshen, T. L., Moon, R. T., Haggarty, S. J., and Tsai, L. H. (2009). Disrupted in schizophrenia 1 regulates neuronal progenitor proliferation via modulation of GSK3beta/beta-catenin signaling. *Cell* 136, 1017–1031.

Marti-Fabregas, J., Romaguera-Ros, M., Gomez-Pinedo, U., Martinez-Ramirez, S., Jimenez-Xarrie, E., Marin, R., Marti-Vilalta, J. L., and Garcia-Verdugo, J. M. (2010). Proliferation in the human ipsilateral subventricular zone after ischemic stroke. *Neurology* 74, 357–365.

Mattiesen, W. R., Tauber, S. C., Gerber, J., Bunkowski, S., Bruck, W., and Nau, R. (2009). Increased neurogenesis after hypoxic-ischemic encephalopathy in humans is age related. *Acta Neuropathol.* 117, 525–534.

McEwen, B. S. (2001). Plasticity of the hippocampus: adaptation to chronic stress and allostatic load. *Ann. N. Y. Acad. Sci.* 933, 265–277.

Mikkonen, M., Soininen, H., Kalvianen, R., Tapiola, T., Ylinen, A., Vapalahti, M., Paljarvi, L., and Pitkanen, A. (1998). Remodeling of neuronal circuitries in human temporal lobe epilepsy: increased expression of highly polysialylated neural cell adhesion molecule in the hippocampus and the entorhinal cortex. *Ann. Neurol.* 44, 923–934.

Miller, M. W., and Nowakowski, R. S. (1988). Use of bromodeoxyuridine-immunohistochemistry to examine the proliferation, migration and time of origin of cells in the central nervous system. *Brain Res.* 457, 44–52.

Minturn, J. E., Geschwind, D. H., Fryer, H. J., and Hockfield, S. (1995). Early postmitotic neurons transiently express TOAD-64, a neural specific protein. *J. Comp. Neurol.* 355, 369–379.

Mirescu, C., and Gould, E. (2006). Stress and adult neurogenesis. *Hippocampus* 16, 233–238.

Miyata, T., Maeda, T., and Lee, J. E. (1999). NeuroD is required for differentiation of the granule cells in the cerebellum and hippocampus. *Genes Dev.* 13, 1647–1652.

Modo, M. B., and Bulte J. W. M. (eds). (2011). *Magnetic Resonance Neuroimaging*, Vol. 711. New York: Springer.

Moe, M. C., Varghese, M., Danilov, A. I., Westerlund, U., Ramm-Pettersen, J., Brundin, L., Svensson, M., Berg-Johnsen, J., and Langmoen, I. A. (2005). Multipotent progenitor cells from the adult human brain: neurophysiological differentiation to mature neurons. *Brain* 128, 2189–2199.

Monje, M. L., Toda, H., and Palmer, T. D. (2003). Inflammatory blockade restores adult hippocampal neurogenesis. *Science* 302, 1760–1765.

Mullen, R. J., Buck, C. R., and Smith, A. M. (1992). NeuN, a neuronal specific nuclear protein in vertebrates. *Development* 116, 201–211.

Nacher, J., Blasco-Ibanez, J. M., and McEwen, B. S. (2002). Non-granule PSA-NCAM immunoreactive neurons in the rat hippocampus. *Brain Res.* 930, 1–11.

Naumann, N., Alpar, A., Ueberham, U., Arendt, T., and Gartner, U. (2010). Transgenic expression of human wild-type amyloid precursor protein decreases neurogenesis in the adult hippocampus. *Hippocampus* 20, 971–979.

Pagano, S. F., Impagnatiello, F., Girelli, M., Cova, L., Grioni, E., Onofri, M., Cavallaro, M., Etteri, S., Vitello, F., Giombini, S., Solero, C. L., and Parati, E. A. (2000). Isolation and characterization of neural stem cells from the adult human olfactory bulb. *Stem Cells* 18, 295–300.

Palmer, T. D., Willhoite, A. R., and Gage, F. H. (2000). Vascular niche for adult hippocampal neurogenesis. *J. Comp. Neurol.* 425, 479–494.

Paradisi, M., Fernandez, M., Del Vecchio, G., Lizzo, G., Marucci, G., Giulioni, M., Pozzati, E., Antonelli, T., Lanzoni, G., Bagnara, G. P., Giardino, L., and Calzà, L. (2010). Ex vivo study of dentate gyrus neurogenesis in human pharmacoresistant temporal lobe epilepsy. *Neuropathol. Appl. Neurobiol.* 36, 535–550.

Parent, J. M. (2002). The role of seizure-induced neurogenesis in epileptogenesis and brain repair. *Epilepsy Res.* 50, 179–189.

Parent, J. M., Valentin, V. V., and Lowenstein, D. H. (2002). Prolonged seizures increase proliferating neuroblasts in the adult rat subventricular zone-olfactory bulb pathway. *J. Neurosci.* 22, 3174–3188.

Parent, J. M., Yu, T. W., Leibowitz, R. T., Geschwind, D. H., Sloviter, R. S., and Lowenstein, D. H. (1997). Dentate granule cell neurogenesis is increased by seizures and contributes to aberrant network reorganization in the adult rat hippocampus. *J. Neurosci.* 17, 3727–3738.

Pencea, V., Bingaman, K. D., Freedman, L. J., and Luskin, M. B. (2001).

Neurogenesis in the subventricular zone and rostral migratory stream of the neonatal and adult primate forebrain. *Exp. Neurol.* 172, 1–16.

Pereira, A. C., Huddleston, D. E., Brickman, A. M., Sosunov, A. A., Hen, R., McKhann, G. M., Sloan, R., Gage, F. H., Brown, T. R., and Small, S. A. (2007). An in vivo correlate of exercise-induced neurogenesis in the adult dentate gyrus. *Proc. Natl. Acad. Sci. U.S.A.* 104, 5638–5643.

Pryce, C. R., and Seifritz, E. (2011). A translational research framework for enhanced validity of mouse models of psychopathological states in depression. *Psychoneuroendocrinology* 36, 308–329

Rakic, P. (1985). DNA synthesis and cell division in the adult primate brain. *Ann. N. Y. Acad. Sci.* 457, 193–211.

Rakic, P. (2002a). Adult neurogenesis in mammals: an identity crisis. *J. Neurosci.* 22, 614–618.

Rakic, P. (2002b). Neurogenesis in adult primate neocortex: an evaluation of the evidence. *Nat. Rev. Neurosci.* 3, 65–71.

Rakic, P., and Nowakowski, R. S. (1981). The time of origin of neurons in the hippocampal region of the rhesus monkey. *J. Comp. Neurol.* 196, 99–128.

Ramm, P., Couillard-Despres, S., Plotz, S., Rivera, F. J., Krampert, M., Lehner, B., Kremer, W., Bogdahn, U., Kalbitzer, H. R., and Aigner, L. (2009). A nuclear magnetic resonance biomarker for neural progenitor cells: is it all neurogenesis? *Stem Cells* 27, 420–423.

Reif, A., Fritzen, S., Finger, M., Strobel, A., Lauer, M., Schmitt, A., and Lesch, K. P. (2006). Neural stem cell proliferation is decreased in schizophrenia, but not in depression. *Mol. Psychiatry* 11, 514–522.

Reynolds, B. A., and Weiss, S. (1992). Generation of neurons and astrocytes from isolated cells of the adult mammalian central nervous system. *Science* 255, 1707–1710.

Rodriguez, J. J., Jones, V. C., Tabuchi, M., Allan, S. M., Knight, E. M., LaFerla, F. M., Oddo, S., and Verkhratsky, A. (2008). Impaired adult neurogenesis in the dentate gyrus of a triple transgenic mouse model of Alzheimer's disease. *PLoS ONE* 3, e2935. doi: 10.1371/journal.pone.0002935

Rodriguez, J. J., Jones, V. C., and Verkhratsky, A. (2009). Impaired cell proliferation in the subventricular zone in an Alzheimer's disease model. *Neuroreport* 20, 907–912.

Romer, B., Sartorius, A., Inta, D., Vollmayr, B., and Gass, P. (2008). Imaging new neurons in vivo: a pioneering tool to study the cellular biology of depression? *Bioessays* 30, 806–810.

Roy, N. S., Wang, S., Jiang, L., Kang, J., Benraiss, A., Harrison-Restelli, C., Fraser, R. A., Couldwell, W. T., Kawaguchi, A., Okano, H., Nedergaard, M., and Goldman, S. A. (2000). In vitro neurogenesis by progenitor cells isolated from the adult human hippocampus. *Nat. Med.* 6, 271-277.

Sakakibara, S., and Okano, H. (1997). Expression of neural RNA-binding proteins in the postnatal CNS: implications of their roles in neuronal and glial cell development. *J. Neurosci.* 17, 8300–8312.

Sanai, N., Berger, M. S., Garcia-Verdugo, J. M., and Alvarez-Buylla, A. (2007). Comment on "human neuroblasts migrate to the olfactory bulb via a lateral ventricular extension". *Science* 318, 393; author reply 393.

Sanai, N., Tramontin, A. D., Quinones-Hinojosa, A., Barbaro, N. M., Gupta, N., Kunwar, S., Lawton, M. T., McDermott, M. W., Parsa, A. T., Manuel-Garcia Verdugo, J., Berger, M. S., and Alvarez-Buylla, A. (2004). Unique astrocyte ribbon in adult human brain contains neural stem cells but lacks chain migration. *Nature* 427, 740–744.

Santarelli, L., Saxe, M., Gross, C., Surget, A., Battaglia, F., Dulawa, S., Weisstaub, N., Lee, J., Duman, R., Arancio, O., Belzung, C., and Hen, R. (2003). Requirement of hippocampal neurogenesis for the behavioral effects of antidepressants. *Science* 301, 805–809.

Scharfman, H. E., Goodman, J. H., and Sollas, A. L. (2000). Granule-like neurons at the hilar/CA3 border after status epilepticus and their synchrony with area CA3 pyramidal cells: functional implications of seizure-induced neurogenesis. *J. Neurosci.* 20, 6144–6158.

Seevinck, P. R., Deddens, L. H., and Dijkhuizen, R. M. (2010). Magnetic resonance imaging of brain angiogenesis after stroke. *Angiogenesis* 13, 101–111.

Seress, L., Abraham, H., Tornoczky, T., and Kosztolanyi, G. (2001). Cell formation in the human hippocampal formation from mid-gestation to the late postnatal period. *Neuroscience* 105, 831–843.

Sgubin, D., Aztiria, E., Perin, A., Longatti, P., and Leanza, G. (2007). Activation of endogenous neural stem cells in the adult human brain following subarachnoid hemorrhage. *J. Neurosci. Res.* 85, 1647–1655.

Sheline, Y. I., Wang, P. W., Gado, M. H., Csernansky, J. G., and Vannier, M. W. (1996). Hippocampal atrophy in recurrent major depression. *Proc. Natl. Acad. Sci. U.S.A.* 93, 3908–3913.

Shen, J., Xie, L., Mao, X., Zhou, Y., Zhan, R., Greenberg, D. A., and Jin, K. (2008). Neurogenesis after primary intracerebral hemorrhage in adult human brain. *J. Cereb. Blood Flow Metab.* 28, 1460–1468.

Sibtain, N. A., Howe, F. A., and Saunders, D. E. (2007). The clinical value of proton magnetic resonance spectroscopy in adult brain tumours. *Clin. Radiol.* 62, 109–119.

Sierra, A., Encinas, J. M., Deudero, J. J., Chancey, J. H., Enikolopov, G., Overstreet-Wadiche, L. S., Tsirka, S. E., and Maletic-Savatic, M. (2010). Microglia shape adult hippocampal neurogenesis through apoptosis-coupled phagocytosis. *Cell Stem Cell* 7, 483–495.

Soares, D. P., and Law, M. (2009). Magnetic resonance spectroscopy of the brain: review of metabolites and clinical applications. *Clin. Radiol.* 64, 12–21.

Sohur, U. S., Emsley, J. G., Mitchell, B. D., and Macklis, J. D. (2006). Adult neurogenesis and cellular brain repair with neural progenitors, precursors and stem cells. *Philos. Trans. R. Soc. Lond. B Biol. Sci.* 361, 1477–1497.

Spalding, K. L., Bhardwaj, R. D., Buchholz, B. A., Druid, H., and Frisen, J. (2005). Retrospective birth dating of cells in humans. *Cell* 122, 133–143.

Spector, R., and Johanson, C. E. (2007). The origin of deoxynucleosides in brain: implications for the study of neurogenesis and stem cell therapy. *Pharm. Res.* 24, 859–867.

Stockmeier, C. A., Mahajan, G. J., Konick, L. C., Overholser, J. C., Jurjus, G. J., Meltzer, H. Y., Uylings, H. B., Friedman, L., and Rajkowska, G. (2004). Cellular changes in the postmortem hippocampus in major depression. *Biol. Psychiatry* 56, 640–650.

Stoeber, K., Tlsty, T. D., Happerfield, L., Thomas, G. A., Romanov, S., Bobrow, L., Williams, E. D., and Williams, G. H. (2001). DNA replication licensing and human cell proliferation. *J. Cell. Sci.* 114, 2027–2041.

Suzuki, K., Okada, K., Wakuda, T., Shinmura, C., Kameno, Y., Iwata, K., Takahashi, T., Suda, S., Matsuzaki, H., Iwata, Y., Hashimoto, K., and Mori, N. (2010). Destruction of dopaminergic neurons in the midbrain by 6-hydroxydopamine decreases hippocampal cell proliferation in rats: reversal by fluoxetine. *PLoS ONE* 5, e9260. doi: 10.1371/journal.pone.0009260

Takasaki, Y., Deng, J. S., and Tan, E. M. (1981). A nuclear antigen associated with cell proliferation and blast transformation. *J. Exp. Med.* 154, 1899–1909.

Tata, D. A., and Anderson, B. J. (2010). The effects of chronic glucocorticoid exposure on dendritic length, synapse numbers and glial volume in animal models: implications for hippocampal volume reductions in depression. *Physiol. Behav.* 99, 186–193.

Tattersfield, A. S., Croon, R. J., Liu, Y. W., Kells, A. P., Faull, R. L., and Connor, B. (2004). Neurogenesis in the striatum of the quinolinic acid lesion model of Huntington's disease. *Neuroscience* 127, 319–332.

Van der Borght, K., Kobor-Nyakas, D. E., Klauke, K., Eggen, B. J., Nyakas, C., Van der Zee, E. A., and Meerlo, P. (2009). Physical exercise leads to rapid adaptations in hippocampal vasculature: temporal dynamics and relationship to cell proliferation and neurogenesis. *Hippocampus* 19, 928–936.

van Praag, H., Shubert, T., Zhao, C., and Gage, F. H. (2005). Exercise enhances learning and hippocampal neurogenesis in aged mice. *J. Neurosci.* 25, 8680–8685.

Veeraraghavalu, K., Choi, S. H., Zhang, X., and Sisodia, S. S. (2010). Presenilin 1 mutants impair the self-renewal and differentiation of adult murine subventricular zone-neuronal progenitors via cell-autonomous mechanisms involving notch signaling. *J. Neurosci.* 30, 6903–6915.

Verret, L., Jankowsky, J. L., Xu, G. M., Borchelt, D. R., and Rampon, C. (2007). Alzheimer's-type amyloidosis in transgenic mice impairs survival of newborn neurons derived from adult hippocampal neurogenesis. *J. Neurosci.* 27, 6771–6780.

Verwer, R. W., Sluiter, A. A., Balesar, R. A., Baayen, J. C., Noske, D. P., Dirven, C. M., Wouda, J., van Dam, A. M., Lucassen, P. J., and Swaab, D. F. (2007). Mature astrocytes in the adult human neocortex express the early neuronal marker doublecortin. *Brain* 130, 3321–3335.

Vollmayr, B., Mahlstedt, M. M., and Henn, F. A. (2007). Neurogenesis and depression: what animal models tell us about the link. *Eur. Arch. Psychiatry Clin. Neurosci.* 257, 300–303.

von Bohlen Und Halbach, O. (2007). Immunohistological markers for staging neurogenesis in adult hippocampus. *Cell Tissue Res.* 329, 409–420.

Watts, C., McConkey, H., Anderson, L., and Caldwell, M. (2005). Anatomical perspectives on adult neural stem cells. *J. Anat.* 207, 197–208.

Wegiel, J., Kuchna, I., Nowicki, K., Imaki, H., Marchi, E., Ma, S. Y., Chauhan, A., Chauhan, V., Bobrowicz, T. W., de Leon, M., Louis, L. A., Cohen, I. L., London, E., Brown, W. T., and Wisniewski, T. (2010). The neuropathology of autism: defects of neurogenesis and neuronal migration, and dysplastic changes. *Acta Neuropathol.* 119, 755–770.

Weickert, C. S., Webster, M. J., Colvin, S. M., Herman, M. M., Hyde, T. M.,

Weinberger, D. R., and Kleinman, J. E. (2000). Localization of epidermal growth factor receptors and putative neuroblasts in human subependymal zone. *J. Comp. Neurol.* 423, 359–372.

Whitman, M. C., and Greer, C. A. (2009). Adult neurogenesis and the olfactory system. *Prog. Neurobiol.* 89, 162–175.

Winner, B., Geyer, M., Couillard-Despres, S., Aigner, R., Bogdahn, U., Aigner, L., Kuhn, G., and Winkler, J. (2006). Striatal deafferentation increases dopaminergic neurogenesis in the adult olfactory bulb. *Exp. Neurol.* 197, 113–121.

Wong, M. L., and Licinio, J. (2001). Research and treatment approaches to depression. *Nat. Rev. Neurosci.* 2, 343–351.

Yerushalmi, R., Woods, R., Ravdin, P. M., Hayes, M. M., and Gelmon, K. A. (2010). Ki67 in breast cancer: prognostic and predictive potential. *Lancet Oncol.* 11, 174–183.

Yoshimi, K., Ren, Y. R., Seki, T., Yamada, M., Ooizumi, H., Onodera, M., Saito, Y., Murayama, S., Okano, H., Mizuno, Y., and Mochizuki, H. (2005). Possibility for neurogenesis in substantia nigra of parkinsonian brain. *Ann. Neurol.* 58, 31–40.

Yu, T. S., Zhang, G., Liebl, D. J., and Kernie, S. G. (2008). Traumatic brain injury-induced hippocampal neurogenesis requires activation of early nestin-expressing progenitors. *J. Neurosci.* 28, 12901–12912.

Yu, Y., He, J., Zhang, Y., Luo, H., Zhu, S., Yang, Y., Zhao, T., Wu, J., Huang, Y., Kong, J., Tan, Q., and Li, X. M. (2009). Increased hippocampal neurogenesis in the progressive stage of Alzheimer's disease phenotype in an APP/PS1 double transgenic mouse model. *Hippocampus* 19, 1247–1253.

Zaharchuk, G. (2007). Theoretical basis of hemodynamic MR imaging techniques to measure cerebral blood volume, cerebral blood flow, and permeability. *AJNR Am. J. Neuroradiol.* 28, 1850–1858.

Zhang, R. L., Zhang, Z. G., Zhang, L., and Chopp, M. (2001). Proliferation and differentiation of progenitor cells in the cortex and the subventricular zone in the adult rat after focal cerebral ischemia. *Neuroscience* 105, 33–41.

Zhang, Z. G., and Chopp, M. (2009). Neurorestorative therapies for stroke: underlying mechanisms and translation to the clinic. *Lancet Neurol.* 8, 491–500.

Zhao, M., Momma, S., Delfani, K., Carlen, M., Cassidy, R. M., Johansson, C. B., Brismar, H., Shupliakov, O., Frisen, J., and Janson, A. M. (2003). Evidence for neurogenesis in the adult mammalian substantia nigra. *Proc. Natl. Acad. Sci. U.S.A.* 100, 7925–7930.

Ziabreva, I., Perry, E., Perry, R., Minger, S. L., Ekonomou, A., Przyborski, S., and Ballard, C. (2006). Altered neurogenesis in Alzheimer's disease. *J. Psychosom. Res.* 61, 311–316.

Conflict of Interest Statement: The authors declare that the research was conducted in the absence of any commercial or financial relationships that could be construed as a potential conflict of interest.

Received: 20 January 2011; accepted: 23 March 2011; published online: 04 April 2011.
*Citation: Sierra A, Encinas JM and Maletic-Savatic M (2011) Adult human neurogenesis: from microscopy to magnetic resonance imaging. Front. Neurosci. **5**:47. doi: 10.3389/fnins.2011.00047*
This article was submitted to Frontiers in Neurogenesis, a specialty of Frontiers in Neuroscience.